EXPLORING NOVEL DYE CONCEPTS IN DYE SENSITIZED SOLAR CELLS.

Laia Pellejà i Puxeu

Dipòsit Legal: T 1663-2014

EXPLORING NOVEL DYE CONCEPTS IN DYE SENSITIZED SOLAR CELLS

Laia Pellejà i Puxeu

Doctoral Thesis 2014

UNIVERSITAT ROVIRA I VIRGILI

ICIQ
Institut Català d'Investigació Química

UNIVERSITAT ROVIRA I VIRGILI
EXPLORING NOVEL DYE CONCEPTS IN DYE SENSITIZED SOLAR CELLS.
Laia Pellejà i Puxeu
Dipòsit Legal: T 1663-2014

UNIVERSITAT ROVIRA I VIRGILI
EXPLORING NOVEL DYE CONCEPTS IN DYE SENSITIZED SOLAR CELLS.
Laia Pellejà i Puxeu
Dipòsit Legal: T 1663-2014

UNIVERSITAT ROVIRA I VIRGILI
EXPLORING NOVEL DYE CONCEPTS IN DYE SENSITIZED SOLAR CELLS.
Laia Pellejà i Puxeu
Dipòsit Legal: T 1663-2014

Ph.D. Thesis

Exploring novel dye concepts in Dye Sensitized Solar Cells

Laia Pellejà i Puxeu

Supervised by Prof. Dr. Emilio Palomares Gil

(Institut Català d'Investigació Química-
Universitat Rovira I Virgili)

Tarragona, March 2014

UNIVERSITAT ROVIRA I VIRGILI

UNIVERSITAT ROVIRA I VIRGILI
EXPLORING NOVEL DYE CONCEPTS IN DYE SENSITIZED SOLAR CELLS.
Laia Pellejà i Puxeu
Dipòsit Legal: T 1663-2014

UNIVERSITAT ROVIRA I VIRGILI
EXPLORING NOVEL DYE CONCEPTS IN DYE SENSITIZED SOLAR CELLS.
Laia Pellejà i Puxeu
Dipòsit Legal: T 1663-2014

Emilio Palomares Gil, Group Leader at the Institut of Chemical Research of Catalonia (ICIQ) in Tarragona and Research Professor of the Catalan Institution for Research and Advanced Studies (ICREA) in Barcelona

CERTIFY:

That the present research study, entitled “Exploring novel dye concept in Dye Sensitized Solar Cells” presented by Laia Pellejà i Puxeu for the award of the degree of Doctor, has been carried out under my supervision in ICIQ and that she fulfils the requirements to obtain a Doctorate Mention.

Tarragona, March 2014

Prof. Dr. Emilio Palomares Gil

UNIVERSITAT ROVIRA I VIRGILI

ICIQ
Institut Català d'Investigació Química

UNIVERSITAT ROVIRA I VIRGILI
EXPLORING NOVEL DYE CONCEPTS IN DYE SENSITIZED SOLAR CELLS.
Laia Pellejà i Puxeu
Dipòsit Legal: T 1663-2014

Al Ferran.
I a l'Abril, l'Agnès i el Damià.

UNIVERSITAT ROVIRA I VIRGILI
EXPLORING NOVEL DYE CONCEPTS IN DYE SENSITIZED SOLAR CELLS.
Laia Pellejà i Puxeu
Dipòsit Legal: T 1663-2014

UNIVERSITAT ROVIRA I VIRGILI
EXPLORING NOVEL DYE CONCEPTS IN DYE SENSITIZED SOLAR CELLS.
Laia Pellejà i Puxeu
Dipòsit Legal: T 1663-2014

El mestre que intenta ensenyar sense inspirar en l'alumne
el desig d'aprendre està tractant de forjar un ferro fred.
H. Mann

Gràcies Emili.

UNIVERSITAT ROVIRA I VIRGILI
EXPLORING NOVEL DYE CONCEPTS IN DYE SENSITIZED SOLAR CELLS.
Laia Pellejà i Puxeu
Dipòsit Legal: T 1663-2014

Resum

Aquesta tesi es basa en un tipus de dispositius fotovoltaics, les cel·les solars sensitivitzades amb colorant (en anglès: DSCs). Des de fa un parell de dècades, l'estudi d'aquests dispositius ha anat en augment i actualment ja s'han publicat resultats amb més d'un 13% d'eficiència. Aquest tipus de dispositius són més econòmics i més fàcils de preparar que les esteses cel·les solars de silici. A part, presenten molts avantatges enfront d'aquestes: són transparents, és a dir, deixen passar la llum del sol, poden ser de diferents colors, i això les fa molt atractives a l'hora d'integrar-les als edificis, i també funcionen a baixa intensitat de llum.

El primer capítol tracta sobre els diferents components d'aquest dispositiu, la seva funció i de què estan formats. També s'explica el funcionament d'aquestes cel·les i totes les reaccions i fenòmens físics que hi tenen lloc.

En el segon capítol s'explica com es prepara aquest tipus de dispositius i com es caracteritzen.

I els capítols tercer, quart, cinquè i sisè es basen en diversos articles publicats i entre ells es diferencien pel tipus de colorant utilitzat. En el tercer, el colorant que s'empra són les porfirines, el quart les ftalocianines, en el cinquè es treballa en colorants orgànics que tenen una estructura anomenada dadora-acceptora amb un pont tipus π entremig i en el sisè s'estudien dos complexes de ruteni.

Abstract

This thesis is based on a type of photovoltaic devices; the dye sensitized solar cells (DSCs). In the last two decades, the study of these devices has been increased and currently results with over 13% efficiency have been published. Such devices are cheaper and easier to prepare than the extended silicon solar cells. In addition, they present many advantages over these: they are transparent, they can have different colours, and this makes very attractive to integrate into buildings, and also work at low light intensity.

The first chapter discusses the various components of this kind of device, its function and its components. It is also explained how these cells work and all the reactions and physical phenomena that take place.

The second chapter explains how to prepare these devices and how are characterized.

And the third, fourth, fifth and sixth chapters are based on diverse articles published and the difference between them is the kind of dye. In chapter 3, the dyes used are porphyrins, chapter 4 is based on phthalocyanines, chapter 5 is centred on organic dyes that have a structure called donor-acceptor with a π-bridge type in between and chapter 6 studies two ruthenium complexes.

General Index

UNIVERSITAT ROVIRA I VIRGILI
EXPLORING NOVEL DYE CONCEPTS IN DYE SENSITIZED SOLAR CELLS.
Laia Pellejà i Puxeu
Dipòsit Legal: T 1663-2014

Chapter 1. Introduction

Index

1. Introduction

Dye sensitized solar cells (DSCs) are one of the most studied photovoltaic devices. These solar cells take sunlight and convert it directly into electricity using very cheap materials, which do not require much energy input as the highest temperature used is about 500ºC. A typical DSCs comprises a mesoporous semiconductor metal oxide sensitized with a dye and a liquid (could also be a hole conductor) red/ox couple.

These type of solar cells are known also as photo-electrochemical solar cells. It was in 1991, when Dr. Brian O'Regan and Prof. Michael Grätzel[1] published their study regarding the principles of operation of this molecular device with efficiencies higher than 7% that was a substantial quantum leap in efficiency. The DSCs perform much better compared with other photovoltaic devices under diffuse light conditions due to the use of the mesoporous semiconductor as the film scatter the sunlight. Last but not least, these solar cells offer also the possibilities to design solar cells with a large and flexible shape, color and transparency, which aims for the integration into different products to opens up new eco-friendly commercial opportunities.

1.1. Principles of operation

The DSCs have well known and easily tuneable photophysical, photochemical and electrochemical properties, and for that are excellent candidates for light harvesting systems and energy conversion devices. All DSCs are composed by a working and a counter electrode and the hole transport material which can be liquid or solid. In the working electrode, a layer of a mesoporous metal oxide semiconductor, often TiO_2, is deposited onto a TCO (transparent conducting oxide). The mesoporous film is coloured with a sensitizer that act as light harvesting material. Upon light absorption the sensitizer inject electrons into the semiconductor and the red/ox electrolyte regenerates the oxidized sensitizer closing the electrical circuit. The external circuit electrons arriving to the counter electrode also regenerate the oxidised electrolyte.at the counter electrode an atomic layer of Pt serves to catalyse this electron transfer. Figure 1.1 illustrates an schematic representation of a typical DSCs.

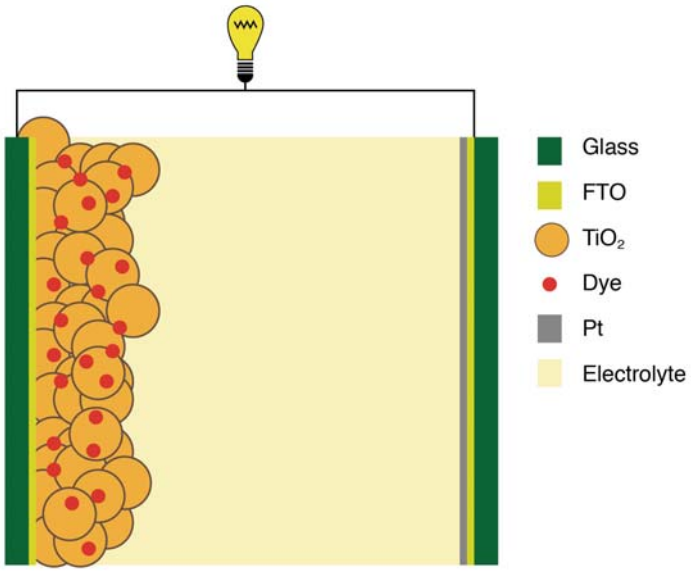

Figure 1.1. Schematic representation of a DSCs.

In Figure 1.2 the major charge transfer steps occurring at the DSCs during illumination are represented.[2]

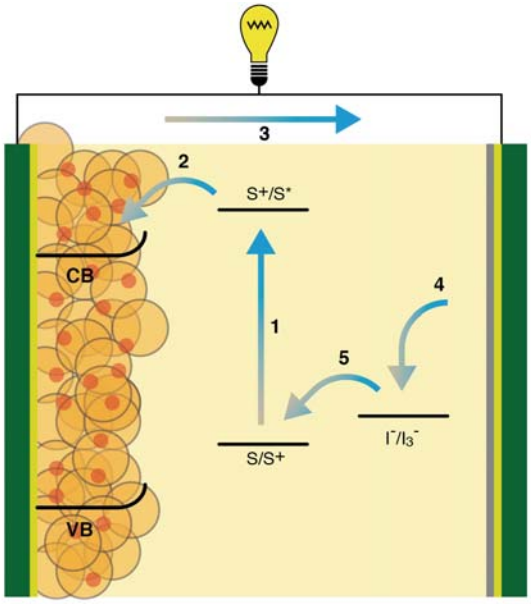

Figure 1.2. Scheme showing the operating principle and energy level diagram of a DSCs. S, S^+ and S* represent the dye in the ground, oxidized and excited state respectively. (1) Photoexcitation of the dye, (2) electron injection from the excited dye to the semiconductor, (3) external circuit, (4) regeneration of the electrolyte and (5) regeneration of the oxydized dye.

1.2. The working electrode

As mentioned above, the mesoporous semiconductor film is attached to the TCO. The TCO consists in a glass coated with a thin layer of a

transparent conductive material. In this type of devices, the most commonly used conductive material is fluorine doped tin oxide (FTO). In other devices, the material used is tin doped indium oxide (ITO), but the fabrication of DSCs implies temperatures higher than 300ºC and although ITO presents higher conductivities, its thermal instability strongly increases the resistance of the material and, hence, most devices are fabricated using FTO.

It is also important to mention that semiconductor TiO_2 still gives the highest efficiencies, but many other metal oxide systems have been tested, such as ZnO, SnO_2, and Nb_2O_5. Besides these simple oxides, ternary oxides, such as $SrTiO_3$ and Zn_2SnO_4, have been investigated, as well as core-shell structures, such as ZnO-coated SnO_2.

The TiO_2 is a stable, nontoxic oxide, which has a high refractive index (n = 2.4-2.5) and is widely used as a white pigment in paint, toothpaste, sunscreen, self-cleaning materials and food (E171). Several crystal forms of TiO_2 occur naturally: rutile, anatase and brookite. Rutile is the thermodynamically most stable form. Anatase is, however, the preferred structure in DSCs, because it has a larger bandgap (3.2 vs 3.0 eV for rutile) and the higher conduction band edge energy, Ec. This leads to a higher Fermi level and V_{oc} in DSCs for the same conduction band electron concentration.

For state-of-the-art DSCs, the employed architecture for the mesoporous TiO_2 electrode is as follows:[2]

- A TiO_2 blocking layer (thickness ~50 nm), coating the FTO plate to prevent contact between the redox mediator in the electrolyte and the FTO, prepared by chemical bath deposition, spray pyrolysis, or sputtering.[3]
- A light absorption layer consisting on a ~10 µm thick film of mesoporous TiO_2 with ~20 nm particle size that provides a large surface area for sensitizer adsorption (in order to anchor a dye monolayer) and good electron transport to the substrate (porosity must be also controlled).
- A light scattering layer on top of the mesoporous film, consisting of a ~4 µm porous layer containing ~400 nm sized TiO_2 particles. The aim of this layer is to reflect the light, which has passed through unabsorbed back into the film where it can be absorbed by the dye.
- An ultrathin overcoating of TiO_2 on the whole structure, deposited by means of chemical bath deposition (using aqueous $TiCl_4$), followed by heat treatment.

The $TiCl_4$ treatment leads to the deposition of an ultrapure TiO_2 shell (~1 nm) on the mesoporous TiO_2 (which may contain impurities or have

carbon residues at the surface). It lowers the acceptor levels in TiO_2 in energy, which can improve the injection efficiency. It also improves electron lifetime significantly, leading to an increase in the electron diffusion length.[4]

Most common methods to deposit the nanoparticles are based on the doctor Blade or the use of screen printing manual or authomatic machines techniques continued with a heating at 500ºC. This process leads in a nanostructured mesoporous TiO_2 electrode.

1.3. The photosensitizer

Best sensitizer for a DSCs must absorb light across the entire visible spectrum, bind strongly to the semiconductor surface, have a suitably high redox potential for regeneration following excitation and be stable over many years of exposure to sunlight. Most of the dyes used in DSCs are linked to the TiO_2 surface through acidic groups, basically carboxylic groups that can form ester linkages with the surface of the semiconductor to obtain a strongly bound and good electronic communication between the two parts. Anchoring to TiO_2 has been also achieved through a number of functional groups, such as phosphonic acid, salicylate, carboxylic acid, sulphonic acid, phosphonic acid and acetyl-acetonate derivatives.

The spectrum of the solar irradiance is shown in Figure 1.3. Currently, the goal is synthesize compounds that absorb light in the red or in in the NIR region of the sun light spectra.

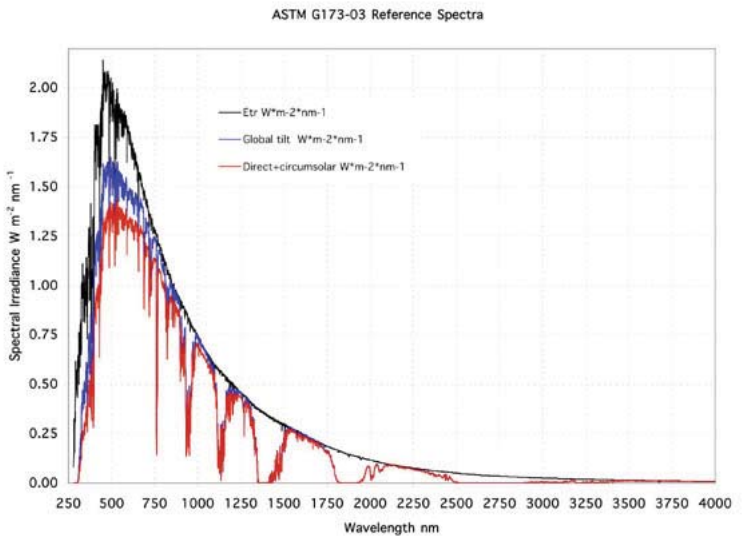

Figure 1.3. Solar irradiation spectrum.

Moreover, the LUMO (Lowest Unoccupied Molecular Orbital) of the dye must remain sufficiently higher than TiO_2 conduction band (CB) edge for efficient charge injection while the HOMO (Highest Occupied Molecular Orbital) must remain sufficiently below the redox level of the electrolyte for efficient regeneration of the dye. The mismatch of these two energy levels with either the TiO_2 CB or the red/ox energy levels leads to unwanted device efficiency losses. The lower energy of longer-wavelength photons the more difficult to make efficient devices as the HOMO–LUMO gap is narrower.[5]

Furthermore, the spatial orientation of the HOMO and LUMO influences not only the electron injection of the dye into the semiconductor conduction band and the photosensitizer regeneration but also the electron recombination between the photoinjected electrons at the TiO_2 and the oxidized dye.[6] In other words, the LUMO should be in close contact with the semiconductor surface and the dye cation should be separated from the electrode surface.

It is also important to prevent dye aggregation, this can be solved through optimization of the molecular structure of the dye or by addition of co-adsorbents that prevent aggregation. The chenodeoxycholic acid is one of the most common co-adsorbents used and it can prevent aggregation because of its bulky size is inserted between the photosensitizers on the TiO_2 surface and it can also reduce the back electron transfer reaction between the red/ox electrolyte and electrons in the TiO_2 nanoparticles, decreasing this recombination process.

The last property that must be taken into account is the chemical, thermal and electrochemical stability of the dye during exposure to solar radiation and in the electrolyte media.

Based on these requirements, many different photosensitizers including metal complexes, porphyrins, phthalocyanines and metal-free organic dyes have been designed and applied to DSCs in the past decades.

1.3.1. Metal complexes. Metal complex photosensitizers consist of a central metal ion with ancillary ligands having at least one anchoring group. Light absorption in the visible part of the solar spectrum is due to a metal to ligand charge transfer (MLCT) transition and this transition leads to moderate absorption coefficients ($\varepsilon < 18000\ cm^{-1}\ M^{-1}$). The central metal ion is a crucial part of the overall properties of the complexes. Ancillary ligands, typically bipyridines or terpyridines, can be tuned by using different substituents (alkyl, aryl, heterocycle, etc.) to change the photophysical and electrochemical properties and therefore improve the photovoltaic performance. Among the

metal complexes, ruthenium complexes have shown the best photovoltaic properties: a broad absorption spectrum, appropriate excited and ground state energy levels, long excited-state lifetime and good electrochemical stability. Several ruthenium complexes used in DSCs have reached more than 10% solar cell efficiency under standard measurement conditions. Some representative ruthenium dyes are depicted in Figure 1.4. Many attempts have also been made to obtain dyes with other metal ions such as Os (II),[7] Re(I),[8] Fe(II),[9] Pt(II)[10] or Cu(I).[11]

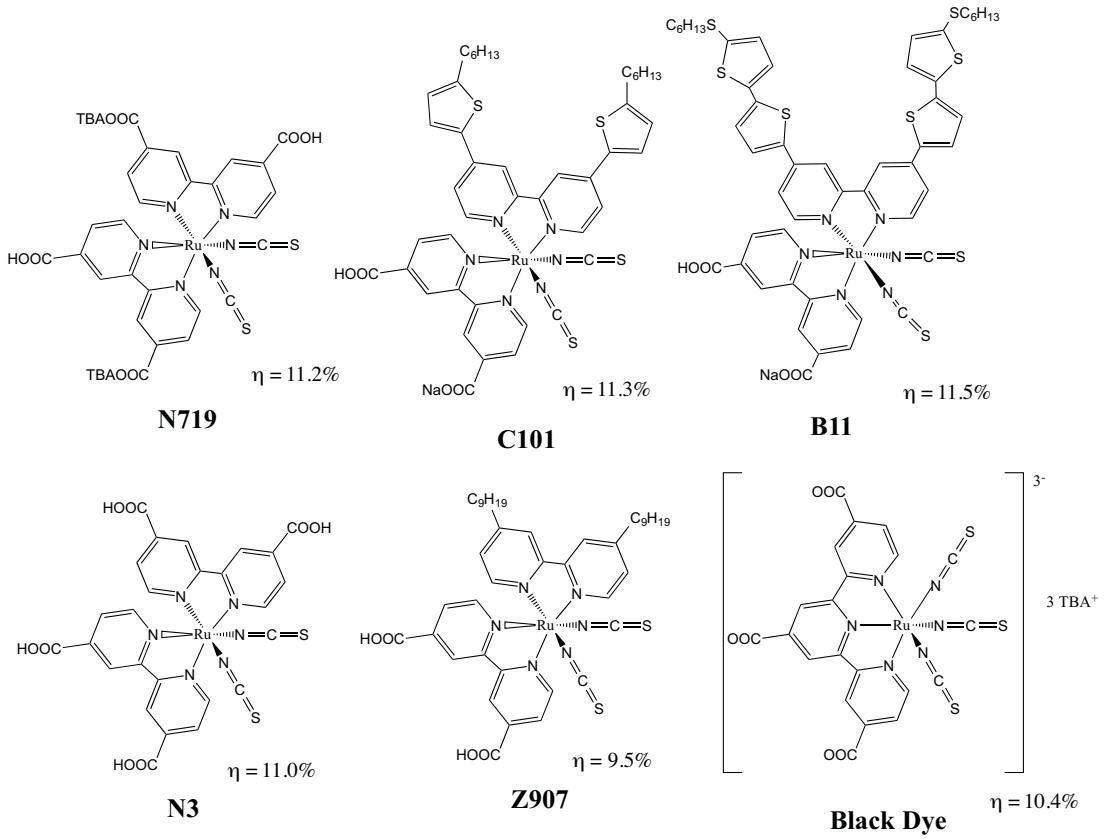

Figure 1.4. Most efficient ruthenium complexes used in DSCs.[12]

1.3.2. Porphyrins. During the last years, an effort was made in order to replace the ruthenium complexes by other dyes. Ideally, earth abundant, non-toxic metals components or no metal ion at all can be easily designed and synthesized. Moreover, avoiding the use of ruthenium will also decrease the production cost of the final device.[5] Porphyrins were introduced as photosensitizers in DSCs due their primary role in photosynthesis and their outstanding absorption properties. Porphyrins are fully conjugated aromatic macrocycles characterized by the presence of four modified pyrrole subunits interconnected at their α carbon atoms via methine bridges. Typical porphyrin absorption spectra consist of an intense Soret band centered at 400-450 nm ($\varepsilon \sim 420000\ cm^{-1}\ M^{-1}$) and a series of moderately absorbing Q bands at 500-

650 nm (ε ~ 15000 cm^{-1} M^{-1}).[13] The most commonly porphyrins used in DSCs are the free base (no ion presence) and the zinc based (Figure 1.5). Porphyrin aggregation problems are usual induced by highly favorable π-π stacking resulted in low electron injection yields due to deactivation of excited state before the electron injection into the TiO_2 CB occurs, so co-adsorbents are usual needed to improve the device performance.

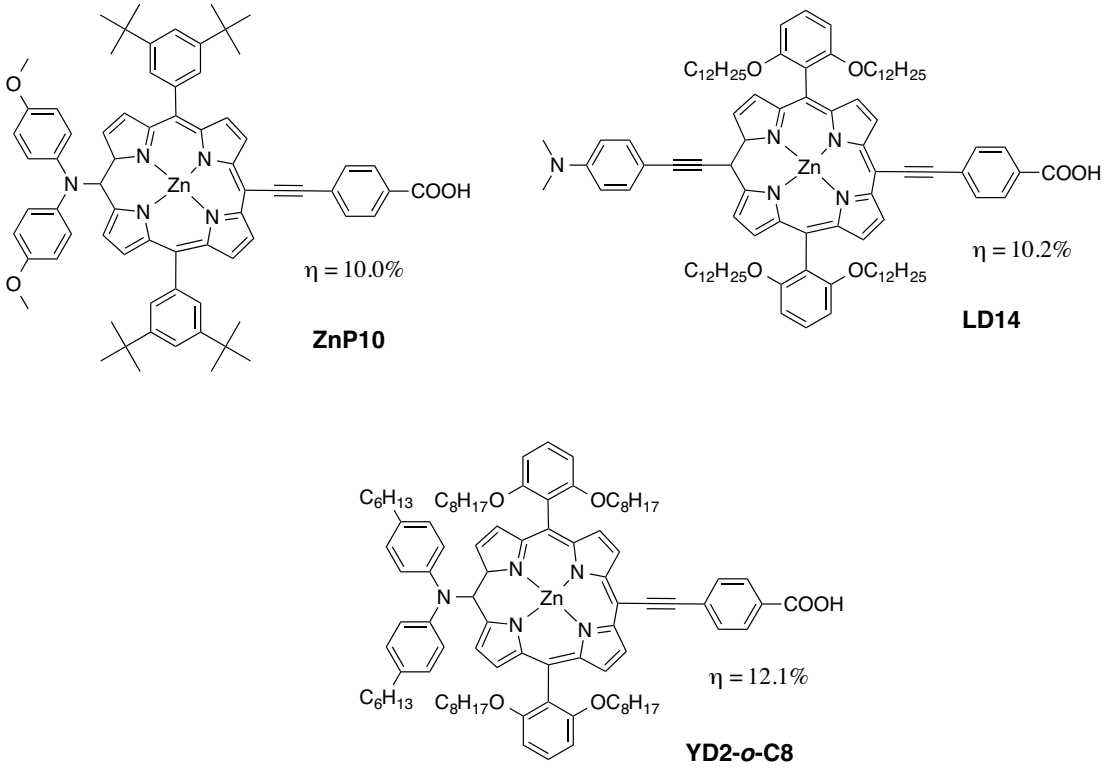

Figure 1.5. Highly efficient porphyrins used in DSCs.[14]

1.3.3. Phtalocyanines. Phtalocyanines are symmetrical 18 π-electron aromatic macrocycles and are extremely used as dyes and pigments. These compounds possess intense absorption in the Q-band (around 700 nm), as well as promising electrochemical, photochemical and thermal properties, and are thus of interest to use as NIR photosensitizers for DSCs. The solubility of these dyes is normally very poor and needs to be improved by structural optimization in order to facilitate the dye-sensitization process. Another major problem with phthalocyanines is their strong tendency to aggregate on the semiconductor surface, which requires a co-adsorbent to suppress dye aggregation. Some examples are shown in Figure 1.6.

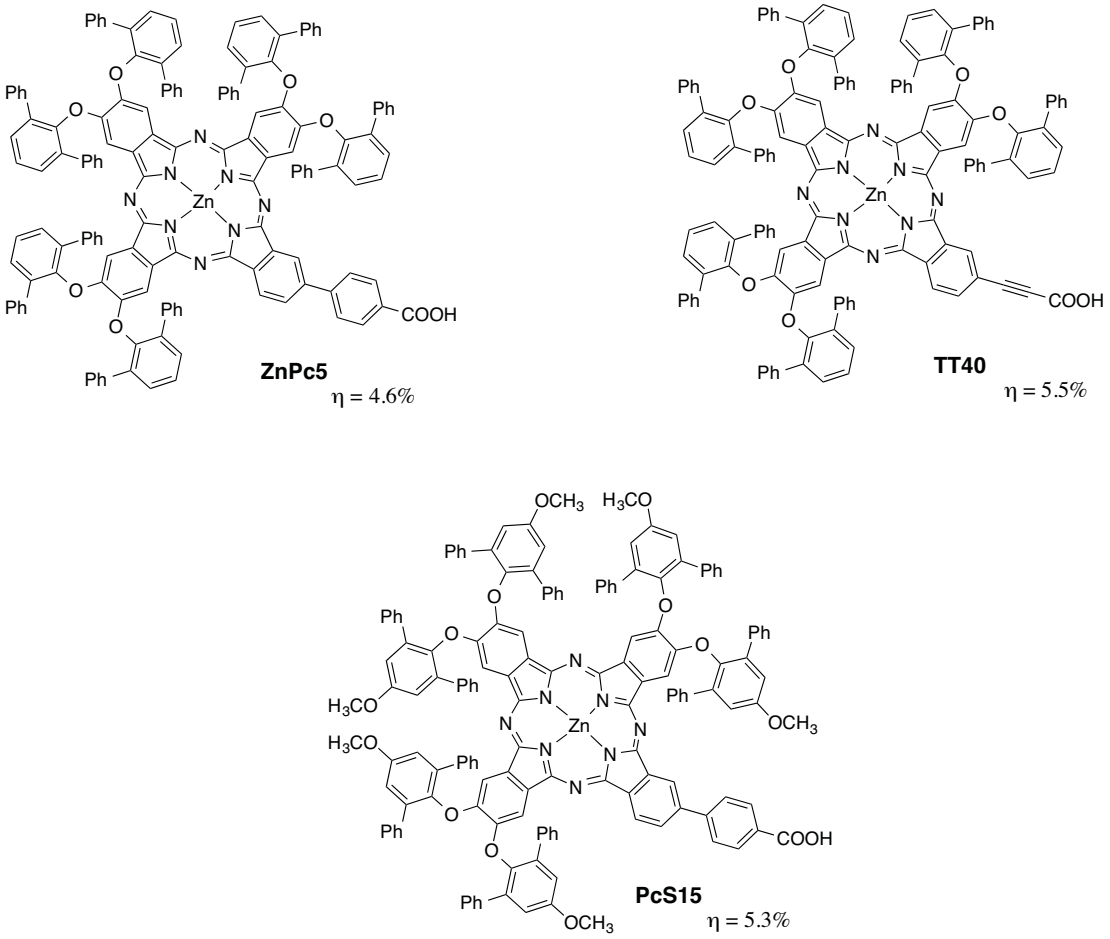

Figure 1.6. Highly efficient phthalocyanines used in DSCs.[15]

1.3.4. Donor-π-bridge-Acceptor conjugated neutral dyes. The D-π-A consists of electron-donating and electron-withdrawing groups linked covalently through a π conjugate spacer. With this construction it is easy to design new dye structures, extend the absorption spectra, adjust the HOMO and LUMO levels and complete the intramolecular charge separation. When a dye absorbs light, the intramolecular charge transfer occurs from subunit A to D through the π-bridge. So this configuration certifies better charge separation and efficient electron injection from the excited state of the photosensitizer into the TiO_2 conduction band. Some examples are shown in Figure 1.7.

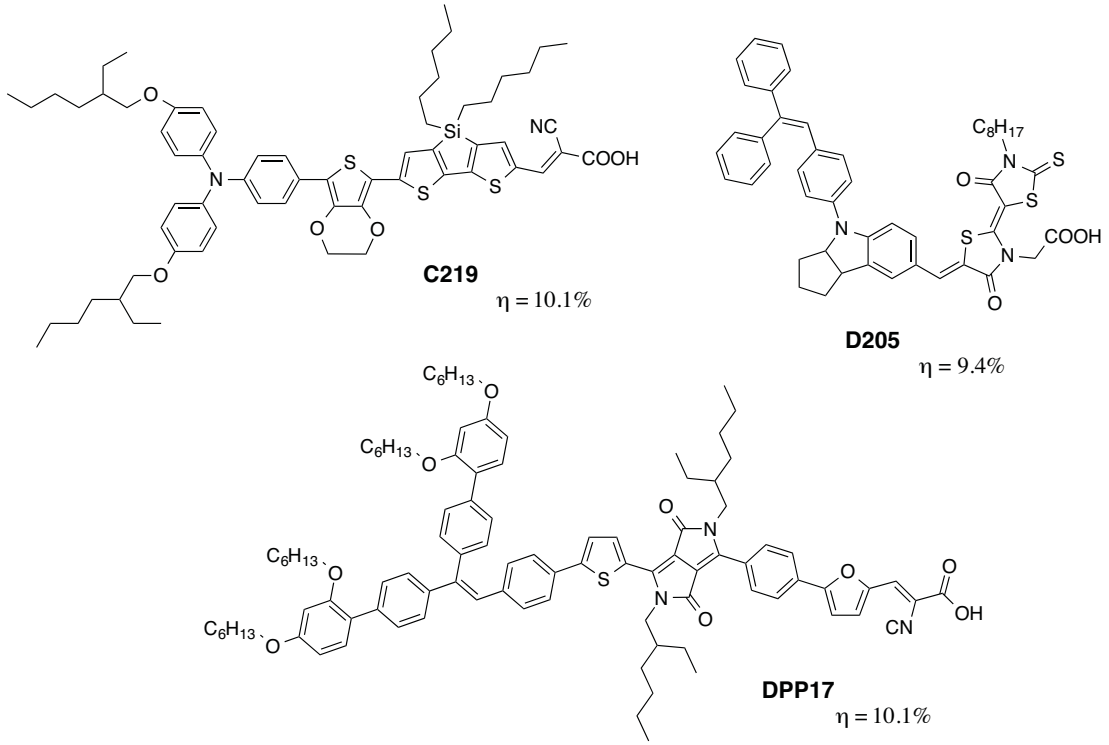

Figure 1.7. Highly efficient donor-π-acceptor dye.[16]

1.3.5. Co-sensitization. This strategy is used in order to increase the spectral response of the DSCs. The idea is to use sensitizers with different absorption spectra that are adsorbed together onto the mesoporous TiO_2 surface, using a mixed dye solution for sensitization. Different dyes absorbing light in the blue, yellow and red regions of the solar spectrum can be used and, thus, increase the DSCs photocurrent.[17] A ruthenium complex can also be used with an organic sensitizer in order to combine both properties.[18] Different sequential dye absorption could be also done applying an ultrathin layer of aluminum oxide between the absorption of the different dyes.[19]

1.4. The electrolyte

The electrolyte is the hole transporting material in a DSCs. Different requirements are needed to have a good electrolyte:

- It must have a good contact between the working and the counter electrodes.
- It needs high conductivity to permit fast charge transport between the platinum counter electrode and the oxidised dye.
- The electrolyte should neither degrade nor desorb the photosensitizer from the metal oxide surface.

- It should also be thermally, optically, chemically and electrochemically stable.
- The redox potentials of the redox par must to allow efficient dye regeneration.

A great number of redox mediators and electrolyte systems have been explored, including I^-/I_3^- in either solid polymer,[20] gel,[21] ionic liquid[22] or plastic crystal[23] systems; solid inorganic materials;[24] Co(II)/Co(III)[25] and $SeCN^-$/$(SeCN)_3^-$ redox couples[22] and hole-conducting organic polymers[26] and small organic molecules.[27] Yet, the best performances have been obtained with I^-/I_3^- or the Co(II)/Co(III) red/ox couple.

Liquid electrolytes. In these electrolytes the redox par is dissolved in organic solvents with high dielectric constants such as acetonitrile, *N*-methylpyrrolidine and valeronitrile or a combination of those solvents.

Ionic liquids. The addition of ionic liquids in organic solvent based electrolytes often increases the ionic conductivity.[28] The ionic liquid electrolytes were divided into two sections, pure ionic liquids and quasi-solid (gel based materials with dispersed amounts of liquid electrolyte) electrolytes based on ionic liquids. The area is vastly dominated by imidazolium-based electrolytes, and some of the main conclusions were that the combination of photochemical stability and low viscosity, and thus ion mobility, remains a challenge.[4] Ionic liquids presents also very low vapor pressure, non-flammability, high ionic conductivity and wide electrochemical window, which are very useful properties for long-lived electrochemical devices.[29]

Solid electrolytes. The most common solid electrolyte is the spiro-OMeTAD. Organic semiconductor materials are of interest as allows the fabrication of solid devices. Yet, the solid hole conductors present several disadvantages as: surface wetting (percolation inside the nanoporous of the semiconductor oxide is an important issue), moderate stability in air that requires a perfect sealing and encapsulation and the materials also absorbs light acting as a filter for the sensitized films.

Additives. These compounds play a central role in the enhancement of photoelectrochemical performance of DSCs. Their effects are often attributed to modification of redox couple potential, band shifts of the semiconducting electrode material, effects of surface blocking or surface dye organization. Most additives that have been reported contain an electron-donating nitrogen heterocycle, such as 4-*tert*-butylpyridine (TBP).[4] as an example, the TBP shift upwards the conduction band edge. This effect

provides an enhancement of the open circuit voltage but at the same time this shift can also decrease the injection driving force, reducing the cell photocurrent.[30]

1.5. The counter electrode

The mean functions of the counter electrode are the reduction of the oxidized species present in the electrolyte redox couple and present low resistance. The best material until the moment is platinum and it is very easy to prepare by thermal decomposition. Another materials have been tested such as carbon as graphite or black carbon, or conducting polymers such as PEDOT or cobalt sulphide.

2. Requirements for efficient DSCs

Efficient photovoltaic conversion in DSCs occurs because of a carefully balanced relationship of different kinetic processes that must be optimized in order to obtain the maximum yield for each device. First of all, in order to convert photons into electrical energy, solar cells must generate a flow of electrons through the external circuit. Therefore, a potential difference between the electrodes is needed, since it will provide the necessary driving force for the electrical current. Below are some of the key issues that must be considered to make an efficient DSCs.

2.1. Fermi level of TiO_2 conduction band

In the dark, the Fermi level of electrons in the semiconductor is equilibrated with the redox energy level of the electrolyte. Under light exposure, the Fermi level is shifted upwards generating enough driving force for electrical current. The open circuit voltage (V_{oc}) is determined by the difference between the Fermi level of the semiconductor conduction band and the electrolyte redox potential.

Changing the surface dipole potential, which means the addition of lithium ions and *tert*-butyl pyridine, modifies the conduction band and so the open circuit voltage. As briefly explained in section 1.4, the addition of lithium ions increase the short current density of the devices, however, at the expense of a lower open circuit voltage and vice versa with *tert*-butyl pyridine, the open circuit voltage increase at the expense of the decrease short circuit

current density.[30] An optimised balance was achieved when both additives were used in combination. Additives can also improve injection in DSCs by blocking aggregation in the dye layer, which deactivates the sensitizer excited state through a self-quenching mechanism. Small molecules such as chenodeoxycholic acid are typically employed for this purpose, as is explained in section 1.3.

2.2. Light absorption and electron injection

When a photon is absorbed by the dye (S), the excited molecule (S*, reaction 1) injects an electron into the conduction band (CB) of the semiconductor on a picosecond timescale (reaction 2) before the sensitizer can relax back to its ground state (reaction 3).

$S + hv \rightarrow S^*$	Photoexcitation	(1)
$S^* \rightarrow S^+ + e^-_{(TiO_2)}$	Charge injection	(2)
$S^* \rightarrow S$	Dye relaxation	(3)

It is important to synthesize dyes with a LUMO component close to the semiconductor surface and an HOMO far from the TiO_2. That ensures that electron density in the excited state is concentrated close to the TiO_2, promoting injection and localizing the resultant positive charge away from the interface.

2.3. Electron transport, recombination and regeneration

Once the dye is oxidized (S^+), it is regenerated by iodide in the electrolyte in a few microseconds (reaction 4), which generally occurs faster than reduction by photoinjected electrons in the semiconductor (reaction 5).

$S^+ + 2I^- \rightarrow S + I_2^-$ and $2I_2^- \rightarrow I_3^- + I^-$	Dye regeneration	(4)
$S^+ + e^-_{(TiO_2)} \rightarrow S$	Recombination via dye	(5)

The tri-iodide formed upon the sensitizer regeneration is reduced at the counter electrode by the Pt (reaction 6). Electrons in the semiconductor are affected by two concomitant processes: in one hand, the recombination with tri-iodide in the electrolyte (reaction 7) and on the other hand diffusion through the mesoporous TiO_2 to the working electrode (Figure 1.8). Recombination

occurs in the millisecond to second range and diffusion ideally occurs on a timescale one or two orders of magnitude smaller such that a large fraction of electrons is separated at the working electrode.

$I_3^- + 2e^- \rightarrow 3I^-$	Electrolyte regeneration	(6)
$2e^-_{(TiO2)} + I_3^- \rightarrow 3I^-$	Recombination via electrolyte	(7)

In an ideal device, every absorbed photon is extracted as an electron but they are losses in solar cells and they can be due to dye relaxation, dye regeneration by the injected electron or recombination of electrons in the semiconductor with the electrolyte (reactions 3, 5 and 7). Electrons injected into the semiconductor have a finite time before recombining, the key is to extract these charges before they found other species to re-establish the electrochemical equilibrium (Figure 1.8). For the standard I^-/I_3^- redox mediator, recombination with I_3^- occurs in 1 ms - 1 s time scale. This surprisingly slow recombination is the principle reason for the high power conversion efficiencies achieved by DSCs.

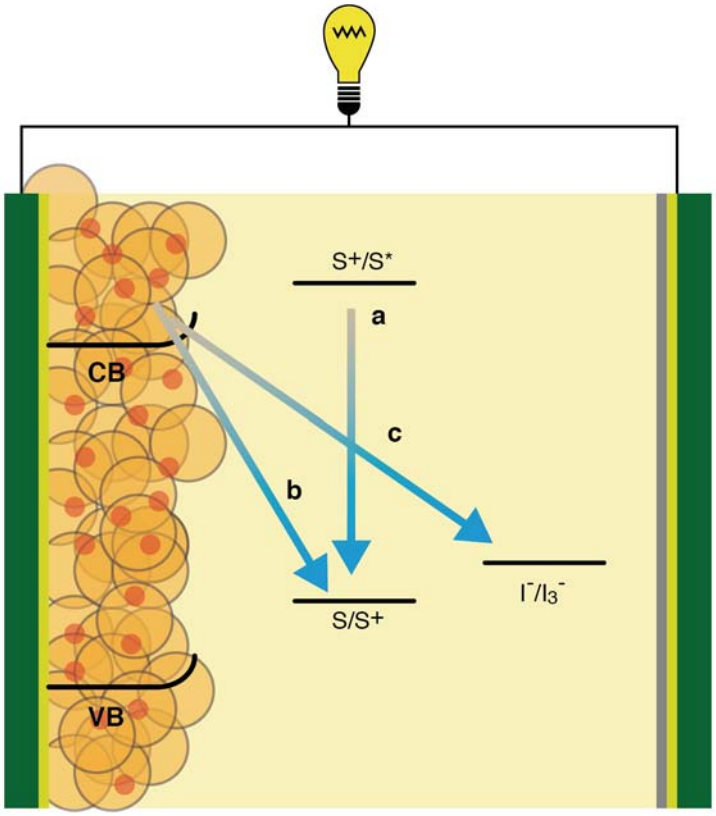

Figure 1.8. Scheme of the rival processes occurring in a DSCs. (a) Dye excited state deactivation, (b) recombination between the photoinjected electrons and the oxydized electrolyte and (c) recombination between the photoinjected electrons and the electrolyte.

References

1. O'Regan, B.; Grätzel, M., A low-cost, high-efficiency solar cell based on dye-sensitized colloidal TiO2 films. *Nature* **1991,** *353*, 737-740.
2. Ardo, S.; Meyer, G. J., Photodriven heterogeneous charge transfer with transition-metal compounds anchored to TiO2 semiconductor surfaces *Chem. Soc. Rev.* **2009,** *38*, 115-164.
3. Ito, S.; Liska, P.; Comte, P.; Charvet, R. L.; Pechy, P.; Bach, U.; Schmidt-Mende, L.; Zakeeruddin, S. M.; Kay, A.; Nazeeruddin, M. K.; Grätzel, M., Control of dark current in photoelectrochemical (TiO2/I−−I3−) and dye-sensitized solar cells. *Chem. Commun.* **2005**, 4351-4353.
4. Hagfeldt, A.; Boschloo, G.; Sun, L.; Kloo, L.; Pettersson, H., Dye-Sensitized Solar Cells. *Chem. Rev.* **2010,** *110*, 6595-6663.
5. Robertson, N., Optimizing dyes for dye-sensitized solar cells. *Angew. Chem., Int. Ed.* **2006,** *45*, 2338-2345.
6. Clifford, J. N.; Palomares, E.; Nazeeruddin, M. K.; Grätzel, M.; Nelson, J.; Li, X.; Long, N. J.; Durrant, J. R., Molecular control of recombination dynamics in dye-sensitized nanocrystalline TiO2 films: free energy vs distance dependence. *J. Am. Chem. Soc.* **2004** *126*, 5225-5233.
7. Altobello, S.; Argazzi, R.; Caramori, S.; Contado, C.; Da Fre, S.; Rubino, P.; Chone, C.; Larramona, G.; Bignozzi, C. A., Sensitization of Nanocrystalline TiO2 with Black Absorbers Based on Os and Ru Polypyridine Complexes. *J. Am. Chem. Soc.* **2005,** *127*, 15342-15343.
8. Hasselmann, G. M.; Meyer, G. J., Diffusion-Limited Interfacial Electron Transfer with Large Apparent Driving Forces. *J. Phys. Chem. B* **1999,** *103*, 7671-7675.
9. Ferrere, S., New photosensitizers based upon [FeII(L)2(CN)2] and [FeIIL3], where L is substituted 2,2′ -bipyridine. *Inorg. Chim. Acta* **2002,** *329*, 79-92.
10. Geary, E. A. M.; McCall, K. L.; Turner, A.; Murray, P. R.; McInness, E. J. L.; Jack, L. A.; Yellwleesa, L. J.; Robertson, N., Spectroscopic, electrochemical and computational study of Pt–diimine–dithiolene complexes: rationalising the properties of solar cell dyes. *Dalton Trans.* **2008**, 3701-3708.
11. Bessho, T.; Constable Edwin, C.; Grätzel, M.; Hernandez Redondo, A.; Housecroft Catherine, E.; Kylberg, W.; Nazeeruddin, M. K.; Neuburger, M.; Schaffner, S., An element of surprise—efficient copper-functionalized dye-sensitized solar cells. *Chem. Commun.* **2008**, 3717-3719.
12. (a) Nazeeruddin, M. K.; Zakeeruddin, S. M.; Humphrey-Baker, R.; Jirousek, M.; Liska, P.; Vlachopoulos, N.; Shklover, V.; Fischer, C.-H.; Grätzel, M., Acid–Base Equilibria of (2,2‘-Bipyridyl-4,4‘-dicarboxylic acid)ruthenium(II) Complexes and the Effect of Protonation on Charge-Transfer Sensitization of Nanocrystalline Titania. *Inorg. Chem.* **1999,** *38*, 6298-6305; (b) Gao, F.; Wang, Y.; Shi, D.; Zhang, J.; Wang, M.; Jing, X.; Humphry-Baker, R.; Wang, P.; Zakeeruddin, S. M.; Grätzel, M., Enhance the Optical Absorptivity of Nanocrystalline TiO2 Film with High Molar Extinction Coefficient Ruthenium Sensitizers for High Performance Dye-Sensitized Solar Cells. *J. Am. Chem. Soc.* **2008,** *130*, 10720-10728; (c) Chen, C.-Y.; Wang, M.; Li, J.-Y.; Pootrakulchote, N.; Alibabaei, L.; Ngoc-le, C.; Decoppet, J.-D.; Tsai, J.-H.;

Grätzel, C.; Wu, C. G.; Zakeeruddin, S. M.; Grätzel, M., Highly Efficient Light-Harvesting Ruthenium Sensitizer for Thin-Film Dye-Sensitized Solar Cells. *ACS Nano* **2009,** *3*, 3103-3109; (d) Nazeeruddin, M. K.; A., K.; Rodicio, I.; Humphry-Baker, R.; Mueller, E.; Liska, P.; Vlachopoulos, N.; Grätzel, M., Conversion of light to electricity by cis-X2bis(2,2'-bipyridyl-4,4'-dicarboxylate)ruthenium(II) charge-transfer sensitizers (X = Cl-, Br-, I-, CN-, and SCN-) on nanocrystalline titanium dioxide electrodes. *J. Am. Chem. Soc.* **1993,** *115*, 6382-6390; (e) Nazeeruddin, M. K.; Zakeeruddin, S. M.; Lagref, J. J.; Liska, P.; Comte, P.; Barolo, C.; Viscardi, G.; Shenk, K.; Grätzel, C., Stepwise assembly of amphiphilic ruthenium sensitizers and their applications in dye-sensitized solar cell. *Coord. Chem. Rev.* **2004,** *248*, 1317-1328; (f) Nazeeruddin, M. K.; Pechy, P.; Renouard, T.; Zakeeruddin, S. M.; Humphrey-Baker, R.; Comte, P.; Liska, P.; Cevey, L.; Costa, E.; Shklover, V.; Spiccia, L.; Deacon, G. B.; Bignozzi, C. A.; Grätzel, C., Engineering of Efficient Panchromatic Sensitizers for Nanocrystalline TiO2-Based Solar Cells. *J. Am. Chem. Soc.* **2001,** *123*, 1613-1624.

13. Gouterman, M., In *Porphyrins*, ed. Dolphin, D., Ed. New York, 1978; Vol. 3, pp 1-166.

14. (a) Yella, A.; Lee, H. W.; Tsao, H. N.; Yi, C. Y.; Chandiran, A. K.; Nazeeruddin, M. K.; Diau, E. W.-G.; Yeh, C.-Y.; Zakeeruddin, S. M.; Grätzel, M., Porphyrin-Sensitized Solar Cells with Cobalt (II/III)–Based Redox Electrolyte Exceed 12 Percent Efficiency. *Science* **2011,** *334*, 629-634; (b) Chang, Y.-C.; Wang, C.-L.; Pan, T.-Y.; Hong, S.-H.; Lan, C.-M.; Kuo, H.-H.; Lo, C.-F.; Hsu, H.-Y.; Lin, C.-Y.; Diau, W.-G., A strategy to design highly efficient porphyrin sensitizers for dye-sensitized solar cells. *Chem. Commun.* **2011,** *47*, 8910-8912.

15. (a) Mori, S.; Nagata, M.; Nakahata, Y.; Yasuta, K.; Goto, R.; Kimura, M.; Taya, M., Enhancement of Incident Photon-to-Current Conversion Efficiency for Phthalocyanine-Sensitized Solar Cells by 3D Molecular Structuralization. *J. Am. Chem. Soc.* **2010,** *132*, 4054-4055; (b) Ragoussi, M. E.; Cid, J. J.; Yum, J. H.; de la Torre, G.; Di Censo, D.; Grätzel, M.; Nazeeruddin, M. K.; Torres, T., Carboxyethynyl Anchoring Ligands: A Means to Improving the Efficiency of Phthalocyanine-Sensitized Solar Cells. *Angew. Chem., Int. Ed.* **2012,** *51*, 4375-4378; (c) Kimura, M.; Nomoto, H.; Masaki, N.; Mori, S., Dye Molecules for Simple Co-Sensitization Process: Fabrication of Mixed-Dye-Sensitized Solar Cells. *Angew. Chem. Int. Ed.* **2012,** *51*, 4371-4374.

16. (a) Zeng, W.; Cao, Y.; Bai, Y.; Wang, Y.; Shi, Y.; Zhang, M.; Wang, F.; Pan, C.; Wang, P., Efficient Dye-Sensitized Solar Cells with an Organic Photosensitizer Featuring Orderly Conjugated Ethylenedioxythiophene and Dithienosilole Blocks. *Chem. Mater.* **2010,** *22*, 1915-1925; (b) Yum, J.-H.; Holcombe, T. W.; Kim, Y.; Rakstys, K.; Moehl, T.; Teuscher, J.; Delcamp, J. H.; Nazeeruddin, M. K.; Grätzel, M., Blue-Coloured Highly Efficient Dye-Sensitized Solar Cells by Implementing the Diketopyrrolopyrrole Chromophore. *Scientific Reports* **2013,** *3*, 2446; (c) Ito, S.; Miura, H.; Uchida, S.; Takata, M.; Sumioka, K.; Liska, P.; Comte, P.; Pechy, P.; Grätzel, C., High-conversion-efficiency organic dye-sensitized solar cells with a novel indoline dye. *Chem. Commun.* **2008**, 5194-5196.

17. Ehret, A.; Stuhl, L.; Spitler, M. T., Spectral Sensitization of TiO2 Nanocrystalline Electrodes with Aggregated Cyanine Dyes. *J. Phys. Chem. B* **2001,** *105*, 9960-9965.
18. Ogura, R. Y.; Nakane, S.; Morooka, M.; Orihashi, M.; Suzuki, Y.; Noda, K., High-performance dye-sensitized solar cell with a multiple dye system. *Appl. Phys. Lett.* **2009,** *94*, 73308.
19. Clifford, J. N.; Palomares, E.; Nazeeruddin, M. K.; Thampi, R.; Grätzel, M.; Durrant, J. R., Multistep Electron Transfer Processes on Dye Co-sensitized Nanocrystalline TiO2 Films. *J. Am. Chem. Soc.* **2004,** *126*, 5670-5671.
20. Kang, M.-S.; Kim, J. H.; Won, J.; Park, N.-G.; Kang, y. S., Dye-sensitized solar cells based on composite solid polymer electrolytes. *Chem. Commun.* **2005**, 889-891.
21. Wang, P.; Zakeeruddin, S. M.; Moser, J. E.; Nazeeruddin, M. K.; Sekiguchi, T.; Grätzel, M., A stable quasi-solid-state dye-sensitized solar cell with an amphiphilic ruthenium sensitizer and polymer gel electrolyte. *Nat. Mater.* **2003,** *2*, 402-407.
22. Wang, P.; Zakeeruddin, S. M.; Moser, J. E.; Humphrey-Baker, R.; Grätzel, M., A Solvent-Free, SeCN-/(SeCN)3- Based Ionic Liquid Electrolyte for High-Efficiency Dye-Sensitized Nanocrystalline Solar Cells. *J. Am. Chem. Soc.* **2004,** *126*, 7164-7165.
23. Wang, P.; Dai, Q.; Zakeeruddin, S. M.; Forsyth, M.; MacFarlane, D. R.; Grätzel, M., Ambient Temperature Plastic Crystal Electrolyte for Efficient, All-Solid-State Dye-Sensitized Solar Cell. *J. Am. Chem. Soc.* **2004,** *126*, 13590-13591.
24. Meng, Q.-B.; Takahashi, K.; Zhang, X.-T.; Sutanto, I.; Rao, T. N.; Sato, O.; Fujishima, A., Fabrication of an Efficient Solid-State Dye-Sensitized Solar Cell. *Langmuir* **2003,** *19*, 3572-3574.
25. Nusbaumer, H.; Zakeeruddin, S. M.; Moser, J. E.; Grätzel, M., An Alternative Efficient Redox Couple for the Dye-Sensitized Solar Cell System. *Chem. Eur. J.* **2003,** *9*, 3756-3763.
26. Sato, Y.; Azechi, T.; Kitamura, T.; Hasegawa, Y.; Wada, Y.; Yanagida, S., Photo-sensitizing ruthenium complexes for solid state dye solar cells in combination with conducting polymers as hole conductors. *Coord. Chem. Rev.* **2004,** *248*, 1469-1478.
27. Krüger, J.; Plass, R.; Cevey, L.; Piccirelli, M.; Grätzel, M.; Bach, U., High efficiency solid-state photovoltaic device due to inhibition of interface charge recombination. *Appl. Phys. Lett.* **2001,** *79*, 2085.
28. Papageorgiou, N.; Athanassov, Y.; Armand, M.; Bonhote, P.; Pettersson, H.; Azam, A.; Grätzel, M., The Performance and Stability of Ambient Temperature Molten Salts for Solar Cell Applications. *J. Electrochem. Soc.* **1996,** *143*, 3099-3108.
29. Welton, T., Room-Temperature Ionic Liquids. Solvents for Synthesis and Catalysis. *Chem. Rev.* **1999,** *99*, 2071-2084.
30. Haque, S. A.; Palomares, E.; Cho, B. M.; Green, A. N. M.; Hirata, N.; Klug, D. R.; Durrant, J. R., Charge Separation versus Recombination in Dye-Sensitized Nanocrystalline Solar Cells: the Minimization of Kinetic Redundancy. *J. Am. Chem. Soc.* **2005,** *127*, 3456-3462.

Chapter 2.
Experimental methods

Chapter 2. Experimental methods

Index

Chapter 2. Experimental methods

1. Device preparation

1.1. TiO_2 layer preparation

Prior to the deposition of the TiO_2 nanoparticle layer, the fluorine doped tin oxide (FTO) conducting glass substrates (Hartford Glass Inc. with 15 Ω cm^{-2} resistance) were cleaned and treated. The cleaning process consists in different bath sonication of the glass slides: 15 minutes in detergent solution, 15 minutes in water and finally 15 minutes in ethanol. Then the slides were heated at 500ºC and cooled to room temperature. The last step for the cleaning process is an ozone treatment in a UV-O_3 cleaning system (UVOCS Inc. $T_{10}X_{10}$/OES/E) for 20 minutes. Then, the substrates were immersed immediately into a 40 mM $TiCl_4$ solution for 30 minutes at 70ºC and then washed with water and ethanol. The introduction of a dense TiO_2 layer with $TiCl_4$ by thermal treatment of FTO (thickness 100-200 nm) avoids the electrolyte from reaching the back contact of the conductive glass surface and so reduces electron recombination. In this thesis, TiO_2 pastes were purchased from Dyesol and Solaronix. Two different nanoparticle sizes were used: 20 nm (Dyesol 18NR-T or Solaronix T/SP) and 400 nm (Dyesol 18NR-AO or Solaronix R/SP). The TiO_2 nanoparticles were deposited onto the conductive side of the substrates using the screen printing technique (Figure 2.1). Several layers were deposited in order to obtain the desired thickness, which was measured with a profilometer. The TiO_2 electrodes were gradually heated under airflow at 325ºC for 5 minutes, 375ºC for 5 minutes, 450ºC for 15 minutes and 500ºC for 15 minutes. After this process, the substrates were immersed again into a 40 mM $TiCl_4$ solution for 30 minutes at 70ºC and then washed with water and ethanol. Finally, films were heated at 500ºC for 30 minutes and cooled to room temperature before dye absorption.

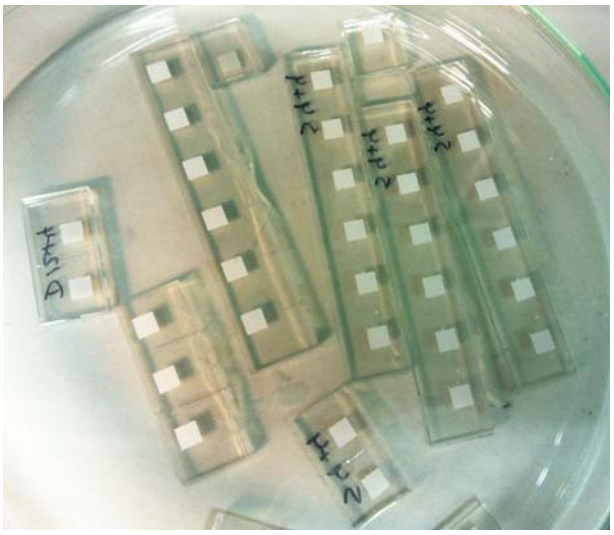

Figure 2.1. Digital photo of the deposited TiO_2 nanoparticles as thin films.

1.2. Dye sensitization

The TiO_2 films were immersed into different dye solutions and left for a specific period of time under dark conditions at a certain temperature (Figure 2.2). Every dye has its optimized conditions in order to obtain the maximum efficiency.

Dye solutions were prepared dissolving the dye in one solvent (such as ethanol, acetonitrile or chlorobenzene) or in a mixture of two solvents (acetonitrile:*tert*-butanol or chloroform:ethanol). In some studies, the addition of chenodeoxydecholic acid as a coadsorbent is needed in order to avoid dye aggregation.

After dye sensitization, films were washed with the same solvent used in the dye solution and dried under air.

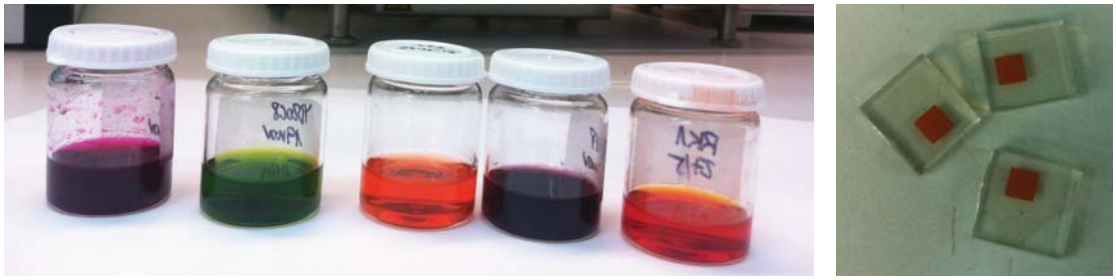

Figure 2.2. Digital photos of several dye solutions (left) and some sensitized films (right).

1.3. Counter electrode preparation

First, a small hole was made in the fluorine doped tin oxide (FTO) conducting glass substrates (Hartford Glass inc. with 15 Ω cm^{-2} resistance) with a drill to allow the introduction of the liquid electrolyte using vacuum. Then, the substrates were cleaned as in the working electrodes. The cleaning process consists in different bath sonication of the glass slides: 15 minutes in detergent solution, 15 minutes in water and finally 15 minutes in ethanol. Then the slides were heated at 500ºC and cooled to room temperature. Several drops of a 5 mM H_2PtCl_6 anhydrous solution in isopropyl alcohol were spread onto the substrate followed by heating at 390ºC for 15 minutes (Figure 2.3).

Figure 2.3. Digital photo of the counter electrodes.

1.4. Electrolyte preparation

The composition of the electrolyte solution differs depending on the dyes used and the study performed. Basically, the electrolyte was based of a redox couple with the presence of different additives (Figure 2.4). In this thesis, 6 type of electrolytes were prepared:

- 0.6 M 1-butyl-3-methylimidazolium iodide (BMII), 0.1 M lithium iodide, 0.05 M iodine and 0.5 M 4-*tert*-butylpyridine in a 1:1 mixture of acetonitrile:valeronitrile.
- 0.5 M 1-butyl-3-methylimidazolium iodide (BMII), 0.1 M lithium iodide, 0.05 M iodine and 0.5 M 4-*tert*-butylpyridine in a 85:15 mixture of acetonitrile:valeronitrile.
- 0.5 M 1-butyl-3-methylimidazolium iodide (BMII), 0.1 M lithium iodide, 0.05 M iodine and 0.5 M 4-*tert*-butylpyridine in acetonitrile (**LP1**).
- 1 M 1-butyl-3-methylimidazolium iodide (BMII), 0.05 M lithium iodide, 0.03 M iodine, 0.1 M guanidinium thiocyanate and 0.5 M 4-*tert*-butylpyridine in a 85:15 mixture of acetonitrile:valeronitrile (**Z960**).
- 0.2 M tris(1,10-phenantroline)cobalt(II)$(TFSI)_2$, 0.02 M tris(1,10-phenantroline)cobalt(III)$(TFSI)_3$, 0.1 M lithium perchlorate and 0.5 M 4-*tert*-butylpyridine in a 85:15 mixture of acetonitrile:valeronitrile.
- 0.6 M 1-butyl-3-methylimidazolium iodide (BMII), 0.1 M lithium iodide and 0.05 M iodine in a 1:1 mixture of acetonitrile:valeronitrile (**LP2**).

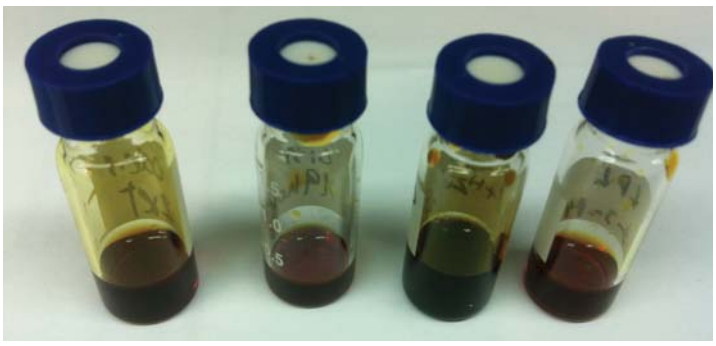

Figure 2.4. Digital photo of different electrolytes.

1.5. Device assembly

Once the electrodes were prepared, they were sandwiched together using a thin thermoplastic film. In this thesis, Surlyn film was used. Surlyn is a polymer that melts at 100ºC, so the two electrode were sealed by applying pressure and temperature (170ºC) for 15 seconds. Then the electrolyte was introduced into the device with a syringe and applying vacuum through the hole previously made at the counter electrode. The hole was sealed by melting a small piece of Surlyn and a cover slide. Finally, a blend of different metals was applied to the cell contacts in order to reduce the resistance (Figure 2.5).

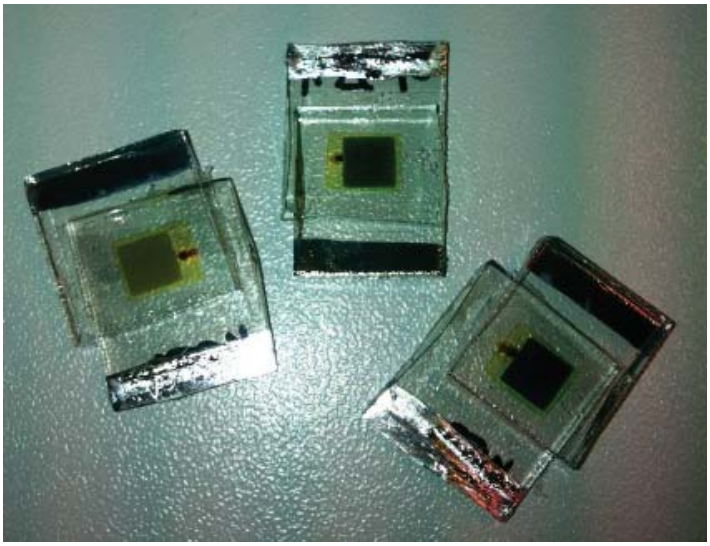

Figure 2.5. Digital photo of final devices.

2. Device characterization

2.1. Power conversion efficiency

DSCs are measured in a solar simulator under AM 1.5G, an universal parameter. When skies are clear, the maximum radiation strikes the earth's surface when the sun is directly overhead, having the shortest path length through the atmosphere. The path length is called the *air mass* (AM) and can be approximated by AM = 1/cosϕ, where ϕ is the angle of elevation of the sun. The standard solar spectrum used for efficiency measurements of solar cells is AM 1.5 G (global), giving that ϕ = 42°. This spectrum is normalized so

that the integrated irradiance (the amount of radiant energy received from the sun per unit area per unit time) is 1000 W m^{-2}.[1]

The current to voltage (I-V) curves were carried out with a 150 W solar simulator from ABET© technologies with the appropriate set of filters for the correct simulation of the AM 1.5G solar spectrum (Figure 2.6). The incident light power was measured at 100 mW cm^{-2} with a calibrated silicon photodiode. The applied potential and cell current were measured with a Keithley model 2400 digital source meter. The I-V curves were measured automatically with a home-built Labview© software. This technique consists of the measurements of the photocurrent generated by a photovoltaic device under light irradiation when a gradually increasing photovoltage is applied to the solar cell.

Figure 2.6. Digital photo of the solar simulator equipment.

The maximum current flow is obtained when the cell operates at short circuit mode, which means the external circuit is closed and the voltage is zero. The solar circuit photocurrent density (J_{sc}, mA cm^{-2}) is obtained as the short circuit photocurrent (I_{sc}, mA) divided by the area of the cell (cm^2) as is depicted in Equation 1. The short circuit photocurrent (I_{sc}) is directly proportional with light intensity and the area of the solar cell.

$$Jsc = \frac{Isc}{Area\ cell} \qquad \text{Equation 1}$$

Photovoltage is the electrical force generated upon light radiation that can drive electrical current from the working electrode to the counter electrode of the device. Under open circuit conditions, the maximum photovoltage (V_{oc}) is obtained when the I_{sc} is zero.

Power is the product of photovoltage multiplied by photocurrent. The maximum power (P_{max}) represents the maximum efficiency of the device in converting sunlight into current flow (Figure 2.7).

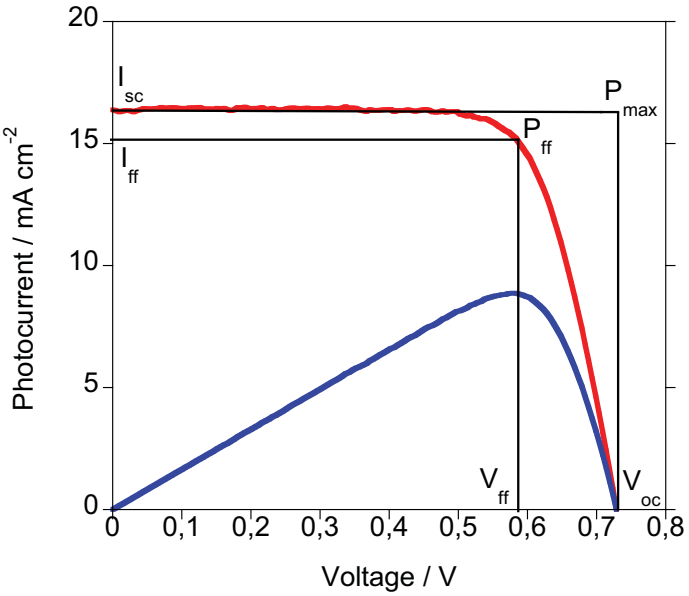

Figure 2.7. Example of current-voltage (I-V) and power-voltage (P-V) curves.

The fill factor (*FF*) represents the "squareness" of the I-V curve and is obtained from the voltage and the current at the maximum power point (Equation 2).

$$FF = \frac{J_{ff} \cdot V_{ff}}{J_{sc} \cdot V_{oc}} \qquad \text{Equation 2}$$

Finally, the power conversion efficiency of a solar cell is determined by the photocurrent density at short circuit, the photovoltage at open circuit, the fill factor and the power of the incident lamp as shown in Equation 3.

$$\eta = \frac{J_{sc} \cdot V_{oc} \cdot FF}{P_{light}} \qquad \text{Equation 3}$$

An example of I-V curve is shown in Figure 2.8.

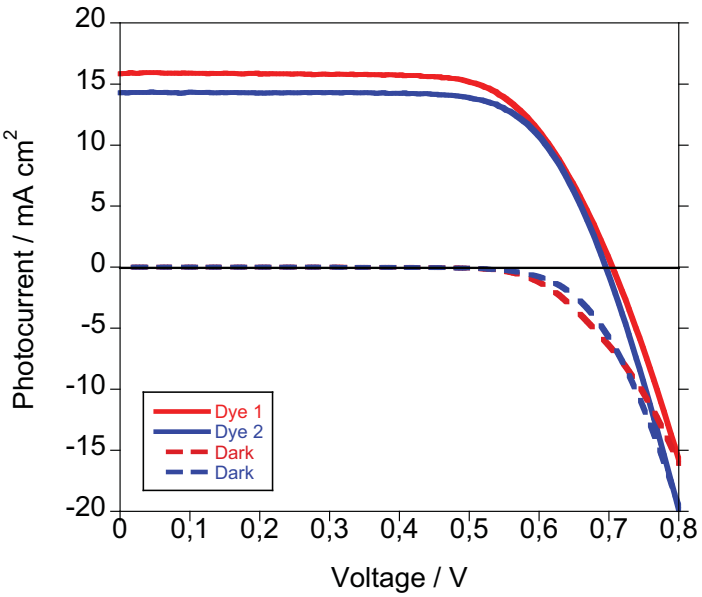

Figure 2.8. Example of I-V curves for two different dyes under illumination (solid lines) and their corresponding I-V curve under dark conditions (dashed lines).

2.2. Incident photon-to-current conversion efficiency (IPCE)

Incident photon-to-current conversion efficiency (IPCE) is defined by the number of electrons generated in the solar device as function of the ratio of the number of incident photons for a given wavelength, hence, is an spectral response.

The IPCE measurements were carried out with a home built system set up, consisting of a 150 W Oriel Xenon lamp as light source, a motorized monochromator which changes the measured wavelength and a Keithley 2400 digital source meter for acquiring the photocurrent generated. An integrating sphere was employed in order to provide homogeneous monochromatic light distribution (Figure 2.9).

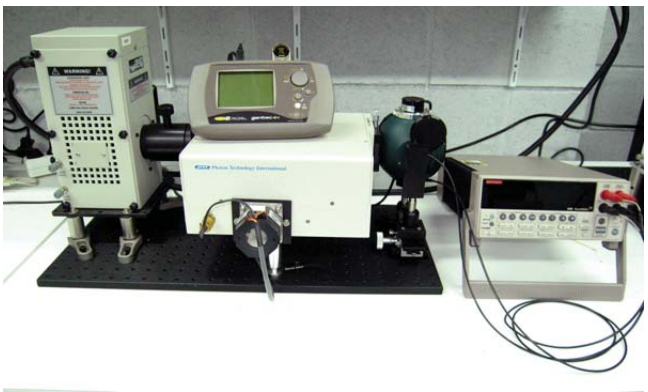

Figure 2.9. Digital photo of the IPCE equipment.

IPCE is determinated by Equation 4, where J_{sc} is photocurrent density at short circuit (mA cm^{-2}), λ is the incident light wavelength (nm), P_{lamp} is the power of the incident light (W m^{-2}) and 1240 is the conversion factor of the energy of photons.

$$IPCE\ (\lambda) = \frac{1240 \cdot J_{sc}\ (\lambda)}{\lambda \cdot P_{light}(\lambda)} \qquad \text{Equation 4}$$

Usually, the IPCE spectrum matches with the absorptance spectrum of the dye. An example of IPCE curve is shown in Figure 2.10.

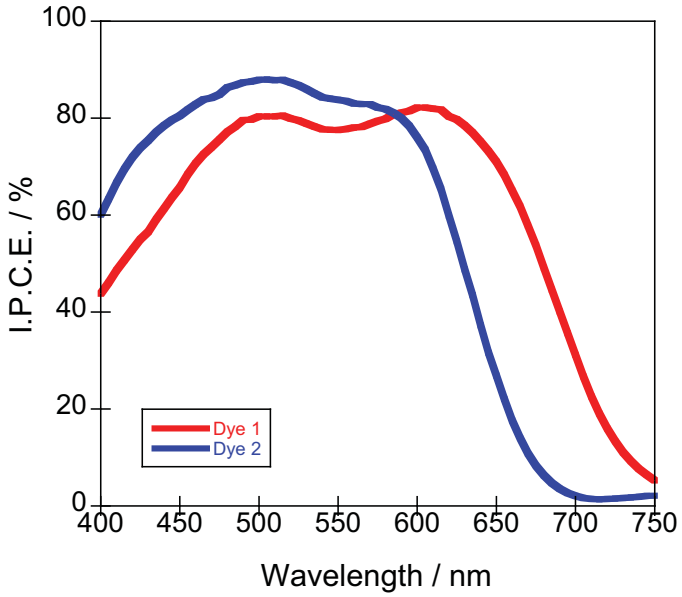

Figure 2.10. Example of IPCE curve for two different dyes.

2.3. Charge extraction measurements

The Charge Extraction (CE) technique provides information about the electron transport, trapping and recombination reactions in DSCs under operating conditions.

The CE measurements were carried out on a system similar to that employed by O'Regan et al. (Figure 2.11)[2] In CE measurements pulses of white light from a series of LEDs are applied to the cell that is allowed to reach a steady state for several seconds under open circuit conditions. When the LEDs are turned off the cell is immediately short-circuited and the charge is extracted allowing electron density in the cells to be calculated. By changing the LED intensity the electron density can be estimated as a function of cell voltage. So the accumulated charges in the TiO_2 film under cell

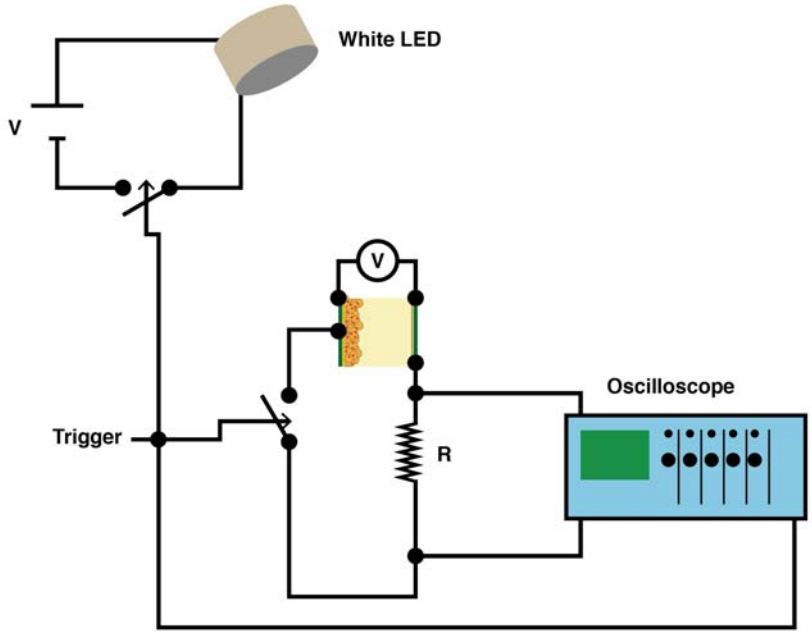

Figure 2.11. Schematic representation of the charge extraction system.

operation conditions are obtained and this value determines de conduction band edge shift of the semiconductor (Figure 2.12).

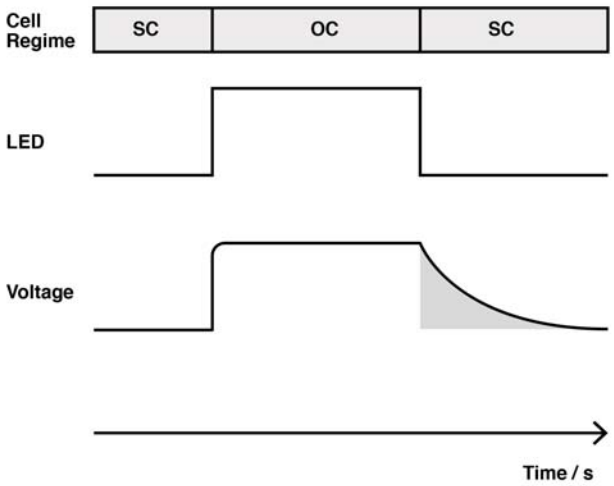

Figure 2.12 Short circuit (SC) and open circuit (OC) sequences showing the relationship between the illumination by white LEDs and the voltage measured in the charge extraction technique. The integrated area (grey) is proportional to the accumulated charge (Equation 5).

The accumulated charge *Q* (C) is defined as:

$$Q = \frac{1}{R}\int_{t=0}^{t=t} V(t)dt \qquad \text{Equation 5}$$

where *R* (Ω) is the resistance and *V*(t) (V) is the voltage measured at each time. The accumulated charge depends on the amount of TiO_2

nanoparticles, thus to obtain the charge accumulated in the films, electron density (e^- cm^{-3}) is needed and it is defined as:

$$e^-_{density} = \mathrm{Q}\frac{1}{C_e}\frac{1000}{d \cdot A \cdot (1-p)} \qquad \text{Equation 6}$$

where C_e (C) is the electronic charge, d (μm) is the thickness and A (cm^2) is the area of the film and p is the porosity of TiO_2.

The graphical representation between the electron density and the voltage applied to the call gives the onset of the conduction band of the semiconductor and is usually represented in a linear-linear plot. The data can be fitted to a single exponential function as shown in Equation 7:

$$e^-_{density}(\mathrm{V}) = A_0 + A_1 e^{V/m_c} \qquad \text{Equation 7}$$

where A_0 and A_1 are constants and m_c (V) is the characteristic energy which describes the curvature distribution.[2b] An example of charge extraction data is shown in Figure 2.13.

Differences in V_{oc} can generally be explained by either shifts in the TiO_2 conduction band edge (manifested by the shift of the exponential distribution of experimental data measured by CE) and/or by TiO_2 electron recombination lifetimes (investigated via TPV measurements).

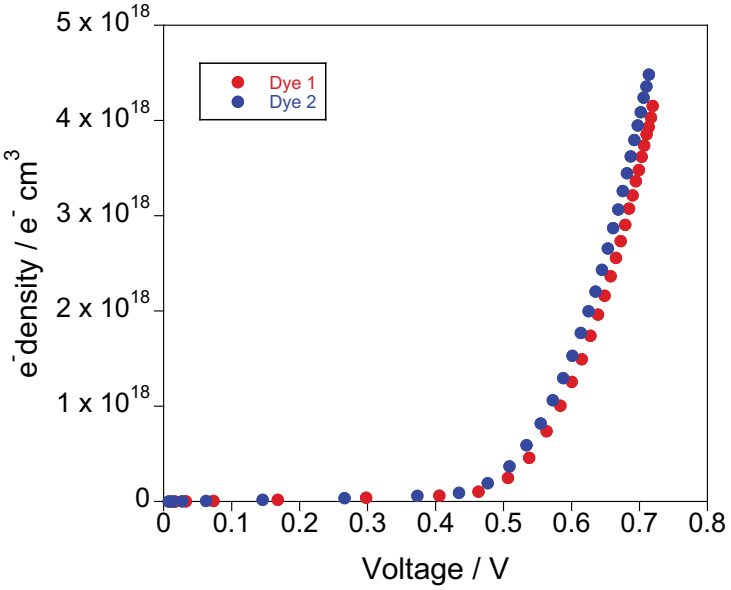

Figure 2.13. Example of charge extraction data where electron density is plotted vs. voltage induced by the light applied.

2.4. Transient photovoltage measurements

Transient photovoltage (TPV) measurements were carried out also on a system similar to that employed by O'Regan et al. (Figure 2.14)[2] This technique provides information about the electron recombination between the photoinjected electrons in the semiconductor conduction band and the redox couple present in the electrolyte under operating conditions.

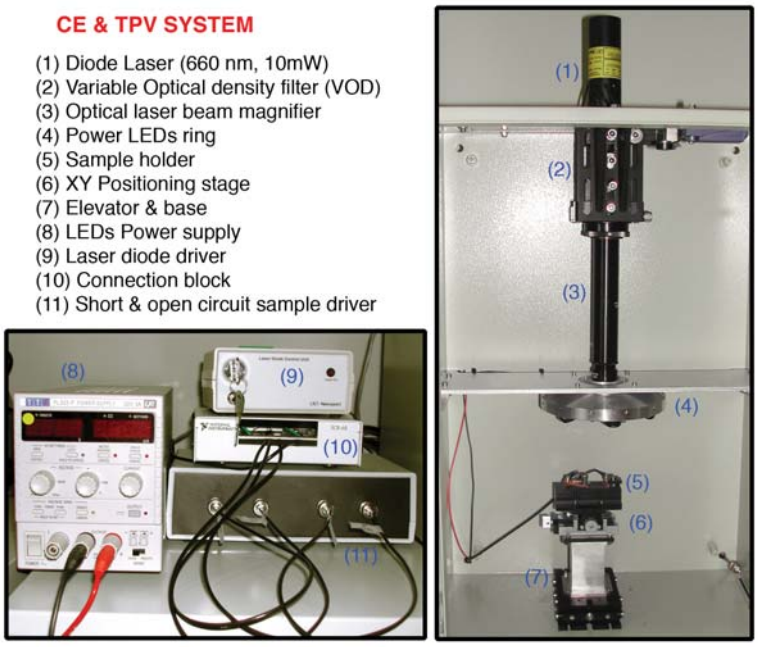

Figure 2.14. Digital photo and scheme of the charge extraction and transient photovoltage equipment.

In TPV measurements a constant background voltage is applied to the cells and again an equilibrium is reached in the cell. However a diode pulse (660 nm, 10 mW) is then applied to the sample inducing a change of approx. 2 mV in the cell. These small perturbations induce extra injected electrons in the conduction band of the TiO_2 and these electrons finally recombine with the oxidized electrolyte due to the open circuit conditions. By modifying the voltage (by modifying the illumination) the small voltage perturbations allow to monitor the recombination of injected electrons with oxidized electrolyte over several voltages (Figure 2.15).

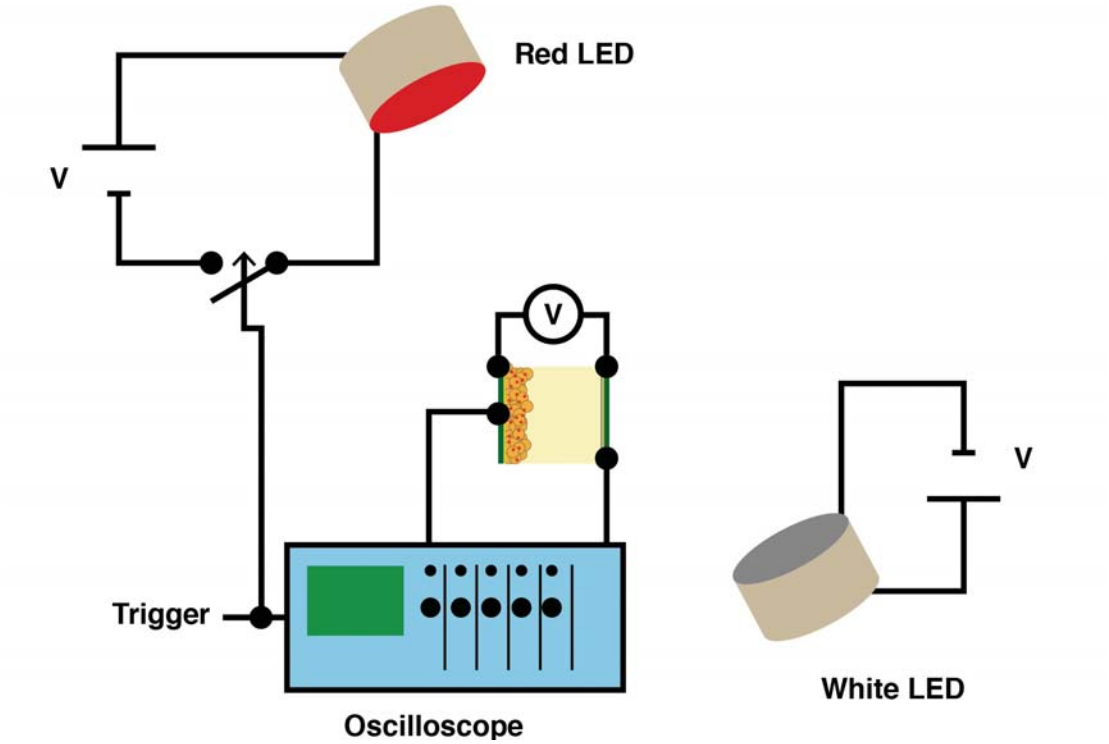

Figure 2.15. Schematic representation of the transient photovoltage system.

The resulting photovoltage decay transients are collected and the τ values are determined by fitting the data to the Equation 8. A programmable USB power supply changed the light bias from the LEDs, and a PCI-6251 card (National Instruments) was used for signal control and acquisition.

$$V\ (t) = V_0 + V_1 \cdot e^{-1/\tau} \qquad \text{Equation 8}$$

where V_o (V) is the voltage at open circuit, V_1 (V) is the voltage amplitude generated by the pulse and τ (s) is the recombination lifetime.

The best useful way to compare electron recombination in different samples is to compare kinetics at similar electron densities. These electron densities are extracted from the charge extraction method explained in the previous section.

The graphical representation between the recombination lifetime and the electron density is usually represented in a logarithmic plot. The data can be fitted to a power law function as shown in Equation 9:

$$\tau = 10^A \cdot (e^-_{density})^k \qquad \text{Equation 9}$$

where A and K are constants. An example of transient photovoltage data is shown in Figure 2.16.

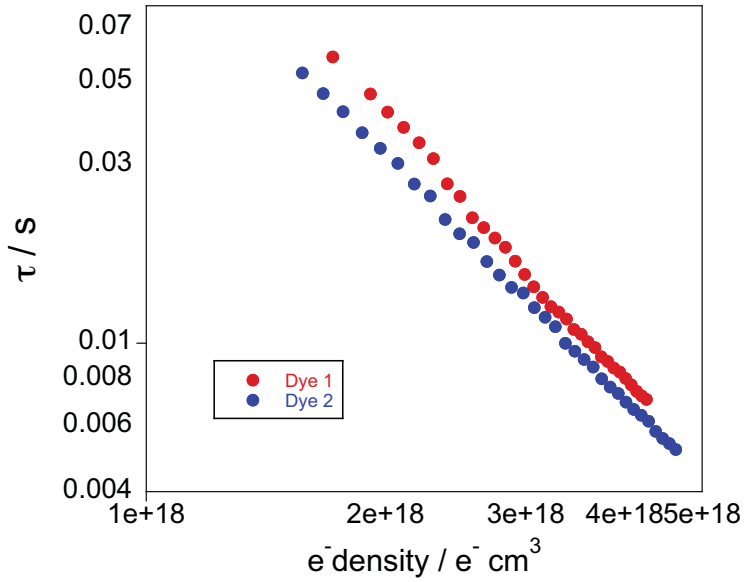

Figure 2.16. Example of transient photovoltage data.

In order to calculate this recombination, other techniques can be used as impedance spectroscopy.[3] However, the improvement of TPV is that it is a much simpler technique in which the cell is measured under illumination close to cell operating conditions.

2.5. Time correlated single-photon counting measurements

Time correlated single-photon counting (TC-SPC) evaluates the electron injection through the luminescence decays of radiative materials. Basically, single photons are detected as a function of time. The lifetime of the excited state is the average time that the dye takes to come back to the ground state from its excited state.

These experiments were carried out with a Lifespec-red picosecond to microsecond fluorescence lifetime spectrometer from Edinburgh Instruments. As excitation sources, different diode lasers with its respective nominal wavelengths were used and the instrument response measured at the full-width at half-maximum (FWHM) was below 350 ps (Figure 2.17).

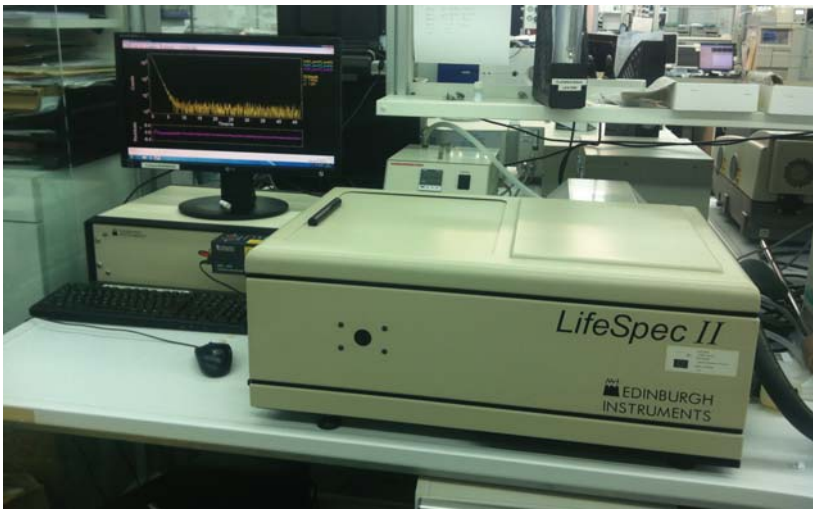

Figure 2.17. Digital photo of the TC-SPC equipment.

The estimation of the electron yield is measured comparing the lifetime decay results between a complete device and a device with Al_2O_3 instead TiO_2. Electron injection could not be possible with the dye anchored to Al_2O_3 because the conduction band of this semiconductor is higher that the excited state of the dye, so Al_2O_3 acts as an insulator.

The TC-SPC decay can be fitted to an exponential decay:

$$I(t) = A_o + \sum_{i=1}^{i=n} A_i e^{-t/\tau_i} \qquad \text{Equation 10}$$

where *I(t)* is the time dependent luminescence intensity, A_n values are pre-exponential factors, *t* is the time and τ is the lifetime.

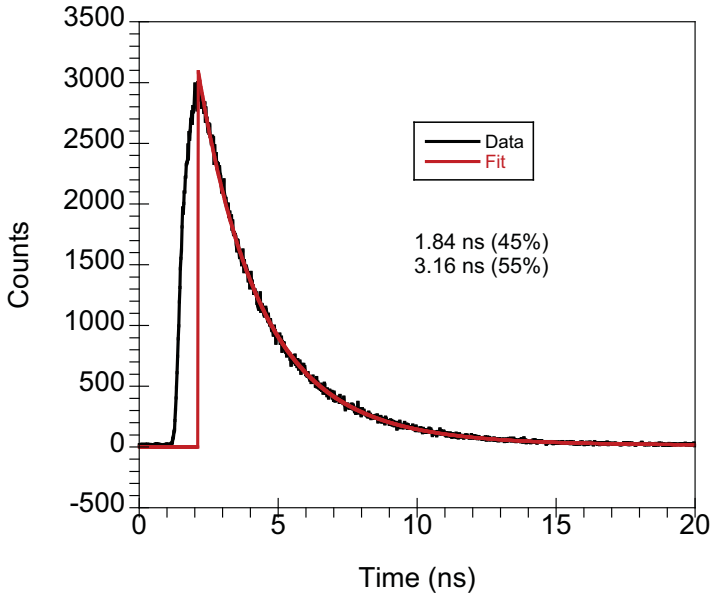

Figure 2.18. Example of TC-SPC data.

However, several times this technique can only be used as an estimation of electron injection yield because injection is too fast to be monitored.[4] An example of TC-SPC is shown in Figure 2.18.

2.6. Laser-transient absorbance spectroscopy

Transient absorption spectroscopy (TAS) measures the electron injection constant by monitoring the formation of the dye cation species (D^+) which appears after electron injection. TAS can determine both the undesired charge recombination of these electrons in the semiconductor with the oxidized dye and the regeneration of the dye cation by the redox electrolyte.[5]

Nanosecond to microsecond TAS measurements were carried out with a home-built system as reported elsewhere.[6] The technique comprises the irradiation of a sample with a short intense pulse of light, called the excitation pulse, and measuring the resulting change in the samples optical density. The optical density is determined by monitoring the transmission of a second and less intense beam of light that passes through the sample, called probe. In addition, probe wavelength can be changed over a broad range (from 400 to 1000 nm) by the use of monochromators giving the absorption spectrum of the transient at a certain time delay.

Figure 2.19. Digital photo of the L-TAS equipment.

The excitation source used was a PTI GL-3300 Nitrogen Laser, which produced pulses at 337 nm with an energy of 1.45 mJ. The pulse was

provided by a TG330 function generator from Thurlby Thandar Instruments© at 1 Hz repetition rate. A PTI GL-301 dye laser head was used in combination with the nitrogen laser to provide a variable source of excitation wavelength, from 360 to 750 nm, as shown in Figure 2.20.

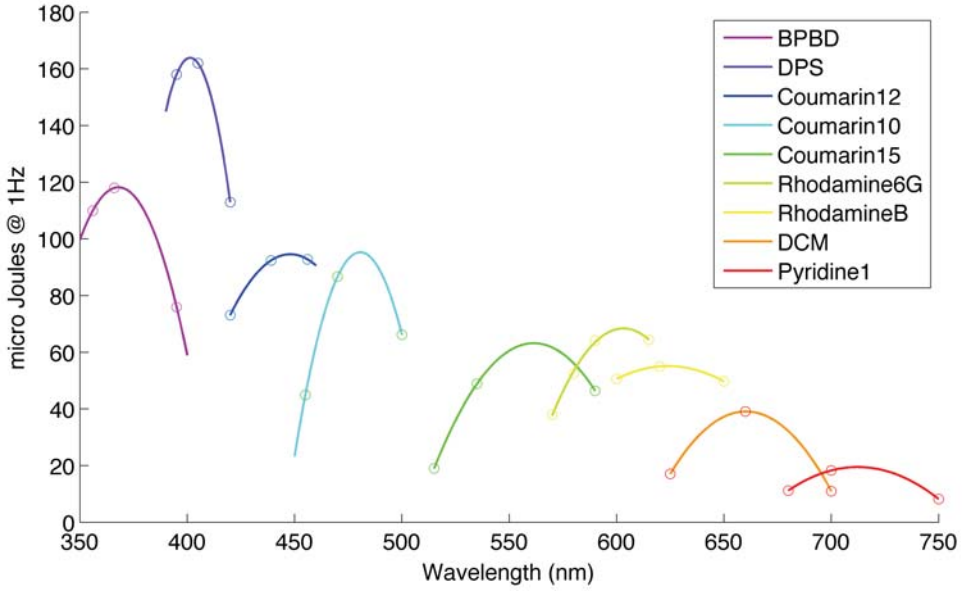

Figure 2.20. Emission spectra of the laser dyes used in the TAS system.

A PTI 150 W tungsten lamp was used as the probe light source. The monitoring wavelength from the lamp was selected by using monochromator 1 (M1). A second monochromator (M2) was used after the sample to reduce the noise from laser light scattering. The optical detector is based on a silicon photodiode, which converts the optical signal into an electrical signal. That signal was amplified and filtered by an electronic system provided by Costronics©. At the end, a TDS 2022 oscilloscope provided by Tektronix© carried out the signal acquisition (Figure 2.21). The data collected was treated using TakeWave software, converting the electrical signal to units of optical density (Δ*O.D.*) as shown in the Equation 11:

$$\Delta O.D.(t) = -\log\left[\frac{I_{probe}}{I_{ref}}\right] \approx \frac{1}{\ln(10)}\frac{I_{probe}-I_{ref}}{I_{ref}} \approx \alpha \cdot \left[\frac{\Delta V(t)}{V_0}\right] \quad \text{Equation 11}$$

where ΔV(t) is the transient signal size which is proportional to the light intensity, V_0 is the DC voltage level, which is proportional to the intensity if the probe and α is the amplification factor constant, which was set to 0.00174 and depends on the equipment used.

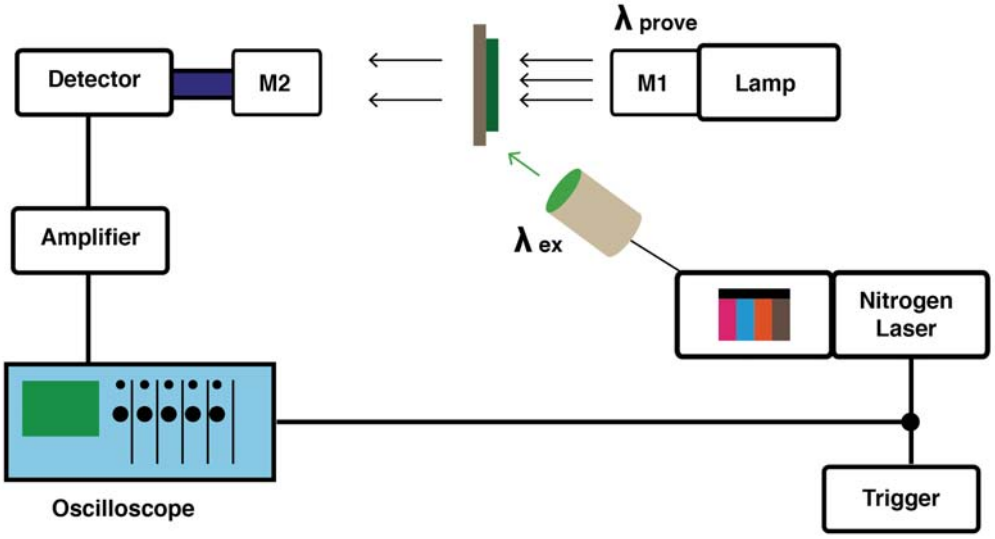

Figure 2.21. Schematic representation of the transient absorption spectroscopy system.

Two different experiments were performed. The first one involved the measurement of the recombination dynamics between the photoinjected electrons in the conduction band of the dye and the oxidized molecule on the semiconductor surface. Following the measurement of the transient absorption spectrum of the sensitized semiconductor film (by measuring signal sizes of the sample at a certain time at approximately 20 nm intervals over the absorption range 400-1000 nm) the change in the optical density of the dye cation at its maximum absorption wavelength was recorded as a function of time. The second experiment involved the measurement of complete devices, which gives an idea of both the regeneration of the dye cation by the electrolyte and also the recombination kinetics between the photoinjected electrons in the conduction band of the TiO_2 and the oxidized form of the redox couple present in the electrolyte. This measurement was performed by monitoring the change in optical density as a function of time at a probe wavelength fixed at 1000 nm using the monochromators.

Transient decays can be fitted to an stretched exponential function:

$$\Delta O.D. = A_o + A_1 \cdot e^{-(t/\tau)^{\alpha}} \qquad \text{Equation 12}$$

where A_n values are pre-exponential factors, t is the time, τ is the lifetime and α is a value between 0 and 1 called the stretching parameter.[7] An example of transient absorption decays is shown in Figure 2.22.

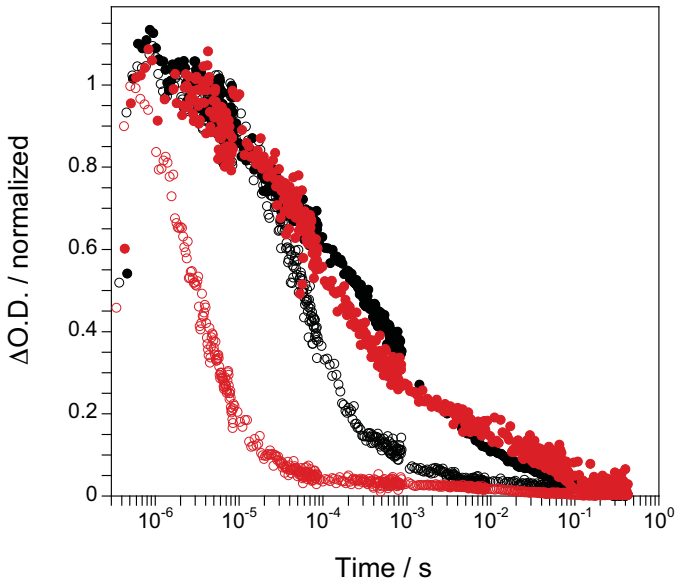

Figure 2.22. Example of TAS data.

References

1. Hagfeldt, A.; Boschloo, G.; Sun, L.; Kloo, L.; Pettersson, H., Dye-Sensitized Solar Cells. *Chem. Rev.* **2010,** *110*, 6595-6663.
2. (a) O'Regan, B.; Bakker, K.; Kroeze, J.; Smit, H.; Sommeling, P.; Durrant, J., Measuring Charge Transport from Transient Photovoltage Rise Times. A New Tool To Investigate Electron Transport in Nanoparticle Films. *J. Phys. Chem. B* **2006,** *110*, 17155-17160; (b) O'Regan, B.; Scully; Mayer, A. C.; Palomares, E.; Durrant, J., The effect of Al2O3 barrier layers in TiO2/dye/CuSCN photovoltaic cells explored by recombination and DOS characterization using transient photovoltage measurements. *J. Phys. Chem. B* **2005,** *109*, 4616-4623.
3. Bisquert, J.; Vikhrenko, V. S., Interpretation of the Time Constants Measured by Kinetic Techniques in Nanostructured Semiconductor Electrodes and Dye-Sensitized Solar Cells. *J. Phys. Chem. B* **2004,** *108*, 2313-2332.
4. Koops, S. E.; Durrant, J., Transient emission studies of electron injection in dye sensitised solar cells. *Inorg. Chim. Acta* **2008,** *361*, 663-670.
5. Haque, S. A.; Tachibana, Y.; Klug, D. R.; Durrant, J., Charge Recombination Kinetics in Dye-Sensitized Nanocrystalline Titanium Dioxide Films under Externally Applied Bias. *J. Phys. Chem. B* **1998,** *102*, 1745-1749.
6. Tachibana, Y.; Moser, J. E.; Grätzel, M.; Klug, D. R.; Durrant, J., Subpicosecond Interfacial Charge Separation in Dye-Sensitized Nanocrystalline Titanium Dioxide Films. *J. Phys. Chem.* **1996,** *100*, 20056-20062.
7. Nelson, J.; Haque, S. A.; Klug, D. R.; Durrant, J., Trap-limited recombination in dye-sensitized nanocrystalline metal oxide electrodes. *Phys. Rev. B* **2001,** *63*, 205321.

Chapter 2. Experimental methods

Chapter 3.
Substitutes porphyrins as sensitizers

The use of porphyrins as light harvesters on DSCs is particularly attractive given their primary role in photosynthesis and the relative ease way, which a variety of covalent or noncovalent porphyrin arrays can be constructed. The attachment of a large porphyrin array to a nanocrystalline semiconductor surface provides a way to dramatically increase the surface dye concentration and therefore, the light energy conversion efficiency of the device.[1]

More advantages are the high molar extinction coefficient, sharp absorption bands and high photostability. In the last three years, the use of cobalt electrolytes has gained much attention in this kind of dyes because of the high efficiencies obtained.

In this chapter, the value of TiO_2 dye loading is investigated. In this line, results obtained in DSC based on the I^-/I_3^- electrolyte are not necessary applicable to DSCs based on cobalt electrolytes. It is also studied the effect of light soaking in one porphyrin with an indoline group. Whit this treatment on the DSCs, the conduction band of the semiconductor and the electron lifetime change notably. A co-sensitization with two dyes with complementary absorbance is also perform in order to enhance the resulting efficiency. All the compounds are fully photophysical and electrochemical characterized and the device properties are completely investigated.

Index

1. Paper 1: Effect of porphyrin loading on performance of dye sensitized solar cells based on iodide/tri-iodide and cobalt electrolytes

Ana Aljarilla,[a] John N. Clifford,*[b] Laia Pellejà,[b] Antonio Moncho,[b] Susana Arrechea,[a] Pilar de la Cruz,[a] Fernando Langa*[a] and Emilio Palomares,[bc]

[a]Institute of Nanoscience, Nanotechnology and Molecular Materials (INAMOL), Campus de la Fábrica de Armas (UCLM), Toledo, Spain. E-mail: Fernando.Langa@uclm.es; Fax: +34 9252 68840; Tel: +34 9252 68843
[b]Institute of Chemical Research of Catalonia (ICIQ), Tarragona, Spain. E-mail: jnclifford@iciq.es
[d]Catalan Institution for Advanced Studies and Research (ICREA), Avda. Lluís Companys, 28. Barcelona. E-08030, Spain

J. Mater. Chem A, **2013**, 3, 13640-13647

Abstract: Two zinc–porphyrin sensitizers, **1a** and **1b**, bearing triphenylamine donor groups, were synthesized and their efficiencies measured in nanocrystalline TiO_2 dye sensitized solar cells employing iodide/tri-iodide and tris(1,10-phenanthroline) cobalt electrolytes. Optimized sensitization time for the TiO_2 photoanode was found to depend on the electrolyte employed: devices based on iodide/tri-iodide showed better efficiencies with shorter sensitization times (1.5 hours) whereas those based on tris(1,10-phenanthroline) cobalt showed better efficiencies with longer sensitization times (6 hours). From UV-Vis absorption spectra it is estimated that there is roughly twice as much dye loaded onto the TiO_2 film sensitized for 6 hours compared to the 1.5 hour film. Interfacial processes were probed using transient photovoltage, transient absorption and fluorescence lifetime measurements. The results indicate that sensitization time does not affect either dye regeneration or interfacial recombination processes in the presence of either electrolyte. However, sensitization time does have a considerable impact on device photocurrent, and moreover, the effect is different for the two electrolytes studied. This work demonstrates how device preparation must be tailored carefully depending on the electrolyte red/ox couple used.

1.1. Introduction

Research into Dye Sensitized Solar Cells (DSCs) continues to be an extremely active area.[2] After considerable time in which DSCs based on Ru(II)polypyridyl sensitizers were clearly the most efficient, DSCs based on

organic sensitizers have recently made huge strides forward in development.[3] In particular, there are many recent examples of DSCs employing iodide/tri-iodide ($I^-/I3^-$) with >10% device efficiency based on D–p–A porphyrins designed by Diau and co-workers.[4] Indeed, with recently developed novel cobalt complex based electrolytes[5] porphyrins have shown their promise with the current highest efficiency recorded for a DSC device of 12.05% being based on a cell containing a porphyrin sensitizer and a tris(bipyridyl) cobalt electrolyte.[6] Regardless of the red/ox couple, porphyrins offer several distinct advantages over Ru(II)polypyridyl sensitizers due to their high molar extinction coefficients, sharp absorption bands and high photostability.[7] However, their properties in DSCs still need to be fully investigated and molecular structure-device function rules need to be outlined to fully understand performance for devices based on these dyes.

In this article we investigate the performance of two porphyrin sensitizers, **1a** and **1b** (Figure 3.1), in DSC devices employing I^-/I_3^- and tris(1,10-phenanthroline) cobalt electrolytes.

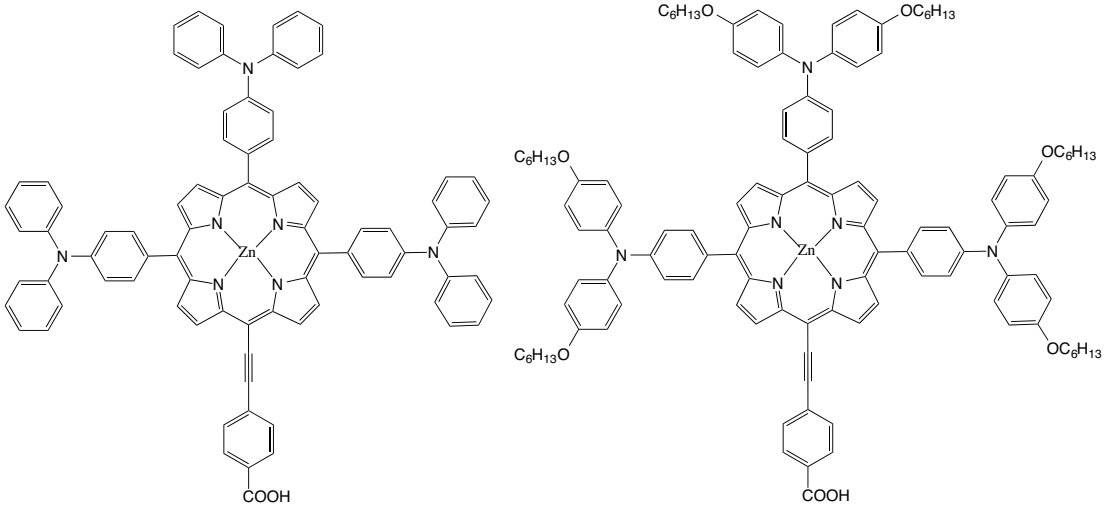

Figure 3.1. Structures of dyes **1a** (left) and **1b** (right).

Interfacial processes were investigated using a number of spectroscopic techniques. In particular, these processes were investigated as a function of TiO_2 dye loading. It was found that device efficiency was very sensitive to dye loading. This study underlines how device rules for DSCs based on the I^-/I_3^- electrolyte are not necessary applicable to DSCs based on cobalt electrolytes. This study is pertinent and timely given the increasing interest in DSCs based on cobalt electrolytes.

1.2. Results and discussion

1.2.1. Synthesis of 1a and 1b

Scheme 3.1 illustrates the synthetic route to dyes **1a** and **1b**. We prepared the free base porphyrins **2a,b** in 14% and 11% yield respectively, according to the Lindsey method.[8] This procedure improves significantly the yield with respect to previous procedures described for similar porphyrins (4–6%).[9] **2a,b** were reacted with zinc acetate in chloroform giving the metallated porphyrins **3a,b** in 91% and 95% yield respectively after purification by column chromatography. Finally, the trimethylsylil group was quantitatively removed by TBAF and in situ reacted with *p*-iodobenzoic acid under Pd-catalyzed Sonogashira coupling conditions affording the target dyes **1a,b** in 70% and 63% yield respectively. The intermediate and final compounds were fully characterized by means of UV-Vis, FT-IR, ^{1}H and ^{13}C NMR spectroscopies; the structures of all compounds were confirmed by MALDI-TOF mass spectrometry (see the Experimental section). The thermal stabilities of compounds **1a** and **1b** were evaluated by thermogravimetric analysis (TGA) under nitrogen, with a heating rate of 10 ºC min^{-1}. The decomposition temperatures (Td) were estimated from the TGA plot as the temperature of the intercept of the leading edge of the weight loss curve. Under these conditions, compounds **1a** and **1b** display excellent thermal stability up to 220ºC which is in principle satisfactory for their application in photovoltaic devices.

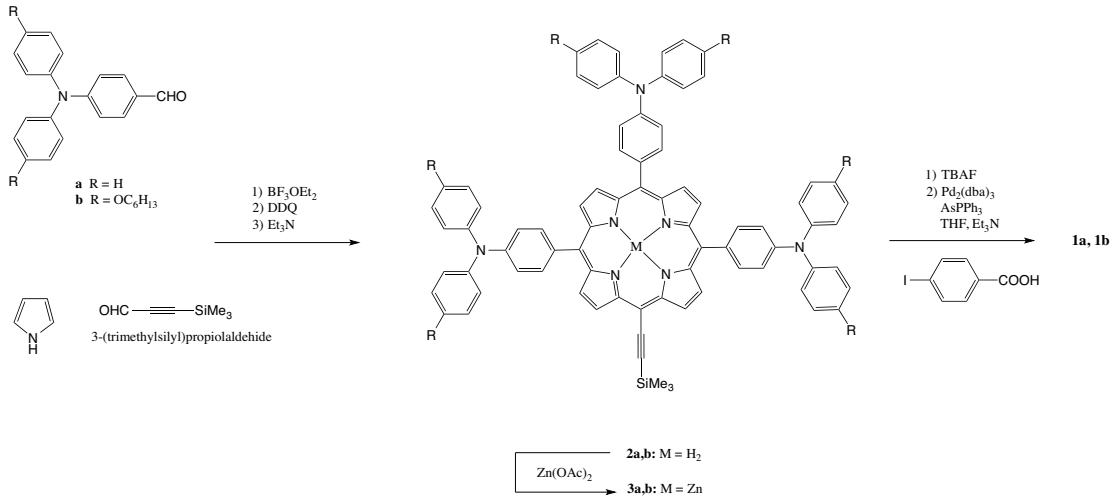

Scheme 3.1. Synthetic route to dyes **1a** and **1b**.

1.2.2. Absorption, emission, electrochemistry and computational calculations

The absorption spectra of dyes **1a,b** in dichloromethane (CH_2Cl_2) solution were shown in Figure 3.2. Both dyes exhibit the typical features of zinc porphyrins, with an intense Soret band between 400 and 500 nm and less intense Q bands in the range 550 to 700 nm (see Table 3.1). As expected, the absorption bands are not very sensitive to the nature of the substituents, pointing to weak electronic interactions between the porphyrin and the attached moiety in the ground state. Due to the presence of the hexyloxy groups in dye **1b**, a bathochromic shift is observed in the Q band, while in the Soret band an enhancement in bandwidth is observed. For the fluorescence spectra in CH_2Cl_2 the trend for the variation of the emission wavelength is similar to that of the absorption bands. The emission bands at 652 nm (**1a**, λ_{exc} = 450 nm) and 669 nm (**1b**, λ_{exc} = 449 nm) (see Figure 1) were totally quenched after adsorption onto TiO_2 indicating efficient photoinduced electron transfer from the dyes to the TiO_2 nanoparticles.

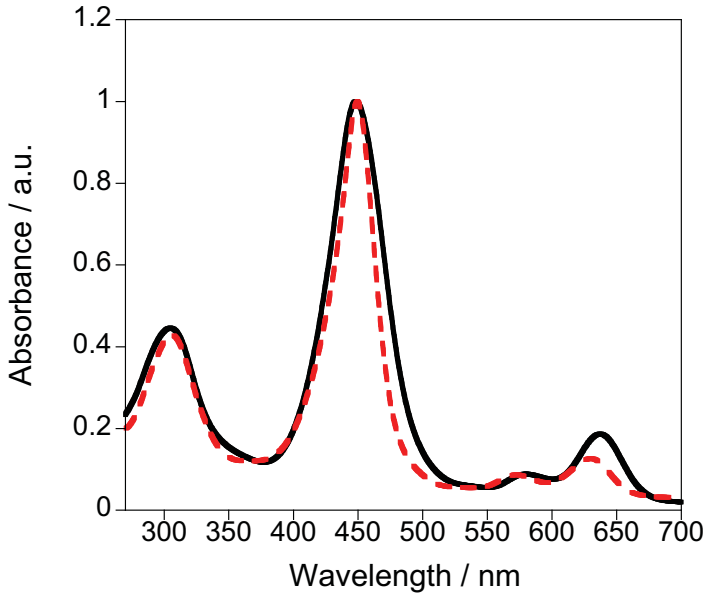

Figure 3.2 Normalized absorption (—) and emission (---) spectra of dyes 1a (red) and 1b (black) in dichloromethane solution (10^{-5} M).

The redox properties of **1a,b** were investigated by cyclic voltammetry and square wave voltammetry in tetrahydrofuran (THF), (see Table 3.1). In the cathodic side, compounds **1a,b** show the first reversible oxidation peaks at 0.33 and 0.28 V respectively; the presence of the electron- donating alkoxy groups significantly reduces the oxidation potential of **1b** compared to **1a**. On the reduction side, both compounds show first reduction potentials at –0.52 V and –0.57 V as irreversible waves, showing that the electron-donating alkoxy

groups in **1b** increase its reduction potential with respect to **1a**, as one would expect. The E_{HOMO} values of **1a** to **1b** vary only by 0.05 eV and were determined as –5.43 eV (**1a**) and –5.38 eV (**1b**), indicating regeneration is energetically feasible by both $I^-/I3^-$ (E_{redox} = –4.75 eV) and $Co(II)(phen)_3/Co(III)(phen)_3$ (E_{redox} = –5.06 eV) red/ox couples. The E_{LUMO} values also indicate that efficient electron injection into the TiO_2 conduction band (E_{TiO2} = –4.00 eV) is energetically possible.

Table 3.1. Absorption, emission and electrochemical data of dyes **1a** and **1b**.

Dye	λ_{abs} [a] / nm (log ε)	λ_{em} [a] / nm	E^1_{red} [b] / V	E^1_{ox} [b] / V	E_{HOMO} [c] / eV	E_{LUMO} [d] / eV
1a	630 (4.18), 572 (4.02) 450 (5.08), 306 (4.71)	652	–0.52	0.33	–5.43	–3.50
1b	637 (4.39), 579 (4.07) 449 (5.12), 305 (4.77)	669	–0.58	0.28	–5.38	–3.49

[a] 10^{-5} M, CH_2Cl_2. [b] 10^{-3} M in THF *versus* Fc/Fc^+, glassy carbon, Pt counter electrode, 20ºC, 0.1 M Bu4NClO4, scan rate = 100 mV s^{-1}. Calculated using equation E_{HOMO} (*vs.* vacuum) = – 5.1 – E^1_{ox} (vs. Fc/Fc^+) in eV.[10] [d] E_{LUMO} was calculated using $E_{LUMO} = E_{HOMO} + E_{0-0}$, where E_{0-0} is the intersection of the absorption and emission spectra.

In order to gain insight into the geometries and electronic properties of dyes **1a** and **1b**, computational studies were performed using density functional theory (DFT) at the B3LYP/6-31G level. Regarding geometry, for both dyes the dihedral angles between the phenyl ring and the porphyrin macrocycle (φ) are similar (φ ~ –65º) and are in agreement with those calculated for similar systems (Figure 3.3). The HOMOs were found to be delocalized through both the porphyrin macrocycle and TPA for both **1a** and **1b**, whereas the LUMOs are extended along the porphyrin system, the linker and the acid group, indicating electronic coupling with the TiO_2 nanocrystals. The HOMO–LUMO gap is similar for both dyes although the LUMO level of dye **1b** is higher (–2.45 eV) than that of **1a** (–2.61 eV) due to the electronic coupling of the alkoxy groups of the TPA moieties. HOMO and LUMO (Figure 3.4) are overlapped, favouring the HOMO to LUMO electronic transitions.

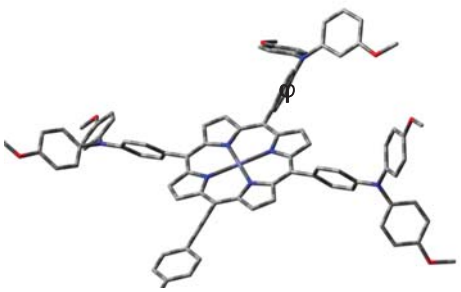

Figure 3.3. Optimized structure for dye **1b** (hexyl groups have been changed by methyl for calculations).

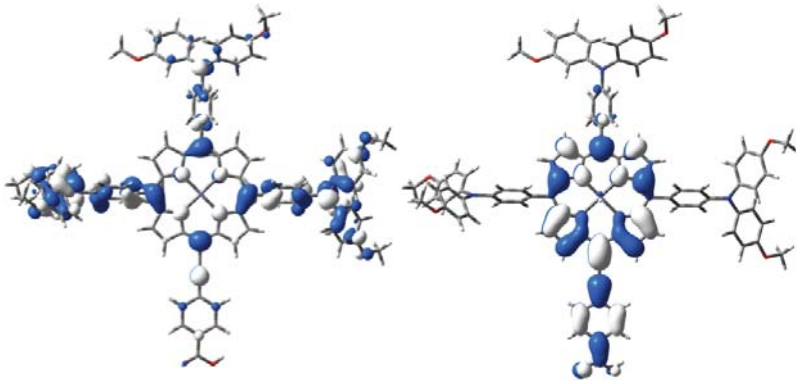

Figure 3.4. Frontier orbitals of dye **1b:** HOMO (left) and LUMO (right).

1.2.3. Device properties

Figure 3.5(a) and 3.5(c) and Table 3.2 show the IV curves and device characteristics, namely J_{sc}, V_{oc}, fill factor (FF) and overall efficiency (η), for sensitizers **1a** and **1b** in DSCs devices based on I^-/I_3^- and $Co(II)(phen)_3/Co(III)(phen)_3$ electro-lytes.

Employing I^-/I_3^- electrolyte, the best device efficiencies (Figure 3.5(a)) were obtained after 1.5 hours sensitization time with maximum efficiencies of 5.14% and 4.15% for **1a** and **1b** respectively (without mask). These values compare well with a recent study by Liu *et al*. involving similar dyes.[9] Upon the longer sensitization time of 6 hours the device efficiency drops to 3.93% and 3.60% for **1a** and **1b** respectively (without mask). The principle reason for this is a loss in J_{sc}. When cobalt electrolyte is used, however, the dependence of device efficiency on sensitization time is reversed (Figure 3.5(c)). The best efficiencies are recorded for 6 hours sensitization (3.11% and 2.45% for **1a** and **1b** respectively). Again, the main difference arising from sensitization time is accounted for by a difference in J_{sc}. The increase in device V_{oc} (approx. 140 mV) afforded by employing $Co(II)(phen)_3/Co(III)(phen)_3$ with respect to I^-/I_3^- is in line with increases observed in other studies.[11] Finally, under similar conditions the **YD2-*o*-C8** device gave an efficiency of 11.20% (without mask) indicating testing conditions are indeed comparable with studies demonstrating the best literature values for porphyrin based DSCs.[12]

Figure 3.5(b) and 3.5(d) show the IPCE spectra for all of the devices measured in this study. These spectra show the contributions to device current from the Soret and Q bands centred at around 450 and 650 nm respectively. Integration of these spectra agrees with the J_{sc} values for the same devices in Figure 3.5(a) and 3.5(c).

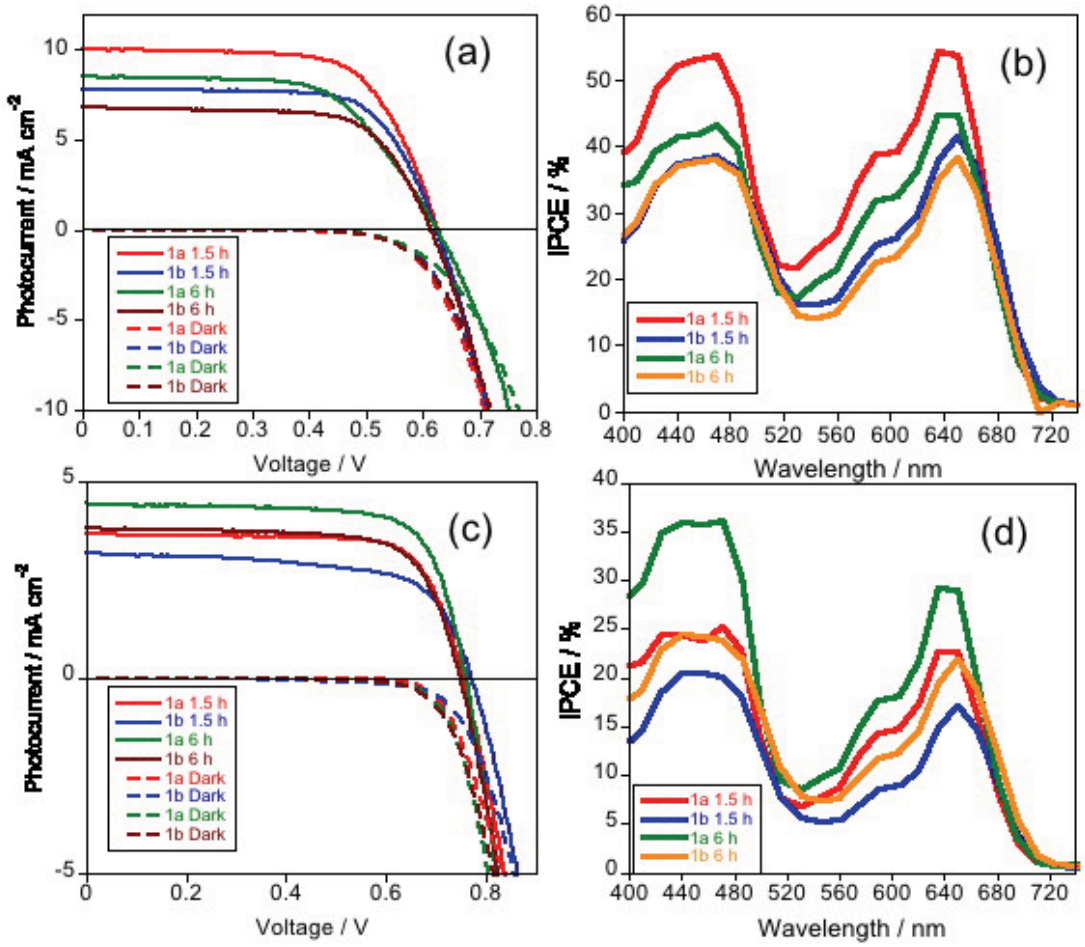

Figure 3.5. I-V curves and IPCE spectra of DSC devices composed of sensitizers **1a** and **1b** based on I^-/I_3^- (a and b) and $Co(II)(phen)_2/(Co(III)(phen)_3$ electrolytes (c and d).

Table 3.2. Photovoltaic performance of cells recorded under AM 1.5G 1 sun illumination.

Dye	Time/h	J_{sc}/mA cm^{-2}	V_{oc}/V	FF (%)	η $^{(\%)d}$
1a	1.5 [a]	10.09	0.63	67	4.19 (5.14)
1a	6 [a]	8.51	0.62	62	3.27 (3.93)
1b	1.5 [a]	7.83	0.62	70	3.40 (4.15)
1b	6 [a]	6.18	0.61	69	2.54 (3.60)
1a	1.5 [b]	3.67	0.75	75	2.06 (2.53)
1a	6 [b]	4.44	0.76	74	2.48 (3.11)
1b	1.5 [b]	3.17	0.77	66	1.61 (2.01)
1b	6 [b]	3.82	0.75	72	2.05 (2.45)
YD2-*o*-C8[c]		15.25	0.76	72	8.42 (11.2)

[a] Electrolyte: 0.6 M 1-butyl-3-methylimidazolium iodide (BMII), 0.1 M lithium iodide, 0.05 M iodine and 0.5 M 4-*tert*-butylpyridine in a 1:1 mixture of acetonitrile/valeronitrile. [b] Electrolyte: 0.2 M tris(1,10-phenantroline)cobalt(II)$(TFSI)_2$, 0.02 M tris(1,10-phenantroline)cobalt(III)$(TFSI)_3$, 0.1 M lithium perchlorate and 0.5 M 4-*tert*-butylpyridine in a 85:15 mixture of acetonitrile/valeronitrile. [c] Electrolyte: 0.5 M 1-butyl-3-methylimidazolium iodide (BMII), 0.1 M lithium iodide, 0.05 M iodine and 0.5 M 4-*tert*-butylpyridine in a 85:15 mixture of acetonitrile/valeronitrile, [d] Data in brackets recorded without mask.

In order to have an indication of dye loading in these devices, the absorption spectra of thin films of transparent TiO_2 films (6 µm) were measured after 1.5 hours and 6 hours sensitization in 0.2 mM solutions of **1a** and **1b** in chlorobenzene (Figure 3.6). These data indicate that there is roughly twice as much dye loading on the film sensitized for 6 hours compared to the equivalent film of 1.5 hours.

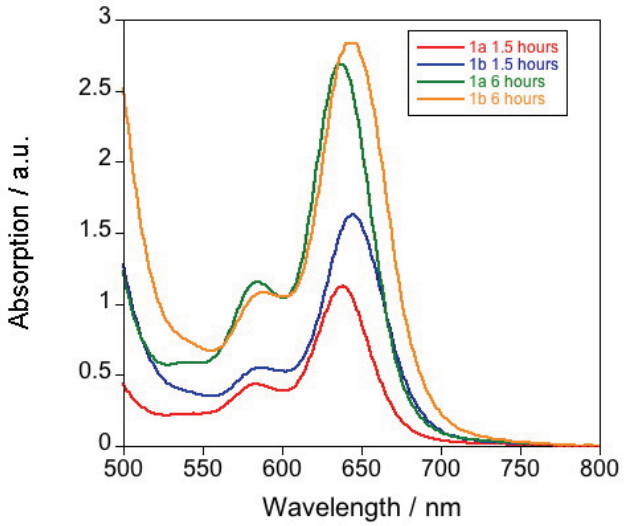

Figure 3.6. Absorption spectra of transparent TiO_2 films (6 µm) following 1.5 and 6 hour sensitization in 0.2 mM solutions of **1a** and **1b** in chlorobenzene.

1.2.4. Charge extraction, transient photovoltage and transient absorption spectroscopy measurements

Device electron densities and electron lifetimes were probed using charge extraction and transient photovoltage measurements respectively (Figure 3.7). To simplify the discussion, and because trends in DSC performance based on **1a** and **1b** are the same, data relating to DSCs fabricated using sensitizer **1a** are presented only.

The data in Figure 3.7 demonstrate that sensitization time has little bearing either on the position of the TiO_2 conduction band or on device electron lifetime for **1a** devices based on the two different electrolytes. This is not surprising if we consider that the V_{oc} for devices does not change with sensitization time. Despite the estimated doubling in dye loading for 6 hours sensitization compared to 1.5 hours, V_{oc}, TiO_2 electron density and electron lifetime do not change. This may be because the TiO_2 film is entirely covered by **1a** following 1.5 hours and any subsequent dye loading does not come into direct contact with TiO_2 or improve the dye blocking effect increasing TiO_2 electron lifetime.

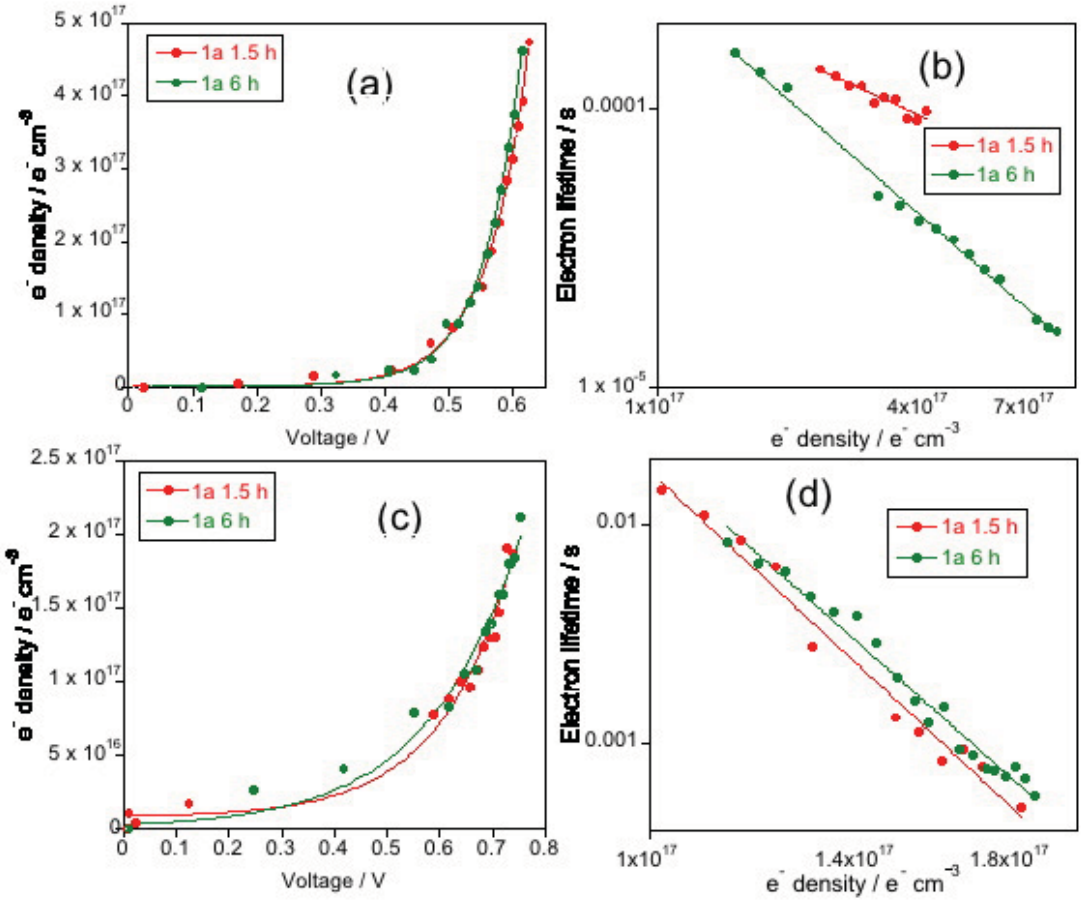

Figure 3.7. Charge density as a function of voltage and electron lifetime as a function of charge density of DSCs devices composed of sensitizer **1a** based on I^-/I_3^- (a and b) and $Co(II)(phen)_2/(Co(III)(phen)_3$ electrolytes (c and d).

Transient absorption spectroscopy was then used to monitor dye regeneration in these devices and these kinetics are shown in Figure 3.8.

In the absence of electrolyte (black decays) the kinetics are slow and dispersive, which become faster when electrolyte is added. The $t_{50\%}$ for the device prepared with 1.5 hour sensitization (0.5 ms) is slightly longer than that prepared with 6 hour sensitization (0.1 ms), probably due to the fewer charge separated species generated in this device due to lower dye loading. On the other hand, sensitization time appears to have little effect on $t_{50\%}$ in the presence of electrolyte (approx. 20 µs (I^-/I_3^-) and 90 µs ($Co(II)(phen)_3$/ $Co(III)(phen)_3$)). It is noted that kinetics recorded in the presence of the I^-/I_3^- electrolyte are faster due to the potential of this red/ox couple according more free energy for regeneration compared to $Co(II)(phen)_3$/ $Co(III)(phen)_3$.

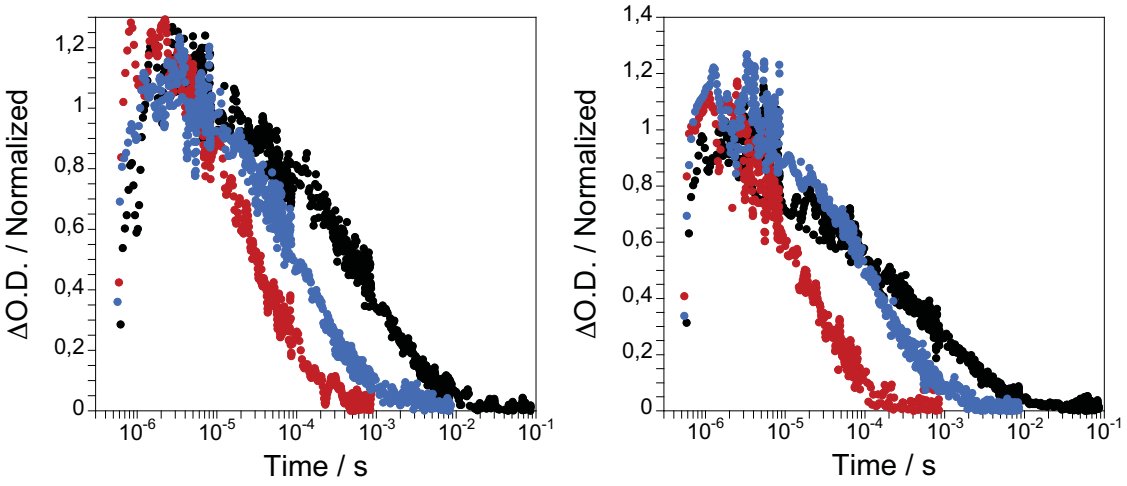

Figure 3.8. Transient absorption kinetics for DSC devices of **1a** prepared following (left) 1.5 hours and (right) 6 hours sensitization. The black, red and blue decays correspond to kinetics recorded in the presence of a blank electrolyte, I^-/I_3^- electrolyte and $Co(II)(phen)_2$/ $(Co(III)(phen)_3$ electrolyte respectively. Kinetics were recorded at 620 nm following excitation at 650 nm.

1.2.5. Fluorescence lifetime measurements

To investigate the difference in the J_{sc} values for **1a** devices, fluorescence emission lifetimes were measured using time-correlated single photon counting (Figure 3.9).

Dye loading of **1a** onto the above films was controlled so that the absorbance of Al_2O_3 and TiO_2 films in each set of samples was the same. Electron injection yields, ϕ, were estimated by integrating the areas under each emission decay, as done previously by Koops *et al.*[13] The results show that as the sensitization time increases from 1.5 to 6 hours, ϕ drops from 77 to 62%, respectively, in the presence of I^-/I_3^-. On the other hand, in the presence of $Co(II)(phen)_3/Co(III)(phen)_3$, ϕ increases from 27 to 40% on increasing sensitization time from 1.5 to 6 hours. Clearly, ϕ values correlate well with J_{sc} for the differently prepared devices.

Dye aggregation has been shown to quench dye excited states in I^-/I_3^- based devices limiting device photocurrent.[14] This would explain the drop in J_{sc} in **1a** and **1b** DSC devices at high dye loading in I^-/I_3^-. However, the higher ϕ and J_{sc} of $Co(II)(phen)_3/Co(III)(phen)_3$ devices at high dye loading indicate that this electrolyte has some influence over, and is able to control, aggregation. This can be explained by the bulky nature of the cobalt complexes allowing them to break-up dye aggregates of the planar porphyrin systems, improving J_{sc} and ultimately device performance.

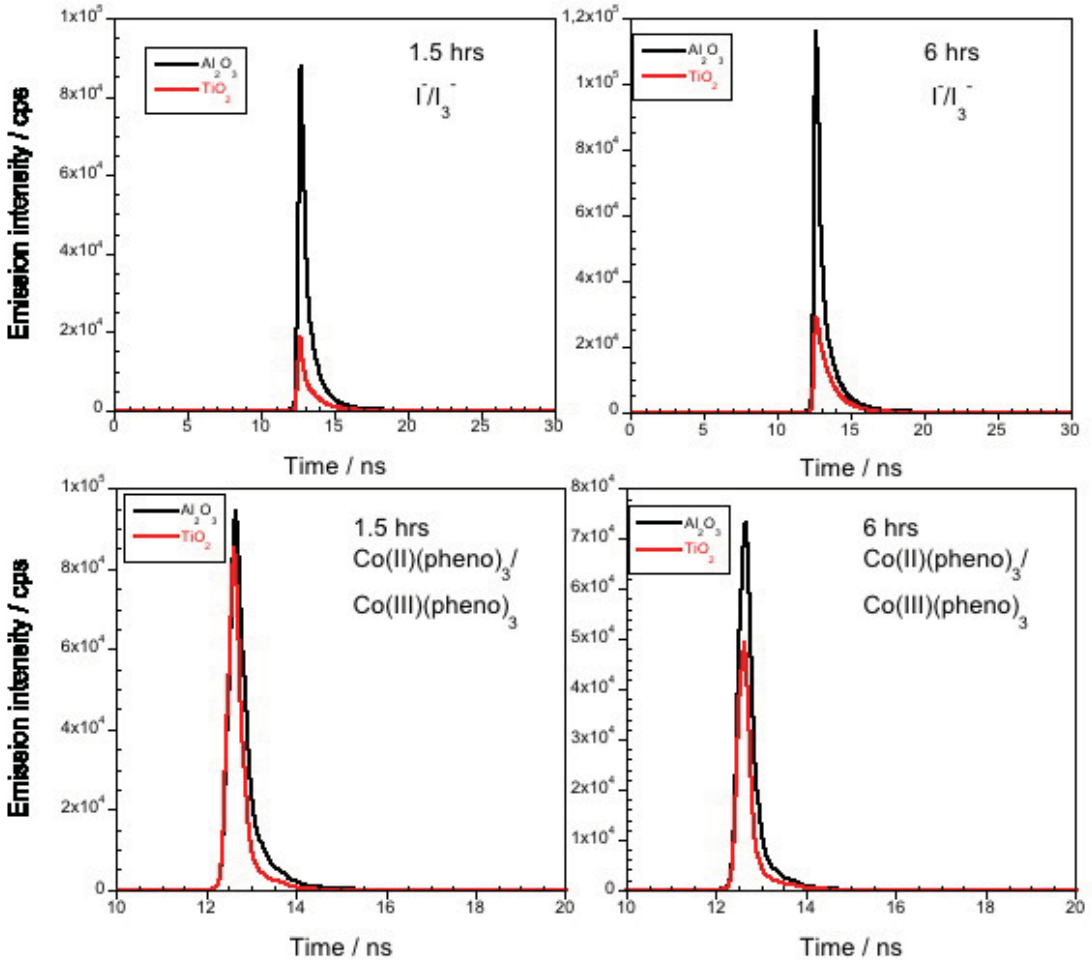

Figure 3.9. Emission lifetime decays of 1a on transparent Al_2O_3 and Tio_2 films following 1.5 h and 6 hours sensitization in the presence of I^-/I_3^- and Co(II)(phen)$_2$/(Co(III)(phen)$_3$ electrolytes. In all cases emission was recorded at 660 nm following excitation at 405 nm.

1.3. Conclusions

Two zinc–porphyrin sensitizers were synthesized and their efficiencies measured in dye sensitized solar cells employing I^-/I_3^- and Co(II)(phen)$_3$/Co(III)(phen)$_3$ electrolytes. Optimized sensitization times were found to depend on the electrolyte used with devices based on I^-/I_3^- showing better efficiencies with shorter sensitization times (1.5 hours) while those based on Co(II)(phen)$_3$/Co(III)(phen)$_3$ showing better efficiencies with longer sensitization times (6 hours). UV-Vis absorption spectra indicate that there is roughly twice as much dye loaded onto the TiO_2 film sensitized for 6 hours. It was found that dye loading had little influence over device V_{oc}, electron density or electron lifetime. However, at shorter sensitization times and lower dye loading, electron injection efficiency and photocurrent were higher in devices based on I^-/I_3^-. The opposite was true for devices based on Co(II)(phen)$_3$/

$Co(III)(phen)_3$ with higher electron injection efficiencies and photocurrents found for longer sensitization times and higher dye loadings. This work demonstrates how device preparation must be tailored carefully depending on the electrolyte red/ox couple used.

1.4. Experimental

1.4.1. Materials

Synthetic procedures were carried out under inert argon atmosphere, in dry solvent unless otherwise noted. All reagents and solvents were reagent grade and were used without further purification. Chromatographic purifications were performed using silica gel 60 SDS (particle size 0.040–0.063 mm).

1.4.2. Instruments

Analytical thin-layer chromatography was performed using Merck TLC silica gel 60 F254. ^{1}H NMR spectra were obtained on Bruker TopSpin AV-400 (400 MHz) spectrometer. Chemical shifts are reported in parts per million (ppm) relative to the solvent residual peak ($CDCl_3$, 7.27 ppm). ^{13}C NMR chemical shifts are reported relative to the solvent residual peak ($CDCl_3$, 77.00 ppm). UV-Vis measurements were carried out on a Shimadzu UV 3600 spectrophotometer. For extinction coefficient determination, solutions of different concentration were prepared in CH_2Cl_2, HPLC grade, with absorption between 0.1 and 1 of absorbance using a 1 cm UV cuvette. The emission measurements were carried out on Cary Eclipse fluorescence spectrophotometer. Mass spectra (MALDI-TOF) were recorded on a VOYAGER DE™ STR mass spectrometer using dithranol as matrix. The thermal stability was evaluated by TGA on Mettler Toledo TGA/DSC Start^e System under nitrogen, with a heating rate of 10ºC min^{-1}. Heating of crystalline samples leads to melting of the solids, but no recrystallization was observed.

1.4.3. Device preparation and characterization

In the present work two different types of TiO_2 films are utilized depending on the measurements being conducted. Highly transparent thin films of 4–8 µm were utilized for L-TAS measurements and also for UV-Vis absorption studies. On the other hand, for efficient DSCs, devices were made using either 4 µm

or 8 µm thick films consisting of 20 nm TiO_2 nanoparticles (Dyesol paste) for $Co(II)(phen)_3/Co(III)(phen)_3$ and I^-/I_3^- electrolytes respectively. A scatter layer of 4 µm of 400 nm TiO_2 particles (Dyesol paste) was then deposited on these films. Prior to the deposition of the TiO_2 paste the conducting glass substrates were immersed in a solution of $TiCl_4$ (40 mM) for 30 min and then dried. The TiO_2 nanoparticle paste was deposited onto a conducting glass substrate (NSG glass with 8 Ω cm^{-2} resistance) using the screen printing technique. The TiO_2 electrodes were gradually heated under airflow at 325 ºC for 5 min, 375 ºC for 5 min, 450 ºC for 15 min and 500 ºC for 15 min. The heated TiO_2 electrodes were immersed again in a solution of $TiCl_4$ (40 mM) at 70 ºC for 30 min and then washed with ethanol. The electrodes were heated again at 500 ºC for 30 min and cooled before sensitization. In order to reduce scattered light from the edge of the glass electrodes of the dyed TiO_2 layer, a light shading mask was used on the DSCs, so the active area of DSCs was fixed to 0.16 cm^2. The counter electrode was made by spreading a 5 mM solution of H_2PtCl_6 in isopropyl alcohol onto a conducting glass substrate (TEC15, Pilkington) with a small hole to allow the introduction of the liquid electrolyte using vacuum, followed by heating at 390 ºC for 15 min. Dye solutions of **1a** and **1b** at concentrations of 0.2 mM in chlorobenzene were prepared and films immersed for different periods of time at r.t. The sensitized electrodes were washed with chlorobenzene and dried under air. Finally, the working and counter electrodes were sandwiched together using a thin thermoplastic (Surlyn) frame that melts at 100 ºC. The iodide/tri-iodide electrolyte used consisted of 0.6 M 1-butyl-3-methylimidazolium iodide (BMII), 0.1 M lithium iodide, 0.05 M iodine and 0.5 M 4-*tert*-butylpyridine in a 1:1 mixture of acetonitrile/valeronitrile. The cobalt electrolyte consisted of 0.2 M tris(1,10-phenanthroline)cobalt(II)$(TFSI)_2$, 0.02 M tris(1,10-phenanthroline)cobalt(III)$(TFSI)_3$, 0.1 M lithium perchlorate and 0.5 M 4-*tert*-butylpyridine in a 85:15 mixture of acetonitrile/valeronitrile.

Reference devices containing **YD2-*o*-C8** dye were made by sensitizing films for approximately 90 minutes consisting of 13 µm transparent and 4 µm scatter TiO_2 in 0.1 mM ethanol solutions containing 0.5 mM chenodeoxycholic acid. The electrolyte consisted of 0.5 M 1-butyl-3-methylimidazolium iodide (BMII), 0.1 M lithium iodide, 0.05 M iodine and 0.5 M 4-*tert*-butylpyridine in 85:15 mixture of acetonitrile/valeronitrile.

The IV characteristics of cells were measured using a Sun 2000 Solar Simulator (150 W, ABET Technologies). The illumination intensity was measured to be 100 mW m^{-2} with a calibrated silicon photodiode. The appropriate filters were utilized to faithfully simulate the AM 1.5G spectrum. The applied potential and cell current were measured with a Keithley 2400

digital source meter. The IPCE (Incident Photon to Current conversion Efficiency) was measured using a homemade set up consisting of a 150 W Oriel Xenon lamp, a motorized monochromator and a Keithley 2400 digital source meter.

Transient photovoltage, charge extraction measurements and transient absorption spectroscopy measurements were carried out on systems described previously.[15] Emission lifetime studies were carried out on transparent 8–10 μm Al_2O_3 and TiO_2 films with a Lifespec© picosecond fluorescence lifetime spectrometer from Edinburgh Instruments© with an instrument response at half width at half maximum (HWHM) of duration 420 ps.

1.4.4. Synthesis and characterization

General procedure for the synthesis of 2a and 2b. To a solution of corresponding (diphenylamino)benzaldehyde (3 mmol), pyrrol (4 mmol) and 3-(trimethylsilyl)propiolaldehyde (1 mmol) in $CHCl_3$ (100 mL $mmol^{-1}$), under argon and degassed, was added $BF_3(OEt)_2$ (0.9 mmol). The mixture was allowed to stir under argon for 3 hours. Then, DDQ (2.8 eq.) was added and stirring for one hour; after addition of Et_3N (2 mL) for 30 min, the solvent was removed by rotary evaporation and the product was purified by column chromatography (silica gel, Hex-$CHCl_3$, 1:1).

*Synthesis of [10,15,20-tri(N,N-diphenylaniline)-5-ethynyltrimethyl-silane] porphyrin (**2a**).* From 3.00 g of (diphenylamino)benzaldehyde (11 mmol), 1.02 mL of pyrrol (14.7 mmol) and 0.547 mL of 3-(trimethylsilyl)propiolaldehyde (3.7 mmol), reacted according to the general procedure, affording 600 mg of **5a** as a green solid (14% yield). ^{1}H NMR (400 MHz, $CDCl_3$) δ/ppm: 9.69 (d, *J* = 4.7 Hz, 2H), 9.05 (d, *J* = 4.7 Hz, 2H), 8.96 (d, *J* = 4.7 Hz, 2H), 8.93 (d, *J* = 4.7 Hz, 2H), 8.07 (dd, *J* = 8.5, 6.4 Hz, 6H), 7.49 (d, *J* = 8.5 Hz, 6H), 7.45–7.42 (t, *J* = 7.0 Hz, 24H), 7.20–7.15 (m, 6H), 0.64 (s, 9H), –2.31 (s, 2H). ^{13}C NMR (100 MHz, $CDCl_3$) δ/ppm: 147.7, 147.6, 135.7, 135.6, 135.5, 135.3, 129.5, 129.2, 124.9, 123.3, 122.1, 121.3, 121.2, 120.9, 107.7, 101.6, 98.6, 0.35. UV-Vis (CH_2Cl_2) λ_{max}/nm (log ε): 670 (3.94), 580 (4.30), 538 (4.02), 435 (5.13), 303 (4.77). FT- IR v/cm^{-1}: 3315, 3058, 3030, 2954, 2137, 1595, 1492, 1328, 1313, 1270, 848, 798, 749, 695. MS (*m/z*) (MALDI-TOF): calculated for $C_{79}H_{61}N_7Si$: 1135.48; found: 1135.5 (M^+).

*Synthesis of [10,15,20-tri(N,N-(bis(4-hexyloxy)phenyl)aniline)-5- ethynyl-trimethylsilane]porphyrin (**2b**).* From 3.00 g of 4-(N,N-di-4- (hexyloxy)

phenylamino)benzaldehyde[16] (6.3 mmol), 0.6 mL of pyrrol (8.5 mmol) and 0.31 mL of (trimethylsilyl)-propiolaldehyde (2.1 mmol) reacted according to the general procedure affording 397 mg of **2b** as yellow solid (11% yield). ^{1}H NMR (400 MHz, $CDCl_3$) δ/ppm: 9.65 (d, *J* = 4.7 Hz, 2H), 9.04 (d, *J* = 4.7 Hz, 2H), 8.94 (d, *J* = 4.7Hz, 2H), 8.92 (d, *J* = 4.7 Hz, 2H), 7.98 (dd, *J* = 8.6, 6.1 Hz, 6H), 7.39–7.34 (m, 12H), 7.30 (t, *J* = 8.6 Hz, 6H), 7.00–6.95 (m, 12H), 4.00 (dd, *J* = 12.6, 6.6 Hz, 12H), 1.87–1.78 (m, 12H), 1.54–1.46 (m, 12H), 1.41–1.35 (m, 24H), 0.96–0.92 (s, 18H), 0.63 (s, 9H), –2.27 (s, 2H). ^{13}C NMR (100 MHz, $CDCl_3$) δ/ppm: 155.7, 148.5, 140.6, 135.5, 133.55, 133.2, 127.1, 122.6, 117.95, 117.8, 115.4, 107.4, 101.3, 98.1, 68.25, 31.6, 29.3, 25.8, 22.6, 14.1, 0.4. UV-Vis (CH_2Cl_2) λ_{max}/nm (log ε): 677 (3.72), 591 (4.15), 422 (5.06), 300 (4.68). FT-IR ν/cm^{-1}: 3314, 2951, 2927, 2857, 2137, 1599, 1504, 1469, 1239. MS (*m/z*) (MALDI-TOF): calculated for $C_{115}H_{133}N_7O_6Si$: 1736.01; found: 1736.00 (M^+).

General procedure for the synthesis of 3a and 3b. To a solution of corresponding porphyrin **2a** or **2b** (1 mmol) in $CHCl_3$ (84 mL mmol^{-1}) under argon was added a solution of $Zn(OAc)_2{\cdot}2H_2O$ (5 mmol) in MeOH (2.5 mL mmol^{-1}). The mixture was stirred at room temperature overnight. The reaction was quenched with water and the mixture extracted with $CHCl_3$ (3 x 50 mL). The combined organic extracts were washed with H_2O and dried over anhydrous $MgSO_4$. The solvent was removed under reduced pressure and the product was purified by column chromatography (silica gel, Hex–$CHCl_3$, 1:1).

*Synthesis of [10,15,20-tri-(N,N-diphenylaniline)-5-ethynyltrimethylsilane] porphinato zinc(II) (**3a**).* From 250 mg of porphyrin **2a** (0.22 mmol), reacted according to the general procedure, affording 251 mg of **3a** as a green solid (95% yield). ^{1}H NMR (400 MHz, $CDCl_3$) δ/ppm: 9.79 (d, *J* = 4.7 Hz, 2H), 9.14 (d, *J* = 4.7 Hz, 2H), 9.07 (d, *J* = 4.7 Hz, 2H), 9.05 (d, *J* = 4.7 Hz, 2H), 8.10–8.05 (m, 6H), 7.49 (t, *J* = 8.4 Hz, 6H), 7.46–7.43 (t, 24H), 7.19–7.14 (m, 6H), 0.66 (s, 9H). ^{13}C NMR (100 MHz, $CDCl_3$) δ/ppm: 150.04, 149.94, 147.85, 147.82, 147.36, 136.32, 135.40, 135.32, 132.23, 131.79, 130.93, 129.48, 124.81, 123.21, 122.93, 121.82, 121.36, 121.26, 107.66, 101.12, 99.37, 0.41. UV-Vis (CH_2Cl_2) λ_{max}/nm (log ε): 619 (4.25), 571 (4.19), 444 (5.31), 305 (4.81). FT-IR ν/cm^{-1}: 3060, 3030, 2955, 1924, 2853, 2138, 1589, 1490, 1329, 1315, 1280, 996, 842, 699. MS (*m/z*) (MALDI-TOF): calculated for $C_{79}H_{59}N_7SiZn$: 1197.39; found (M + H^+): 1197.6, 1198.6, 1199.6, 1200.5, 1201.5, 1202.5.

*Synthesis of [10,15,20-tri-(N,N-(bis(4-hexyloxy)phenyl)aniline)-5-ethynyl-trimethylsilane]porphinato zinc(II) (**3b**).* From 230 mg of porphyrin **2b** (0.13 mmol), reacted according to the general procedure, affording 217 mg of **3b** as

green solid (91% yield). ^{1}H NMR (400 MHz, $CDCl_3$) δ/ppm: 9.75 (d, *J* = 4.7 Hz, 2H), 9.13 (d, *J* = 4.7 Hz, 2H), 9.05 (d, *J* = 4.7 Hz, 2H), 9.03 (d, *J* = 4.7 Hz, 2H), 7.98 (dd, *J* = 8.6, 7.0 Hz, 6H), 7.36 (dd, *J* = 9.0, 5.8 Hz, 12H), 7.30 (t, *J* = 8.6 Hz, 6H), 6.95 (dd, *J* = 9.0, 6.7 Hz, 12H), 3.97 (dd, *J* = 13.0, 6.5 Hz, 12H), 1.85–1.75 (m, 12H), 1.54–1.45 (m, 12H), 1.41– 1.35 (m, 24H), 0.95–0.91 (m, 18H), 0.63 (s, 9H). ^{13}C NMR (100 MHz, $CDCl_3$) δ/ppm: 152.45, 150.9, 150.2, 150.1, 148.3, 140.8, 140.8, 135.3, 135.2, 134.1, 133.0, 132.2, 131.7, 130.7, 127.0, 123.4, 122.15, 118.0, 117.9, 115.4, 107.95, 100.9, 99.0, 68.3, 31.6, 29.3, 25.8, 22.6, 14.1, 0.4. UV-Vis (CH_2Cl_2) λ_{max}/nm (log ε): 623 (4.22), 570 (4.10), 441 (5.09), 301 (4.79). FT-IR v/cm^{-1}: 2954, 2951, 2854, 2138, 1604, 1503, 1235. MS (*m/z*) (MALDI-TOF): calculated for $C_{115}H_{131}N_7O_6SiZn$: 1797.92; found: 1798.5 (M^+).

General procedure for the synthesis of 1a and 1b. To a solution of the corresponding porphyrin **3a** or **3b** (1 mmol) in CH_2Cl_2 (200 mL mmol^{-1}), TBAF (1.25 mmol, 1 M in THF) was added under argon. The solution was stirred at room temperature for 1 hour. The mixture was quenched with H_2O and extracted with CH_2Cl_2 (3x50 mL). The combined organic layer was dried over anhydrous $MgSO_4$ and the solvent was removed under reducer pressure. The residue and 4-iodobenzoic acid (5 mmol) were dissolved in dry THF (200 mL mmol^{-1}) and Et_3N (120 mL mmol^{-1}). The solution was degassed with argon for 15 min, $Pd_2(dba)_3$ (0.3 mmol) and $AsPh_3$ (2 mmol) were added to the mixture and the solution was refluxed overnight. The solvent was removed under reduced pressure. The product was purified by column chromatography (silica gel, $CHCl_3$:MeOH 95:5).

*Synthesis of [10,15,20-tri(N,N-diphenylaniline)-5-carboxyphenyl- ethynyl-porphyrinato] zinc(II) (**1a**).* From 100 mg of porphyrin **3a** (0.22 mmol) reacted according to the general procedure giving 73 mg of **1a** as a green solid (70% yield). ^{1}H NMR (400 MHz, $CDCl_3$/d_5-pyridine) δ/ppm: 9.80 (d, *J* = 4.6 Hz, 2H), 9.09 (d, *J* = 4.6 Hz, 2H), 8.97 (d, *J* = 4.6 Hz, 2H), 8.94 (d, *J* = 4.6 Hz, 2H), 8.34 (d, *J* = 8.3 Hz, 2H), 8.11 (d, *J* = 8.3 Hz, 2H), 8.05 (t, *J* = 8.3 Hz, 6H), 7.70– 7.64 (m, 4H), 7.57–7.52 (m, 2H), 7.49–7.38 (m, 24H), 7.16–7.11 (m, 6H). ^{13}C NMR (100 MHz, $CDCl_3$/d_5-pyridine) δ/ppm: 207.05, 152.8, 152.3, 150.7, 149.8, 147.9, 147.1, 137.0, 132.0, 132.7, 132.1, 132.1, 132.0, 131.9, 131.9, 131.4, 131.1, 130.25, 130.1, 128.5, 128.4, 124.6, 121.4, 121.3. UV-Vis (CH_2Cl_2) λ_{max}/nm (log ε): 630 (4.18), 572 (4.02), 450 (5.08), 306 (4.71). FT-IR v/cm^{-1}: 3436, 3061, 3031, 2956, 2924, 2186, 1738, 1589, 1405, 1330, 1316, 1278, 1173, 698. MS (*m/z*) (MALDI-TOF): calculated for $C_{83}H_{55}N_7O_2Zn$: 1245.37; found: 1245.4 (M^+).

Synthesis of [10,15,20-tri(N,N-(bis(4-hexyloxy)phenyl)aniline)-5-5-carbo-

*xy-phenylethynyl-porphyrinato] zinc(II) (**1b**).* From 100 mg of porphyrin **3b** (0.13 mmol) reacted according to the general procedure giving 65 mg of **1b** as a green solid (63% yield). ^{1}H NMR (400 MHz, $CDCl_3$/d_5-pyridine) δ/ppm: 9.71 (d, *J* = 4.5 Hz, 2H), 9.03 (d, *J* = 4.5 Hz, 2H), 8.90 (d, *J* = 4.5 Hz, 2H), 8.87 (d, *J* = 4.5 Hz, 2H), 8.27 (d, *J* = 6.8 Hz, 2H), 8.03 (d, *J* = 6.8 Hz, 2H), 7.90 (dd, *J* = 8.5, 6.7 Hz, 6H), 7.30–7.19 (m, 24H), 6.91–6.86 (m, 6H), 3.93–3.88 (m, 12H), 1.72 (q, *J* = 6.7 Hz, 12H), 1.45–1.37 (m, 12H), 1.31–1.24 (m, 24H), 0.83 (t, *J* = 7.0 Hz, 18H). ^{13}C NMR (100 MHz, $CDCl_3$/d_5-pyridine) δ/ppm: 207.0, 155.6, 125.2, 150.9, 149.9, 149.9, 148.0, 140.9, 140.8, 134.9, 134.8, 132.8, 131.9, 131.4, 131.0, 130.1, 126.9, 122.05, 118.0, 117.9, 115.4, 97.4, 95.1, 68.2, 31.6, 30.9, 29.3, 25.75, 22.6, 14.0. UV-Vis (CH_2Cl_2) λ_{max}/nm (log ε): 637 (4.39), 579 (4.07), 449 (5.12), 305 (4.77). FT-IR ν/cm^{-1}: 3424, 3120, 3039, 2852, 2927, 2859, 2185, 1799, 1688, 1603, 1503, 1467, 1314, 1278, 1240, 1167, 998, 828, 794. MS (*m/z*) (MALDI-TOF): calculated for $C_{119}H_{127}N_7O_8Zn$: 1845.90; found: 1846.4 (M^+).

Acknowledgements

Financial support from the Ministry of Science and Innovation of Spain, (CTQ2010-17498, PLE2009-0038 and Consolider-Ingenio Projects HOPE CSD2007-00007) is gratefully acknowledged. EP would also like to thank the EU for the ERCstg PolyDot, and the Catalan government for the 2009 SGR-207 projects.

2. Paper 2: Novel D-π-A Porphyrin Employing an Indoline Donor Group for High Efficiency Dye Sensitized Solar Cells

Laia Pellejà,[a] Challuri Vijay Kumar,[a] John N. Clifford,[a] and Emilio Palomares,*[ab]

[b]Institute of Chemical Research of Catalonia (ICIQ), Tarragona, Spain. E-mail: epalomares@iciq.es
[b]Catalan Institution for Advanced Studies and Research (ICREA), Avda. Lluís Companys, 28. Barcelona. E-08030, Spain

Abstract: Dye Sensitized Solar Cell (DSC) devices were fabricated using a novel donor-(π bridge)-acceptor (D-π-A) porphyrin sensitizer, **VC-70**, in which an indoline is linked directly to the porphyrin core and functions as the donor group. The best efficiencies of **VC-70** and reference **YD2-*o*-C8** devices were found to be 7.31 and 7.60% respectively under standar AMG 1.5 illumination and device properties were fully characterized using transient absorption, charge extraction and transient photovoltage techniques. A notable effect on TiO_2 conduction band energetics and electron lifetime was observed following light soaking of **VC-70** devices under AM 1.5G illumination. Upon co-sensitization of **VC-70** with the organic dye **D205** an improved efficiency of 8.10% was obtained.

Journal of Physical Chemistry C, **2014**, article ASAP.

2.1. Introduction

The emergence of Dye Sensitized Solar Cells (DSCs)[2a, 17] based on organic sensitizers is evident in the recent literature.[3a, 6, 18] The development of porphyrin sensitizers with D-π-A structure in which the porphyrin ring core constitutes the π-bridge has led to efficiencies which rival the best Ru(II) polypyridal dyes employing the iodide/tri-iodide (I^-/I_3^-) electrolyte.[4a, 19] For such structures the best acceptor has been found to be carboxylic acid providing optimal electronic contact with the nanocrystalline TiO_2.[20] Donor groups have included triphenylamine,[19a] diphenylamine,[4a, 6] pyrene[19c] and bulky fluorenyl groups,[21] amongst others. In this work, for the first time an indoline group as the donor is incorporated into a D-π-A porphyrin, **VC-70** (Figure 3.10). Indoline has been used in several recent studies as a donor in D-π-A organic sensitizers.[22] In agreement with a recent study by this group on a related indoline D-π-A organic dye,[22a] the efficiency of DSCs fabricated with **VC-70** was found to increase with post fabrication light soaking.

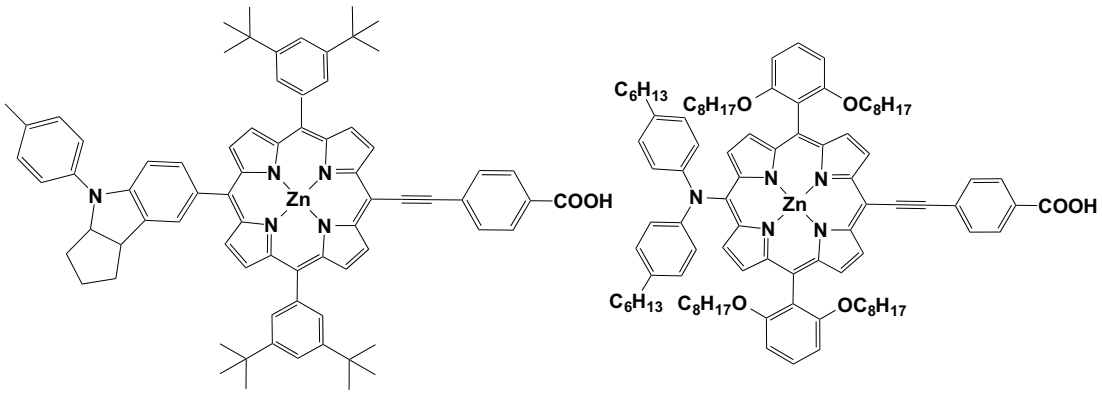

VC-70 **YD2-*o*-C8**

Figure 3.10 Molecular structures of **VC-70** and **YD2-*o*-C8**.

2.2. Experimental

2.2.1. Device preparation

The working and counter electrodes consisted of TiO_2 and thermalized platinum films, respectively, were deposited onto F-doped tin oxide (FTO, Pilkington Glass Inc., with 15 Ω sq-1 sheet resistance) conducting glass substrates. Two different types of TiO_2 films were utilized depending on the measurements being conducted. Highly transparent thin films (4 µm) were utilized for L-TAS (Laser Transient Absorption Spectroscopy) measurements and efficient DSCs devices were made using 13 µm thick films consisting of 20 nm TiO_2 nanoparticles (Dyesol© paste) and a scattering layer of 4 µm of 400 nm TiO_2 particles (Dyesol© paste). Prior to the deposition of the TiO_2 paste, the conducting glass substrates were immersed in a solution of $TiCl_4$ (40 mM) at 70 ºC for 30 minutes and then dried. The TiO_2 nanoparticle paste was deposited onto a conducting glass substrate using the screen-printing technique. The TiO_2 electrodes were gradually heated under an airflow at 325 ºC for 5 min, 375 ºC for 5 min, 450 ºC for 15 min and 500 ºC for 15 min. The heated TiO_2 electrodes were immersed again in a solution of $TiCl_4$ (40 mM) at 70 ºC for 30 min and then washed with ethanol. The electrodes were heated again at 500 ºC for 30 min and cooled before dye adsorption. The active area for devices was 0.16 cm^2. The counter electrode was made by spreading a 5 mM solution of H_2PtCl_6 in isopropyl alcohol onto a conducting glass substrate containing a small hole to allow the introduction of the liquid electrolyte using vacuum, followed by heating at 390 ºC for 15 minutes. Films were sensitized in 0.1 mM of **VC-70** solutions in ethanol containing 0.5 mM of chenoxydecholic acid overnight at room temperature. For co-sensitized devices, films were first sensitized for 3 hours in a 0.5 mM solution of **D205** in

acetonitrile/*tert*-butanol (1:1) containing 1 mM of chenoxydecholic acid followed by 3 hours sensitization in the **VC-70** solution. Finally, the working and counter electrodes were sandwiched together using a thin thermoplastic (Surlyn) frame that melts at 100 ºC. The electrolyte for all devices measured consisted of 0.5 M 1-butyl-3-methylimidazolium iodide (BMII), 0.1 M lithium iodide, 0.05 M iodine and 0.5 M *tert*-butylpyridine in a mixture of acetonitrile:valeronitrile (85:15).

2.2.2. Characterization techniques

UV-vis absorption spectra were measured in a 1 cm path-length quartz cell using a Shimadzu model 1700 spectrophotometer. Steady state fluorescence spectra were recorded using a Spex model Fluoromax-3 spectrofluorometer using a 1 cm quartz cell. ^{1}H NMR spectra were recorded at 300 MHz on a Bruker 300Avance NMR spectrometer with X-WIN NMR software. ^{1}H spectra were referenced to tetramethylsilane. ESI mass spectra were recorded on a Water Quattro micro (Water Inc, USA). Cyclic voltammetric experiments were carried out with a PC-controlled CH instruments model CHI620C electrochemical analyser.

The IV characteristics of cells were measured using a Sun 2000 Solar Simulator (150 W, ABET Technologies). The illumination intensity was measured to be 100 mW m^{-2} with a calibrated silicon photodiode. The appropriate filters were utilized to faithfully simulate the AM 1.5G spectrum. The applied potential and cell current were measured with a Keithley 2400 digital source meter.

Transient photovoltage and charge extraction measurements were carried out on a system described elsewhere.[15] In charge extraction, white light from a series of LEDs was used as the light source. When the LEDs are turned off the cell is immediately short-circuited and the charge is extracted allowing electron density in the cells to be calculated. By changing the LEDs intensity the electron density can be estimated as a function of cell voltage. In transient photovoltage measurements, in addition to the white light applied by the LEDS, constant background voltage is applied to the cells and again, a diode pulse (660 nm, 10 mW) is then applied to the sample inducing a change of 2-3 mV within the cell. The resulting photovoltage decay transients are collected and the τ values are determined by fitting the data to the equation $\exp(-t/\tau)$.

Laser-transient absorption spectroscopy measurements were carried out using a system described previously.[15] Kinetics were recorded in a blank electrolyte consisting of 0.5 M *tert*-butylpyridine in acetonitrile and the iodide/ tri-iodide electrolyte used for optimized 0.16 cm^2 devices.

2.3. Results and discussion

The synthetic route of porphyrin dye **VC-70** is depicted in Scheme 3.2. An ethyne bridge provides a well-defined and rigid structural arrangement and for this reason ethynyl benzoic acid was selected as the electron acceptor and the anchoring group. The synthesis of the target dye **VC-70** was achieved using a convergent synthetic strategy on the basis of Suzuki coupling of indoline borate with bromo porphyrin (**1**) in the presence of $Pd(PPh_3)_4$ and K_2CO_3 in dry THF (tetrahydrofurane) and a simple bromination was performed on the reactive porphyrin unit (**4**). The ethynyl benzoic acid group was attached to the meso position via catalyzed Sonagashira coupling. The important intermediates and the targeted dye **VC-70** were well characterized by ^{1}H-NMR, ^{13}C-NMR and MALDI (Matrix-Assisted Laser Desorption/Ionization) mass spectroscopy.

Scheme 3.2. Synthetic route of **VC-70**[a]

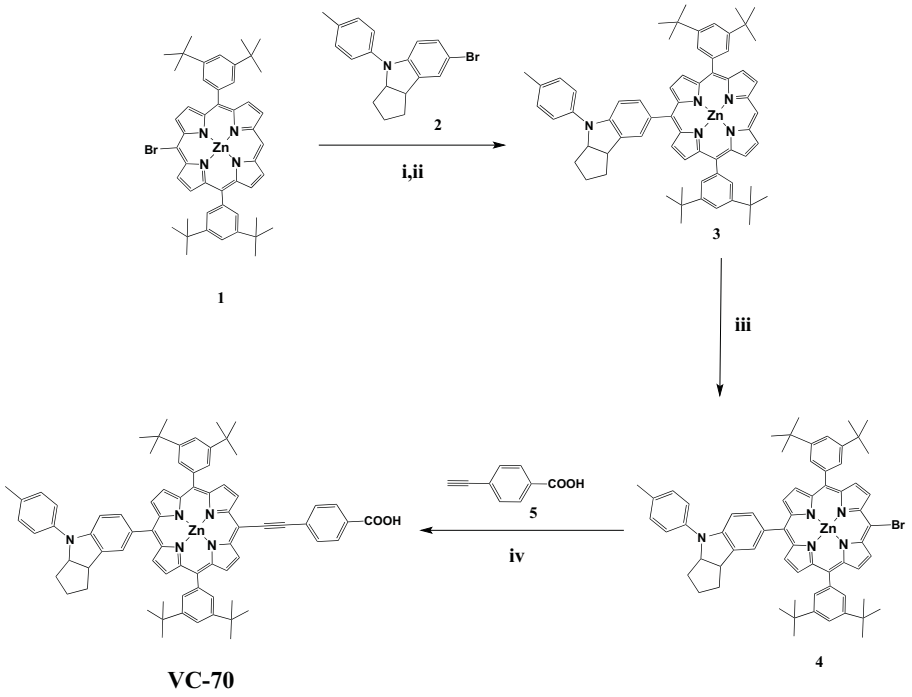

[a] *Reaction conditions:* (i) *n*-BuLi, THF, $B(OCH_3)_3$, -78 ºC ; (ii) $Pd(PPh_3)_4$, 2 M K_2CO_3 aqueous solution, THF, 6 h, 80 ºC; (iii) NBS, DCM, Pyridine, R.T. (iv) $Pd_2(dba)_3$, $AsPh_3$, dry THF, NEt_3, reflux 6 h.

The absorption and emission spectra of **VC-70** and **YD2-*o*-C8** in solution are shown in Figure 3.11 and their photophysical and electrochemical characteristics are collected in Table 3.3.

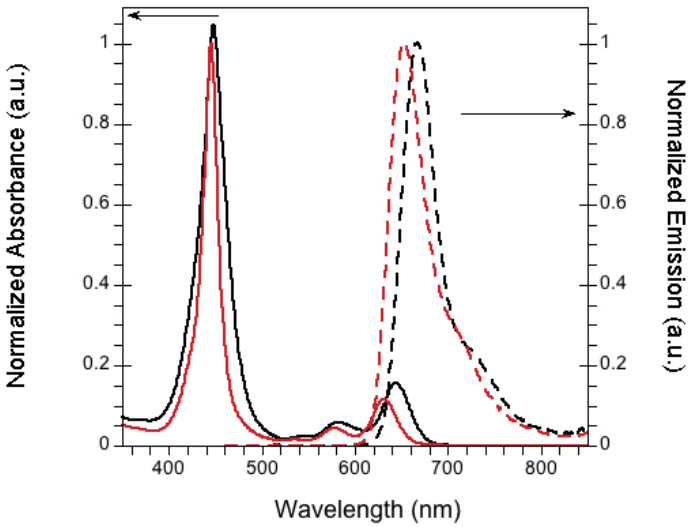

Figure 3.11. Normalized absorption (solid) and emission (dashed) specta of **YD2-*o*-C8** (black) and **VC-70** (red) in THF.

Both dyes show typical absorption bands associated with porphyrins, namely an intense Soret band at around 445 nm and a series of lower intensity Q bands at longer wavelength (550-700 nm). It is noticeable that though the molar extinction co-efficients of the Q-bands are comparable, the Soret band of **VC-70** is nearly double that of **YD2-*o*-C8** (Figure 3.16, Supporting Information). Strong emission at around 660 nm was observed for both dyes. There is a clear shift of 15 nm both in absorption and emission for **VC-70** towards the blue. Cyclic voltammetry studies measured in solution (Figure 3.17, Supporting Information) show that the ground state oxidation potential (E_{ox}) of **VC-70** is 70 mV more positive than that of **YD2-*o*-C8**. Both photophysical and electrochemical studies suggest that the band gap of **VC-70** is larger than that of **YD2-*o*-C8**. This may be due to a lack of co-planarity between the planar indolene and porphyrin core in **VC-70**, making the indolene a weaker electron-donating group than the diphenylamine of **YD2-*o*-C8**. This is also indicated by the stronger and more blue absorbing Soret band in **VC-70**, which has been observed in other D-π-A dyes where no or weakly electron-donating groups have been placed in the *meso*-position opposite to the anchoring group.[4b, 23] It is noted that the *meso*-phenyls in **YD2-*o*-C8** are functionalized at the *ortho*-positions with electron-donating dioctyloxy substituents whereas the *meso*-phenyls in **VC-70** contain *tert*-butyl groups. This may also contribute to the differences in photochemical and electrochemical properties observed as noted elsewhere.[6]

The E_{HOMO} and E_{LUMO} values calculated from photophysical and electrochemical data in Table 3.3 indicate that efficient dye regeneration by the I^-/I_3^- redox electrolyte (E_{redox} = –4.75 eV) and also efficient electron injection into the TiO_2 conduction band (E_{TiO2} = –4.0 eV) is energetically favourable for these sensitizers.

Table 3.3. Absorption, emission and electrochemical properties of **YD2-*o*-C8** and **VC-70.**

Dye	λ_{abs} [a]/nm	λ_{em} [a]/nm	E_{ox} [b]/V (*vs.* Fc/Fc^+)	$E_{0\text{-}0}$ [c]/eV	E_{HOMO} [d]/eV	E_{LUMO} [e]/eV
YD2-*o*-C8	448 (21.04), 583 (1.17), 642 (3.01)	667	0.165	1.90	–5.05	–3.15
VC-70	445 (41.46), 557 (1.83), 630 (4.46)	653	0.235	1.94	–5.12	–3.18

[a] Measured in THF. In parenthesis molar extinction efficient (ε) at λ_{abs} (10^3 M^{-1} cm^{-1}). [b] Measured in 0.1 M tetrabutylammonium hexafluorophosphate in THF at scan rates of 50 mV s^{-1} (**YD2-o-C8**) and 100 mV s^{-1} (**VC-70**). The working electrode consisting of a platinum wire and the counter electrode a platinum mesh. The reference electrode was the silver calomel electrode (saturated KCl). All solutions were degassed with argon for 5 min prior to measurement. [c] E_{0-0} (Energy for the electronic transition to and from the lowest vibrational states of a molecule) was determined from the intersection of absorption and emission spectra in dilute solutions. [d] E_{HOMO} was calculated using E_{HOMO} (vs. vacuum) = –4.88 – E_{ox} (vs.Fc/Fc^+). [e] E_{LUMO} was calculated using $E_{LUMO} = E_{HOMO} + E_{0-0}$.

YD2-*o*-C8 and **VC-70** were used to fabricate DSCs solar cells and measured under standard illumination conditions (AM 1.5G 100 mW m^{-2}). Device properties are listed in Table 3.4. Devices were measured before and after 90 minutes of continuous illumination to investigate the effect of light soaking on device performance.

Table 3.4. Device properties of **YD2-*o*-C8** and **VC-70** devices.

Dye	J_{sc}/mA cm^{-2}	V_{oc}/V	FF (%)	η [(%)c]
YD2-*o*-C8 (0 min)[a]	13.48	0.774	73	7.60
YD2-*o*-C8 (90 min)[b]	12.83	0.774	75	7.43
VC-70 (0 min)[a]	12.20	0.674	67	5.59
VC-70 (90 min)[b]	14.47	0.699	72	7.31

[a] Recorded after 0 minutes illumination. [b] Recorded after 90 minutes illumination. [c] Efficiencies recorded with mask.

The **YD2-*o*-C8** device shows an efficiency of 7.60% which compares extremely well with literature values.[22b] Upon 90 minutes light soaking there is little difference in device performance. On the other hand, the efficiency of the **VC-70** device increases markedly from 5.59 to 7.31% with light soaking, an increase of 31%. The reasons for this increase will be discussed further on. The much higher V_{oc} for the **YD2-*o*-C8** device can be ascribed to the hexyl chains on the diphenylamine donor and the dioctyloxy substituents on the *meso*-phenyls which are superior to blocking recombination of TiO_2 electrons with the electrolyte and also preventing aggregation than the *tert*-butyl groups of **VC-70**.[6, 20] The I-V curves are shown in Figure 3.12.

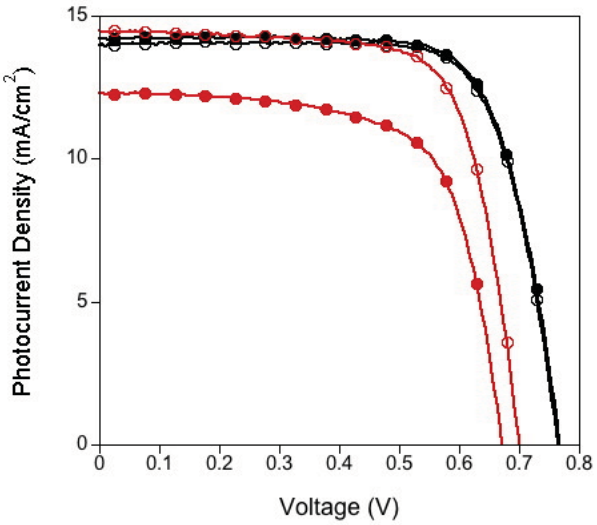

Figure 3.12. I-V curves recorded under AM 1.5G illumination for **YD2-*o*-C8** (black) and **VC-70** (red) DSC devices before (solid circles) and after (open circles) light soaking.

Electron density and electron lifetimes in these devices were probed using charge extraction and transient photovoltage measurements, respectively (Figure 3.13). Before light soaking **YD2-*o*-C8** and **VC-70** devices show similar charge densities but electron lifetimes in the **YD2-*o*-C8** device are considerably longer than those of the **VC-70** device at the same electron density. This explains the 100 mV higher V_{oc} for the reference **YD2-*o*-C8** device. Upon light soaking for 90 mins, the charge extraction data show an increase in charge density for the **VC-70** device suggesting a downward shift in the TiO_2 conduction band. Electron density in the **YD2-*o*-C8** device remains unchanged. Transient photovoltage data also show no effect on electron lifetimes in the **YD2-*o*-C8** device whereas electron lifetimes become much longer for the **VC-70** device, even longer than for the **YD2-*o*-C8** device in fact. This helps explain the 25 mV increase in V_{oc} for the **VC-70** device upon light soaking, though the V_{oc} of the **YD2-*o*-C8** device is still considerably larger (75 mV).

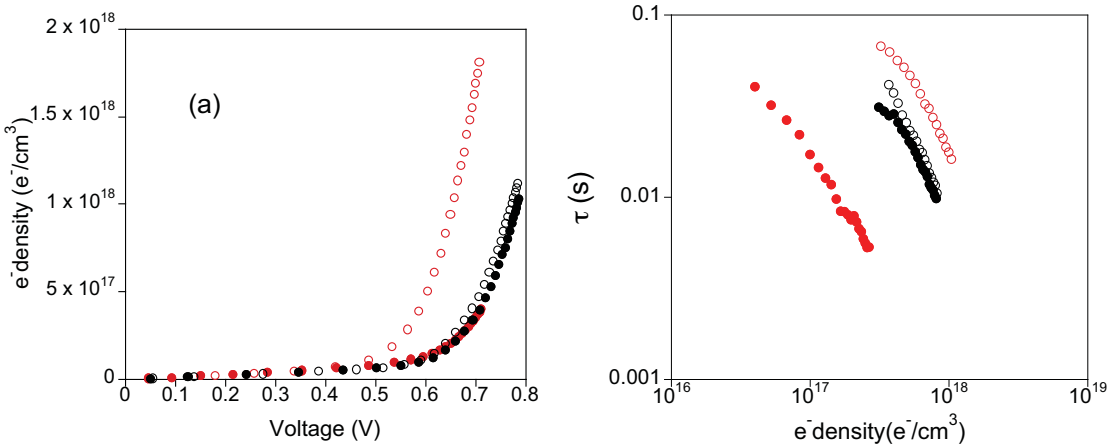

Figure 3.13. (a) Electron density as a function of cell voltage and (b) device electron lifetime τ as a function of charge density for **YD2-*o*-C8** (black) and **VC-70** (red) devices measured before (solid circles) and after (open circles) light soaking.

Transient absorption spectroscopy was used to probe charge recombination and regeneration by the I^-/I_3^- redox couple in transparent DSC devices (Figure 3.14). The data recorded in the absence of redox active electrolyte (black decays) show similar long-lived decays for both devices assigned to the dye cation formed following photo-excitation and charge separation. These kinetics are similar to those which we have observed previously in DSCs containing similar porphyrin dyes.[24] In the presence of the redox couple the kinetics become bi-phasic with the loss of the cation signal due to regeneration by I^- and the appearance of a long-lived signal assigned to TiO_2 injected electrons and/or $I_2^{\bullet-}$ (red decays). The $t_{50\%}$ (time taken for 50% of signal to disappear) for the regeneration reaction is estimated as 40 and 3 μs for **YD2-*o*-C8** and **VC-70** respectively. This difference may be explained by the difference in ground state oxidation (E_{ox}) potential for these dyes, with the more positive potential of **VC-70** of 70 mV providing greater driving force for the regeneration reaction as we have observed previously.[22a]

Returning to the effect of light soaking on device efficiency, similar observations were observed in two other studies involving DSCs employing porphyrin sensitizers.[25,26] In both cases notable increases in device V_{oc} and J_{sc} were observed following light soaking. Furthermore, though increases in device electron lifetime were observed, no change in device electron density was recorded in either study and improvements in device performance where therefore attributed to increased charge injection and reduced charge recombination rather than a shift in the TiO_2 conduction band. Griffith *et al.*[26] explained the effect of light soaking as a result of a cation exchange at the TiO_2 surface between Li^+ (from LiI) and $DMPI^+$ (from 1,2-dimethyl-3-propyl-imidazolium) ions present in the electrolyte. It was noted that the light soaking

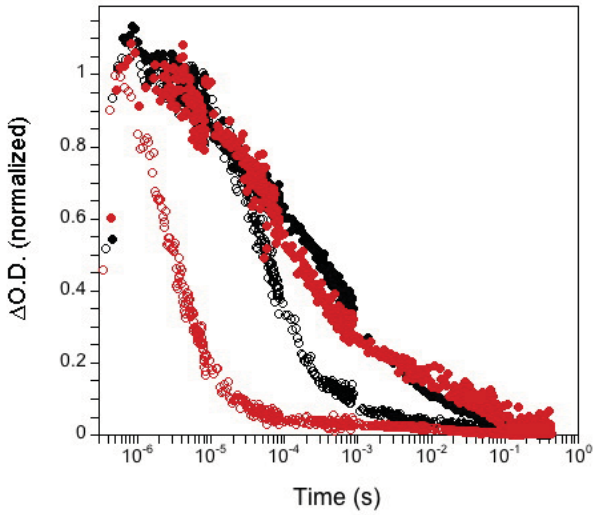

Figure 3.14. Transient absorption kinetics of **YD2-*o*-C8** (black) and **VC-70** (red) for 1 cm^2 area devices comprising transparent TiO_2 films in the presence of a blank electrolyte and an I_3^-/I^- redox electrolyte. Open symbols correspond to the samples with I_3^-/I^- electrolyte. Kinetics were recorded at 800 nm (**YD2-*o*-C8**) and 850 nm (**VC-70**) following excitation at 470 nm. Δ O.D. (Change in Optical Density)

effect was greater in devices where lower TiO_2 dye loadings were used suggesting that the presence of large exposed spaces on the film could lead to a greater degree of cation exchange. A similar scenario may also explain the light soaking effect we observe in our study with ineffective packing on the surface of the TiO_2 caused by the bulky indoline group not being co-planar with the porphyrin ring in **VC-70** facilitating cation exchange to some extent. We note that our electrolye is identical to that used in the two studies mentioned except that 0.5 M 1-butyl-3-methylimidazolium iodide (BMII) was used instead of 0.6 M 1,2-dimethyl-3-propylimidazolium (DMPII). This could be a reason why we observe a shift in the TiO_2 conduction, though we are still unsure why. We note we also observed a shift in the TiO_2 conduction band following light soaking for devices containing an organic dye with the same electrolyte in a previous study.[22a]

Finally, in an effort to improve device efficiency, **VC-70** was co-sensitized with the indoline dye **D205**[27] which has a complementary absorption band centred at 525 nm. Sensitizing conditions for optimized devices were found to be 3 hours in **D205** solution followed by a further 3 hours in **VC-70** solution. With this dual dye system the best device gave a J_{sc} of 17.18 mA cm^{-2}, a V_{oc} of 0.71 V and a fill factor of 66% resulting in an overall cell efficiency of 8.10%, which is higher than the corresponding device based on **VC-70** alone (7.31%). Again, light soaking of 90 minutes was used to optimize efficiency in co-sensitized devices. The I-V curve for the **D205/VC-70** co-sensitized DSC device is shown in Figure 3.15.

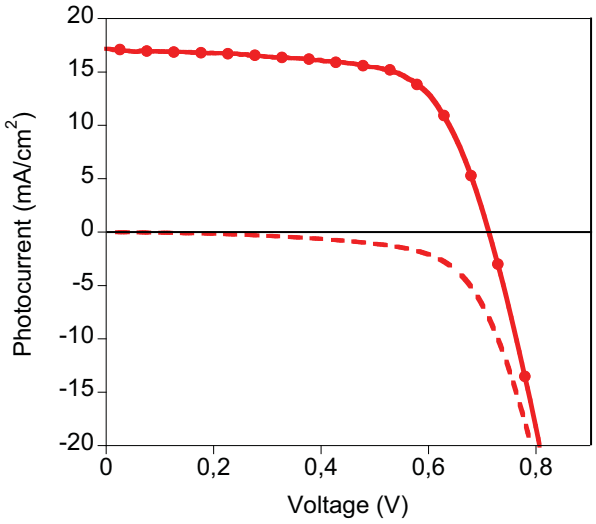

Figure 3.15. I-V curves recorded under AM 1.5G illumination and in the dark for a DSC device co-sensitized with **D205** and **VC-70**.

2.4. Conclusions

A novel D-π-A porphyrin sensitizer, **VC-70**, in which an indoline unit is employed as the donor group, was synthesized and its photophysical and electrochemical properties fully characterized. In DSC devices an efficiency of 7.31% compared extremely favourably with devices based on the reference porphyrin **YD2-*o*-C8** (7.60%). The efficiency of **VC-70** devices was found to depend upon exposure to illumination (light soaking) with maximum efficiencies observed after 90 minutes with increases in both V_{oc} and J_{sc} observed. Charge extraction and transient photovoltage data indicate that the increase in J_{sc} is due to a downward shift of the TiO_2 conduction band while the increase in V_{oc} is due to an increase in device electron lifetime, which may be related to the migration of ions in the electrolyte to the TiO_2 surface due to bad dye packing of **VC-70** on the TiO_2 film. Finally, when **VC-70** is co-sensitized with the indoline dye **D205** having complementary absorbance, device efficiency was improved further to 8.10%.

Acknowledgements

The Spanish MINECO under grants CTQ2010-18859 and CONSOLIDER CDS-007 HOPE-2007 supports this work. EP would like also thanks the EU for the ERCstg PolyDot, and the Catalan government for the 2009 SGR-207 projects.

2.5. Supporting Information

2.5.1. Materials

Dichloromethane, Pyrrole, Pyridine and THF were distilled before use. 3,5-*tert*-butyl-benzaldehyde, DDQ, $Pd(PPh_3)_4$, $Pd_2(dba)_3$, $AsPh_3$, N-bromo-succinimide (NBS), potassium carbonate, 4-*tert*-butylpyridine (TBP), NEt_3,$B(OMe)_3$ and *n*-butyl lithium (2.0 M in hexane) were purchased from Sigma-Aldrich. Dye **YD2-*o*-C8** was obtained from Solaronix and **D205** was purchased from Mitsubishi Paper Mills Limited.

2.5.2. Synthetic Procedures.

Synthesis of 3: 7-bromo-1,2,3,3a,4,8b-hexahydro-4-(4-methylphenyl)-cyclopent[b]indole[28] (**2**) and bromo porphyrin (**1**) was synthesized as reported procedure. Indoline borate was prepared with the published method[29] from the raw material of 7-bromo-1,2,3,3a,4,8bhexahydro-4-(4-methylphenyl)-cyclo-pent[b]indole (0.120 g, 0.367 mmol) was added to a round flask with 20 mL of THF and was stirred under nitrogen atmosphere at –78ºC. *n*BuLi 2M in hexane (0.035 ml, 0.433 mmol) was added and the mixture was stirred for 15 minutes at –78ºC. After that, $B(OMe)_3$ (0.06 ml, 0.55 mmol) was added and the reaction was stirred overnight at –78ºC. The crude was warmed to room temperature. In another schlenk, $Pd(PPh_3)_4$ (0.045 g, 0.03 mmol), **1** (0.303 g, 0.367 mmol), K_2CO_3 2M (2ml). The borate crude material and THF (20ml) was added and the reaction was stirred at 70ºC for 6 hours. Then water was added. The crude product was extracted into $CHCl_3$, and the organic layer was dried over Na_2SO_4. The residue was purified by silica gel column chromatography (Hexane/Dichloromethane 6:4) to obtain a purple solid (0.125 g, 40% yield).^{1}H-NMR (400 MHz, $CDCl_3$) δ/ppm: 10.21 (s, 1H); 9.38 (d, *J* = 4.5 Hz, 2H); 9.16 (d, *J* = 4.5 Hz, 2H); 9.13 (dd, *J* = 4.5 Hz, 2.1 Hz, 2H); 9.04 (dd, *J* = 12.6 Hz, 4.5 Hz, 2H); 8.11 (m, 4H); 7.95 (s, 1H); 7.86 (dd, *J* = 8.1 Hz, 2.1 Hz, 1H); 7.81 (d, *J* = 2 Hz, 2H); 7.43 (d, *J* = 8.5 Hz, 2H); 7.22 (m, 4H); 5.00 (m, 1H); 4.10 (m, 1H); 2.34 (s, 3H); 2.11 (m, 4H); 1.95 (m, 1H); 1.82 (m,1H); 1.54 (s, 36H). ^{13}CNMR (100MHZ, $CDCl_3$) δ/ppm: 150.66; 150.64; 150.59; 150.55; 150.52; 150.48; 150.09; 148.80; 147.47; 141.99; 141.10; 134.20; 133.42; 133.23; 133.16; 133.05; 132.46; 132.39; 132.22; 132.10; 131.92; 131.63; 131.42; 131.33; 130.28; 130.16; 130.06; 129.95; 122.95; 122.02; 120.97; 120.05; 105.97; 105.57; 69.57; 45.83; 35.56; 35.29; 34.00; 32.00; 24.94; 21.04. MS (*m/z*) MALDI: calc for $C_{66}H_{69}N_5Zn$ 995.48, found 995.7

Synthesis of 4: To a stirred solution of porphyrin **3** (110 mg, 0.11 mmol) in dichloromethane (50 mL) and pyridine (2 mL) NBS (23.4 mg, 0.80 mmol) was added at 23 °C. After stirring for 30 min, the reaction was quenched with acetone (20 mL). The solvent was removed under reduced pressure. The residue was purified by silica gel column chromatography using dichloromethane/hexane (1:4) as eluent to give the product (98 mg, 84%). ^{1}H-NMR (400 MHz, $CDCl_3$) δ/ppm: 9.75 (d, *J* = 4.5 Hz, 2H); 9.09 (d, *J* = 4.5 Hz, 2H); 9.03 (d, *J* = 4.5 Hz, 2H); 8.95 (dd, *J* = 8.0 Hz, 4.5 Hz, 2H); 8.07 (m, 4H); 7.91 (s, 1H); 7.81 (d, *J* = 2 Hz, 2H); 7.43 (d, *J* = 8.5 Hz, 2H); 7.22 (m, *J* = 4H); 5.01 (m, 1H); 4.09 (m, 1H); 2.38 (s, 3H); 2.11 (m, 4H); 1.96 (m, 1H); 1.80 (m, 1H); 1.54 (s, 36H). ^{13}CNMR (100MHZ, $CDCl_3$) δ/ppm: 151.29; 150.93; 150.89; 150.77; 150.72; 150.69; 149.92; 149.64; 148.67; 148.48; 147.43; 141.59; 140.82; 134.01; 133.48; 133.39; 132.67; 132.61; 132.52; 132.37; 131.86; 131.27; 131.15; 129.89; 129.79; 129.69; 129.63; 123.24; 123.00; 120.97; 119.95; 119.90; 105.84; 103.83; 69.41; 45.64; 35.40; 35.11; 34.92; 31.82; 24.80; 20.88. MS (*m/z*) MALDI: calc for $C_{66}H_{68}BrN_5Zn$ 1075.39, found 1075.4

Synthesis of VC70: In a dry Schlenck tube **4** (64 mg, 0.05 mmol) and 4-ethynyl benzoic acid (42.5 mg, 0.29 mmol) were dissolved in a mixture of dry tetrahydrofurane (18 mL) and NEt_3 (3.5 mL) and the solution was degassed with nitrogen for 10 min; $Pd_2(dba)_3$ (16.5 mg, 0.01 m mol) and $AsPh_3$ (36 mg, 0.11 m mol) were added to the mixture. The solution was refluxed for 6 h under nitrogen atmosphere. The solvent was removed under reduced pressure and the crude product was purified by silica gel column chromatography (dichloromethane:methanol, 6:4) to afford pure product as a green solid (42 mg, yield 62%). ^{1}H-NMR (400 MHz, THF-d8) δ/ppm: 9.81 (d, *J* = 4.5 Hz, 2H); 8.96 (t, *J* = 4.5 Hz, 4H); 8.81 (t, *J* = 4.5 Hz, 2H); 8.25 (d, *J* = 8.0 Hz, 2H); 8.16 (m, 6H); 7.93 (d, *J* = 8.5 Hz, 3H); 7.80 (d, *J* = 8.5 Hz, 1H); 7.45 (d, *J* = 8.0 Hz, 2H); 7.26 (m, 3H); 5.08 (m, 1H); 4.13 (m, 1H); 2.37 (s, 3H); 2.16 (m, 4H); 1.98 (m, 1H); 1.83 (m,1H); 1.59 (s, 36H). ^{13}C NMR (126 MHz, THF-d8) δ/ppm: 152.20, 150.76, 150.66, 150.46, 150.43, 150.02, 149.72, 148.52, 148.43, 148.42, 148.40, 147.38, 142.30, 140.81, 133.83, 133.16, 133.13, 132.53, 131.13, 131.07, 130.99, 130.91, 130.87, 129.83, 129.57, 124.26, 122.93, 122.91, 120.60, 119.84, 105.32, 97.31, 94.77, 69.25, 66.93, 66.76, 66.58, 66.40, 66.23, 66.05, 45.56, 35.90, 35.23, 34.91, 34.71, 33.90, 31.08, 31.07, 29.64, 24.82, 24.65, 24.49, 24.42, 24.33, 24.17, 24.01, 19.91. MS (*m/z*) MALDI: calc for $C_{75}H_{73}N_5O_2Zn$ 1139.51, found 1139.5

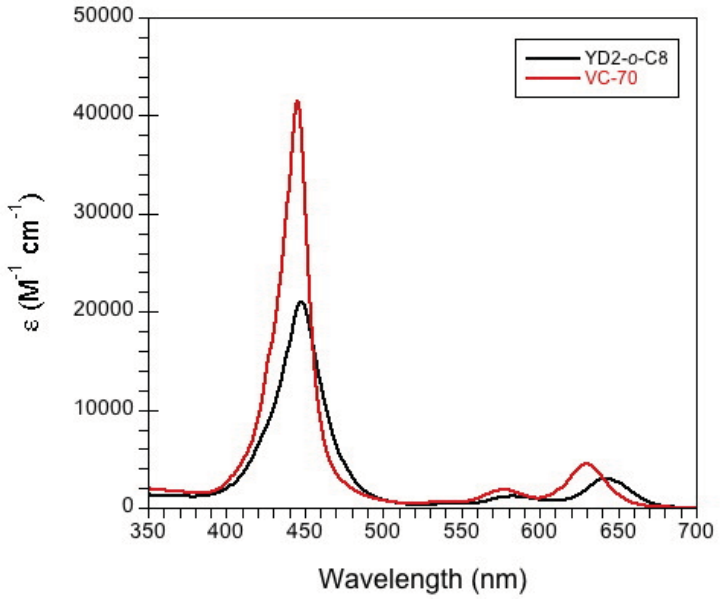

Figure 3.16. Molar extinction co-efficients of **YD2-*o*-C8** and **VC-70** in THF. The concentration was 1x 10^{-4} M.

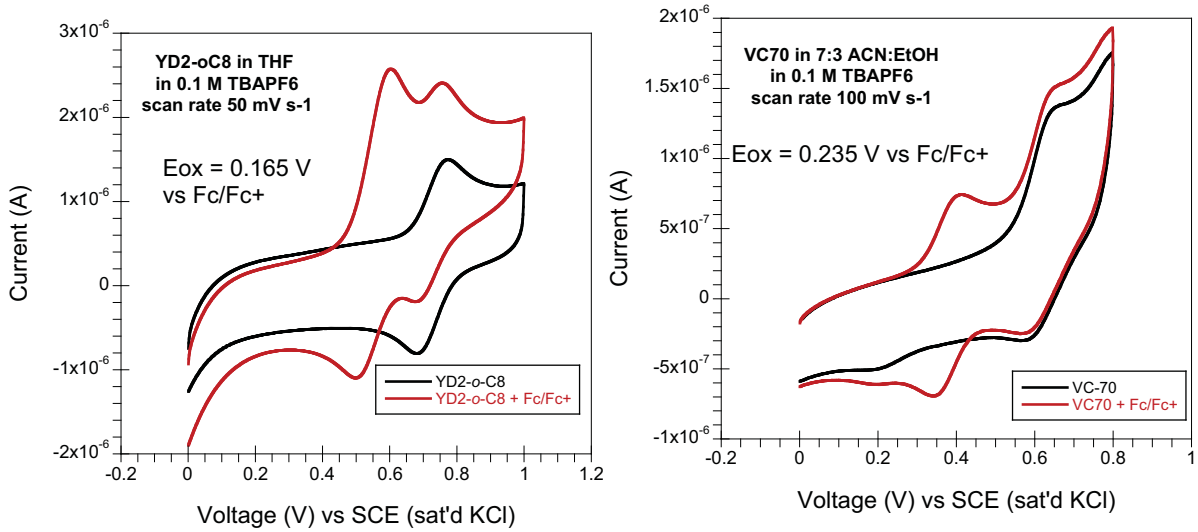

Figure 3.17. Cyclic voltammetry of **YD2-*o*-C8** (left) and **VC-70** (right) recorded in 0.1M tetrabutylammonium hexafluorphosphate in THF at scan rates of 50 mV s^{-1} (**YD2-*o*-C8**) and 100 mV s^{-1} (**VC-70**). The working electrode consisted of a platinum wire and the counter electrode a platinum mesh. The reference electrode was the silver calomel electrode (saturated KCl). All solutions were degassed with argon for 5 mins prior to measurement. The red and black scans were recorded in the presence and absence of Ferrocene/Ferrocenium^{+}.

2.5.3. Device fabrication and optimization conditions

Several conditions were tested for **VC-70** trying to optimize the device efficiency in our conditions. The following data gives an overview of the work carried out.

Devices were made using the following specifications: same dye concentration and different solvent.

Polymer: Surlyn

Working and counter electrodes: TEC15

Blocking Layer

Paste: Dyesol 8+4 and 12+4 (20 nm, 400 nm)

Area cell: 0,16 cm^2

Electrolyte: ***Z960:*** 1 M BMII, 0.03 M I_2, 0.5 M TBP, 0.1 M Guan and 0.05 M LiI in ACN/VAL (85:15)

LP1: 0,5 M BMII, 0,05 M I_2, 0,5 M TBP and 0,1 M LiI in ACN

Solution: 0,2 mM Dye (1,14 mg) and 0,4 mM cheno (0,81 mg) in ethanol or acetonitrile/t-butanol (1:1). Overnight at RT

Table 3.5. Device properties of **VC-70** devices using ethanol as solvent in the dye solution.

Thickness (µm)	Electrolyte	J_{sc}/mA cm^{-2}	V_{oc}/V	FF (%)	$\eta^{(\%)a}$
8+4	LP1	13.41	0.704	73	6.86
8+4	Z960	14.72	0.739	67	7.31
12+4	LP1	12.90	0.680	73	6.39
12+4	Z960	14.00	0.730	68	6.97

[c] Efficiencies recorded with mask.

Table 3.6. Device properties of **VC-70** devices using acetonitrile/*t*-buthanol (1:1) as solvent in the dye solution.

Thickness (µm)	Electrolyte	J_{sc}/mA cm^{-2}	V_{oc}/V	FF (%)	$\eta^{(\%)a}$
8+4	LP1	13.68	0.685	71	6.66
8+4	Z960	14.97	0.734	65	7.10
12+4	LP1	14.17	0.675	72	6.91
12+4	Z960	15.06	0.734	67	7.36

[c] Efficiencies recorded with mask.

References

1. Campbell, W. M.; Burrell, A. K.; Officer, D. L.; Jolley, K. W., Porphyrins as light harvesters in the dye-sensitised TiO2 solar cell. *Coord. Chem. Rev.* **2004,** *248*, 1363-1379.
2. (a) O'Regan, B.; Grätzel, M., A low-cost, high-efficiency solar cell based on dye-sensitized colloidal TiO2 films. *Nature* **1991,** *353*, 737-740; (b) Hagfeldt, A.; Boschloo, G.; Sun, L.; Kloo, L.; Pettersson, H., Dye-Sensitized Solar Cells. *Chem. Rev.* **2010,** *110*, 6595-6663; (c) Clifford, J. N.; Martinez-Ferrero, E.; Palomares, E., Dye mediated charge recombination dynamics in nanocrystalline TiO2 dye sensitized solar cells. *J. Mater. Chem.* **2012,** *22*, 12415-12422; (d) Robertson, N., Catching the Rainbow: Light Harvesting in Dye-Sensitized Solar Cells. *Angew. Chem., Int. Ed.* **2008,** *47*, 1012-1014.
3. (a) Clifford, J. N.; Planells, M.; Palomares, E., Dye mediated charge recombination dynamics in nanocrystalline TiO2 dye sensitized solar cells. *J. Mater. Chem.* **2012,** *22*, 24195-24201; (b) Mishra, A.; Fischer, M. K. R.; Bäuerle, P., Metal-Free Organic Dyes for Dye-Sensitized Solar Cells: From Structure: Property Relationships to Design Rules. *Angew. Chem., Int. Ed.* **2009,** *48*, 2474-2499.
4. (a) Bessho, T.; Zakeeruddin, S. M.; Yeh, C.-Y.; Diau, E. W.-G.; Grätzel, M., Highly Efficient Mesoscopic Dye-Sensitized Solar Cells Based on Donor–Acceptor-Substituted Porphyrins. *Angew. Chem., Int. Ed.* **2010,** *49*, 6646-6649; (b) Chang, Y.-C.; Wang, C.-L.; Pan, T.-Y.; Hong, S.-H.; Lan, C.-M.; Kuo, H.-H.; Lo, C.-F.; Hsu, H.-Y.; Lin, C.-Y.; Diau, E. W.-G., A strategy to design highly efficient porphyrin sensitizers for dye-sensitized solar cells. *Cem. Commun.* **2011,** *47*, 8910-8912; (c) Wang, C.-L.; Chang, Y.-C.; Lan, C.-M.; Lo, C.-F.; Diau, E. W.-G.; Lin, C.-Y., Enhanced light harvesting with π-conjugated cyclic aromatic hydrocarbons for porphyrin-sensitized solar cells. *Energy Environ. Sci.* **2011,** *4*, 1788-1795.
5. (a) Feldt, S. M.; Gibson, E. A.; Gabrielsson, E.; Sun, L.; Boschloo, G.; Hagfeldt, A., Design of Organic Dyes and Cobalt Polypyridine Redox Mediators for High-Efficiency Dye-Sensitized Solar Cells. *J. Am. Chem. Soc.* **2010,** *132*, 16714-16724; (b) Wang, M.; Grätzel, C.; Zakeeruddin, S. M.; Grätzel, M., Recent developments in redox electrolytes for dye-sensitized solar cells. *Energy Environ. Sci.* **2012,** *5*, 9394-9405; (c) Cong, J.; Yang, X.; Kloo, L.; Sun, L., Iodine/iodide-free redox shuttles for liquid electrolyte-based dye-sensitized solar cells *Energy Environ. Sci.* **2012,** *5*, 9180-9194; (d) Mosconi, E.; Yum, J.-H.; Kessler, F.; Gomez-Garcia, C. J.; Zuccaccia, C.; Cinti, A.; Nazeeruddin, M. K.; Grätzel, M.; De Angelis, F., Cobalt electrolyte/dye interactions in dye-sensitized solar cells: a combined computational and experimental study. *J. Am. Chem. Soc.* **2012,** *134*, 19438-19453.
6. Yella, A.; Lee, H. W.; Tsao, H. N.; Yi, C. Y.; Chandiran, A. K.; Nazeeruddin, M. K.; Diau, E. W.-G.; Yeh, C.-Y.; Zakeeruddin, S. M.; Grätzel, M., Porphyrin-Sensitized Solar Cells with Cobalt (II/III)–Based Redox Electrolyte Exceed 12 Percent Efficiency. *Science* **2011,** *334*, 629-634.
7. (a) Li, L. L.; Diau, E. W.-G., Porphyrin-sensitized solar cells. *Chem. Soc. Rev.* **2013,** *42*, 291-304; (b) Imahori, H.; Hayashi, S.; Hayashi, H.;

Oguro, A.; Eu, S.; Umeyama, T.; Matano, Y., Effects of Porphyrin Substituents and Adsorption Conditions on Photovoltaic Properties of Porphyrin-Sensitized TiO2 Cells. *J. Phys. Chem. C* **2009,** *113*, 18406-18413; (c) Martinez-Diaz, M. V.; de la Torre, G.; Torres, T., Lighting porphyrins and phthalocyanines for molecular photovoltaics. *Chem. Commun.* **2010,** *46*, 7090-7108.

8. Lindsey, J. S.; Prathapan, S.; Johnson, T. E.; Wagner, R. W., Porphyrin building blocks for modular construction of bioorganic model systems. *Tetrahedron* **1994,** *50*, 8941-8968.

9. Liu, B.; Zhu, W.; Wang, Y.; Wu, W.; Li, X.; Chen, B.; Long, Y.-T.; Xie, Y., Modulation of energy levels by donor groups: an effective approach for optimizing the efficiency of zinc-porphyrin based solar cells. *J. Mater. Chem.* **2012,** *22*, 7434-7444.

10. Cardona, C. M.; Li, W.; Kaifer, A. E.; Stockdale, D.; Bazan, G. C., Electrochemical Considerations for Determining Absolute Frontier Orbital Energy Levels of Conjugated Polymers for Solar Cell Applications *Adv. Mater.* **2011,** *23*, 2367-2371.

11. Bai, Y.; Zhang, J.; Zhou, D.; Wang, Y.; Zhang, M.; Wang, P., Engineering Organic Sensitizers for Iodine-Free Dye-Sensitized Solar Cells: Red-Shifted Current Response Concomitant with Attenuated Charge Recombination. *J. Am. Chem. Soc.* **2011,** *133* (11442-11445).

12. Wu, H.-P.; Ou, Z.-W.; Pan, T.-Y.; Lan, C.-M.; Huang, W.-K.; Lee, H. W.; Reddy, N. M.; Chen, C.-T.; Chao, W.-S.; Yeh, C.-Y.; Diau, E. W.-G., Molecular engineering of cocktail co-sensitization for efficient panchromatic porphyrin sensitized solar cells. *Energy Environ. Sci.* **2012,** *5*, 9845-9848.

13. Koops, S. E.; Barnes, P. R. F.; O'Regan, B.; Durrant, J. R., Kinetic Competition in a Coumarin Dye-Sensitized Solar Cell: Injection and Recombination Limitations upon Device Performance. *J. Phys. Chem. C* **2010,** *114*, 8054-8061.

14. Tatay, S.; Haque, S. A.; O'Regan, B.; Durrant, J. R.; Verhees, W. J. H.; Kroon, J. M.; Vidal-Ferran, A.; Gavina, P.; Palomares, E., Kinetic competition in liquid electrolyte and solid-state cyanine dye sensitized solar cells. *J. Mater. Chem.* **2007,** *17*, 3037-3044.

15. Zewdu, T.; Clifford, J. N.; Hernandez, J. P.; Palomares, E., Photo-induced charge transfer dynamics in efficient TiO2/CdS/CdSe sensitized solar cells. *Energy Environ. Sci.* **2011,** *4*, 4633-4638.

16. Nguyen, H.-M.; Mane, R. S.; Ganesh, T.; Han, S.-H.; Kim, N., Aggregation-Free ZnO Nanocrystals Coupled HMP-2 Dye of Higher Extinction Coefficient for Enhancing Energy Conversion Efficiency. *J. Phys. Chem. C* **2009,** *113*, 9206-9209.

17. Jung, H. S.; Lee, J. K., Dye Sensitized Solar Cells for Economically Viable Photovoltaic Systems. *J. Phys. Chem. Lett.* **2013,** *4*, 1682-1693.

18. (a) Zeng, W.; Cao, Y.; Bai, Y.; Wang, Y.; Shi, Y.; Zhang, M.; Wang, F.; Pan, C.; Wang, P., Efficient Dye-Sensitized Solar Cells with an Organic Photosensitizer Featuring Orderly Conjugated Ethylenedioxythiophene and Dithienosilole Blocks. *Chem. Mater.* **2010,** *22*, 1915-1925; (b) Yum, J.-H.; Holcombe, T. W.; Kim, Y.; Rakstys, K.; Moehl, T.; Teuscher, J.; Delcamp, J. H.; Nazeeruddin, M. K.; Grätzel, M., Blue-Coloured Highly Efficient Dye-

Sensitized Solar Cells by Implementing the Diketopyrrolopyrrole Chromophore. *Scientific Reports* **2013,** *3*, 2446.
19. (a) Wang, C.-L.; Lan, C.-M.; Hong, S.-H.; Wang, Y.-F.; Pan, T.-Y.; Chang, C.-W.; Kuo, H.-H.; Kuo, M.-Y.; Diau, E. W.-G.; Lin, C.-Y., Enveloping porphyrins for efficient dye-sensitized solar cells. *Energy Environ. Sci.* **2012,** *5*, 6933-6940; (b) Campbell, W. M.; Jolley, K. W.; Wagner, P.; Wagner, K.; Walsh, P. J.; Gordon, K. C.; Schmidt-Mende, L.; Nazeeruddin, M. K.; Wang, Q.; Grätzel, M., Highly Efficient Porphyrin Sensitizers for Dye-Sensitized Solar Cells. *J. Phys. Chem. C* **2007,** *111*, 11760-11762; (c) Wang, C.-L.; Chang, Y.-C.; Lan, C.-M.; Lo, C.-F.; Wei-Guang Diau, E.; Lin, C.-Y., Enhanced light harvesting with [small pi]-conjugated cyclic aromatic hydrocarbons for porphyrin-sensitized solar cells. *Energy & Environmental Science* **2011,** *4* (5), 1788-1795.
20. Masi Reddy, N.; Pan, T.-Y.; Christu Rajan, Y.; Guo, B.-C.; Lan, C.-M.; Wei-Guang Diau, E.; Yeh, C.-Y., Porphyrin sensitizers with [small pi]-extended pull units for dye-sensitized solar cells. *Physical Chemistry Chemical Physics* **2013,** *15* (21), 8409-8415.
21. Kang, M. S.; Choi, I. T.; Kim, Y. W.; You, B. S.; Kang, S. H.; Hong, J. Y.; Ju, M. J.; Kim, H. K., Novel D-[small pi]-A structured Zn(ii)-porphyrin dyes with bulky fluorenyl substituted electron donor moieties for dye-sensitized solar cells. *Journal of Materials Chemistry A* **2013,** *1* (34), 9848-9852.
22. (a) Cabau, L.; Pelleja, L.; Clifford, J. N.; Kumar, C. V.; Palomares, E., Light soaking effects on charge recombination and device performance in dye sensitized solar cells based on indoline-cyclopentadithiophene chromophores. *Journal of Materials Chemistry A* **2013,** *1* (31), 8994-9000; (b) Wu, H.-P.; Ou, Z.-W.; Pan, T.-Y.; Lan, C.-M.; Huang, W.-K.; Lee, H.-W.; Masi Reddy, N.; Chen, C.-T.; Chao, W.-S.; Yeh, C.-Y.; Diau, E. W.-G., Molecular engineering of cocktail co-sensitization for efficient panchromatic porphyrin-sensitized solar cells *Energy & Environmental Science* **2012,** *5*, 9843-9848; (c) Wu, Y.; Zhang, X.; Li, W.; Wang, Z.-S.; Tian, H.; Zhu, W., Hexylthiophene-Featured D–A–π–A Structural Indoline Chromophores for Coadsorbent-Free and Panchromatic Dye-Sensitized Solar Cells. *Adv. Energy Mat.* **2012,** *2*, 149-156.
23. Hsieh, C.-P.; Lu, H.-P.; Chiu, C.-L.; Lee, C.-W.; Chuang, S.-H.; Mai, C.-L.; Yen, W.-N.; Hsu, S.-J.; Diau, E. W.-G.; Yeh, C.-Y., Synthesis and characterization of porphyrin sensitizers with various electron-donating substituents for highly efficient dye-sensitized solar cells. *J. Mater. Chem.* **2010,** *20*, 1127-1134.
24. Aljarilla, A.; Clifford, J. N.; Pellejà, L.; Moncho, A.; Arrechea, S.; de la Cruz, P.; Langa, F.; Palomares, E., Effect of porphyrin loading on performance of dye sensitized solar cells based on iodide/tri-iodide and cobalt electrolytes. *J. Mater. Chem.* **2013,** *1*, 13640-13647.
25. Wagner, K.; Griffith, M. J.; James, M.; Mozer, A. J.; Wagner, P.; Triani, G.; Officer, D. L.; Wallace, G. G., Significant Performance Improvement of Porphyrin-Sensitized TiO2 Solar Cells under White Light Illumination. *J. Phys. Chem. C* **2011,** *115*, 317-326.
26. Griffith, M. J.; Sunahara, K.; Furube, A.; Mozer, A. J.; Officer, D. L.; Wagner, P.; Wallace, G. G.; Mori, S., Cation Exchange at Semiconducting

Oxide Surfaces: Origin of Light-Induced Performance Increases in Porphyrin Dye-Sensitized Solar Cells. *J. Phys. Chem. C* **2013,** *117*, 11885-11898.
27. Ito, S.; Miura, H.; Uchida, S.; Takata, M.; Sumioka, K.; Liska, P.; Comte, P.; Pechy, P.; Grätzel, M., High-conversion-efficiency organic dye-sensitized solar cells with a novel indoline dye. *Chem. Commun.* **2008,** *41*, 5194-5196.
28. Miyata, O.; Takeda, N.; Kimura, Y.; Takemoto, Y.; Tohnai, N.; Miyata, M.; Naito, T., Efficient synthesis of indoles using [3,3]-sigmatropic rearrangement of N-trifluoroacetyl enehydrazines. *Tetrahedron* **2006,** *62*, 3629-3647.
29. Zhu, W.; Wu, Y.; Wang, S.; Li, W.; Li, X.; Chen, J.; Wang, Z.-S.; Tian, H., Organic D-A-π-A Solar Cell Sensitizers with Improved Stability and Spectral Response. *Adv. Funct. Mater.* **2011,** *21* (756-763).

Chapter 4.
Anchoring effects on phtalocyanines

The use of phthalocyanine dyes is an approach to long-wavelength sensitization. Phtalocyanines display an intense absorption in the Q band at low energy as well as a higher energy Soret band. However, studies on phthalocyanines are troubled by poor solubility and also by their tendency to aggregate on the TiO_2 surface, which leads to deactivation of the excited state of the dye.

In this chapter, in order to avoid aggregation of the photosensitizer, three phtalocyanines based DSCs with Ti(IV) as the central metal were studied. In principle, this configuration introduces strongly attached axial ligands that prevent aggregation of the macrocycles. All the compounds are fully photophysical and electrochemical characterized and the device properties are completely investigated.

Index

Chapter 4. Anchoring effects on phtalocyanines

1. Paper 3: Ti(IV) phtalocyanines for dye sensitized solar cells

M. Salomé Rodríguez-Morgade,[a] Laia Pellejà,[b] Tomás Torres,*[a,c] and Emilio Palomares*[bd]

[a]Departamento de Química Orgánica, Universidad Autónoma de Madrid, Cantoblanco, 28049 Madrid, Spain. E-mail: tomas.torres@uam.es
[b]Institute of Chemical Research of Catalonia (ICIQ), 43007 Tarragona, Spain. E-mail: epalomares@iciq.es
[c]IMDEA-Nanociencia, Faraday 9, Campus de Cantoblanco, 28049 Madrid, Spain.
[d]ICREA, Passeig Lluís Companys 23, 08010 Barcelona, Spain

Dedicated to Professor Evgeny Luk'yanets on the occasion of his 75th birthday.

J. Porphyrins Phtalocyanines **2013**, 17, 816-820

Abstract: Ti(IV) phthalocyanines axially coordinated to 2,3- and 1,8-naphthalenediols have been prepared and characterized. The naphthalene axial ligands have been endowed with none, one or two sulfonate anchoring groups in order to study the performance of the dyes as DSSC photosensitizers. All studied compounds showed the same efficiency. The unexpected results suggest displacement of the axial ligand with concomitant formation of a di-μ-oxotitanium-type anchoring moiety between the hydroxylated TiO_2 surface and the Ti-phthalocyanine. This is probably the reason why the type of axial ligand does not play any role on the overall device efficiency. The titanium phthalocyanine absorbed in this way shows state selective electron injection were only those photons absorbed by the Soret band are capable to inject electrons into the TiO_2, while photons absorbed by the Q-band result in negligible photocurrent. This fact could explain the low efficiency of the Ti-phthalocyanines.

1.1. Introduction

Solar energy is one of the essential energy sources that is expected to provide energy for the future. However, harvesting solar light and converting it into chemical fuels or electricity at low cost remains a huge challenge. One of the most promising areas is that of organic photovoltaic cells (OPV), which employs organic constituents for light harvesting or charge carrier transport. In particular, dye-sensitized solar cells (DSCs)[1] and related electrochemical systems have emerged as a promising technology for converting solar light into electricity. Their main advantages rely on their low processing costs

together with their versatility, owing to the possibility of tuning the photophysical behavior of the organic dye thus adapting the device to every particular application.[2] Therefore, one of the main components in DSCs is a suitable photosensitizer with strong spectral response in the red and near-IR regions.

As an alternative to ruthenium complexes, porphyrins and their synthetic analogs are being tested as the organic components of photovoltaic and artificial photosynthetic devices. Among them, phthalocyanines show high potential as DSCs photosensitizers. In fact, they exhibit very high extinction coefficients in a wavelength range that extends to around 700 nm, where the maximum of the solar photon flux occurs.[3] Importantly, the NIR features the majority of the sunlight intensity, so their optical properties make the phthalocyanines inevitable donor participants in photovoltaics. On the other hand, Pcs have emerged as excellent light harvesting antennas for their incorporation into donor–acceptor systems, mainly in connection with carbon nanostructures as acceptor moieties.[4] Lastly, the electronic properties of phthalocyanines can be fine-tuned by synthetic modification, which can be performed by functionalizing their peripheral positions, replacing the central metal ion and/or providing these metallorganic dyes with axial ligands. So far, the photovoltaic conversion efficiency record for a phthalocyanine-based DSC is 5.5% and 6.1% under 100 and 9.5 mW cm^{-2} intensities of standard AM 1.5G, respectively.[5]

Titanium(IV) phthalocyanines have been comprehensively investigated for the photogeneration of charge carriers,[6] NLO properties[7] and DSC photosensitizers.[8] Here, we report the synthesis of new titanium phthalocyanines **1** and **2**, bearing sulfonic acid moieties at their axial ligands for their application to the sensitization of nanocrystalline, mesoporous TiO_2 films. The use of Ti(IV) as the phthalocyanine central metal allows to introduce robustly attached axial ligands that prevent aggregation of the macrocycles. Besides, the sulfonic acid moieties are employed to strongly anchor the dye to the nanocrystalline TiO_2 particles.[9] By using this axial ligation approach, we wish to control the distance between the HOMO orbital of the chromophore and the TiO_2 surface and thereby the electron injection and recombination dynamics.

1.2. Results and discussion

1.2.1. Synthesis

The macrocycles were substituted with four peripheral *tert*-butyl groups in order to provide good solubility in organic solvents and prevent aggregation. The preparation of the axially substituted titanium(IV) phthalocyanines was carried out based on a reported procedure in which oxotitaniumphthalocyanine **4** was used as the synthetic precursor an treated with a diol.[10] The reaction is based upon the rupture of the Ti=O double bond in Pc **4** and the successive formation of two Ti–O single bonds. As the diol donor ligands, we employed two naphthalene derivatives containing the two alcohol functions at different positions, namely, 2,3- and 1,8-naphthalenediols, so that the distance and hence, the communication between the dye and the TiO_2 should be different in each case. In order to enhance solubility in organic solvents, commercially available sodium sulfonates were converted into the corresponding tetrabutylammonium salts by treating the sodium salt with tetrabutylammonium fluoride. Phthalocyanine **1**, containing tetrabutylammonium 6,7-dihydroxynaphthalene-2-sulfonate as the axial ligand, was synthesized in 74% yield by reaction of Pc **4** with the corresponding diol in acetonitrile at 80°C (Scheme 4.1).

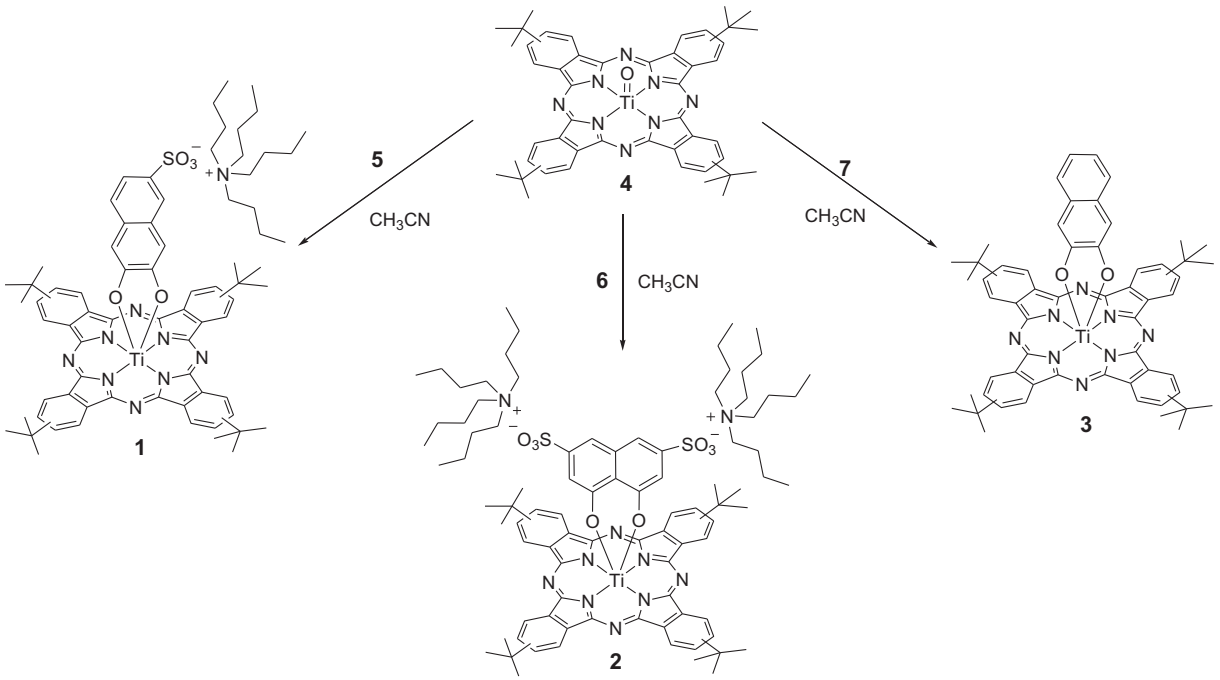

5: tetrabutylammonium 6,7-dihydroxynaphthalene-2-sulfonate
6: tetrabutylammonium 4,5-dihydroxynaphthalene-2,7-disulfonic acid
7: 6,7-dihydroxynaphthalene-2-sulfonate

Scheme 4.1. Synthesis of titanium phtalocyanines **1**, **2** and **3**.

Phthalocyanine **2** was obtained under similar conditions using tetrabutylammonium 4,5-dihydroxynaphthalene-2,7-disulfonate as the diol. Additionally, phthalocyanine **3** (Scheme 4.1), lacking any anchoring group, was prepared as a reference following a similar protocol but doing the reaction in chloroform.[7]

All new compounds were characterized by ^{1}H and ^{13}C NMR, UV-vis and IR spectroscopies and mass spectrometry. Phthalocyanine **3** displayed its molecular ion in MALDI-TOF MS, positive mode, at *m*/z = 942 $[M]^+$. Likewise, phthalocyanine **1** exhibited in negative mode its molecular ion at *m*/z = 1021 $[M - NBu_4]^-$, while the two-fold charged phthalocyanine **2** showed in FAB, negative mode, three main peaks at *m*/z = 1342 $[M - NBu_4]^-$, *m*/z = 1101 $[M–2NBu_4 +H]^-$ and *m*/z = 550 $[M - 2NBu_4]^{2-}$. ^{1}H NMR provided very useful information for the structural characterization of **1-3**. In these macrocycles, the axial ligands are placed under the influence of the phthalocyanine diatropic ring current, in the shielding cone. Therefore, all signals corresponding to those ligands are strongly shifted to high field as a function of their distance to the macrocycle's geometric center. Thus, for example, phthalocyanine **3** exhibits its closer naphthalene $H^{1',4'}$ protons as a singlet at 4.76 ppm and the further $H^{5',6',7',8'}$ protons as a multiplet at 6.5-6.6 ppm. Similarly, phthalocyanine **1** displayed their closer $H^{5',8'}$ naphthalene protons as two singlets at 4.72 and 4.70 ppm, that are by 2.5 ppm shielded with respect to the precursor, while the furthest $H^{3'}$ proton is shifted only 0.4 ppm (Figure 4.1). Finally, the closer $H^{3',6'}$ protons in **2** appear at 5.58 ppm, whereas the further $H^{1',8'}$ signals are seen at 7.15 ppm (1.8 and 0.7 ppm high-field shifted, respectively, Figure 4.1).

IR spectroscopy reveals strong bands at 1022 and 1036 cm^{-1} corresponding to the stretching vibration of the SO_3^- groups in phthalocyanines **1** and **2**, respectively. Moreover, the bands corresponding to O–H stretching at 3000–3400 cm^{-1} disappear on going from the diols to the diolates **1** and **2**. UV-vis spectrum of phthalocyanine **3** displays a single Q-band at 703 nm and a Soret absorption at 353 nm. The introduction of a sulfonic group at the naphthalene axial ligand does not significantly alter the optical properties of the Pc ring. However, on going from phthalocyanines **1** and **3**, with the axial ligand attached to the central titanium(IV) ion through the 2 and 3 naphthalene positions, to phthalocyanine **2**, with the axial ligand attached through the 1 and 8 naphthalene positions, small bathochromic shifts of 3-4 nm both in the Q- and B-bands are detected. Whether this small change in phthalocyanine **2** arises from the naphthalene attachment mode, or the closer proximity of the two electron-withdrawing sulfonic groups to the Pc

ring, remains unclear.[7]

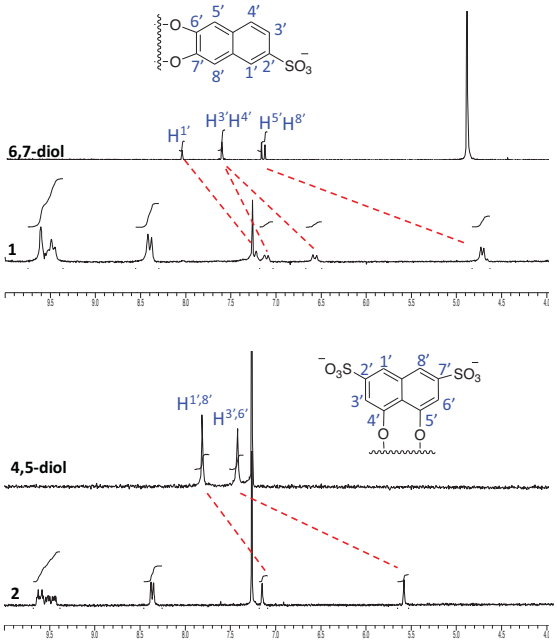

Figure 4.1. Comparison between ^{1}H NMR spectra (aromatic protons) of phtalocyanines **1** and **2** and their diol precursors.

1.2.2. Device preparation and characterization

In the present work for efficient DSCs, devices were made using 8 µm thick films consisting of 20 nm TiO_2 nanoparticles (Dyesol paste) and a scatter layer of 4 µm of 400 nm TiO_2 particles (Dyesol paste). Prior to the deposition of the TiO_2 paste, the conducting glass substrates were immersed in a solution of $TiCl_4$ (40 mM) for 30 min and then dried. The TiO_2 nanoparticle paste was deposited onto a conducting glass substrate (TEC15, Pilkington) using the screen printing technique. The TiO_2 electrodes were gradually heated under an airflow at 325°C for 5 min, 375ºC for 5 min, 450ºC for 15 min and 500ºC for 15 min. The heated TiO_2 electrodes were immersed again in a solution of $TiCl_4$ (40 mM) at 70ºC for 30 min and then washed with ethanol. The electrodes were heated again at 500ºC for 30 min and cooled before sensitization. The counter electrode was made by spreading a 5 mM solution of H_2PtCl_6 in isopropyl alcohol onto a conducting glass substrate (TEC15, Pilkington) with a small hole to allow the introduction of the liquid electrolyte using vacuum, followed by heating at 390ºC for 15 min. Dye solutions of phthalocyanines **1**, **2** and **3** at concentrations of 0.3 mM in chloroform were prepared and films immersed for two hours at room temperature. The sensitized electrodes were washed with chloroform and dried under air. Finally, the working and counter electrodes were sandwiched together using a

thin thermoplastic (Surlyn) frame that melts at 100ºC. For these solar cells the electrolyte used consisted of 0.5 M 1-butyl-3-methylimidazolium iodide (BMII), 0.1 M lithium iodide, 0.05 M iodine and 0.5 M 4-*tert*-butylpyridine in acetonitrile.

The IV characteristics of cells were measured using a Sun 2000 Solar Simulator (150 W, ABET Technologies). The illumination intensity was measured to be 100 mW m^{-2} with a calibrated silicon photodiode. The appropriate filters were utilized to faithfully simulate the AM 1.5G spectrum. The applied potential and cell current were measured with a Keithley 2400 digital source meter.

1.2.3. Device properties

Figure 4.2 and Table 4.1 show the IV curves and cell characteristics, namely J_{sc}, V_{oc}, fill factor (FF) and overall efficiency (η) for phthalocyanines **1**, **2** and **3** DSC devices.

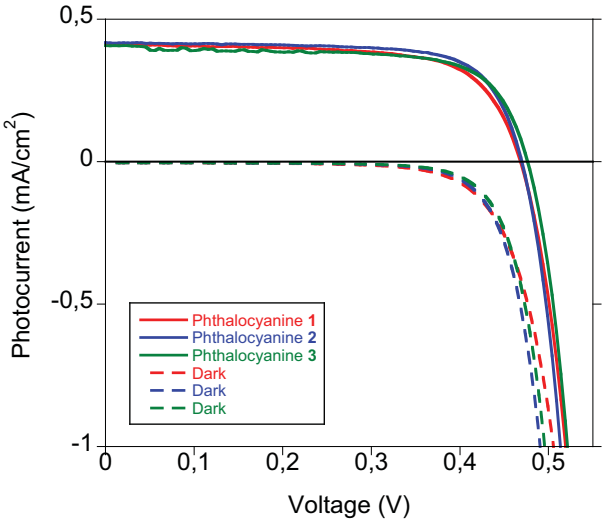

Figure 4.2. IV curves of phtalocyanines **1**, **2** and **3** DSC devices recorded with mask under AM 1.5G 1 sun illumination and in the dark.

Table 4.1. Photovoltaic performance of cells recorded under AM 1.5G 1 sun illumination.

Dye	J_{sc}/mA cm^{-2}	V_{oc}/V	FF (%)	$\eta^{a\ (\%)}$
1	0.42	0.469	72	0.14
2	0.41	0.479	69	0.13
3	0.41	0.469	69	0.13

As it can be seen in Figure 4.2, all sensitizers lead to identical photovoltage and photocurrent with outstanding fill factor values. Interestingly,

reference compound **3**, lacking any anchoring group, gave similar results to **1** and **2**. Thus, the device parameters under working conditions (sun simulated light at 100 mW m^{-2}) are not influenced by the axial ligand structure. It is very likely that the anchoring process onto the TiO_2 surface leads to the displacement of the axial ligand, thus generating a di-μ-oxodi- or trititanium-type anchoring moiety between the hydroxylated TiO_2 surface and the Ti-phthalocyanine (Figure 4.3).[10] In other words, molecules **1-3** are not stable in these conditions. Most probably, all three compounds undergo a ligand exchange with the TiO_2, giving rise to the same species adsorbed on the inorganic semiconductor, namely the one(s) represented in Figure 4.3. This interchange takes place only with the catecholates **1-3**, since a DSC experiment carried out with "free" oxotitaniumphthalocyanine **4**, in the same conditions mentioned above for **1-3**, afforded a negligible efficiency of 0.001%, thus indicating that this Pc is not adsorbed on the TiO_2.

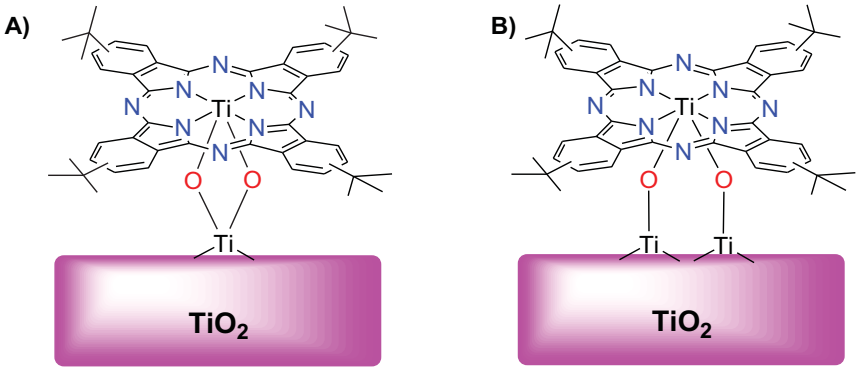

Figure 4.3. Possible bidentate chelating (di-μ-oxodititanium) and bidentate bridging (di-μ-oxotrititanium) modes for titanium(IV) phtalocyanines.

The lower photocurrent observed for this TiO_2-adsorbed Ti-Pc (Figure 4.2) is mainly due to the low efficiency of the electron injection process from the molecule excited state to the TiO_2 conduction band (CB). As it has been reported before,[8] Ti-phthalocyanine shows state selective electron injection were only those photons absorbed by the Soret band are capable to inject electrons into the TiO_2 while photons absorbed by the Q-band result in negligible photocurrent.

1.3. Experimental

1.3.1. General

UV-vis spectra were recorded with a Hewlett-Packard 8453 instrument. IR spectra were recorded with Bruker Vector 22 spectrophotometer. FAB-MS

spectra were determined on a VG AutoSpec instrument. MALDI-TOF MS spectra were recorded with a Bruker Reflex III spectrometer. NMR spectra were recorded with a Bruker WM-200-SY and Bruker AC-300 instruments. Column chromatographies were carried out on silica gel Merck-60 (230–400 mesh, 60 Å). TLC was performed on aluminium sheets precoated with silica gel 60 F_{254} (E. Merck). Chemicals were purchased from Aldrich Chemical Co. and used as received without further purification. Oxotitaniumphthalocyanine **4** was prepared using a reported procedure.[7]

1.3.2. Synthesis

Preparation of tetrabutylammonium 6,7-dihydro-xynaphthalene-2-sulfonate. To a solution of sodium 6,7-dihydroxynaphthalene-2-sulfonate hydrate (500 mg, 1.84 mmol) in water (10 mL), a solution of tetrabutylammonium fluoride (2.09 g, 8 mmol) in water (10 mL) was added. The mixture was stirred for 10 min and the obtained white precipitate was filtered, washed with water and dried, affording 535 mg (60%) of tetrabutylammonium 6,7-dihydroxynaphthalene-2-sulfonate as a white, crystalline solid. ^{1}H NMR (200 MHz; MeOD): δ_H, ppm 8.04 (s, 1H, $H^{1'}$), 7.60 (s, 2H, $H^{3',4'}$), 7.17, 7.13 (2s, 2H, $H^{5',8'}$), 3.1-3.2 (m, 12H, NCH_2), 1.6-1.7 (m, 12H, NCH_2CH_2), 1.3-1.5 (m, 12H, $NCH_2CH_2CH_2$), 1.02 (t, 16H, CH_3). ^{13}C NMR (50 MHz; MeOD): δ_C, ppm 149.2, 148.7, 141.1, 131.4, 129.5, 127.0, 124.6, 121.6, 111.3, 110.5, 59.3 ($C^{1'}$), 24.7, 20.6 ($C^{2'}$, $C^{3'}$), 13.9 ($C^{4'}$). IR (KBr): v, cm^{-1} 3418, 3221, 3040 (OH), 2964, 2874 (C–H), 1622, 1539, 1477, 1412, 1387, 1254, 1225, 1159, 1092, 1030 (SO_3^-), 864, 806, 781, 719, 748, 625. MS (FAB$^-$, NBA): *m*/z 239 $[M - Nbu_4]^-$.

Preparation of tetrabutylammonium 4,5-dihydro- xynaphthalene-2,7-disulfonate. A mixture of sodium 4,5-dihydroxynaphthalene-2,7-disulfonate (500 mg, 1.25 mmol) and tetrabutylammonium fluoride (719 mg, 2.75 mmol) in ethanol (200 mL), was stirred for 60 min until a fine suspension of NaF was observed. The mixture was filtered over Celite and the solvent was rotary evaporated. The residue was resuspended in ethyl acetate, filtered, repeatedly washed with this solvent and dried, affording 709 mg (71%) of tetrabutylammonium 4,5-dihydroxynaphthalene-2,7-disulfonate as a white, crystalline solid. ^{1}H NMR (200 MHz; $CDCl_3$): δ_H, ppm 10.81 (s, 2H, OH), 7.81 (s, 2H, $H^{1',8'}$), 7.42 (s, 2H, $H^{3',6'}$), 3.0-3.1 (m, 12H, NCH_2), 1.3-1.4 (m, 12H, NCH_2CH_2), 1.2-1.3 (m, 12H, $NCH_2CH_2CH_2$), 0.89 (t, 16H, CH_3). ^{13}C NMR (50 MHz; $CDCl_3$): δ_C, ppm 126.0, 145.8, 136.6, 118.7, 117.1, 108.3, 59.5 ($C^{1'}$), 24.7, 20.8 ($C^{2'}$, $C^{3'}$), 14.0 ($C^{4'}$). IR (KBr): v, cm^{-1} 3420, 3231 (OH), 2966, 2872 (C–H), 1693, 1481, 1379, 1292, 1225, 1184, 1057, 1030 (SO_3^-), 887, 789, 739, 633. MS (FAB$^-$, NBA): *m*/z 560 $[M - NBu_4]^-$, 319 $[M - 2NBu_4 +$

H]$^-$.

Tetrabutylammonium 6,7-naphthalenediolate-2- sulfonate-2,(3)-(tetra-*tert*-butylphthalocyaninato)-titanium(IV) 1. A mixture of oxotitanium-phthalocyanine **4** (50 mg, 0.062 mmol) and tetrabutylammonium 6,7-dihydroxynaphthalene-2-sulfonate (30 mg, 0.062 mmol) in acetonitrile (30 mL), was stirred at 80ºC for 60 min. The solvent was rotary evaporated and the residue was resuspended in dichloromethane and filtered over Celite. The solvent was rotary evaporated and the residue was recrystallized from ethanol/hexane, filtered, repeatedly washed with hexane and dried, affording 58 mg (74%) of **1** as a green, crystalline solid. ^{1}H NMR (300 MHz; $CDCl_3$): δ_H, ppm 9.4-9.6 (m, 8H, Pc^{Hortho}), 8.41 (d, 4H, Pc^{Hmeta}), 7.22 (s, 1H, $H^{1'}$), 7.10 (d, J = 8 Hz, 2H, $H^{3'}$), 6.56 (d, J = 8 Hz, 2H, $H^{4'}$), 4.73, 4.70 (2 s, 2H, $H^{5',8'}$), 2.8-2.9 (m, 8H, NCH_2), 1.81-1.82 (4s, 36H, 4 *t*-Bu), 1.2-1.3 (m, 12H, NCH_2CH_2), 1.0-1.1 (m, 12H, $NCH_2CH_2CH_2$), 0.72 (t, 16H, CH_3). ^{13}C NMR (50 MHz; $CDCl_3$): δ_C, ppm 159.2, 155.1, 152.7, 152.5, 136.7, 136.6, 136.5, 134.3, 134.2, 134.1, 129.4, 129.2, 126.5, 124.3, 123.5, 121.2, 119.8, 103.0, 102.0, 58.3 ($C^{1'}$), 36.2 [$C(CH_3)_3$], 32.0 [$C(CH_3)_3$], 23.6, 19.4 ($C^{2'}$, $C^{3'}$), 13.4 ($C^{4'}$). IR (KBr): v, cm^{-1} 3024 (C–H), 2964, 2870 (C–H), 1610, 1448, 1394, 1367, 1329, 1250, 1196, 1155, 1063, 1022 (SO_3^-), 926, 862, 750, 671, 644. UV-vis ($CHCl_3$): λ_{max}, nm (log ε) 243 (5.14), 269 (5.11), 351 (4.92), 636 (4.54), 703 (5.26). MS (MALDI-TOF$^-$, TCNQ): *m*/z 1021 [M – NBu_4]$^-$.

Tetrabutylammonium 4,5-naphthalenediolate-2,7- disulfonate-2,(3)-(tetra-*tert*-butylphthalocyaninato)-titanium(IV) 2. A mixture of oxotitanium-phthalocyanine **4** (50 mg, 0.062 mmol) and tetrabutylammonium 4,5-dihydroxynaphthalene-2,7-disulfonate (50 mg, 0.062 mmol) in acetonitrile (30 mL), was stirred at 80ºC for 90 min. The solvent was rotary evaporated and the residue was resuspended in dichloromethane and filtered over Celite. The solvent was rotary evaporated and the residue was recrystallized from ethanol/hexane, filtered, repeatedly washed with hexane and dried, affording 69 mg (70%) of **2** as a blue-green, crystalline solid. ^{1}H NMR (300 MHz; $CDCl_3$): δ_H, ppm 9.4-9.6 (m, 8H, Pc^{Hortho}), 8.36 (dd, 4H, Pc^{Hmeta}), 7.15 (s, 2H, $H^{1',8'}$), 5.58 (s, 2H, $H^{3',6'}$), 2.5-2.6 (m, 8H, NCH_2), 1.82, 1.79 (2s, 36H, 4 *t*-Bu), 1.0–1.1 (m, 12H, NCH_2CH_2), 0.8-1.0 (m, 12H, $NCH_2CH_2CH_2$), 0.59 (t, 16H, CH_3). ^{13}C NMR (50 MHz, $CDCl_3$): δ_C, ppm 156.2, 154.8, 152.7, 152.5, 136.5, 134.1, 134.0, 131.9, 128.8, 123.3, 123.2, 123.1, 120.0, 119.9, 118.5, 105.8, 58.3 ($C^{1'}$), 36.2 [$C(CH_3)_3$], 32.0 [$C(CH_3)_3$], 23.4, 19.2 ($C^{2'}$, $C^{3'}$), 13.3 ($C^{4'}$). IR (KBr): v, cm^{-1} 3024 (C–H), 2949, 2868 (C–H), 1612, 1564, 1464, 1358, 1331, 1279, 1198, 1063, 1036 (SO_3^-), 926, 878, 829, 756, 667, 640. UV-vis ($CHCl_3$): λ_{max}, nm (log ε) 243 (3.88), 282 (3.91), 323 (3.84), 357 (3.79), 636 (3.52), 706 (4.16). MS (FAB$^-$, NBA): *m*/z 1343 [M – NBu_4]$^-$, 1101 [M – 2NBu_4 + H]$^-$, 550

$[M - 2NBu_4]^{2-}$.

2,3-naphthalenediolate-2,(3)-(tetra-*tert*-butyl-phthalocyaninato)titanium (IV) 3. A mixture of oxotitanium phthalocyanine **4** (50 mg, 0.062 mmol) and 2,3-dihydroxynaphthalene (20 mg, 0.125 mmol) in chloroform (30 mL), was refluxed for 60 min. The solvent was rotary evaporated and the residue was recrystallized from dichloromethane/methanol and dried, affording 55 mg (94%) of **3** as a green, crystalline solid. ^{1}H NMR (300 MHz; $CDCl_3$): δ_H, ppm 9.5-9.7 (m, 8H, Pc^{Hortho}), 8.42 (dd, 4H, Pc^{Hmeta}), 6.5-6.6 (m, 4H, $H^{5',6',7',8'}$), 4.77 (s, 2H, $H^{1',4'}$), 1.83, 1.82 (4s, 36H, 4*t*-Bu). ^{13}C NMR (50 MHz; $CDCl_3$): δ_C, ppm 155.2, 155.0, 152.5, 152.4, 152.3, 136.8, 136.7, 136.6, 136.5, 134.3, 134.2, 129.2, 129.1, 36.2 [$C(CH_3)_3$], 32.0 [$C(CH_3)_3$]. IR (KBr): v, cm^{-1} 3047 (C–H), 2964, 2924, 2858 (C–H), 1616, 1508, 1441, 1400, 1337, 1323, 1259, 1198, 1149, 1063, 933, 860, 835, 748, 673, 646. UV-vis ($CHCl_3$): λ_{max}, nm (log ε) 242 (4.74), 275 (4.75), 353 (4.68), 636 (4.36), 704 (5.09). MS (MALDI-TOF^+, TCNQ): *m*/z 942 $[M]^+$.

1.4. Conclusion

This study reports the performance as DSC photosensitizers of Ti(IV) phthalocyanines, axially coordinated to 2,3- and 1,8-naphthalenediols, which are endowed with none, one or two sulfonate anchoring groups. All studied compounds showed the same efficiency. Thus, unexpectedly, we can conclude, that at least with the three chatecolate titanium phthalocyanines **1-3** studied in this work, a ligand exchange with the TiO_2 takes place, giving rise to the same species adsorbed on the inorganic semiconductor (Fig. 4.3). This is probably the reason why, in the current case, the type of axial ligand does not play any role on the overall device efficiency, since the injecting species is the same in all the three cases. The titanium phthalocyanine absorbed in this way shows a low efficiency.

Acknowledgements

Support is acknowledged from the Spanish MICINN (CTQ2011-24187/BQU and CONSOLIDER INGENIO 2010, CSD2007-00010 on Molecular Nanoscience) and the CAM (MADRISOLAR-2, S2009/PPQ/1533). EP would like to acknowledge the European Research Council starting Grant ERCstg-POLYDOT and the national projects CONSOLIDER HOPE 0007-2007 and MICINN CTQ-2007-60746-BQU as well as Catalonian regional government for the project 2009 SGR 207.

References

1. (a) O'Regan, B.; Grätzel, M., A low-cost, high-efficiency solar cell based on dye-sensitized colloidal TiO2 films. *Nature* **1991,** *353*, 737-740; (b) Cao, Y. M.; Bai, Y.; Yu, Q. J.; Cheng, Y. M.; Liu, S.; Shi, D.; Gao, F. F.; Wang, P., Dye-Sensitized Solar Cells with a High Absorptivity Ruthenium Sensitizer Featuring a 2-(Hexylthio)thiophene Conjugated Bipyridine. *J. Phys. Chem. C* **2009,** *113* (6290-6297); (c) Grätzel, M., Recent Advances in Sensitized Mesoscopic Solar Cells. *Acc. Chem. Res.* **2009,** *42*, 1788-1798.

2. Hagfeldt, A.; Boschloo, G.; Sun, L.; Kloo, L.; Pettersson, H., Dye-Sensitized Solar Cells. *Chem. Rev.* **2010,** *110*, 6595-6663.

3. Rio, Y.; Rodríguez-Morgade, M. S.; Torres, T., Modulating the electronic properties of porphyrinoids: a voyage from the violet to the infrared regions of the electromagnetic spectrum. *Org. Biomol. Chem.* **2008,** *6*, 1877-1894.

4. (a) Ohkubo, K.; Fukuzumi, S., Long-lived charge-separated states of simple electron donor-acceptor dyads using porphyrins and phthalocyanines. *J. Porphyrins Phtalocyanines* **2008,** *12*, 993-1004; (b) Bottari, G.; de la Torre, G.; Guldi, D. M.; Torres, T., Covalent and Noncovalent Phthalocyanine–Carbon Nanostructure Systems: Synthesis, Photoinduced Electron Transfer, and Application to Molecular Photovoltaics. *Chem. Rev.* **2010,** *110*, 6768-6816; (c) Bottari, G.; Trukhina, O.; Ince, M.; Torres, T., Towards artificial photosynthesis: Supramolecular, donor–acceptor, porphyrin- and phthalocyanine/carbon nanostructure ensembles. *Chem. Rev.* **2012,** *256*, 2453-2477.

5. Ragoussi, M. E.; Cid, J. J.; Yum, J. H.; de la Torre, G.; Di Censo, D.; Grätzel, M.; Nazeeruddin, M. K.; Torres, T., Carboxyethynyl Anchoring Ligands: A Means to Improving the Efficiency of Phthalocyanine-Sensitized Solar Cells. *Angew. Chem., Int. Ed.* **2012,** *51*, 4375-4378.

6. Winter, G.; Heckmann, H.; Haisch, P.; Eberhardt, W.; Hanack, M.; Lüer, L.; Egelhaaf, H. J.; Oelkrug, D., Study of Substituent Effects on the Photoconductivity of Soluble 2,(3)- and 1,(4)-Substituted Phthalocyaninato- and Naphthalocyaninatotitanium(IV) Oxides. *J. Am. Chem. Soc.* **1998,** *120*, 11663-11673.

7. Barthel, M.; Dini, D.; Vagin, S.; Hanack, M., An Easy Route for the Synthesis of New Axially Substituted Titanium(IV) Phthalocyanines. *Eur. J. Org. Chem.* **2002,** *22*, 3756-3762.

8. Palomares, E.; Martínez-Díaz, M. V.; Haque, S. A.; Torres, T.; Durrant, J. R., State selective electron injection in non-aggregated titanium phthalocyanine sensitised nanocrystalline TiO2 films. *Chem. Commun.* **2004**, 2112-2113.

9. (a) Yan, Z.; Guang, S.; Su, X.; Xu, H., Near-Infrared Absorbing Squaraine Dyes for Solar Cells: Relationship between Architecture and Performance. *J. Phys. Chem. C* **2012,** *116*, 8894-8900; (b) Campbell, W. M.; Burrell, A. K.; Officer, D. L.; Jolley, K. W., Porphyrins as light harvesters in the dye-sensitised TiO2 solar cell. *Coord. Chem. Rev.* **2004,** *248*, 1363-1379.
10. Thomas, A. G.; Syres, K. L., Adsorption of organic molecules on rutile TiO2 and anatase TiO2 single crystal surfaces. *Chem. Soc. Rev.* **2012,** *41*, 4207-4217.

Chapter 5.
Organic dyes as sensitizers

Organic dyes, as porphyrins, have several advantages compared to the ruthenium based complexes. As is said various times in this thesis, organic dyes shown higher molar extinction coefficient and that leads that thinner semiconductor layer are needed. Organic dyes presents also sharp absorption bands, high photostability and environmental free compounds.

In this chapter, one simple, easy to prepare and efficient novel donor-acceptor organic dye based on a dissymmetric central core embedding a benzothiadiazole cromophoric unit is studied and a remarkable power conversion efficiendy of 10.2% is obtained. On the other hand, two series of organic dyes with alkene and alkyne bridges are also investigated in order to study the effects of these bridges on the molecule backbone. All the compounds are fully photophysical and electrochemical characterized and the device properties are completely investigated.

Index

Chapter 5. Organic dyes as sensitizers

1. Paper 4: A Robust Organic Dye for Dye Sensitized Solar Cells Based on Iodine/Iodide Electrolytes Combining High Efficiency and Outstanding Stability

Damien Joly,[a] Laia Pellejà,[b] Stéphanie Narbey,[c] Frédéric Oswald,[c] Julien Chiron,[d] John N. Clifford,[b] Emilio Palomares,[b,e] and Renaud Demadrille[a]

[a]INAC/SPrAM UMR 5819 (CEA-CNRS-U.J.F-Grenoble 1) 17 Rue des Martyrs, 38054 Grenoble Cedex 9, France
[b]Institute of Chemical Research of Catalonia (ICIQ), Av. Països Catalans 16,Tarragona, E-43007 Spain.
[c]Solaronix SA, Rue de l'Ouriette 129, 1170 Aubonne, Switzerland.
[d]KaïronKem, 20 Rue Marc Donadille, Technopole Chateau Gombert, 13013 Marseille, France.
[e]Catalan Institution for Advanced Studies and Research (ICREA), Passeig Lluís Companys 23, 08010 Barcelona, Spain.

Scientific Reports **2014**, 4, 4033; DOI:10.1038/srep04033

Abstract: Among the new photovoltaic technologies, the Dye Sensitized Solar Cell (DSCs) is becoming a realistic approach towards energy markets such as BIPV (Building Integrated PhotoVoltaics). In order to improve the performances of DSCs and to increase their commercial attractiveness, cheap, colourful, stable and highly efficient ruthenium-free dyes must be developed. Here we report the synthesis and complete characterization of a new purely organic sensitizer (**RK1**) that can be prepared and synthetically upscaled rapidly. Solar cells containing this orange dye show a power conversion efficiency of 10.2% under standard conditions (AM 1.5G, 1000 W m^{-2}) using iodine/iodide as the electrolyte redox shuttle in the electrolyte, which is among the few examples of DSC using an organic dyes and iodine/iodide red/ox pair to overcome the 10% efficiency barrier. We demonstrate that the combination of this dye with an ionic liquid electrolyte allows the fabrication of solar cells that show power conversion efficiencies of up to 7.36% that are highly stable with no measurable degradation of initial performances after 2200 h of light soaking at 65ºC under standard irradiation conditions. **RK1** achieves one of the best output power conversion efficiencies for a solar cell based on the iodine/iodide electrolyte, combining high efficiency and outstanding stability.

1.1. Introduction

Dye Sensitized Solar Cells (DSCs) are attracting much attention because of their relatively high conversion efficiencies, low cost production processes and short energy payback time.[1] In these devices, sunlight is absorbed by photoactive molecules that are attached to the surface of a wide band gap semiconductor oxide (typically TiO_2 or ZnO) forming a dense monolayer. The system is completed using a hole transporting material which is usually a liquid electrolyte containing the iodide/tri-iodide (I_2/I_3^-) red/ox couple.[2] The molecules act as sensitizers and upon photo-excitation inject an electron into the conduction band of the metal oxide. While the electrons are conducted through the nanostructured metal oxide to reach the external circuit, the oxidized dye is regenerated by the red/ox couple, which is itself regenerated at the counter electrode.[3] The complete description of the basic working principles of a DSC can be found elsewhere.[4]

Several different classes of materials are employed to fabricate a DSCs, but the sensitizer is probably the key element since it governs the photon harvesting and the creation of free charges after injection of electrons into the nanostructured semi-conducting oxide. Moreover, the sensitizer structure has also been shown to control key electron transfer processes at the TiO_2/dye/electrolyte interface such as the recombination of TiO_2 electrons with electrolyte species or with dye cations themselves. For this reason many efforts have recently focused on the development of new efficient sensitizers that could help improve device performance and allow for practical and real use of this technology beyond the laboratory.

For many years, ruthenium based complexes were the ‘‘champion’’ dyes of DSCs and some of them were distinguished by achieving more than 11% efficiency.[5] However, despite the fact that high power conversion efficiencies and relatively stable DSCs have been fabricated using ruthenium sensitizers, ruthenium cannot be considered an ‘‘earth abundant material’’ and, thus, it is desirable to look for alternative dyes. Besides, even though some ruthenium complexes show broad absorption spectra, they generally have modest molar extinction coefficients[6] which limit their performances when employed to sensitize thin electrodes. As a consequence, this class of sensitizer is not ideal for DSCs based on ionic-liquids as thin electrodes are preferable due to the high inherent viscosity of these electrolytes.[7]

To overcome this problem, the use of organic sensitizers has been demonstrated to be a useful strategy. Organic sensitizers have attracted great interest because of their potentially lower production costs, easier and more

versatile synthesis, and much larger molar absorption coefficients. In addition, some of them have shown satisfactory stability.[8] Many different organic dyes with conversion efficiencies in the range of 6-8% have been reported in the last years but only a few examples have overcome efficiencies of 10%.[9] To date, the highest efficiency for a DSC employing a purely organic sensitizer has been achieved by Wang and co-workers using an electrolyte based on iodide/tri-iodide in a volatile electrolyte. Using C219, a high absorbing dye prepared in ten steps, they reported 10.1% power conversion efficiency under 1 Sun irradiation.[10]

In addition to purely organic dyes, metallated porphyrins showing strong absorption in the visible region, have been synthesized and tested in DSCs by Grätzel and co-workers.[11] After appropriate tailoring of the chemical structure and employment of a cobalt electrolyte, the porphyrin dye YD2-*o*-C8 showed power conversion efficiencies of up to 11.9% under standard conditions (AM 1.5 G, 100 mW cm^{-2} intensity) which was further improved to 12.3% when co-sensitized with an organic dye.[12] However, porphyrins usually require complicated synthetic strategies with relatively low yields, especially when an anchoring function and a redox group have to be introduced at specific positions.[13] For this reason, our motivation in this work was to design a simple, easy to prepare and efficient organic sensitizer. Our strategy was principally driven by the possibility to reduce the number of chemical steps involved in its preparation, the availability of the organic precursors and the possibility to confer to the dye tailored optical and electrochemical properties. In the literature, most of the new organic sensitizers are prepared using the very well-known donor-π-acceptor design approach, where the donor bears alkyls chains and the π conjugated bridge is mainly based on symmetrical chromophoric units. Our approach, on the other hand, is based on the use of a dissymmetric π-conjugated bridge that embeds an alkyls chain and an electro deficient unit localized close to the electron-withdrawing anchoring function and an electron-rich unit close to the aryl amine donating group.[14] The introduction of a phenyl ring between acceptor benzothiadiazole (BTD) and the cyanoacrylic acid group should stabilize the dye radical cation and decrease recombination rate as showed by Haid *et al*.[15]

Herein we report the preparation of a new purely organic dye, **RK1**, whose synthesis involves just five steps which starts from low cost precursors, resulting in a solar to electrical power conversion efficiency of 10.2% under standard conditions (AM 1.5 G, 100 mW cm^{-2} intensity). To the best of our knowledge, this represents one of the best power conversion efficiencies ever reported for a DSC based on a purely organic dye. Moreover, this high efficiency is coupled with outstanding long-term stability as

demonstrated by devices based on an ionic liquid electrolyte.

1.2. Results

1.2.1. RK1 synthesis

The chemical structure of **RK1** is shown in Scheme 5.1. The thiophene BTD phenyl chromophore constitutes the π bridge in this D–π–A structure. **RK1** has a very simple chemical structure, and its preparation does not require complicated synthetic procedures or purification steps allowing for its preparation in the tens of grams scale.

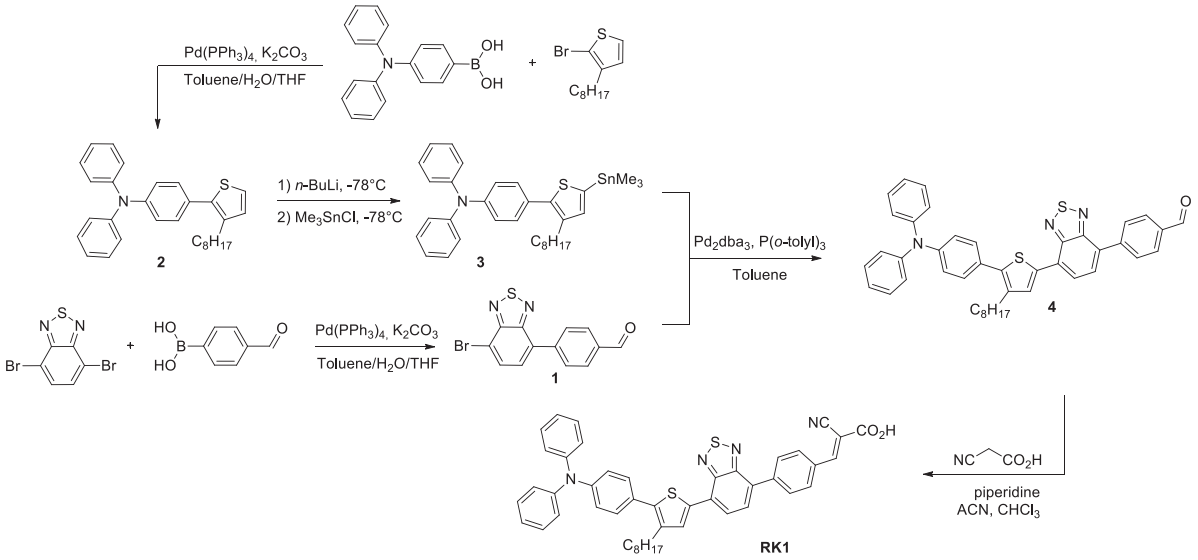

Scheme 5.1. Synthetic route and reaction conditions for the preparation of **RK1**.

The convergent synthetic strategy to access **RK1** relies on the preparation of two key building blocks (1 and 2) that are subsequently coupled together via a Suzuki or a Stille cross coupling reaction (see Scheme 5.1). The preparation of these two intermediates is based on the use of low cost and commercially available precursors and a classical palladium cross coupling reaction. With the idea in mind of potential future synthesis of this dye at an industrial level, toxic reaction solvents such as DMF were purposely not used in our synthetic scheme. In addition, the replacement of DMF by a mixture of toluene, THF and water helped us to strongly improve the yields of the Suzuki coupling reaction. The overall yield of preparation for **RK1** is 50% after just five steps.

1.2.2. Optical and electrochemical data

The optical properties of the dye were investigated by UV-Visible spectroscopy in ethanol solution and compared to those of N719 which was used as a reference compound in this study (Figure 5.1 and Table 5.1). The UV-Vis spectrum of **RK1** shows, as expected, two absorption bands between 300 and 580 nm. The first one which is located in the UV region (λ = 366 nm, ε = 45000 M^{-1} cm^{-1}) is assigned to the π-π* transition of the aromatic rings, whereas the second absorption band in the visible region (λ = 470 nm, ε = 26600 M^{-1} cm^{-1}) is attributed to the internal charge transfer (ICT) transition that occurs between the electron-withdrawing and electron-donating segments of the molecule. This band is at shorter wavelength with respect to that of N719 but the measured molar extinction coefficient at 470 nm for **RK1** is almost two times higher than the corresponding values for N719. As a consequence, **RK1** shows an aesthetically pleasing orange colour both in solution and on TiO_2 films.

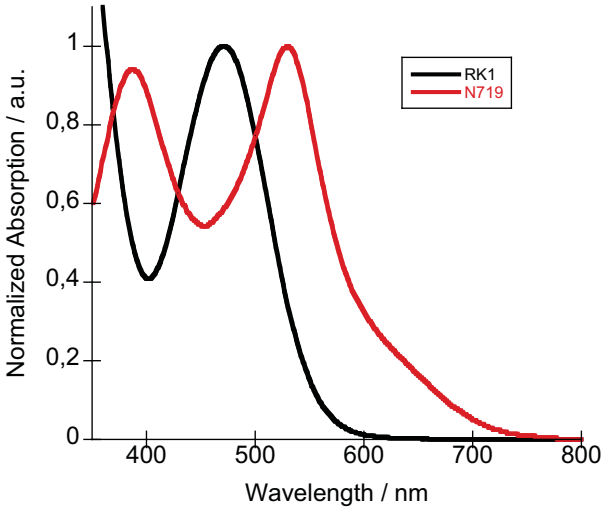

Figure 5.1. UV-visible spectra of RK1 and N719 in ethanol solution.

Table 5.1. Optical and electrochemical data of **RK1**.

	λ_{abs} /nm[a]	ε /M^{-1} cm^{-1} [a]	Eg_{opt} /eV[b]	$Eox1$[c] /V vs NHE	$Eox2$[c] /V vs NHE	$Ered$[c] /V vs NHE	HOMO[d] /V vs NHE	LUMO[d] /V vs NHE	Eg_{cv} /eV[e]
RK1	366 470	45000 26600	2.17	0.98	1.41	–0.74	0.93	–0.72	1.65

[a] Measured in Ethanol. [b] Measured from λ_{onset}. [c] All potentials were obtained during cyclic voltammetric investigations in 0.2 M Bu_4NPF_6 in Ch_2Cl_2. Platinum electrode diameter 1 mm, sweep rate: 200 mV s^{-1}. Potentials measured vs Fc^+/Fc were converted to NHE by addition of +0.69 V. [d] Determined from oxidation onset and reduction onset. [e] Calculated Eg_{cv} = HOMO – LUMO.

The electrochemical properties of **RK1** were investigated by cyclic voltammetry (CV) with the goal to determine the energy level positions of

frontier orbitals. Upon the application of negative potentials, the dye undergoes a quasi-reversible reduction/re-oxidation process, and upon the application of positive potentials it showed two reversible oxidation waves corresponding to an oxidation/re-reduction process. The first oxidation peak (E_{ox1}) was found at 0.98 V versus NHE which can be assigned to the oxidation of the triphenylamine donor moiety. The second oxidation potential (E_{ox2}) was observed at 1.41 V and is attributed to the oxidation of the π-conjugated backbone. The HOMO and LUMO energy level positions determined from the onset of the first oxidation and reduction potential were 0.93 and –0.72 V vs. NHE. **RK1** therefore showed a bandgap (Eg_{CV}) of 1.65 eV. The experimentally determined LUMO energy level of **RK1** lies above the conduction band edge of TiO_2 (0.40 V versus NHE), which ensures the necessary driving force for electron injection from the dye into the conduction band of the semi-conductor. Moreover, the HOMO energy level positioned at 0.93 V versus NHE also indicates that there is a sufficient energy offset for regeneration by the I^-/I_3^- redox couple at –0.35 V versus NHE.[16]

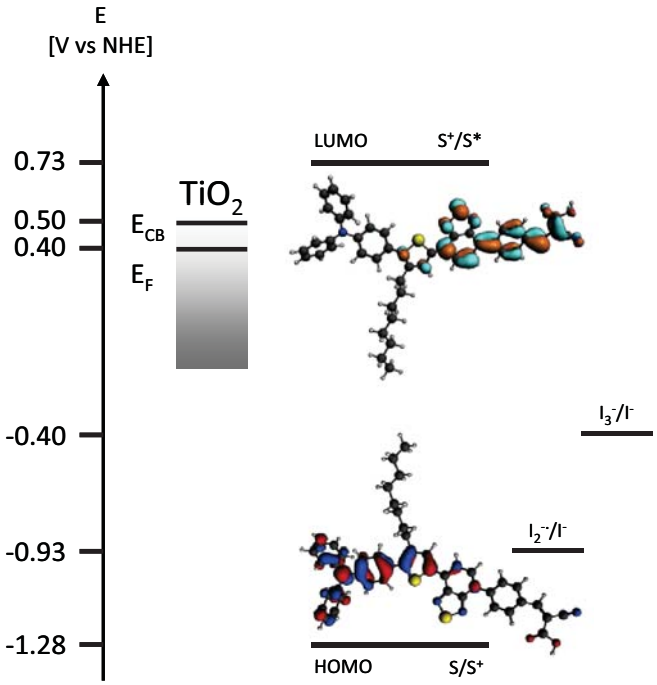

Figure 5.2. Frontier molecular orbitals of RK1 calculated at B3LYP level of theory.

In order to compare these experimental values and to gain insight into structural properties, the electron density distribution of the frontier orbitals of **RK1** was determined by density functional theory (DFT) using the B3LYP hybrid functional (see Experimental Section for details). We report in Figure 5.2 the calculated molecular orbital energy diagram for **RK1**, along with *iso* density plots of the HOMO and LUMO. The dyes show a directional electron distribution, with the delocalization of the HOMO on the triphenylamine group

and the thiophene of the π-conjugated bridge. On the other hand, the LUMO is predominantly delocalized on the BTD-phenylvinylcyanoacetic units. This directional electron distribution is consistent with the dissymmetrisation of the core and should facilitate the reduction of the oxidized dyes by the I^-/I_3^- based electrolyte, and the injection of electrons into the conduction band of TiO_2.

1.2.3. Dye sensitized solar cells

Solar cells with liquid electrolyte. The photovoltaic parameters of the best **RK1** DSCs using a standard acetonitrile based electrolyte are shown in Table 5.2 alongside those for a device made using the ruthenium sensitizer N719 for comparison. The photoactive electrodes of these devices were fabricated using standard double layer structure consisting of mesoporous TiO_2 and a TiO_2 scatter layer. The I-V curves of champion cells recorded under AM 1.5G, 1 Sun illumination and in the dark and their photocurrent response (IPCE) are shown in Figure 5.3. It should be underlined that the results presented here were reproduced in two different laboratories (ICIQ and Solaronix) and that three different cells were fabricated for each entry of the table.

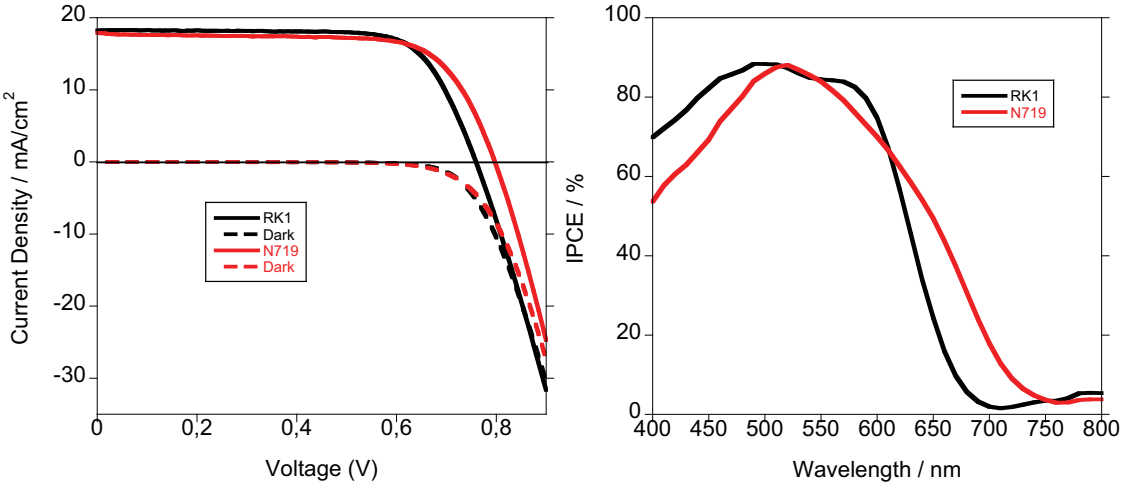

Figure 5.3. I-V curves recorded under AM 1.5G illumination and in the dark (right) and IPCE spectra (left) for RK1 and N719 devices.

Table 5.2. Photovoltaic parameters of DSCs with an acetonitrile electrolyte.

Adsorbing Solution	TiO_2 Thickness / μm	J_{sc} / mA cm^{-2}	V_{oc} / V	FF (%)	η^{a} (%)
RK1 (0.2 mM)/Cheno (10 mM)[a]	4 + 3.5[c]	12.44	0.744	76	7.07
RK1 (0.2 mM)/Cheno (10 mM)[a]	8 + 3.5[c]	13.60	0.719	76	7.50
RK1 (0.2 mM) without Cheno	13 + 3.5[c]	20.25	0.691	64	8.89
RK1 (0.2 mM)/Cheno (2 mM)[b]	13 + 3.5[d]	20.25	0.715	68	9.89

RK1 (0.2 mM)/Cheno (4 mM)[b]	13 + 3.5[d]	19.45	0.704	66	8.98
RK1 (0.2 mM)/Cheno (2 mM)[b]	3.5 + 6.5 + 3.5[d]	18.33	0.734	71	9.52
RK1 (0.2 mM)/Cheno (2 mM)[b]	3.5 + 9.5 + 3.5[d]	19.50	0.713	72	10.00
RK1 (0.5 mM)/Cheno (5 mM)[a]	13 + 4[e]	18.26	0.760	74	10.20
N719 (0.5 mM)/Cheno (5 mMa[b]	13 + 4[e]	17.91	0.800	71	10.19

[a] In Ethanol. [b] In Methanol. [c] TiO_2 Solaronix (HT/SP + R/SP). [d] TiO_2 macrochannel Solaronix (HT/SP + MC/SP + R/SP). [e] TiO_2 Dyesol (18NR-T + 18NR-AO) , all measurements were carried out with a mask of 0.36 cm2.

In order to investigate and optimize the DSC performances of the new dye, the TiO_2 film thickness was varied between 4 and 13 µm onto which a 3.5 to 4 µm scattering layer was deposited. For the dyeing of the TiO_2 electrodes, 0.2 to 0.5 mM solutions of **RK1** containing various amounts of 3α, 7α-dihydroxy-5β-cholic acid (chenodeoxycholic acid) were employed. Though the use of chenodeoxycholic acid with organic sensitizers is known to reduce the sensitizer's loading, it has also been shown to diminish the undesirable formation of dye aggregates on the TiO_2 surface and decrease recombination processes between TiO_2 electrons and electrolyte species.[17]

Interestingly for **RK1** devices performances remain higher than 7% even for low TiO_2 film thicknesses. When thicker electrodes (10 to 13 µm) are employed, very high current densities of up to 20.25 mA cm^{-2} can be attained. This results in a power conversion efficiency of 10.2% for the **RK1** champion cell which is outstanding for an organic sensitizer.

The J_{sc}, FF and V_{oc} for champion cells of N719 and **RK1** with power conversion efficiencies of over 10%, are rather similar. The dark current in both devices is nearly identical. The photocurrent response (IPCE) shows that though the N719 device performs better at longer wavelengths, **RK1** performs significantly better at shorter wavelengths, in agreement with the respective absorption spectra of these dyes (Figure 5.3).

The V_{oc} of a DSC is determined by the quasi-Fermi-level of the metal oxide semiconductor, which is correlated with its conduction band edge (Ec) and electron density. Electron density is itself dependent on rate of recombination between semiconductor electrons and oxidized electrolyte species. To investigate the difference in voltage for these devices, charge extraction and transient photovoltage measurements were conducted. Charge extraction data (Figure 5.4 (left)) show that the **RK1** device has a slightly higher charge density with respect to the N719. This indicates that the TiO_2 con- duction band in **RK1** devices is shifted downward somewhat compared to N719 devices. Electron lifetime measured using transient photovoltage

measurements (Figure 5.4 (right)) for the **RK1** device is shorter than for the N719 device. This is routinely observed for DSCs employing organic sensitizers.[18] Therefore, the combined effect of the lower lying TiO_2 conduction band and shorter electron lifetime explains the general trend of lower V_{oc} for **RK1** devices.

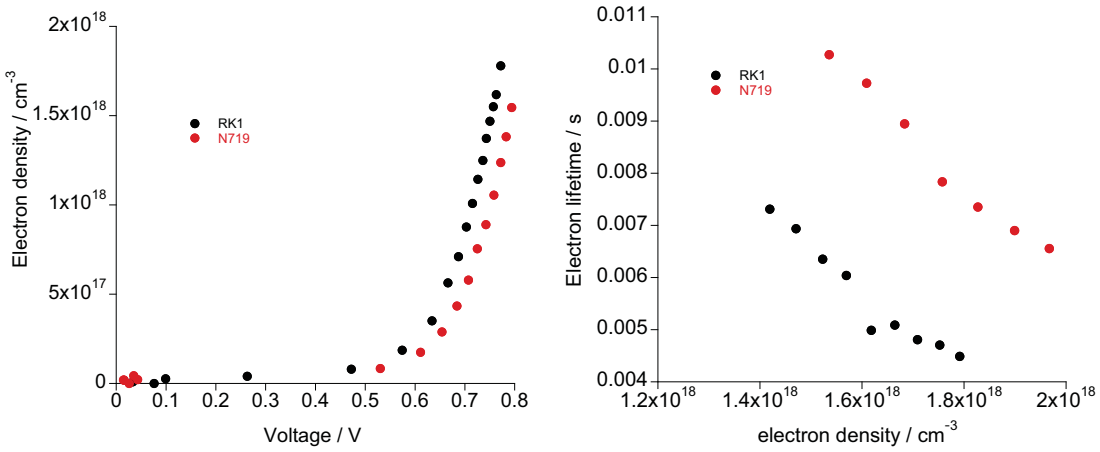

Figure 5.4. Charge extraction data showing electron density as a function of induced voltage (left) and transient photovoltage data showing electron lifetimes versus electron density (left) for RK1 and N719 devices.

Solar cells with ionic liquid electrolyte. For the practical application of dye-sensitized solar cells (DSCs), in addition to high performances, long device lifetime is a major requirement. Because highly volatile solvents such as acetonitrile are inappropriate for stability measurements, a solvent-free ionic liquid electrolyte was used instead in order to evaluate the lifetime of the **RK1** sensitizer under thermal stress and light soaking. The photovoltaic parameters of these solar cells are given in Table 5.3. Two different types of electrodes were used to fabricate the devices. In addition to regular mesoporous TiO_2, to further increase the thickness of the electrode, a macro channel TiO_2 paste was employed. This strategy was found to be particularly efficient to improve the light-harvesting capacity of these devices without alteration of the capability of the viscous ionic liquid electrolyte to penetrate deeply into the nanostructured electrode. With 8 µm thick TiO_2 film coated with a 3.5 µm thick reflecting layer, devices showing a J_{sc} of 15.40 mA cm^{-2}, a V_{oc} of 0.665 V, a FF of 69% and a power conversion efficiency of 7.36% at 1 Sun were obtained. This performance ranks among the best reported for organic sensitizers using ionic liquid electrolyte and is considerably better than most of the performances reported for Ruthenium based dyes.[19] The fabricated DSCs were irradiated continuously in a solar simulator with a light intensity of 1000 W cm^{-2} at 65ºC. The evolution of the photovoltaic parameters of a cell measured under the irradiance of AM 1.5G sunlight during successive full-sun visible-light soaking is presented in Figure 5.5. After light

soaking, the power conversion efficiency of the solar cell significantly increases; this behaviour is related to the improved penetration of the ionic liquid electrolyte through the complete thickness of the electrode and the "activation" of the entire electrode.[20] After this period we observed a stabilisation of the performances and no degradation; this cell exhibits outstanding stability with no measurable degradation of the initial performances after 2200 h of irradiation. After this period the cells start to undergo a linear degradation of their performances but it is noteworthy that after 5000 h continuous irradiation at 65ºC, the degraded solar cells still show 75% of their initial power conversion efficiency. From the best of our knowledge this stability performance is the best ever achieved for an organic sensitizer.

Table 5.3. Photovoltaic parameters of DSCs with an ionic liquid electrolyte.

Adsorbing Solution	TiO_2 Thickness / µm	J_{sc} / mA cm^{-2}	V_{oc} / V	FF (%)	η^{a} (%)
RK1 (0.2 mM)/ Cheno (10 mM)[a]	4 + 3.5[c]	12.22	0.684	72	6.04
RK1 (0.2 mM)/ Cheno (2 mM)[a]	6 + 3.5[c]	13.70	0.671	66	6.06
RK1 (0.2 mM)/ Cheno (2 mM)[b]	4 + 4 + 3.5[d]	15.40	0.665	69	7.36

[a] In Ethanol. [b] In Methanol. [c] TiO_2 Solaronix (HT/SP + R/SP). [d] TiO_2 macrochannel Solaronix (HT/SP + MC/SP + R/SP), all measurements were carried out with a mask of 0.36 cm^2.

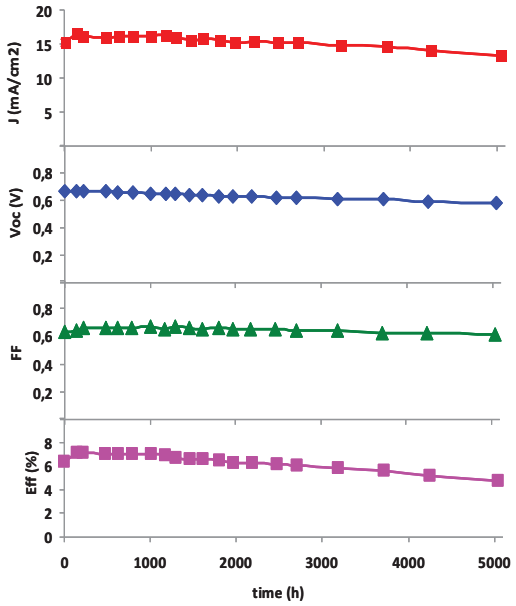

Figure 5.5. Detailed photovoltaic parameters of a cell measured under the irradiance of AM 1.5G sunlight during successive full-sun visible-light soaking (1sun 100 mW cm^{-2}) at 65°C. J_{sc}: short-circuit photocurrent density; V_{oc}: open-circuit voltage; FF: fill factor; Eff: power conversion efficiency.

1.3. Discussion

We have designed and synthesized a novel donor-acceptor organic dye (**RK1**) based on a dissymmetric central core embedding a benzothiadiazole chromophoric unit. This dye has a simple chemical structure and can be prepared very easily in five steps with an overall yield of 50%. When employed in DSCs with liquid electrolytes containing the I^-/I_3^- redox couple, under standard conditions a high short circuit current of 18.26 mA cm^{-2}, an open circuit voltage of 0.76 V and a FF of 74% were achieved leading to an overall power conversion efficiency of 10.2%. This represents one of the highest efficiencies ever recorded for a DSC device employing a fully organic dye and iodine/iodide electrolytes. In addition, when a solvent-free ionic liquid electrolyte was used a short circuit current of 15.40 mA cm^{-2}, an open circuit voltage of 0.665 V and a FF of 69% leading to a power conversion efficiency of 7.36% under standard conditions was achieved. These DSC devices showed outstanding stability when irradiated continuously with 1000 W cm^{-2} light intensity at 65ºC with no measurable degradation of the initial performances after 2200 h and only a loss of circa 25% after 5000 h. We note that these results are obtained with iodide/tri-iodide that has a strong absorption band located at 360 nm[21] and that the photocurrent generated by the sensitizer could be further improved in the blue part of the spectrum with the replacement of this electrolyte by a cobalt redox shuttle. In addition, such redox shuttles can be used to increase V_{oc} further improving device performance. To conclude, we believe that **RK1** is a most promising organic dye for future low cost, stable and efficient dye sensitized solar cells.

1.4. Methods

Materials synthesis. 2-bromo-3-octylthiophene, 4-(N,N-diphenylamine) phenylboronic acid, 4-formylphenyl-boronic acid, 2-cyanoacetic acid, piperidine, *n*-BuLi [2.5 M solution in Tetrahydrofuran (THF)] and trimethyl tin chloride solution [1 M solution in *n*-hexane] were purchased from Aldrich or TCI chemicals and used as received. N-Bromo-Succinimide (NBS) was purchased from Fisher Chemicals and 4,7-dibromo-2,1,3-benzothiadiazole from Orgalight or provided by Kaïronkem. The solvents, such as anhydrous toluene, chloroform and acetonitrile from Aldrich were used as received. THF was used after distillation under sodium and benzophenone. Spectroscopic grade solvents from Aldrich were used for spectral measurements. 4-bromo-7-(4-formyl-benzyl)-2,1,3-benzothiadiazole was synthesised according to literature.[22]

Synthesis of 4-(3-Octylthien-2-yl)-N,N-dipphenylamine (2). Under argon, 4-(diphenylamino)phenylboronic acid (1.65 g, 4.63 mmol), 2-bromo-3-octylthiophene (1.16 g, 4.21 mmol), K_2CO_3 (700 mg, 5.05 mmol) and $Pd(PPh_3)_4$ (200 mg, 0.17 mmol) were dissolved in a degased toluene/ THF/water solution (30 mL, 20/7.5/2.5). The mixture was stirred overnight at 75ºC before being poured into water. The organic phase was recovered with Et_2O, washed with brine, dried on Na_2SO_4 and concentrated under reduced pressure. The crude oil was purified by chromatography on silica gel using *n*-hexane/CH_2Cl_2 2:1 to afford pale yellow oil **2** (1.67 g, 3.62 mmol, 86,0%). ^{1}H NMR (CD_2Cl_2, 200 MHz): δ = 7.33-7.96 (m, 16H), 2.66 (t, 2H, *J* = 7.8 Hz), 1.64-1.53 (m, 2H), 1.41-1.20 (m, 10H), 0.88 (t, 3H, *J* = 3 Hz). ^{13}C NMR (CD_2Cl_2, 50 MHz): δ =148.10, 147.52, 138.76, 138.09, 130.48, 130.09, 129.83, 129.17, 125.06, 124.63, 123.69, 123.60, 32.45, 31.60, 30.030, 29.95, 29.83, 29.20, 23.25, 14.55. HRMS (ESI): $[M + Na]^+$ = 439.23 (calcd. for $C_{30}H_{33}NS$: 439.23); Anal. Calcd for $C_{30}H_{33}NS$: C, 81.96; H, 7.57; N, 3.19; S, 7.29. Found: C, 81.66; H, 7.67; N, 3.22; S, 7.47.

Synthesis of 4-(7-(5-(4-(diphenylamino)phenyl-4-octylthien-2-yl)benzo[c][1,2,5]thiadia-zol-4-yl)benzaldehyde (4). Under argon, **2** (200 mg, 0.45 mmol) was dissolved in distilled THF (8 mL) then *n*-BuLi (0.32 mL, 0.58 mmol) was added at –78ºC. The solution was stirred for an hour at –50ºC before adding a *n*-hexane solution of Me_3SnCl (0.73 mL, 0.72 µmol) at –781C. The solution was allowed to reach room temperature and stirred for 2 hours. The reaction was quenched with water and the organic phase was extracted with *n*-hexane, dried with Na_2SO_4, filtered and concentrated under reduced pressure. The resulting oil **3** was engaged without any further purification in a Stille coupling with **1**. Under argon, solids **3**, **1** (174 mg, 0.55 mmol), Pd_2dba_3 (16 mg, 18 µmol) and P(*o*-tolyl)$_3$ (44 mg, 0.14 mmol) were dissolved in anhydrous toluene (8 mL) and refluxed for 24 hours. The mixture was then poured into HCl (1 M). The organic phase was extracted with Et_2O, washed with HCl (1 M), dried over Na_2SO_4 and concentrated under reduced pressure. The crude solid was purified by chromatography on silica gel using DCM/*n*-hexane 6:4 first then DCM as eluent to afford red solid **4** (270 mg, 0.40 mmol, 87%). ^{1}H NMR ($CDCl_3$, 200 MHz): δ = 10.11 (s, 1H), 8.19 (d, 2H, *J* = 8.4 Hz), 8.08 (s, 1H), 8.07 (d, 2H, *J* = 8.2 Hz), 7.96 (d, 1H, *J* = 7.6 Hz), 7.82 (d, 1H, *J* = 7.6 Hz), 7.42-7.26 (m, 6H), 7.19-7.03 (m, 8H), 2.77 (t, 2H, *J* = 7.8 Hz), 1.80-1.66 (m, 2H), 1.45-1.19 (m, 10H), 0.87 (t, 3H, *J* = 6.6 Hz); ^{13}C NMR ($CDCl_3$, 50 MHz): δ = 191.83, 153.68, 152.64, 147.42, 147.36, 143.23, 140.30, 139.46, 136.11, 135.632, 131.03, 130.50, 129.93, 129.81, 129.66, 129.33, 128.94, 127.84, 127.71, 124.74, 123.24, 122.87, 31.880, 31.04, 29.56, 29.42, 29.27, 28.97, 22.67, 14.13; HRMS (ESI): $[M + Na]^+$ = 677.25 (calcd. For

$C_{43}H_{39}N_3OS_2$: 677.25); Anal. Calcd for $C_{43}H_{39}N_3OS_2$: C, 76.18; H, 5.80; N, 6.20; S, 9.46. Found C, 76.07; H, 5.73; N, 6.17; S, 9.65.

Synthesis of RK1 dye. Under argon, **4** (134 mg, 0.18 mmol), cyano-acetic acid (78 mg, 0.90 mmol), were dissolved in a mixture of acetonitrile (6 mL) and chloroform (4 mL). A catalytic amount of piperidine was added and the solution was refluxed for 3 hours. Solvent was removed under reduced pressure and the solid dissolved in chloroform. The organic phase was washed with HCl solution (1.5 M), dried on Na_2SO_4 and concentrated. The crude solid was purified by chromatography on silica gel using DCM/MeOH/ Acetic acid 90:5:5 as eluent to afford **RK1** as red solid **5** (128 mg, 0.16 mmol, 87%). ^{1}H NMR ($CDCl_3$, 200 MHz): δ = 8.36 (s, 1H), 16 (s, 4H), 8.06 (s, 1H), 7,91 (d, 1H, *J* = 7.4 Hz), 7.79 (d, 1H, *J* = 7.6 Hz), 7.40-7.26 (m, 6H), 7.18-7.03 (m, 8H), 2.74 (t, 2H, *J* = 7.8 Hz), 1.78-1.66 (m, 2H), 1.42-1.21 (m, 10H), 0.87 (t, 3H, *J* = 6.6 Hz); ^{13}C NMR (THF-d_8, 50 MHz): δ = 163.57, 154.40, 153.76, 153.38, 148.32, 148.29, 142.22, 140.94, 139.85, 137.13, 132.27, 131.70, 131.65, 130.84, 130.39, 130.28, 129.99, 129.53, 128.78, 128.15, 125.44, 125.36, 123.95, 123.47, 116.17, 104.35, 32.681, 31.75, 30.31, 30.22, 30.09, 29.61, 23.38, 14.29; HRMS (Q-TOF): $[M - H]^-$ = 743.25145 (calcd. for $C_{46}H_{39}N_4O_2S_2$: 743.2519), $[M\text{-}CO_2H]^-$ = 699.2616 (calcd. for $C_{45}H_{39}N_4S_2$: 699.2628); Anal. Calcd for $C_{46}H_{40}N_4O_2S_2$: C, 74.16; H, 5.41; N, 7.52; S, 8.61. Found: C, 73.87; H, 5.51; N, 7.41; S, 8.89.

Optical and electrochemical characterizations. UV-vis absorption spectra were recorded in solution on a Perkin-Elmer Lambda 2 spectrometer (wavelength range: 180-820 nm; resolution: 2 nm). Electrochemical studies of the synthesized molecules were carried out in a one compartment, three-electrode electrochemical cell equipped with a flat platinum working electrode (7 mm^2), a Pt wire counter electrode, and a Ag wire pseudo-reference electrode, whose potential was checked using the Fc/Fc^+ couple as an internal standard. The electrolyte consisted of 0.1 M tetrabutylammonium tetrafluoroborate (Bu_4NBF_4) solution in dichloromethane containing 2 x 10^{-3} M of the dye. The experiments were carried out in a glove box.

Modelling. The density functional theory (DFT) calculations were performed on the two organic sensitizers by using the Amsterdam Density Functional package (ADF 2010.01) [ADF2010, SCM, Theoretical Chemistry, Vrije Universiteit, The Netherlands Amsterdam, http://www.scm.com (scientific computing and modelling accessed 21-01-2014)][23]. The structures of the dyes have been fully optimized at a GGA level using the Perdew-Burke-Ernzerhof (PBE) functional and triple zeta plus 2 polarization Slater functions (TZ2P set in ADF) basis sets for all atoms, with 1 s orbitals frozen for C, N and O atoms.

On these optimized geometries, B3LYP hybrid functional calculations with TZ2P all electron basis sets were then performed to yield more reliable frontier orbital energies. Acetonitrile solvent was taken into account using a polarizable continuum model (COSMO in ADF)[24] for all geometry optimizations and B3LYP single point calculations. Orbitals were drawn using the graphical interface of ADF (ADF-GUI).

Solar cell fabrication and characterization. For optimized DSC devices employing acetonitrile electrolyte, photoanodes consisted of a 13 µm layer of mesoporous TiO_2 and a 4 µm scatter layer were prepared. Prior to the deposition of the TiO_2 paste the conducting glass substrates were immersed in a solution of $TiCl_4$ (40 mM) at 70ºC for 30 min, washed with water and ethanol and then dried. The TiO_2 nanoparticle paste was deposited onto a conducting glass substrate (NSG glass with 8 Ω cm^{-2} resistance) using the screen printing technique. The TiO_2 electrodes were gradually heated under airflow at 325ºC for 5 min, 375ºC for 5 min, 450ºC for 15 min and 500ºC for 15 min. The heated TiO_2 electrodes were immersed again in a solution of $TiCl_4$ (40 mM) at 70ºC for 30 min and then washed with water and ethanol. The electrodes were heated again at 500ºC for 30 min and cooled before sensitization. In order to reduce scattered light from the edge of the glass electrodes of the dyed TiO_2 layer, a light shading mask was used on the DSCs, so the active area of DSCs was fixed to 0.16 cm^2. The counter electrode was made by spreading a 5 mM solution of H_2PtCl_6 in isopropyl alcohol onto a conducting glass substrate (TEC15, Pilkington) with a small hole to allow the introduction of the liquid electrolyte using vacuum, followed by heating at 390ºC for 15 min. TiO_2 films were dipped overnight in the corresponding dye solution. The sensitized electrodes were washed with ethanol and dried under air. Finally, the working and counter electrodes were sandwiched together using a thin thermoplastic (Surlyn) frame that melts at 100ºC. The volatile electrolyte used consisted of 0.5 M 1-butyl-3-methylimidazolium iodide (BMII), 0.1 M lithium iodide, 0.05 M iodine and 0.5 M *tert*-butylpyridine in acetonitrile. The non-volatile electrolyte used consisted of (molar ratio) DMII (12), EMII (12), EMITCB (16), iodine (1.67), *n*-butyl benzimida-zole (3.33) and guanidinium thiocyanate (0.67).

Charge extraction and transient photovoltage measurements. For charge extraction white light from a series of LEDs was used as the light source. When the LEDs are turned off, the cell is immediately short circuited and the charge is extracted allowing the electron density in the cells to be calculated. By changing the intensity of the LEDs, the electron density can be estimated as a function of cell voltage. In transient photovoltage measurements, in addition to the white light applied by the LEDS, a diode

pulse (660 nm, 10 mW) is applied to the sample inducing a change of 2-3 mV within the cell. The resulting photovoltage decay transients are collected and the τ values are determined by fitting the data to the equation exp(–t/τ).

Acknowledgments

Gaelle Berthoux and Yann Kervella are acknowledged for their assistance in the synthesis of some of the intermediates. Dr Pascale Maldivi is acknowledged for the density functional theory (DFT) calculations. Authors acknowledge the European Union Research Executive Agency for funding through the Adios-Ru research project. This project is funded by the European Union Research Executive Agency (contract 315131) on the Research for SMEs programme. Emilio Palomares would like to thank ICIQ and ICREA for economic support.

Author contributions

D.J. synthesized and characterized the dye. F.O., S.N., L.P. and J.N.C. carried out the fabrication and the optimisation of the solar cells and designed and analysed the experiments. L.P. and J.N.C. performed the photophysical characterization of the devices. F.O. and S.N. performed the lifetime measurements and stability tests of the solar cells. J.C. contributed to the optimization of the synthesis of the dye. R.D. designed the dye, R.D. and E.P. designed the experiments, contributed to the analysis of the data and wrote the paper. All the authors revised the manuscript.

2. Paper 5: Use of vinyl and Ethynyl Molecular Bridges in Organic Dyes for Dye Sensitized Solar Cells: Implications in Device Performance

Laia Pellejà,[1]‡ Rocío Dominguez,[2]‡ Ana Aljarilla,[2]‡ John N. Clifford,[1] Pilar de la Cruz,[2] Fernando Langa[2]* and Emilio Palomares.[1,3]*

[1]Institute of Chemical Research of Catalonia (ICIQ), Av. Països Catalans 16, Tarragona. E-43007 Spain.
[2]Instituto de Nanociencia, Nanotecnologia y Materiales Moleculares (INAMOL), Universidad de Castilla-La Mancha, Campus de la Fábrica de Armas, Toledo. E-45071, Spain.
[3]Catalan Institution for Advanced Studies and Research (ICREA), Passeig Lluís Companys 23, Barcelona. E-08010 Spain.

Submitted to ChemElectroChem

Abstract: A series of organic dyes with alkene and alkyne bridges were synthesized, fully characterized and used as light-harvesting chromophores in TiO_2 based photo-electrochemical Dye Sensitized Solar Cells (DSCs). A maximum light-to-energy conversion efficiency of η = 5.47% under standard conditions was obtained for the organic dye labelled as **FL16**, which consists of a *N,N*-bis(4-hexyloxyphenyl)aniline donor moiety, an ethynylthieno[3,2-b]thiophene π-bridge and a 2-cyanoacrylic acid acceptor group. Device properties were investigated using charge extraction and transient photo-voltage measurements.

2.1. Introduction

Organic sensitizers have pushed the efficiency of mesoporous nanocrystalline TiO_2 based Dye Sensitized Solar Cells (DSSC) to record light-to-energy conversion efficiencies of over 12%.[12] For this type of solar cells to be competitive and low cost it is required that the sensitizer preparation involves the minimum number of synthetic steps and to be carried out on a multi-gram scale.

A great number of sensitizers have been developed all having in their chemical structure “push-pull” molecular architecture,[7,25] including recently high efficiency porphyrins.[26] In fact, the fine-tuning of the “molecular bridge” between the donor (often a substituted triphenylamine) and the acceptor (commonly a cyanoacrylic acid anchoring group) groups is achieved by

molecular design through, for example, the introduction of double bonds or other different conjugated units (with the aim of broadening the dyes absorption spectra) or increasing the number of bulky groups to minimize dye aggregation. All these chemical strategies are focused to enhance the device efficiency.[18]

On the other hand, less often has been studied the effects that these changes on the molecule backbone, causes on the device interfacial charge transfer kinetics. In other words, it is necessary more work to clarify the fundamental reasons affecting such increase or decrease of the device efficiency when we introduce new functionalities in the D-π-A organic dye.

In the present work we have synthesized a series of organic sensitizers (Scheme 5.2) with different bridges between the *N,N*-bis(4-hexyloxy-phenyl)aniline (A-TPA) donor moiety and the cyanoacrylic acid acceptor-anchoring group.

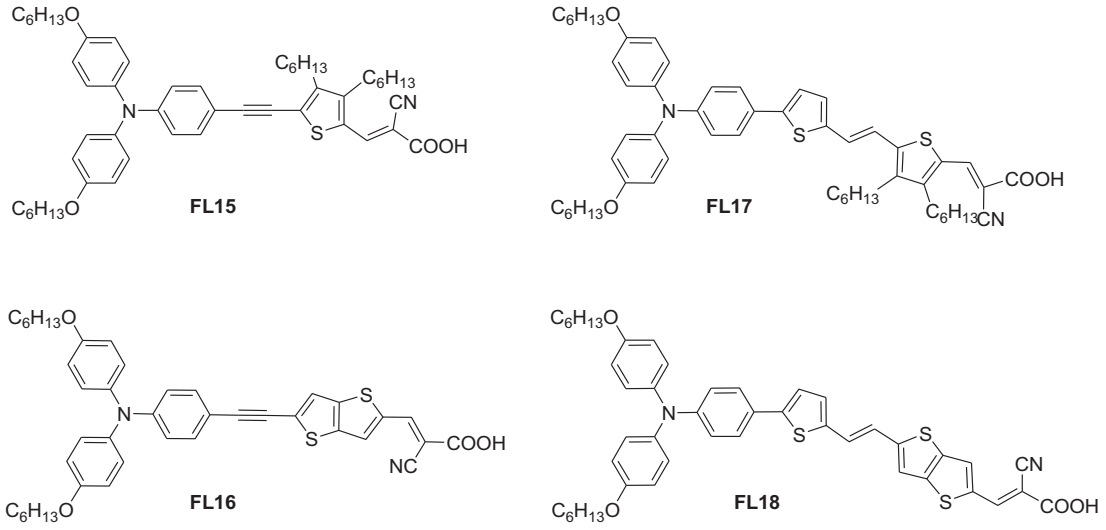

Scheme 5.2. Chemical structures of **FL15-18**.

Dyes **FL15** and **FL16** were synthesized according to Scheme 5.3, starting from alkyne **1**.[27] Sonogashira coupling between **1** and 2-iodothiophene derivatives **2a** (see experimental procedure) and **2b**[28] afforded aldehydes **3a,b** in 87% and 66% yield respectively after purification by column chromatography. The formation of **3a,b** was evidenced in ^{1}H NMR by the presence of the aldehyde fingertip at δ = 9.96 ppm in both cases. With compounds **3a,b** in hand, the desired dyes **FL15** and **FL16** were readily accessible via Knoevenagel condensation with cyanoacetic acid, in the presence of piperidine, in satisfactory yields (FL15: 71% and FL16: 85%).

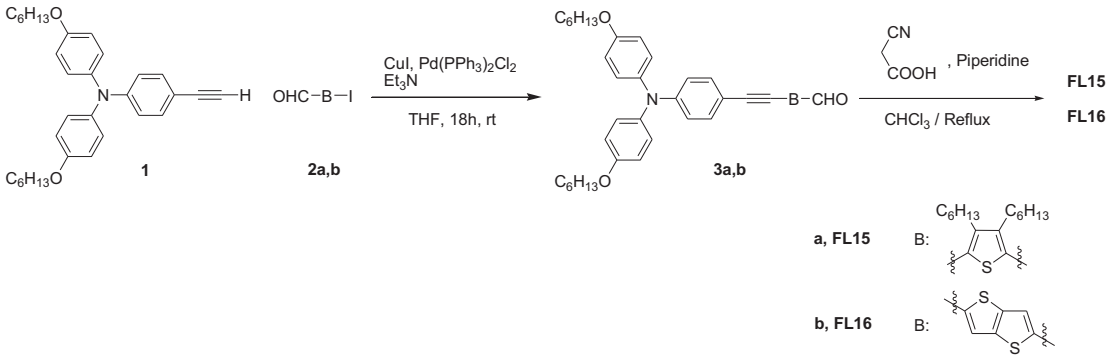

Scheme 5.3. Synthesis of dyes **FL15** and **FL16**.

On the other hand, dyes **FL17** and **FL18** were prepared, as indicated in Scheme 5.4, by the Wittig-Horner reaction between A-TPA-based phosphonate **5**[29] and aldehydes **6**[30] or **8**[31] (in this case, under careful stoichiometric conditions); after purification by column chromatography, **7** and **4b** were obtained in 62% and 45% yield respectively. The *trans* character of the newly formed double bond was evidenced by a coupling constant value of J = 15.0 Hz measured by ^{1}H NMR. Aldehyde **4a** was prepared in 70% yield by Vilsmeier formilation of **7**. Finally, Knoevenagel condensation of **4a,b** with cyanoacetic acid yielded dyes **FL17** and **FL18** in 83% and 75% yield respectively. The formation of the cyanoacrylic double bond is shown in the ^{1}H NMR spectra by the singlet at around 8.20-8.40 ppm. All new compounds were fully characterized by ^{1}H and ^{13}C NMR, FT-IR and MALDI-MS spectrometry. The data were confirmed to be consistent with the expected structures.

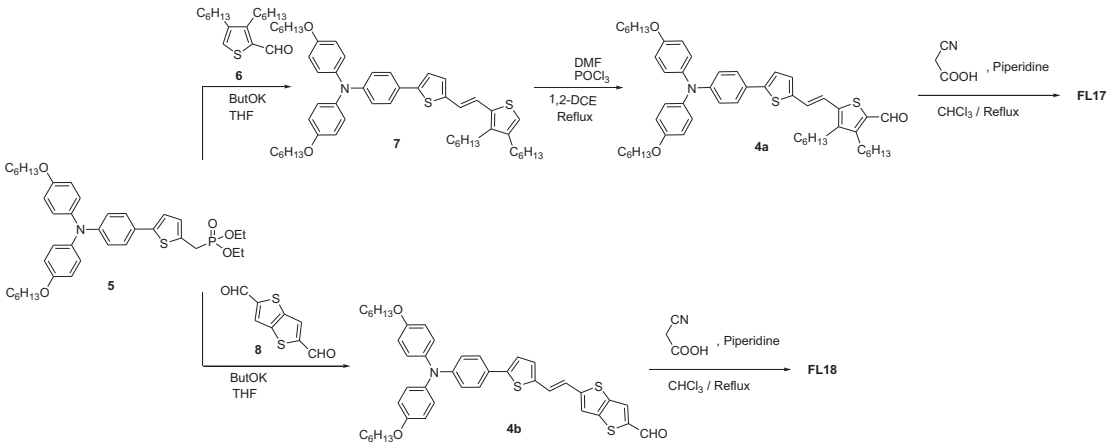

Scheme 5.4. Synthesis of dyes **FL17** and **FL18**.

2.2. Optical and electrochemical properties

The optical and electrochemical properties of the new dyes were studied

by UV-Visible spectroscopy and cyclic (CV) and Osteryoung square wave (OSWV) voltammetries and the data are displayed in Table 5.4.

Table 5.4. Absorption and electrochemical data of dyes **FL15**, **FL16**, **FL17** and **FL18**.

Dye	λ_{em} [a] / nm	E^1_{ox} [b] / V	E^2_{ox} [b] / V	E_{HOMO} [c] / eV
FL15	327 (4.36), 471 (4.41)	0.29	0.80	–5.39
FL16	361 (4.37), 463 (4.41)	0.30	0.64	–5.40
FL17	356 (3.06), 532 (4.47)	0.17	0.55	–5.27
FL18	374 (4.27), 490 (4.41)	0.21	0.55	–5.31

[a] Solvent: CH_2Cl_2. [b] Measured by OSWV; [10^{-3} M] in ODCB:ACN *vs.* Fc/Fc^+, glassy carbon, Pt counter electrode, 20ºC, 0.1 M Bu_4NClO_4, scan rate = 100 mV s^{-1}. [c] Calculated using equation E_{HOMO} (vs. vacuum) = -5.1 - E^1_{ox} (vs. Fc/Fc^+) in eV.

In dichloromethane solution, all dyes show intense absorption in the visible region up to 600-650 nm. Both dyes with a thiophene bridge, **FL15** and **FL17**, showed maxima at 471 nm and 532 nm respectively; the bathochromic shift of the absorption for dye **FL17** is attributed to the increased conjugation. On the other hand, dyes **FL16** and **FL18**, based on thieno[3,2-b]thiophene, show a broader absorption (see Figure 5.6, right) with maxima at 463 and 490 nm.

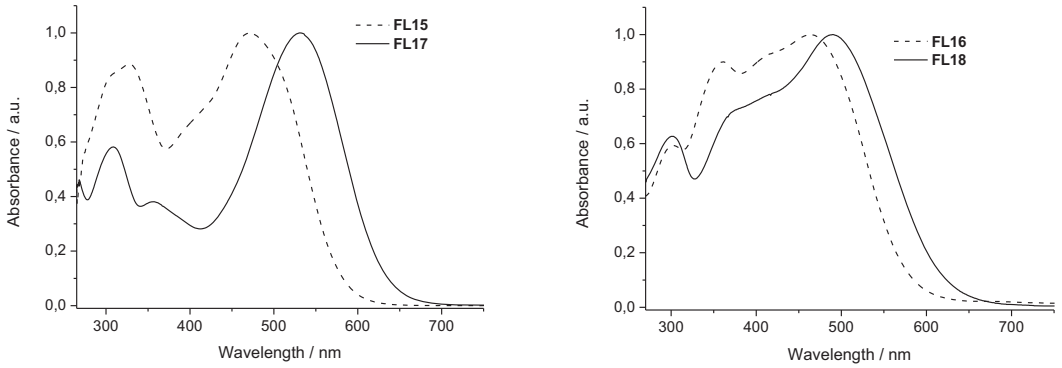

Figure 5.6. (left) Normalized absorption spectra of compound **FL15** and **FL17** and (right) **FL16** and **FL18** in CH_2Cl_2 solution.

The charge transfer character of the most intense band can be confirmed by the positive solvatochromism found when increasing the solvent polarity. As for example, for dye **FL17** the maximum absorption peak is shifted by 21 nm as the solvent polarity increases (λ_{max} = 510 nm in Et_2O, 520 nm in THF and 531 nm in CH_2Cl_2, Figure 5.7). The bathochromic shift (up to 27.5 nm) is higher in thieno[3,2-b]thiophene bridged dye **FL16** (λ_{max} = 436 nm in Et_2O, 449 nm in THF and 463 nm in CH_2Cl_2, Figure 5.7). Moreover, a good correlation (correlation coefficient > 0.99) was found in both cases between the absorption maxima and the Kamlet-Taft constants (π*) (Figure 5.8). The

slope (S) of the Kamlet-Taft equation ($E = E^{\circ} + S\pi^*$) is higher, in absolute value, for **FL16** (S = 7.1) than for **FL17** (S =3.9) (Figure 5.8) indicating a higher polarizability of **FL16** and, consequently, better ability for charge transfer between the A-TPA moiety and the acceptor unit through the thiophene than thieno[3,2-b]thiophene than thiophene moieties. The fact is reflected in a higher efficiency of the solar cell for **FL16** than **FL17** (see Table 5.5).

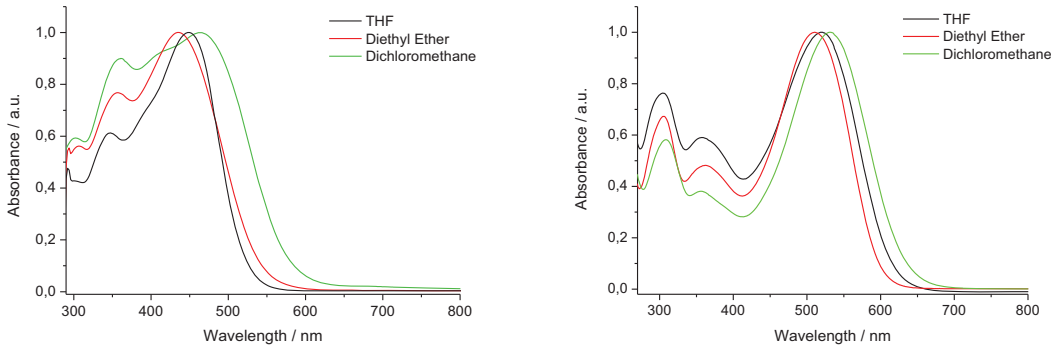

Figure 5.7. UV-visible spectra of compound **FL16** (left) and **FL17** (right) in three different solvents with different polarity.

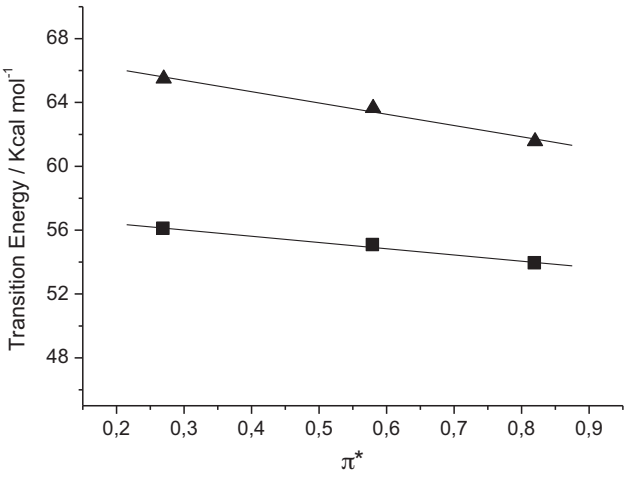

Figure 5.8. Energy transitions of the low energy band for dyes **FL16** (▲) and **FL17** (■) *vs* Taft constant of solvents.

The redox properties for all dyes were investigated at room temperature by employing CV and OSWV in *o*-dichlorobenzene-acetonitrile (4:1), (Table 4.4). In the cathodic region, all compounds show a first reversible (determined by CV) oxidation wave between 0.17 and 0.30 V (vs Fc/Fc^{+}), assigned to the TPA moiety (this assignment is consistent with the oxidation potential of TPA). A second oxidation potential is observed and assigned to the thiophene molecular bridge.

The E_{HOMO} values (calculated with respect to ferrocene as reference, E_{HOMO}: -5.1 eV)[32] were determined to be between -5.27 eV and -5.40 eV (see Table 4.4), indicating that efficient dye regeneration by the I^-/I_3^- redox electrolyte (E_{redox} = -4.75 eV) is energetically favorable for these sensitizers.

2.3. Devices characteristics

FL15-18 were used to fabricate DSSC solar cells and measured under standard sun-simulated illumination conditions (AM 1.5G 100 mW m^{-2}). The I-V curves (photocurrent-voltage curves) recorded under illumination and in the dark are shown in Figure 5.9 and device properties are listed in Table 5.5.

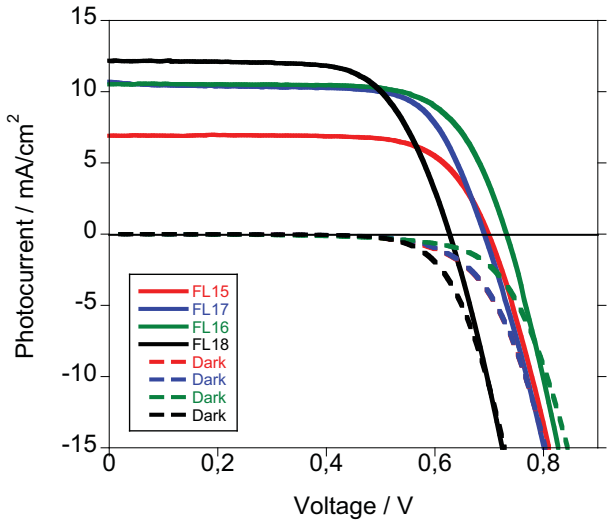

Figure 5.9. I-V curves for **FL15-18** devices recorded under AM 1.5G (100 mW m^{-2}) illumination and in the dark.

Table 5.5. DSCs parameters at 1 sun (100 mW m^{-2} sun simulated AM 1.5G irradiation).

Dye	I_{sc} / mA cm^{-2}	V_{oc} / V	FF / %	μ * / %
FL15	6.91	0.70	72	3.50 (4.5)
FL16	10.51	0.73	71	5.47 (6.7)
FL17	10.71	0.69	71	5.21 (6.3)
FL18	12.18	0.63	67	5.15 (6.2)

* In parenthesis, efficiency without mask. I_{sc}: short-circuit photocurrent, V_{oc}: open circuit voltage, FF: fill factor and μ: device efficiency.

Once the solar cells efficiency was measured and we observed the differences in performance we carried out the photo-induced charge extraction and transient photovoltage measurements (see details about the techniques at the SI). As can be observed in Figure 5.10, for devices made using dyes

FL15, **FL17** and **FL18** the measured charge lies within the same exponential curve. Such observation implies that these dyes, despite their different molecular bridge, do not induce a shift of the TiO_2 conduction band. On the other hand, the dye **FL16** that leads to the device with higher open circuit voltage has a 30 mV shift indicating, therefore, an upward shift of the TiO_2 conduction band.[33] This observation is in good agreement with the higher polarizability measured for **FL16**. The formation of molecular dipoles at the TiO_2 surface, has been reported by several authors as one of the main factors affecting the device V_{oc} too.[34] Moreover, the comparison between **FL15** and **FL16**, both dyes having the ethynyl bridge unit, illustrates that the presence of alkyl chains in **FL15** do not blocks the back-electron transfer reaction between the photo-injected electrons at the TiO_2 and the oxidized electrolyte. As can be seen in Figure 5.10(b), for the same number of charges the charge lifetime follows the same trend ($\tau \approx 0.1$s) for **FL15** and **FL16** based solar cells.

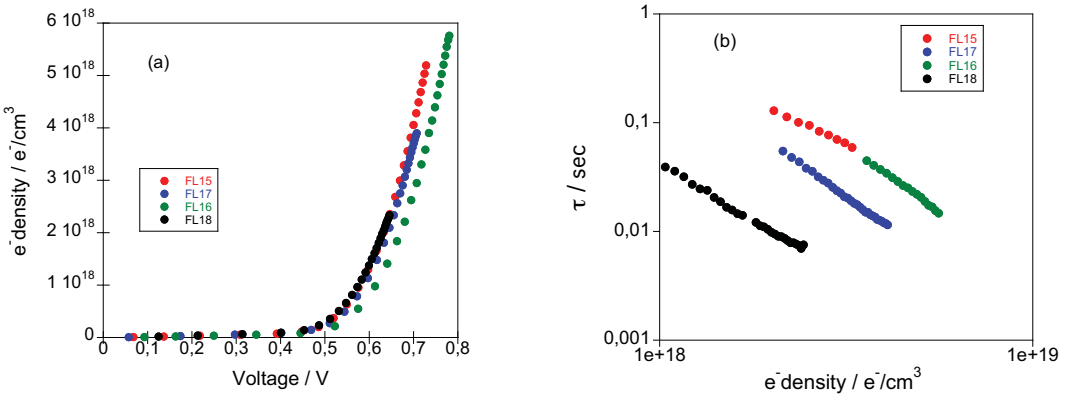

Figure 5.10. (a) Electron density as a function of cell voltage and (b) device charge lifetime, τ, as a function of charge density.

Thus, we can conclude that for the dyes studied herein, which "push-pull" structure is certainly very similar to most of the organic sensitizers used in DSSC, the presence of a alkyne bridge does not consistently leads to faster recombination dynamics between the photo-injected electrons at the TiO_2 and the oxidized electrolyte.

In fact, in our study the slower recombination dynamics in functional devices is achieved with one of the dyes (**FL16**) having a triple bond bridge in their molecular structure. Moreover, we show that dye polarizability must be also taken into account when designing the sensitizer as the formation of dipoles at the surface of the TiO_2 can influence the charge recombination kinetics and, thus, the device V_{oc}.

Author Contributions

Emilio Palomares designed the experiments. Fernando Langa designed the organic dyes. Laia Pellejà carried out the device preparation and characterization. John N. Clifford characterized the devices using photo-induced spectroscopic techniques. Rocío Domínguez, Ana Aljarilla and Pilar de la Cruz carried out the synthesis and characterized the organic dyes. All authors discussed the results and contributed to write the manuscript. ‡ These scientists contributed equally to this work

Acknowledgements

EP would like to thank the Spanish MINECO grant CTQ2010-18859 and the EU for the ERCstg PolyDot. ICREA and ICIQ economical support is also acknowledged. FL thanks the Spanish MINECO grant CTQ2010–17498/BQ.

2.4. Supporting information

2.4.1. Experimental conditions

Synthetic procedures were carried out under inert argon atmosphere, in dry solvent unless otherwise noted. All reagents and solvents were reagent grade and were used without further purification. Chromatographic purifications were performed using silica gel 60 SDS (particle size 0.040-0.063 mm). Analytical thin-layer chromatography was performed using Merck TLC silica gel 60 F254. ^{1}H NMR spectra were obtained on Bruker TopSpin AV-400 (400 MHz) spectrometer. Chemical shifts are reported in parts per million (ppm) relative to the solvent residual peak ($CDCl_3$, 7.27 ppm; DMSO-d_6, 2.50 ppm). ^{13}C NMR chemical shifts are reported relative to the solvent residual peak ($CDCl_3$, 77.00 ppm; DMSO-d_6, 39.52 ppm). UV-Vis measurements were carried out on a Shimadzu UV 3600 spectrophotometer. For extinction coefficient determination, solutions of different concentration were prepared in CH_2Cl_2, HPLC grade, with absorption between 0.1-1 of absorbance using a 1 cm UV cuvette. The emission measurements were carried out on Cary Eclipse fluorescence spectrophotometer. Mass spectra (MALDI-TOF) were recorded on a VOYAGER DE^{TM} STR mass spectrometer using dithranol as matrix. Melting points are uncorrected.

The molecular geometries and frontier molecular orbitals of these new dyes have been optimized by density functional theory (DFT) calculations at the B3LYP/6-31G* level.

Cyclic voltammetry was performed in *o*-dichlorobenzene/acetonitrile 4:1 solutions. Tetrabutylammonium perchlorate (0.1 M as supporting electrolyte) were purchased from Acros and used without purification. Solutions were deoxygenated by argon bubbling prior to each experiment which was run under argon atmosphere. Experiments were done in a one-compartment cell equipped with a glassy carbon working electrode (∅ = 2 mm) and a platinum wire counter electrode. An $Ag/AgNO_3$ (0.01 M in the supporting electrolyte) electrode was used as reference and checked against the ferrocene/ ferrocenium couple (Fc/Fc^+) before and after each experiment.

2.4.2. Synthetic procedures and analytical data

Synthesis of 3,4-dihexyl-5-iodo-2-thiophencarboxaldehyde (2a).

3,4-di-hexyl-2-thiophencarboxaldehyde (**6**) (100 mg, 0.36 mmol) was dissolved in CCl_4 (10 mL) and treated with iodine (45 mg, 0.18 mmol) and *bis*-(trifluoro-acetoxy)iodobenzene (83 mg, 0.19 mmol). The reaction mixture was stirred at room temperature for 3 h and washed with aq. $Na_2S_2O_3$. The organic layer was dried and the solvent was evaporated under vacuum. The residue was purified by column chromatography using silica gel and hexane/$CHCl_3$ 3:2 as eluent to give the pure product as yellow oil in a 72% (105 mg, 0.26 mmol). ^{1}H NMR (400 MHz, $CDCl_3$) δ/ppm: 9.90 (s, 1H), 2.93-2.89 (m, 2H), 2.56-2.52 (m, 2H), 1.62-1.54 (m, 4H), 1.38-1.30 (m, 12H), 0.94-0.89 (m, 6H); ^{13}C NMR (100 MHz, $CDCl_3$) δ/ppm: 181.2, 150.5, 148.4, 143.0, 32.4, 31.5, 31.4, 30.6, 29.7, 29.3, 29.2, 27.8, 22.6, 22.5, 14.0; UV-Vis (CH_2Cl_2) λ_{max}/nm (log ε): 316 (4.24); FT-IR (ATR) ν/cm^{-1}: 2924, 2854, 1657, 1362, 673; MS (*m/z*) (MALDI-TOF): calculated $C_{17}H_{27}IOS$: 406.08; found: 406.08 (M^+).

General procedure for the synthesis of aldehydes 3a and 3b.

A flame-dried Schlenk flask was charged with 4-ethynyl-*N*,*N*-bis(4-hexyloxy-phenyl)aniline (**1**) (0.26 mmol), the corresponding iodide derivative (**2a**,**b**) (0.17 mmol), $Pd(PPh_3)_2Cl_2$ (0.02 mmol), and CuI (0.03 mmol). After three successive vacuum/argon cycles, THF (30 mL) and triethylamine (20 mL) were introduced via syringe. The mixture was stirred at room temperature for 18 h and filtered through celite. The solution was concentrated to obtain

the reaction crude, which was chromatographed on silica gel (hexane/$CHCl_3$ 1:1).

Synthesis of 3a: 0.55 mmol of 4-ethynyl-*N*,*N*-bis(4-hexyloxyphenyl) aniline (**1**) and 0.37 mmol of 3,4-dihexyl-5-iodo-2-thiophencarboxaldehyde (**2a**) give **3a** as a red oil in 67% yield (185 mg, 0.25 mmol).^{1}H NMR (400 MHz, $CDCl_3$) δ/ppm: 9.96 (s, 1H), 7.29-7.27 (m, 2H), 7.07 (d, 4H, *J* = 9.0 Hz), 6.86-6.83 (m, 6H), 3.94 (t, 4H, *J* = 6.4 Hz), 2.86 (t, 2H, *J* = 8.0 Hz), 2.68 (t, 2H, *J* = 8.0 Hz), 1.82-1.75 (m, 4H), 1.64-1.55 (m, 2H), 1.50-1.46 (m, 6H), 1.37-1.29 (m, 20H), 0.94-0.86 (m, 12H); ^{13}C NMR (100 MHz, $CDCl_3$) δ/ppm: 181.9, 156.2, 1513, 149.5, 147.5, 139.6, 136.7, 132.4, 129.4, 127.3, 118.6, 115.4, 112.4, 100.9, 68.2, 32.2, 31.6, 31.5, 30.1, 29.4, 29.3, 27.9, 27.4, 25.8, 22.7, 22.6, 22.5, 14.1, 14.0; UV-Vis (CH_2Cl_2) λ_{max} /nm (log ε): 422 (4.31), 303 (4.29); FT-IR (ATR) υ/cm^{-1}: 2924, 2858, 1655, 1500, 1236, 825. MS (*m/z*) (MALDI-TOF): calculated $C_{49}H_{65}NO_3S$: 747.47; found: 747.62 (M^+).

Synthesis of 3b: 0.42 mmol of 4-ethynyl-*N*,*N*-bis(4-hexyloxyphenyl) aniline (**1**) and 0.28 mmol of 2-formyl-5-iodothieno[3,2-b]thiophene (**2b**) yield **3b** as an orange oil in 56% (101 mg, 0.16 mmol). ^{1}H NMR (400 MHz, $CDCl_3$) δ/ppm: 9.96 (s, 1H), 7.85 (s, 1H), 7.38 (s, 1H), 7.31 (d, 2H, *J* = 8.8 Hz), 7.08 (d, 4H, *J* = 9.0 Hz), 6.87-6.84 (m, 6H), 3.95 (t, 4H, *J* = 6.4 Hz), 1.83-1.76 (m, 4H), 1.49-1.44 (m, 4H), 1.37-1.35 (m, 8H), 0.94-0.91 (m, 6H); ^{13}C NMR (100 MHz, $CDCl_3$) δ/ppm: 183.2, 156.2, 149.7, 145.9, 145.2, 139.5, 138.9, 132.5, 132.2, 128.9, 127.4, 123.4, 118.4, 115.4, 111.8, 98.6, 81.4, 68.2, 31.6, 29.3, 25.8, 22.7, 14.1; UV-Vis (CH_2Cl_2) λ_{max}/nm (log ε): 427 (4.68), 332 (4.58); FT-IR (ATR) υ/cm^{-1}: 2926, 2856, 2191, 1662, 1502, 1225, 825; MS (*m/z*) (MALDI-TOF): calculated $C_{39}H_{41}NO_3S_2$: 635.25; found (M^+): 635.34.

General procedure for the synthesis of 7 and 4b.

Potassium *tert*-butoxide was slowly added to a solution of phosphonate (**5**) the corresponding aldehyde **6** or **8** in dry THF under argon atmosphere. The reaction mixture was stirred at room temperature, hydrolyzed with water (10 mL) and extracted with CH_2Cl_2 (3×20 mL). The organic phases were dried with $MgSO_4$, filtrated and the solvent was removed *in vacuo*. The product was purified by column chromatography (silica gel, hexane: $CHCl_3$ 7:3).

Synthesis of 7: 0.52 mmol of phosphonate **5**, 1.50 mmol of aldehyde **6** in 10 mL of THF after 2 h afford **7** as an orange oil in 62% yield (259 mg, 0.32 mmol). ^{1}H NMR (400 MHz, $CDCl_3$) δ/ppm: 7.40 (d, 2H, *J* = 8.8 Hz), 7.07 (d, 4H, *J* = 9.0 Hz), 7.05 (d, 1H, *J* = 4.0 Hz), 7.02 (d, 1H, *J* = 15.7 Hz), 6.95 (d, 1H, *J* = 4.0 Hz), 6.94 (d, 1H, *J* = 15.7 Hz), 6.91 (d, 2H, *J* = 8.8 Hz), 6.84 (d,

4H, *J* = 9.0 Hz), 6.76 (s, 1H), 3.94 (t, 4H, *J* = 7.5 Hz), 2.61 (t, 2H, *J* = 8.0 Hz), 2.47 (t, 2H, *J* = 8.0 Hz), 1.81 (t, 2H, *J* = 6.4 Hz), 1.77 (t, 2H, *J* = 6.4 Hz), 1.65-1.58 (m, 4H), 1.51-1.25 (m, 24H), 0.94-0.89 (m, 12H); ^{13}C NMR (100 MHz, $CDCl_3$) δ/ppm: 155.6, 148.3, 143.3, 142.9, 141.1, 140.4, 140.1, 136.5, 126.9, 126.6, 126.2, 122.0, 120.6, 120.3, 119.8, 118.0, 115.2, 68.2, 31.7, 31.6, 31.0, 29.7, 29.6, 29.3, 29.3, 29.0, 26.9, 25.7, 22.7, 22.6, 14.2, 14.1, 14.0; FT-IR (KBr) υ/cm^{-1}: 2953, 2924, 2854, 1502, 1238, 825; MS (m/z) (MALDI-TOF): calculated $C_{52}H_{69}NO_2S_2$: 803.48; found: 803.56 (M^+).

Synthesis of 4b: 0.38 mmol of **5**, 0.42 mmol of thieno[3,2-b]thiophene-2,5-dicarbaldehyde (**8**) in 38 mL of THF after 5 h yield **4b** as a red oil in 45% (123 mg, 0.17 mmol). ^{1}H NMR (400 MHz, $CDCl_3$) δ/ppm: 9.93 (s, 1H), 7.86 (d,1H, *J* = 0.75 Hz), 7.40 (d, 2H, *J* = 8.8 Hz), 7.20 (d,1H, *J* = 0.75 Hz), 7.13 (d, 1H, *J* = 15.4 Hz), 7.11 (d, 1H, *J* = 3.7 Hz), 7.07 (d, 4H, *J* = 9.0 Hz), 7.06 (d, 1H, *J* = 3.7 Hz), 7.01 (d, 1H, *J* = 15.4 Hz), 6.91 (d, 2H, *J* = 8.8 Hz), 6.85 (d, 4H, *J* = 9.0 Hz), 3.94 (t, 4H, *J* = 6.5 Hz), 1.80 (t, 2H, *J* = 6.5 Hz), 1.77 (t, 2H, *J* = 6.5 Hz), 1.50-1.45 (m, 4H), 1.37-1.33 (m, 8H), 0.95-0.91 (m, 6H); ^{13}C NMR (100 MHz, $CDCl_3$) δ/ppm: 207.0, 183.0, 155.7, 151.4, 148.7, 146.6, 145.2, 144.6, 140.1, 139.2, 137.3, 129.3, 129.1, 126.8, 126.3, 125.5, 124.9, 122.2, 119.9, 118.1, 115.3, 68.2, 31.6, 30.9, 29.3, 25.7, 22.6, 14.0; UV-Vis (CH_2Cl_2) λ_{max}/nm (log ε): 301 (4.47), 503 (4.80); FT-IR (KBr) υ/cm^{-1}: 2928, 2854, 1662, 1597, 1504, 1238, 825; MS (*m/z*) (MALDI-TOF): calculated $C_{43}H_{45}NO_3S_3$: 719.26; found: 719.33 (M^+).

Synthesis of compound 4a.

To a solution of of **7** (210 mg, 0.25 mmol) and 0.03 mL of dry DMF (0.39 mmol) in 13 mL of 1,2-dichloroethane (50 mL/mmol) at 0 ºC was slowly added phosphorus oxychloride (0.03 mL, 0.33 mmol). The reaction mixture was refluxed during 6 h, hydrolyzed with a saturated solution of NaOAc (50 mL) and extracted with CH_2Cl_2 (3×35 mL). The organic phases were dried with $MgSO_4$, filtrated and the solvent was removed *in vacuo*. The product was purified by column chromatography (silica gel, Hex/AcOEt, 95:5) to give **4a** (152 mg, 0.175 mmol) as a red oil in 70 % yield. ^{1}H NMR (400 MHz, $CDCl_3$) δ/ppm: 9.98 (s, 1H), 7.41 (d, 2H, *J* = 8.7 Hz), 7.20 (d, 1H, *J* = 15.4 Hz), 7.11 (d, 1H, *J* = 3.8 Hz), 7.07 (d, 4H, *J* = 9.0 Hz), 7.05 (d, 1H, *J* = 3.8 Hz), 6.96 (d, 1H, *J* = 15.4 Hz), 6.91 (d, 2H, *J* = 8.7 Hz), 6.84 (d, 4H, *J* = 9.0 Hz), 3.94 (t, 4H, *J* = 6.5 Hz), 2.85 (t, 2H, *J* = 6.5 Hz), 2.62 (t, 2H, *J* = 6.5 Hz), 1.81 (t, 2H, *J* = 6.5 Hz), 1.77 (dt, 2H, *J* = 6.5 Hz), 1.50-1.30 (m, 28H), 0.94-0.89 (m, 12H); ^{13}C NMR (100 MHz, $CDCl_3$) δ/ppm: 181.8, 155.7, 152.9, 148.7, 146.7, 145.1, 141.6, 140.2, 139.8, 134.7, 129.4, 126.8, 126.7, 126.4, 125.6, 125.4, 122.3, 120.0, 118.2, 115.3, 68.3, 32.3, 31.6, 31.5, 31.1, 29.7, 29.6, 29.4, 29.3, 29.3,

27.2, 26.4, 25.8, 22.7, 22.6, 22.5, 14.1, 14.0; UV-Vis (CH_2Cl_2) λ_{max}/nm (log ε): 465 (4.56); FT-IR (ATR) υ/cm^{-1}: 2953, 2924, 2854, 1649, 1597, 1500, 1238, 825; MS (*m/z*) (MALDI-TOF): calculated $C_{53}H_{69}NO_3S_2$: 831.47; found: 831.60 (M^+).

General procedure for the synthesis of FL15, FL17, FL16 and FL18.

A solution of the corresponding aldehyde (**3a**,**b** or **4a**,**b**) (1 mmol) and cyanoacetic acid (1.5 mmol) in $CHCl_3$ (20 mL/mmol) was refluxed, under argon, in the presence of piperidine (0.1 mmol). After removing the solvent, the residue was purified by column chromatography using silica gel and $CHCl_3$/MeOH 10:1 mixture as the eluent.

Synthesis of FL15: 0.11 mmol of **3a** and 0.17 mmol of cyanoacetic acid were reacted for 5 h to yield **FL15** as a red oil in 87% (81 mg, 0.10 mmol). ^{1}H NMR (400 MHz, $CDCl_3$) δ/ppm: 8.42 (s, 1H), 7.30-7.27 (m, 2H), 7.09 (d, 4H, *J* = 8.8 Hz), 6.87-6.84 (m, 6H), 3.95 (t, 4H, *J* = 6.4 Hz), 2.77-2.68 (m, 4H), 1.82-1.75 (m, 4H), 1.62-1.58 (m, 2H), 1.52-1.44 (m, 6H), 1.42-1.34 (m, 20H), 0.94-0.88 (m, 12H); ^{13}C NMR (100 MHz, $CDCl_3$) δ/ppm: 168.4, 156.3, 154.4, 149.8, 146.5, 145.4, 139.4, 132.6, 131.7, 130.1, 127.4, 118.4, 116.2, 115.4, 112.0, 104.2, 94.5, 81.6, 68.3, 32.1, 31.6, 31.5, 31.4, 30.0, 29.3, 29.2, 28.1, 27.8, 25.8, 22.7, 22.6, 22.5, 14.2, 14.1, 14.0; UV-Vis (CH_2Cl_2) λ_{max}/nm (log ε): 471 (4.41), 327 (4.36); FT-IR (ATR) υ/cm^{-1}: 2926, 2856, 1578, 1502, 1236, 825; MS (*m/z*) (MALDI-TOF): calculated $C_{52}H_{66}N_2O_4S$: 814.47; found: 814.62 (M^+).

Synthesis of FL16: 0.07 mmol of **3b** and 0.10 mmol of cyanoacetic acid were reacted for 5 h giving **FL16** as a purple solid in 66% (32 mg, 0.05 mmol). ^{1}H NMR (400 MHz, DMSO-d_6) δ/ppm: 8.22 (s, 1H), 8.01 (s, 1H), 7.75 (s, 1H), 7.35 (d, 2H, *J* = 8.7 Hz), 7.10 (d, 4H, *J* = 8.7 Hz), 6.94 (d, 4H, *J* = 8.7 Hz), 6.65 (d, 2H, *J* = 8.7 Hz), 3.94 (t, 4H, *J* = 6.4 Hz), 1.71-1.68 (m, 4H), 1.40 (s, 4H), 1.30-1.29 (m, 8H), 0.87 (s, 6H); ^{13}C NMR (100 MHz, DMSO-d_6) δ/ppm: 163.8, 156.6, 149.9, 143.0, 142.2, 140.8, 139.1, 139.0, 132.9, 128.3, 128.2, 125.0, 119.2, 117.3, 116.1, 110.9, 97.6, 82.1, 72.7, 68.1, 60.7, 31.5, 29.1, 25.7, 22.6, 14.4; UV-Vis (CH_2Cl_2) λ_{max} (nm) (log ε): 463.5 (4.41), 361 (4.37), 302.5 (4.18); FT-IR (KBr) υ/cm^{-1}: 3403, 2926, 2856, 2190, 1601, 1506, 1384, 1240, 826; MS (*m/z*) (MALDI-TOF): calculated $C_{42}H_{42}N_2O_4S_2$: 702.26; found: 702.38 (M^+).

Synthesis of FL17: 0.09 mmol of **4a** and 0.14 mmol of cyanoacetic acid were reacted for 2 h giving **FL17** as a blue solid in 83% (67 mg, 0.075 mmol). ^{1}H NMR (400 MHz, $CDCl_3$) δ/ppm: 8.41 (s, 1H), 7.41 (d, 2H, *J* = 8.8

Hz), 7.33 (d, 1H, *J* = 15.5 Hz), 7.13 (d, 1H, *J* = 3.9 Hz), 7.11 (d, 1H, *J* = 3.9 Hz), 7.08 (d, 4H, *J* = 8.9 Hz), 6.98 (d, 1H, *J* = 15.5 Hz), 6.91 (d, 2H, *J* = 8.8 Hz), 6.84 (d, 4H, *J* = 8.9 Hz), 3.95 (t, 4H, *J* = 6.5 Hz), 2.74 (t, 2H, *J* = 7.6 Hz), 2.64 (t, 2H, *J* = 6.5 Hz), 1.81 (t, 2H, *J* = 6.5 Hz), 1.77 (t, 2H, *J* = 6.5 Hz), 1.54-1.31 (m, 28H), 0.94-0.90 (m, 12 H); ^{13}C NMR (100 MHz, $CDCl_3$) δ/ppm: 168.2, 156.2, 155.8, 149.0, 148.8, 146.0, 145.0, 139.6, 130.5, 128.3, 127.2, 126.9, 126.4, 125.4, 122.5, 119.9, 117.3, 116.6, 115.3, 94.3, 68.2, 32.1, 31.6, 31.5, 31.0, 29.4, 29.23, 29.2, 27.8, 26.8, 25.7, 22.6, 22.5, 22.4, 14.1, 14.0; UV-Vis (CH_2Cl_2) λ_{max}/nm (log ε): 308 (4.24), 356 (3.06), 532 (4.47); FT-IR (KBr) ν/cm^{-1}: 2954, 2922, 2852, 1728, 1601,1493, 1460, 1184, 1080, 968, 895, 823; MS (*m/z*) (MALDI-TOF): calculated $C_{56}H_{70}N_2O_4S_2$: 898.48; found: 898.65 (M^+).

Synthesis of FL18: 0.09 mmol of **4b** and 0.10 mmol of cyanoacetic acid were reacted for 4 h giving **FL18** as a red solid in 75% yield (41 mg, 0.067 mmol). ^{1}H NMR (400 MHz, DMSO-d_6) δ/ppm: 8.20 (s, 1H), 8.02 (s, 1H), 7.60 (s, 1H), 7.47 (d, 2H, *J* = 8.8 Hz), 7.30 (d, 1H, *J* = 3.8 Hz), 7.26 (t, 1H, *J* = 3.8 Hz), 7.25 (d, 1H, *J* = 15.5 Hz), 7.19 (d, 1H, *J* = 15.5 Hz), 7.04 (d, 4H, *J* = 9.0 Hz), 6.92 (d, 4H, *J* = 9.0 Hz), 6.76 (d, 2H, *J* = 8.8 Hz), 3.94 (t, 4H, *J* = 6.4 Hz), 1.72 (t, 2H, *J* = 6.4 Hz), 1.68 (t, 2H, *J* = 6.4 Hz), 1.43-1.39 (m, 4H), 1.32-1.29 (m, 8H), 0.90-0.86 (m, 6H); ^{13}C NMR (100 MHz, DMSO-d_6) δ/ppm: 156.0, 139.9, 139.7, 137.6, 129.3, 127.5, 126.7, 119.3, 116.0, 79.4, 68.1, 31.5, 31.2, 29.2, 25.7, 22.5, 14.4; UV-Vis (CH_2Cl_2) λ_{max}/nm (log ε): 301 (4.22), 374 (4.27), 490 (4.41); FT-IR (ATR) ν/cm^{-1}: 2954, 2922, 2852, 1728, 1601, 1493, 1460, 1184, 1080, 968, 895, 823; MS (*m/z*) (MALDI-TOF): calculated $C_{46}H_{46}N_2O_4S_3$: 786.26; found: 786.36 (M^+).

2.4.3. Device fabrication and characterization.

The working and counter electrodes consisted of TiO_2 and thermalized platinum films, respectively, and were deposited onto F-doped tin oxide (FTO, Pilkington Glass Inc., with 15 Ω sq^{-1} sheet resistance) conducting glass substrates. DSCs devices were made using 8 μm thick films consisting of 20 nm TiO_2 nanoparticles (Dyesol© paste) and a scattering layer of 4 μm of 400 nm TiO_2 particles (Dyesol© paste). Prior to the deposition of the TiO_2 paste, the conducting glass substrates were immersed in a solution of $TiCl_4$ (40 mM) at 70ºC for 30 minutes and then dried. The TiO_2 nanoparticle paste was deposited onto a conducting glass substrate using the screen-printing technique. The TiO_2 electrodes were gradually heated under an airflow at 325ºC for 5 min, 375ºC for 5 min, 450ºC for 15 min and 500ºC for 15 min. The heated TiO_2 electrodes were immersed again in a solution of $TiCl_4$ (40 mM) at 70ºC for 30 minutes and then washed with water and ethanol. The electrodes

were heated again at 500ºC for 30 minutes and cooled before dye adsorption. The active area for devices was 0.16 cm^2. The counter electrode was made by spreading a 5 mM solution of H_2PtCl_6 in isopropyl alcohol onto a conducting glass substrate containing a small hole to allow the introduction of the liquid electrolyte using vacuum, followed by heating at 390ºC for 15 minutes. Films were sensitized in 0.3 mM dye solutions in chlorobenzene containing 0.2 mM chenoxydecholic acid overnight at room temperature. Finally, the working and counter electrodes were sandwiched together using a thin thermoplastic (Surlyn) frame that melts at 100ºC. The electrolyte for all devices measured consisted of 0.5 M 1-butyl-3-methylimidazolium iodide (BMII), 0.1 M lithium iodide, 0.05 M iodine and 0.5 M *tert*-butylpyridine in acetonitrile.

The IV characteristics of cells were measured using a Sun 2000 Solar Simulator (150 W, ABET Technologies). The illumination intensity was measured to be 100 mW m^{-2} with a calibrated silicon photodiode. The appropriate filters were utilized to faithfully simulate the AM 1.5G spectrum. The applied potential and cell current were measured with a Keithley 2400 digital source meter. The IPCE (Incident Photon to Current conversion Efficiency) was measured using a homemade set up consisting of a 150 W Oriel Xenon lamp, a motorized monochromator and a Keithley 2400 digital source meter.

Transient photovoltage and charge extraction measurements were carried out on a system described elsewhere. In charge extraction, white light from a series of LEDs was used as the light source. When the LEDs are turned off the cell is immediately short circuited and the charge is extracted allowing electron density in the cells to be calculated. By changing the LEDs intensity the electron density can be estimated as a function of cell voltage. In transient photovoltage measurements, in addition to the white light applied by the LEDS, constant background voltage is applied to the cells and again, a diode pulse (660 nm, 10 mW) is then applied to the sample inducing a change of 2-3 mV within the cell. The resulting photovoltage decay transients are collected and the τ values are determined by fitting the data to the equation $\exp(-t/\tau)$.

References

1. Hardin, B. E.; Snaith, H. J.; McGehee, M. D., The renaissance of dye-sensitized solar cells. *Nature Photon.* **2012,** *6*, 162-169.
2. Boschloo, G.; Hagfeldt, A., Characteristics of the Iodide/Triiodide Redox Mediator in Dye-Sensitized Solar Cells. *Acc. Chem. Res.* **2009,** *42*, 1819-1826.
3. (a) O'Regan, B.; Grätzel, M., A low-cost, high-efficiency solar cell based on dye-sensitized colloidal TiO2 films. *Nature* **1991,** *353*, 737-740; (b) Grätzel, M., Recent Advances in Sensitized Mesoscopic Solar Cells. *Acc. Chem. Res.* **2009,** *42*, 1788-1798.
4. (a) Ardo, S.; Meyer, G. J., Photodriven heterogeneous charge transfer with transition-metal compounds anchored to TiO2 semiconductor surfaces *Chem. Soc. Rev.* **2009,** *38*, 115-164; (b) Hagfeldt, A.; Boschloo, G.; Sun, L.; Kloo, L.; Pettersson, H., Dye-Sensitized Solar Cells. *Chem. Rev.* **2010,** *110*, 6595-6663.
5. Yu, Q.; Wang, Y.; Yi, Z.; Zu, N.; Zhang, J.; Zhang, M.; Wang, P., High-efficiency dye-sensitized solar cells: the influence of lithium ions on exciton dissociation, charge recombination, and surface states. *ACS Nano* **2010,** *4*, 6032-6038.
6. (a) Nazeeruddin, M. K.; A., K.; Rodicio, I.; Humphry-Baker, R.; Mueller, E.; Liska, P.; Vlachopoulos, N.; Grätzel, M., Conversion of light to electricity by cis-X2bis(2,2'-bipyridyl-4,4'-dicarboxylate)ruthenium(II) charge-transfer sensitizers (X = Cl-, Br-, I-, CN-, and SCN-) on nanocrystalline titanium dioxide electrodes. *J. Am. Chem. Soc.* **1993,** *115*, 6382-6390; (b) Gao, F.; Wang, Y.; Shi, D.; Zhang, J.; Wang, M.; Jing, X.; Humphry-Baker, R.; Wang, P.; Zakeeruddin, S. M.; Grätzel, M., Enhance the Optical Absorptivity of Nanocrystalline TiO2 Film with High Molar Extinction Coefficient Ruthenium Sensitizers for High Performance Dye-Sensitized Solar Cells. *J. Am. Chem. Soc.* **2008,** *130*, 10720-10728.
7. Choi, S.-H.; Hwang, D.; Kim, D. Y.; Kervella, Y.; Maldivi, P.; Jang, S. Y.; Demadrille, R.; Kim, I. D., Amorphous Zinc Stannate (Zn2SnO4) Nanofibers Networks as Photoelectrodes for Organic Dye-Sensitized Solar Cells. *Adv. Funct. Mater.* **2013,** *23*, 3146-3155.
8. (a) Ryuzi Katoh, R.; Furube, A.; Mori, S.; Miyashita, M.; Sunahara, K.; Koumuraa, N.; Hara, K., Highly stable sensitizer dyes for dye-sensitized solar cells: role of the oligothiophene moiety. *Energy Environ. Sci.* **2009,** *2*, 542-546; (b) Wang, S.; Cui, Y.; Dan-oh, Y.; Kasada, C.; Shinpo, A.; Hara, K., Molecular Design of Coumarin Dyes for Stable and Efficient Organic Dye-Sensitized Solar Cells. *J. Phys. Chem. C* **2008,** *112*, 17011-17017.
9. (a) Mishra, A.; Fischer, M. K. R.; Bäuerle, P., Metal-Free Organic Dyes for Dye-Sensitized Solar Cells: From Structure: Property Relationships to

Design Rules. *Angew. Chem., Int. Ed.* **2009,** *48*, 2474-2499; (b) Yum, J.-H.; Holcombe, T. W.; Kim, Y.; Rakstys, K.; Moehl, T.; Teuscher, J.; Delcamp, J. H.; Nazeeruddin, M. K.; Grätzel, M., Blue-Coloured Highly Efficient Dye-Sensitized Solar Cells by Implementing the Diketopyrrolopyrrole Chromophore. *Scientific Reports* **2013,** *3*, 2446; (c) Zhang, M.; Wang, Y.; Xu, M.; Ma, W.; Lia, R.; Wang, P., Design of high-efficiency organic dyes for titania solar cells based on the chromophoric core of cyclopentadithiophene-benzothiadiazole. *Energy Environ. Sci.* **2013,** *6*, 2944-2949; (d) Wu, Y.; Zhu, W., Organic sensitizers from D–p–A to D–A–p–A: effect of the internal electron-withdrawing units on molecular absorption, energy levels and photovoltaic performances. *Chem. Soc. Rev.* **2013,** *42*, 2039-2058.

10. Zeng, W.; Cao, Y.; Bai, Y.; Wang, Y.; Shi, Y.; Zhang, M.; Wang, F.; Pan, C.; Wang, P., Efficient Dye-Sensitized Solar Cells with an Organic Photosensitizer Featuring Orderly Conjugated Ethylenedioxythiophene and Dithienosilole Blocks. *Chem. Mater.* **2010,** *22*, 1915-1925.

11. Bessho, T.; Zakeeruddin, S. M.; Yeh, C.-Y.; Diau, E. W.-G.; Grätzel, M., Highly Efficient Mesoscopic Dye-Sensitized Solar Cells Based on Donor–Acceptor Substituted Porphyrins. *Angew. Chem.* **2010,** *122*, 6796-6799.

12. Yella, A.; Lee, H. W.; Tsao, H. N.; Yi, C. Y.; Chandiran, A. K.; Nazeeruddin, M. K.; Diau, E. W.-G.; Yeh, C.-Y.; Zakeeruddin, S. M.; Grätzel, M., Porphyrin-Sensitized Solar Cells with Cobalt (II/III)–Based Redox Electrolyte Exceed 12 Percent Efficiency. *Science* **2011,** *334*, 629-634.

13. Kurotobi, K.; Toude, Y.; Kawamoto, K.; Fujimori, Y.; Ito, S.; Chabera, P.; Sundström, V.; Imahori, H., Highly Asymmetrical Porphyrins with Enhanced Push–Pull Character for Dye-Sensitized Solar Cells. *Chem. Eur. J.* **2013,** *19*, 17075-17081.

14. (a) Kim, J.; Choi, H.; Lee, J. W.; Kang, M. S.; Song, K.; Kang, S. O.; Ko, J., A polymer gel electrolyte to achieve ≥6% power conversion efficiency with a novel organic dye incorporating a low-band-gap chromophore. *J. Mater. Chem.* **2008,** *18*, 5223-5229; (b) Zhu, W.; Wu, Y.; Wang, S.; Li, W.; Li, X.; Chen, J.; Wang, Z.-S.; Tian, H., Organic D-A-π-A Solar Cell Sensitizers with Improved Stability and Spectral Response. *Adv. Funct. Mater.* **2011,** *21* (756-763).

15. Haid, S.; Marszalek, M.; Mishra, A.; Wielopolski, M.; Teusche, J.; Moser, J.-E.; Humphry-Baker, R.; Zakeeruddin, S. M.; Grätzel, M.; Bäuerle, P., Significant Improvement of Dye-Sensitized Solar Cell Performance by Small Structural Modification in π-Conjugated Donor–Acceptor Dyes. *Adv. Funct. Mater.* **2012,** *22*, 1291-1302.

16. Clifford, J. N.; Palomares, E.; Nazeeruddin, M. K.; Grätzel, M.; Durrant, J. R., Dye Dependent Regeneration Dynamics in Dye Sensitized Nanocrystalline Solar Cells: Evidence for the Formation of a Ruthenium Bipyridyl Cation/Iodide Intermediate. *J. Phys. Chem. C* **2007,** *111*, 6561-6567.

17. Yum, J.-H.; Moon, S. J.; Humphry-Baker, R.; Walter, P.; Geiger, T.; Nüesch, F.; Grätzel, M.; Nazeeruddin, M. K., Effect of coadsorbent on the photovoltaic performance of squaraine sensitized nanocrystalline solar cells *Nanotechnology* **2008,** *19*, 424005.
18. Clifford, J. N.; Planells, M.; Palomares, E., Advances in high efficiency dye sensitized solar cells based on Ru(II) free sensitizers and a liquid redox electrolyte. *J. Mater. Chem.* **2012,** *22*, 24195-24201.
19. (a) Zakeeruddin, S. M.; Grätzel, M., Solvent-Free Ionic Liquid Electrolytes for Mesoscopic Dye-Sensitized Solar Cells. *Adv. Funct. Mater.* **2009,** *19*, 2187-2202; (b) Gorlov, M.; Kloo, L., Ionic liquid electrolytes for dye-sensitized solar cells. *Dalton Trans.* **2008**, 2655-2666.
20. Zhang, Z.; Ito, S.; Moser, J.-E.; Zakeeruddin, S. M.; Grätzel, M., Influence of Iodide Concentration on the Efficiency and Stability of Dye-Sensitized Solar Cell Containing Non-Volatile Electrolyte. *Chem. Phys. Chem.* **2009,** *10*, 1834-1838.
21. Popov, A. I.; Swensen, R. F., Studies on the Chemistry of Halogens and of Polyhalides. V. Spectrophotometric Study of Polyhalogen Complexes in Acetonitrile and in Ethylene Dichloride. *J. Am. Chem. Soc.* **1955,** *77*, 3724-3726.
22. Sandanayaka, A. S. D.; Taguri, Y.; Araki, Y.; Ishi-i, T.; Mataka, S.; Ito, O., Photoinduced Charge Separation and Charge Recombination in the [60]Fullerene–Diphenylbenzothiadiazole–Triphenylamine Triad: Role of Diphenylbenzothiadiazole as Bridge. *J. Phys. Chem. B* **2005,** *109*, 22502-22512.
23. (a) te Velde, G.; Bickelhaupt, F. M.; Baerends, E. J.; Fonseca-Guerra, C.; van Gisbergen, S. J. A.; Snijders, J. G.; Ziegler, T., Chemistry with ADF. *J. Comput. Chem.* **2001,** *22*, 931-967; (b) Fonseca-Guerra, C.; Snijders, J. G.; te Velde, G.; Baerends, E. J., Towards an order-N DFT method. *Theor. Chem. Acc.* **1998,** *99*, 391-403.
24. Pye, C. C.; Ziegler, T., An implementation of the conductor-like screening model of solvation within the Amsterdam density functional package. *Theor. Chem. Acc.* **1999,** *101*, 396-408.
25. (a) Cai, N.; Zhang, J.; Xu, M.; Zhang, M.; Wang, P., Improving the Photovoltage of Dithienopyrrole Dye-Sensitized Solar Cells via Attaching the Bulky Bis(octyloxy)biphenyl Moiety to the Conjugated π-Linker. *Adv. Funct. Mater.* **2013,** *23*, 3539-3547; (b) Planells, M.; Pellejà, L.; Clifford, J. N.; Pastore, M.; De Angelis, F.; Lopez, N.; Marder, S. R.; Palomares, E., Energy levels, charge injection, charge recombination and dye regeneration dynamics for donor–acceptor π-conjugated organic dyes in mesoscopic TiO2 sensitized solar cells. *Energy Environ. Sci.* **2011,** *4*, 1820-1829.
26. Wang, C.-L.; Lan, C.-M.; Hong, S.-H.; Wang, Y.-F.; Pan, T.-Y.; Chang, C.-W.; Kuo, H.-H.; Kuo, M.-Y.; Diau, E. W.-G.; Lin, C.-Y., Enveloping

porphyrins for efficient dye-sensitized solar cells. *Energy Environ. Sci.* **2012,** *5*, 6933-6940.

27. Pati, P. B.; Zade, S. S., Selective Colorimetric and "Turn-on" Fluorimetric Detection of Cyanide Using a Chemodosimeter Comprising Salicylaldehyde and Triphenylamine Groups. *Eur. J. Org. Chem.* **2012,** *2012*, 6555-6561.

28. Sato, M.; Kitamura, T.; Masiko, T.; Unoura, K., *J. Organom. Chem.* **2008,** *693*, 247-256.

29. Aljarilla, A.; Lopez-Arroyo, L.; de la Cruz, P.; Oswald, F.; Meyer, T. B.; Langa, F., Organic Dyes Incorporating Oligothienylenevinylene for Efficient Dye-Sensitized Solar Cells. *Org. Lett.* **2012,** *14*, 5732-5735.

30. Oswald, F.; Islam, D. M. S.; Araki, Y.; Troiani, V.; de la Cruz, P.; Moreno, A.; Ito, O.; Langa, F., Synthesis and Photoinduced Intramolecular Processes of Fulleropyrrolidine Oligothienylenevinylene–Ferrocene Triads. *Chem. Eur. J.* **2007,** *13*, 3924-3933.

31. Leriche, P.; Raimundo, J.-M.; Turbiez, M.; Monroche, V.; Allain, M.; Sauvage, F.-X.; Roncali, J.; Frere, P.; Skabara, P. J., Linearly extended tetrathiafulvalene analogues with fused thiophene units as π-conjugated spacers. *J. Mater. Chem.* **2003,** *13*, 1324-1332.

32. Cardona, C. M.; Li, W.; Kaifer, A. E.; Stockdale, D.; Bazan, G. C., Electrochemical Considerations for Determining Absolute Frontier Orbital Energy Levels of Conjugated Polymers for Solar Cell Applications *Adv. Mat.* **2011,** *23*, 2367-2371.

33. Barnes, P. R. F.; Miettunen, K.; Li, X.; Anderson, A. Y.; Bessho, T.; Grätzel, M.; O'Regan, B., Interpretation of Optoelectronic Transient and Charge Extraction Measurements in Dye Sensitized Solar Cells. *Adv. Mat.* **2013,** *25*, 1881-1922.

34. Miyashita, M.; Sunahara, K.; Nishikawa, T.; Uemura, Y.; Koumuraa, N.; Hara, K.; Mori, A.; Abe, T.; Suzuki, E.; Mori, S., Interfacial electron-transfer kinetics in metal-free organic dye-sensitized solar cells: combined effects of molecular structure of dyes and electrolytes. *J. Am. Chem. Soc.* **2008,** *130*, 17874-17881.

Chapter 5. Organic dyes as sensitizers

Chapter 6.
Ruthenium heteroleptic complexes

Ruthenium complexes are the most used compounds by far in DSCs. The easily tunable redox and photophysical properties and the synthetic approach of these complexes, which allows the sequential introduction of different ligands, make these compounds excellent potential candidates for semiconductor sensitization.

In this chapter, two novel heteroleptic ruthenium dyes with bulky groups are studied in order to demonstrate that the use of coadsorbants is not needed. These bulku groups can be used as an effective strategy to prevent aggregation and improve the photocurrent. All the compounds are fully photophysical and electrochemical characterized and the device properties are completely investigated.

Chapter 6. Ruthenium heteroleptic complexes

Index

Chapter 6. Ruthenium heteroleptic complexes

1. Paper 6: Effect of bulky group in ruthenium heteroleptic sensitizers on dye sensitized solar cell performance

Miguel García-Iglesias,[a] Laia Pellejà,[b] Jun-Ho Yum,[c] David González-Rodríguez,[a] Mohammad K. Nazeeruddin,*[c] Michael Grätzel,[c] John N. Clifford,*[b] Emilio Palomares,[bd] Purificación Vásquez[a] and Tomás Torres*[ae]

[a]Universidad Autónoma de Madrid, Facultad de Ciencias, 28049 Madrid, Spain. E-mail: tomas.torres@uam.es
[b]Institute of Chemical Research of Catalonia (ICIQ), Tarragona, Spain. E-mail: jnclifford@iciq.es
[c]Laboratory for Photonics and Interfaces, Institute of Chemical Sciences and Engineering, School of Basic Sciences, Swiss Federal Institute of Technology, CH-1015 Lausanne, Switzerland. E-mail: mdkhaja. nazeeruddin@epfl.ch
[d]Catalan Institution for Advanced Studies and Research (ICREA), Avda. Països Catalans 16, 43007 Tarragona, Spain
[e]Instituto Madrileño de Estudios Avanzados en Nanociencia (IMDEA-Nanociencia), 28049, Madrid, Spain

Chem. Sci. **2012**, 3, 1177

Abstract: Two novel heteroleptic ruthenium sensitizers, **TT204** and **TT205**, containing bulky substituents at the 4,4-positions of the ancillary 2,2-bipyridine ligand, were synthesized and characterized. They exhibit absorption maxima in the visible region at 520-530 nm due to metal-to-ligand charge transfer (MLCT) transitions. The E_{HOMO} and E_{LUMO} values indicate sufficient driving force for efficient dye regeneration by the iodide/tri-iodide redox electrolyte and efficient electron injection into the TiO_2 conduction band following photoexcitation, respectively. The performance of these heteroleptic sensitizers in dye sensitized solar cells was investigated where TiO_2 sensitization was carried out both in the presence and absence of chenodeoxycholic acid. The best efficiency among these sensitizers was recorded in the presence of chenodeoxycholic acid which generated a high short circuit current of 18.7 mA cm^{-2}, an open circuit potential of 0.72 V and a fill factor of 73% with a resulting total power conversion efficiency of 9.81% under AM 1.5G 1 sun illumination. Comparison with the reference dye C101 indicates that though bulky groups can prevent aggregation resulting in high photocurrents even in the absence of chenodeoxycholic acid, they can also lead to lower cell voltages due to inefficient dye packing on the TiO_2 surface.

1.1. Introduction

Since the seminal paper by O'Regan and Grätzel,[1] many efforts have been devoted to the synthesis of molecular dyes that are capable of harvesting light and injecting electrons efficiently into the semiconductor metal-oxide conduction band.[2] A large part of the bibliography dealing with investigations into new sensitizers has focused on ruthenium-based sensitizers.[3] The paradigm for this class of dye is generally considered to be **N719**[4] (Figure 6.1) and it is still among the most efficient ruthenium complexes used in Dye Sensitized Solar Cells (DSCs). More recently, sensitizers such as **C101**[5] and **B11**[6] (Figure 6.1) have been designed in order to absorb longer wavelengths in the visible region. This has been achieved through increased conjugation on the ancillary bipyridine ligand by the incorporation of one or more thiophene units. In fact, these novel ruthenium polypyridine complexes show outstanding photocurrents leading to light-to-energy conversion efficiencies of higher than 11%.

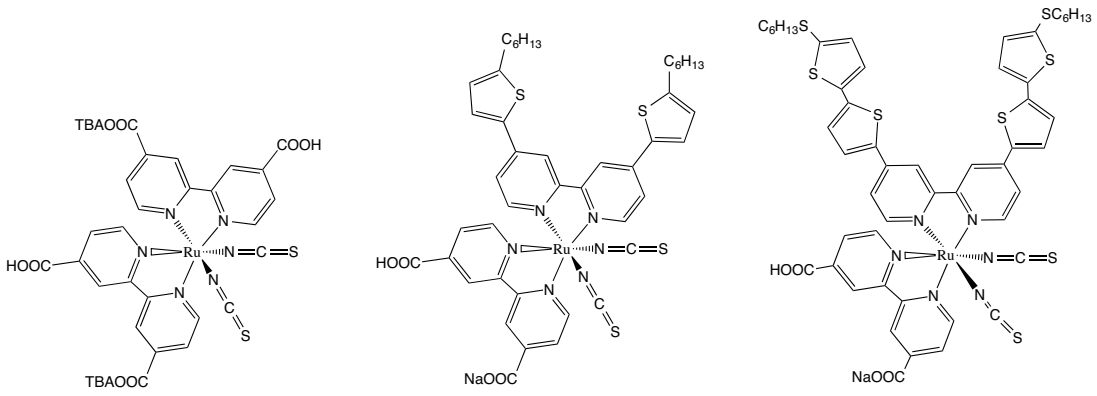

N719 **C101** **B11**

Figure 6.1. Structures of ruthenium polypyridine complexes **N719**, **C101** and **B11**.

Most of the published reports using efficient ruthenium polypyridine complexes require the presence of co-adsorbents (as for example cheno-deoxycholic acid) that minimize the formation of molecular aggregates on the surface of the TiO_2 nanocrystalline film. Several studies have detailed the negative effect of aggregation on device performance[7] and the improvement resulting from using co-adsorbents.[8] Bulky groups in the sensitizer molecular structure can also reduce aggregation, however, such groups have not been employed in ruthenium polypyridine complexes and little is known of the effect of such groups on dye packing and cell performance. Alkyl chains have, however, been incorporated into ruthenium complexes on the 4,4´-positions of the 2,2´-bipyridine, as for example in the dye **Z907**,[9] leading to improvements in cell stability over long periods of

continuous illumination. Moreover, ruthenium complexes have been shown to display improved efficiencies with increasing alkyl chain length.[10] Indeed, many research groups have adopted a similar strategy, using alkyl chains in the molecular design of dye sensitizers, with increased efficiencies observed.[11] The reason for such efficiency improvements has often been cited as the reduction in the back electron transfer reactions between the photo-injected electrons and the oxidized species in the electrolyte. The presence of the alkyl chains retards such interfacial charge transfer recombination reactions leading to an increase in electron lifetime.

The use of more bulky structures present in sensitizers has generally only been exploited for phthalocyanine and porphyrin sensitizers. Mori and co-workers[12] increased device efficiency in a series of phthalocyanines bearing bulky aryl groups. The outstanding porphyrin **YD-2**[13] bears both alkyl chains and bulky *tert*-butyl groups. In this paper we report the synthesis and characterization of two novel **C101** analogues, **TT204** and **TT205** (Figure 6.2) that contain bulky groups on the ancillary bipyridine ligand. We analyse their performances in DSC devices under working conditions and, moreover, the interfacial charge transfer reactions are investigated. Furthermore, we correlate dye structure with function for these novel sensitizers. This study allows for further understanding of ruthenium complexes in DSCs, which it is hoped will ultimately lead to higher light-to-energy conversion efficiencies and improvements in device stability.

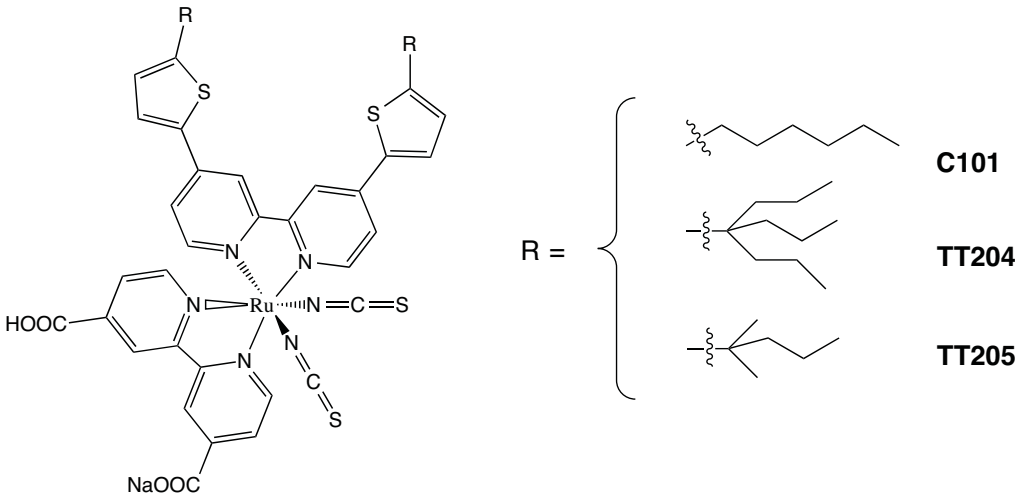

Figure 6.2. Molecular structures of Ru(II) complexes **TT204** and **TT205** employed in this work.

1.2. Experimental section

1.2.1. Materials and reagents

Chemicals employed in this work were purchased from Aldrich Chemical Co. and used as received without further purification. **C101** dye was supplied by the EU FP7 research project ROBUST. Dry solvents were purchased from SDS in anhydrous grade and further dried over activated molecular sieves. The monitoring of the reactions was carried out by TLC, employing aluminium sheets coated with silica gel 60 F_{254} (normal phase) or with LiChroprep RP-18 $F_{254\text{-}S}$ (reverse phase), both purchased from Merck. Purification of compounds was performed by flash column chromatography using silica gel Merck-60 (230-400 mesh, 0.040-0.063 mm) or Aldrich Sephadex LH-20. EI-MS spectra were determined on a VG AutoSpec instrument, MALDI-TOF MS and HRMS spectra were recorded with a Bruker Reflex III spectrometer. NMR spectra were recorded with a Bruker AC-300 instrument with a laser beam operating at 337 nm. Dithranol (1,8,9-anthracenetriol) and PEGNa1000 poly(ethylenglycol)-1000 were used as matrix and internal reference, respectively. FT-IR spectra were recorded on a Bruker Vector 22 spectrophotometer from solid samples embedded in pressed disks of KBr.

1.2.2. Synthesis

Synthesis of thiophenes 1 and 2. To a stirred solution of thiophene (40 mL, 0.48 mol) and 4-propylheptan-4-ol (for **1**) or 2-methylhexan-2-ol (for **2**) (0.022 mol), $BF_3{\cdot}OEt_2$ (3.5 mL, 0.025 mol) was added dropwise under inert atmosphere. The mixture was stirred for 5 h at room temperature in both cases. After vacuum evaporation of thiophene, the crude product was purified by column chromatography on silica gel using hexane as eluent to afford **1** (90%) or **2** (88%) as colourless oils.

*2-(1,1-dipropylbutyl)thiophene (**1**).* ^{1}H-NMR (300 MHz, $CDCl_3$), δ (ppm): 7.19 (dd, J = 5.1 Hz, J'' = 1.2 Hz, 1H), 6.97 (dd, J = 5.1 Hz, J' = 3.5 Hz, 1H), 6.84 (dd, J' = 3.5 Hz, J'' = 1.2 Hz, 1H), 1.72–1.64 (m, 6H), 1.26–1.15 (m, 6H), 0.95 (t, J = 7.0 Hz, 9H). ^{13}C-NMR (75.5 MHz, $CDCl_3$), δ (ppm): 155.4, 126.2, 122.9, 122.4, 43.8, 41.4, 15.0, 14.4. MS (EI), *m/z*: 224.4 $[M]^+$ (100%).

*2-(1,1-dimethylhexyl)thiophene (**2**).* ^{1}H-NMR (300 MHz, $CDCl_3$), δ (ppm): 7.17 (dd, J = 5.1 Hz, J' = 0.94 Hz, 1H), 6.96 (dd, J = 5.1 Hz, J' = 3.6 Hz, 1H), 6.85 (dd, J' = 3.6 Hz, J'' = 1.05 Hz, 1H, H-3), 1.71–1.60 (m, 2H), 1.42 /s, 6H), 1.35–1.20 (m, 4H), 0.93 (t, J = 7.0 Hz, 3H). ^{13}C-NMR (75.5 MHz, $CDCl_3$), δ (ppm): 156.4, 126.3, 123.4, 121.9, 45.6, 37.5, 30.3, 27.0, 23.2, 14.1. MS (EI), *m/z*: 182.3 $[M]^+$ (100%).

Synthesis of bipyridines 3 and 4. *n*-Butyllithium (5.72 mL, 2.5 M in hexane, 14.0 mmol) was added dropwise to a solution of **1** (for **3**) or **2** (for **4**) (11.9 mmol) in anhydrous THF (15 mL) at -78 ºC under argon atmosphere. The mixture was stirred at this temperature for 30 min and then for 1.5 h at room temperature. The reaction was cooled again to -78 ºC and tributyltin chloride (5.0 g, 15.0 mmol) was added. After stirring for 4 h at room temperature, the reaction was quenched by adding saturated NH_4Cl aqueous solution (5 mL). The mixture was then extracted with CH_2Cl_2 and dried over $MgSO_4$. After the removal of the solvent, the crude of the corresponding tributylstannylthiophene (10 mmol) was mixed with 4,40-di-bromo-2,20-bipyridine (1.00 g, 3.2 mmol) in 100 mL of dry DMF. The catalyst $Pd(PPh_3)_4$ (0.13 g, 0.16 mmol) was added to the solution and the mixture was stirred at 85 ºC under argon overnight. After vacuum evaporation of DMF, the resulting solid was purified by column chromatography on silica gel using CH_2Cl_2 as eluent to afford 1.15 g (60%) of **3** or 900 mg (55%) of **4** as ivory white solids.

*4,4´-Bis(5-(1,1-dipropylbutyl)thien-2-yl)-2,2´-bipyridine (**3**).* ^{1}H-NMR (300 MHz, $CDCl_3$), δ (ppm): 8.57 (d, J = 5.3 Hz, 2H), 8.52 (d, J = 1.03 Hz, 2H), 7.4 (m, 4H), 6.74 (d, J = 3.5 Hz, 2H), 1.60–1.50 (m, 12H), 1.34–1.22 (m, 12H), 1.24–1.22 (m, 12H), 0.84 (t, J = 7.0 Hz, 27H). ^{13}C-NMR (75.5 MHz, $CDCl_3$), δ (ppm): 158.0, 156.5, 149.5, 142.8, 138.1, 124.9, 124.4, 119.3, 116.8, 44.2, 41.6, 16.8, 14.7. HR-MS (EI), *m/z*: 601.3611 $[M+H]^+$. calcd. ($C_{38}H_{52}N_2S_2$): 601.3605.

*4,4´-Bis(5-(1,1-dimethylhexyl)thien-2-yl)-2,2´-bipyridine (**4**).* ^{1}H-NMR (300 MHz, $CDCl_3$), δ (ppm): 8.68 (d, J = 5.2 Hz, 2H), 8.64 (d, J = 1.1 Hz, 2H), 7.5 (m, 4H), 6.87 (d, J = 3.7 Hz, 2H), 1.74–1.66 (m, 4H), 1.44 (s, 12H), 1.35–1.20 (m, 8H), 0.91 (t, J = 7.0 Hz, 6H). ^{13}C-NMR (75.5 MHz, $CDCl_3$), δ (ppm): 158.9, 156.5, 149.5, 142.8, 138.2, 125.1, 123.5, 119.5, 116.5, 42.8, 37.9, 29.9, 27.0, 23.2, 14.0. HR-MS (EI), *m/z*: 517.2630 $[M+H]^+$. calcd. ($C_{32}H_{40}N_2S_2$): 517.2666

Synthesis of Ru(II) complexes TT204 and TT205. Dichloro(*p*-cymene)ruthenium(II) dimer (195.8 mg, 0.32 mmol) and **3** (for **TT204**) or **4** (for **TT205**) (0.64 mmol) were dissolved in dry DMF. The reaction mixture was stirred at 80 ºC for 4 h under argon in the dark. Subsequently, 4,4´-dicarboxylic acid-2,2´-bipyridine (156 mg, 0.64 mmol) was added into the flask and the reaction mixture was stirred at 140 ºC for 4 h. Finally, an excess of NH_4NCS (2.0 g, 26.5 mmol) was added to the resulting dark solution and the reaction was stirred for another 4 hours at the same temperature. The crude was cooled down to room temperature and the solvent was removed under vacuum. Water was then added to obtain a dark precipitate. The solid was collected by suction filtration, washed with water (200 mL) and Et_2O (2 x 60 mL), and dried under vacuum. The crude complex was dissolved in basic methanol (NaOH) and purified on a Sephadex LH-20 column with methanol as eluent. The solution obtained was acidified with a mixture of methanol and HNO_3 and the solvent was removed under vacuum. The crude was dissolved in THF (100 mL), and 1 eq of NaOH was added. Then, the solution was washed with brine (2 x 50 mL) and the solvent was removed obtaining the complexes **TT204** (230 mg, 35%) and **TT205** (272 mg, 45%) as brown solids.

*Ru complex **TT204**.* ^{1}H-NMR (300 MHz, $CDCl_3$), δ (ppm): 9.58 (d, J = 5.7 Hz, 1H), 9.18 (s (br), 1H), 9.07 (d, $J´$ = 5.7 Hz, 1H), 9.0 (s (br), 1H), 8.83 (s (br), 1H), 8.68 (s (br), 1H), 8.41 (d, J = 5.7 Hz, 1H), 8.15 (m, 2H), 7.63 (d, J = 6.1 Hz, 1H), 7.2-6.9 (m, 4H), 1.8–1.5 (m, 12H), 1.3–1.0 (m, 12H), 1.0–0.8 (m, 27H). FT-IR (KBr) ν (cm^{-1}): 3447, 3069, 2961, 2100 (–N=C=S as. st.), 1722 (C=O), 1614, 1545, 1464, 1261, 1018, 897, 816 (–N= C=S sym. st.), 669. UV-Vis (THF), λ_{max} (nm) (log ε): 571 (4.1), 411 (4.3), 338 (4.5), 308 (4.6), 306 (4.6), 279 (4.6), 213 (4.7). MS (MALDI, dithranol), *m/z*: 1004.2860 [$(M\text{-}NCS)^+$], calcd. ($C_{51}H_{60}N_5O_4RuS_3$): 1004.2851.

*Ru complex **TT205**.* ^{1}H-NMR (300 MHz, $CDCl_3$), δ (ppm): 9.52 (d, J = 5.9 Hz, 1H), 9.12 (m, 2H), 8.90 (s, 1H), 8.78 (s, 1H), 8.70 (s, 1H), 8.39 (d, J = 5.7 Hz, 1H), 8.10 (s, 1H), 8.03 (s, 1H), 7.96 (m, 2H), 7.68 (a (br), 1H), 7.30 (d, J = 6.2 Hz, 1H), 7.19 (s (br), 1H), 7.13 (s (br), 1H), 7.04 (s (br), 1H), 1.57 (m, 4H), 1.50 (s, 6H), 1.48 (s, 6H), 1.5–1.0 (m, 8H), 0.74 (t, J = 7.1 Hz, 3H), 0.70 (t, J = 7.1 Hz, 3H). ^{13}C-NMR (75.5 MHz, $CDCl_3$), δ (ppm): 165.8, 165.4, 160.75, 160.71, 159.5, 158.6, 158.1, 157.2, 153.7, 153.0, 152.5, 152.0, 142.3, 141.5, 136.5, 135.9, 135.1, 134.2, 129.2, 129.1, 126.6, 125.6, 125.3, 122.3, 123.2, 122.8, 121.8, 119.0, 118.8, 45.2, 45.0, 38.3, 38.2, 30.2, 30.0, 27.1, 26.9, 23.1, 23.0, 14.4, 14.3. FT-IR (KBr) ν (cm^{-1}): 3460, 3081, 2961, 2106 (–N=C=S as. st.), 1720 (C=O), 1612, 1556, 1489, 1448, 1259,

1016, 999, 804 (–N= C=S sym. st.), 658. UV-Vis (THF), λ_{max} (nm) (log ε): 571 (4.2), 411 (4.3), 338 (4.5), 308 (4.6), 306 (4.6), 279 (4.6), 213 (4.7). MS (MALDI, dithranol), *m/z*: 920.1917 [$(M\text{-}NCS)^+$], calcd. ($C_{45}H_{48}N_5O_4RuS_3$): 920.1920.

1.2.3. Optical, electrochemical and spectroscopic measurements

The UV-Visible and fluorescence spectra of solutions in 1 cm path length quartz cells were recorded using a Shimadzu™ UV-1700 spectrophotometer and an Aminco-Bowman™ Series 2 luminescence spectrometer with a temperature controller, respectively. The electrochemical data were obtained by employing a conventional three-electrode cell connected to a Model 600C Series CH Instruments potentiostat. For square wave voltammetry, a platinum wire working electrode, an SCE reference electrode and a platinum mesh as the auxiliary electrode were used. The laser transient absorption spectroscopy (L-TAS) measurements were carried out by the same procedure as Clifford *et al.*[14] employing a PTI nitrogen dye laser and a 150 W tungsten lamp as the light probe. The charge extraction and transient photovoltage decay measurements were carried out with a set-up similar to that employed by O'Regan et al.[15]

1.2.4. Device preparation

In the present work two different types of TiO_2 films are utilized depending on the measurements being conducted. Highly transparent thin films (4-7 µm) were utilized for L-TAS measurements and also for monitoring dye adsorption kinetics. L-TAS experiments were conducted on devices consisting of transparent TiO_2 films with optical densities of around 0.5 a.u. at the maximum absorption wavelength. On the other hand, for efficient DSCs, devices were made using either 6 or 12 µm thick films consisting of 20 nm TiO_2 nanoparticles (Dyesol© paste) and a scatter layer of 5 µm of 400 nm TiO_2 particles (CCIC, HPW-400). Prior to the deposition of the TiO_2 paste the conducting glass substrates were immersed in a solution of $TiCl_4$ (40 mM) for 30 min and then dried. The TiO_2 nanoparticle paste was deposited onto a conducting glass substrate (NSG glass with 8 Ω cm^{-2} resistance) using the screen printing technique. The TiO_2 electrodes were gradually heated under an airflow at 325 ºC for 5 min, 375 ºC for 5 min, 450 ºC for 15 min and 500 ºC for 15 min. The heated TiO_2 electrodes were immersed again in a solution of $TiCl_4$ (40 mM) at 70 ºC for 30 min and

then washed with ethanol. The electrodes were heated again at 500 ºC for 30 min and cooled before dye adsorption. In order to reduce scattered light from the edge of the glass electrodes of the dyed TiO_2 layer, a light shading mask was used onto the DSCs, so the active area of DSCs was fixed to 0.16 cm^2. The counter electrode was made by spreading a 5 mM solution of H_2PtCl_6 in isopropyl alcohol onto a conducting glass substrate (TEC15, Pilkington) with a small hole to allow the introduction of the liquid electrolyte using vacuum, followed by heating at 400 ºC for 15 min. Dye solutions at concentrations of 300 μM in ethanol (containing chenodeoxycholic acid where indicated) were prepared and the film immersed overnight at R.T. The sensitized electrodes were washed with ethanol and dried under air. Finally, the working and counter electrodes were sandwiched together using a thin thermoplastic (Surlyn) frame that melts at 100 ºC. For these solar cells the electrolyte used consisted of 1 M dimethyl-methyl imidazolium iodide (DMII), 0.05 M lithium iodide, 0.03 M iodine, 0.1 M guanidinium thiocyanate (GNCS) and 0.5 M 4-*tert*-butylpyridine in a mixture of acetonitrile/valeronitrile (85 : 15). For L-TAS, charge extraction and transient photovoltage measurements, 1-butyl-3-methyl- imidazolium iodide (BMII) was used instead of dimethyl-methyl imidazolium iodide (DMII) in the electrolyte.

1.2.5. Device characterization

The photovoltaic measurements were carried out with a 450 W xenon light source (Osram XBO 450, Germany) with a filter (Schott 113), whose power was regulated to the AM 1.5G solar standard by using a reference Si photodiode equipped with a colour matched filter (KG-3, Schott) in order to reduce the mismatch in the region of 350-750 nm between the simulated light and AM 1.5G to less than 4%. The applied potential and cell current were measured with a Keithley™ 2400 digital source meter. The incident photon-to-current conversion efficiency (IPCE) measurement was plotted as a function of wavelength by using the light from a 300 W xenon lamp (ILC Technology, USA), which was focused through a Gemini-180 double monochromator (Jobin Yvon Ltd., UK) onto the photovoltaic cell under testing. A computer controlled monochromator was incremented through the spectral range (300-900 nm) to generate a photocurrent action spectrum with a sampling interval of 10 nm and a current sampling time of 4 s. In addition, photocurrent and continuous irradiated light intensity were measured simultaneously at each wavelength.

1.3. Results and discussion

The synthetic route to the new ligands involves three main steps, as depicted in Scheme 6.1. In the first one, thiophene was monoalkylated by a Friedel-Crafts reaction with the corresponding tertiary alcohol (4-propyl-heptan-4-ol (for **1**) or 2-methylhexan-2-ol (for **2**)) in the presence of $BF_3{\cdot}Et_2O$. In order to avoid the formation of the respective dialkylated products, thiophene was used in a large excess (solvent). Subsequently, 4,4´-disubstituted bipyridines **3** and **4** were prepared by means of a palladium-catalyzed Stille coupling reaction between 4,4´-dibromo-2,2´-bi-pyridine and the corresponding tetrabutyl-stannylthiophenes. The latter were generated in situ by lithiation of **1** or **2** and quenching with tributyltin chloride. Finally, the ruthenium(II) complexes **TT204** and **TT205** were prepared in a typical one-pot synthesis[16] and were fully characterized by NMR, MS, HR-MS, UV-vis and FT-IR.

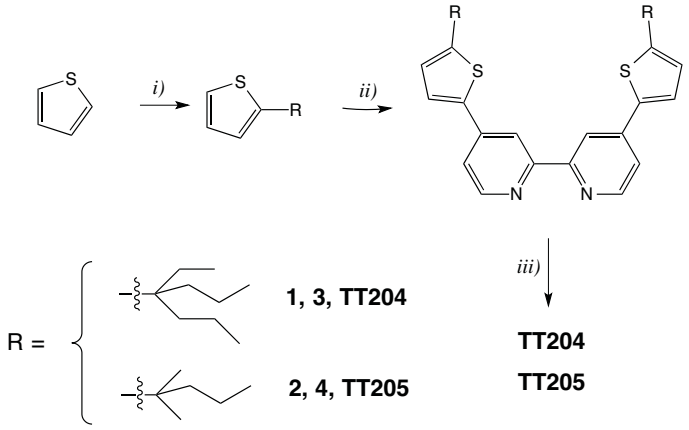

Scheme 6.1. Synthesis of ligands and their Ru(II) complexes **TT204** and **TT205**. ***i)*** Thiophene, $BF_3{\cdot}Et_2O$, 4-propylheptan-4-ol (for **1**; 90%) or 2-methylhexan-2-ol (for **2**; 88%). ***ii)*** *a*) *n*-butyllithium, **1** (for **3**) or **2** (for **4**), *b*) tributylstannyl chloride, THF, −78 ºC, *c*) 4,4'-dibromo-2,2'-bipyridine, $Pd(PPh_3)_2Cl_2$, DMF, 85 ºC; 60% (for **3**), 55% (for **4**). ***iii)*** *a*) Dichloro(*p*-cymene)ruthenium(II) dimer, **3** (for **TT204**) or **4** (for **TT205**), DMF, 80 ºC. *b*) 4,4'-dicarboxylic acid-2,2'-bipyridine, DMF, 140 ºC. *c*) NH_4Cl, DMF, 140 ºC; 35% (for **TT204**), 45% (for **TT205**).

The photophysical and electrochemical properties of **C101**, **TT204** and **TT205** were investigated and are summarized in Table 6.1. The absorption and emission spectra are shown in Figure 6.3.

The broad absorptions for all complexes in ethanol in the visible region centred on 520-530 nm are ascribed to the metal-to-ligand charge transfer (MLCT) transitions, which are typical for ruthenium polypyridal complexes. Excitation of this band produces very weak emission at 700-800

nm. The above data for **C101** corresponds well with that already reported by Gao *et al*.[5] HOMO and LUMO values calculated were quite similar for these three complexes indicating that the nature of the group on the 2-position of the thiophene unit on the ancillary bipyridal ligand has little bearing on the electronic properties of the dye. Furthermore, E_{HOMO} and E_{LUMO} values indicate efficient dye regeneration by the iodide/tri-iodide redox electrolyte (E_{redox} = –4.75 eV) and also efficient electron injection into the TiO_2 conduction band (E_{TiO2} = –4.0 eV). A small shift in the absorption and emission spectra of **TT204** was observed and it is most likely due to dissociation of protons in solution[17] in other words, less number of protons in **TT204** compared to the **TT205**.

Table 6.1. Photophysical and electrochemical properties of **C101**, **TT204** and **TT205**.

Dye	λ_{abs}[a]/nm	λ_{em}[a]/nm	E_{ox}[b]/V (*vs.* Fc/Fc^+)	$E_{0\text{-}0}$[c]/eV	E_{HOMO}[d]/eV	E_{LUMO}[e]/eV
C101	531	755	0.280	1.92	–5.16	–3.24
TT204	694	694	0.333	2.04	–5.21	–3.17
TT205	747	747	0.297	1.96	–5.18	–3.22

[a] Measured in ethanol. [b] Measured in ethanol containing 0.1 M tetrabutylammonium perchlorate. The working electrode consisting of a platinum wire and the counter electrode a platinum mesh. The reference electrode was the silver calomel electrode. All solutions were degassed with argon for 10 min prior to measurement. [c] E_{0-0} was determined from the intersection of absorption and emission spectra in dilute ethanol solutions. [d] E_{HOMO} was calculated using E_{HOMO} (vs. vacuum) = –4.88 – E_{ox} (vs.Fc/Fc^+). [e] E_{LUMO} was calculated using $E_{LUMO} = E_{HOMO} + E_{0-0}$.

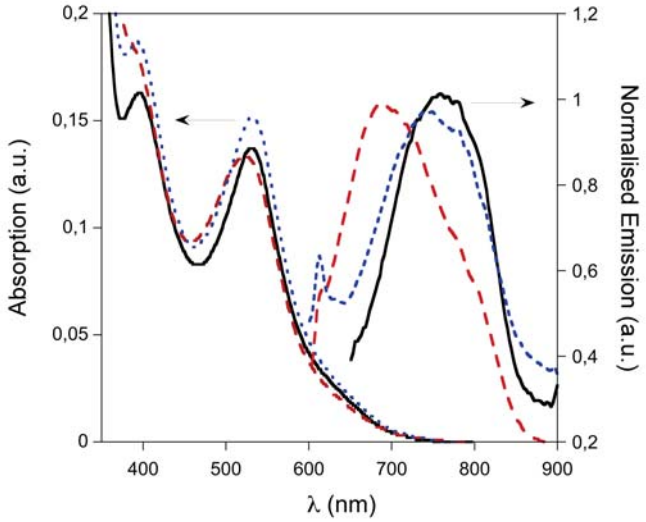

Figure 6.3. Absorption and emission spectra of C101 (–), TT204 (---) and TT205 (···) in ethanol.

The absorption of thin TiO_2 films (~7 µm) was measured with time

following sensitization in 300 μM solutions of **C101**, **TT204** and **TT205** at R.T. in the presence and absence of 1 mM chenodeoxycholic acid (Figure 6.4). The adsorption rate constant for each dye onto the TiO_2 electrode K_{ads} (min^{-1}) could be obtained by fitting these data to the Lagargren Equation, as has been done previously:[18]

$$Abs(t) = Abs_{max} (1 - e^{-(Kadst)}) \quad (1)$$

In the case of the solutions containing chenodeoxycholic acid (Figure 6.4(a)) K_{ads} for all dyes was found to be almost identical (0.014 min^{-1}, 0.014 min^{-1} and 0.013 min^{-1} for **C101**, **TT204**, **TT205** respectively) indicating that the presence of the bulky groups in **TT204** and **TT205** with respect to the alkyl chain on **C101** have little effect upon dye adsorption kinetics. Surprisingly, K_{ads} for films sensitized in the absence of chenodeoxycholic acid (Figure 6.4(b)) appear quite similar (0.015 min^{-1}, 0.012 min^{-1} and 0.010 min^{-1} for **C101**, **TT204**, **TT205** respectively), despite the absence of any co-adsorbent that can compete for space on the TiO_2 film. It is noted, however, that **TT204** films generally show lower optical densities than **TT205** and **C101** films. As all three dyes have similar molar extinction coefficients this indicates that there are lower dye concentrations on **TT204** films. This is especially marked in the case where no chenodeoxycholic acid is present in the sensitizing solution (Figure 6.4(b)). This suggests different dye packing on the TiO_2. The significance of this is discussed hereafter when comparing V_{oc} for optimized DSCs devices.

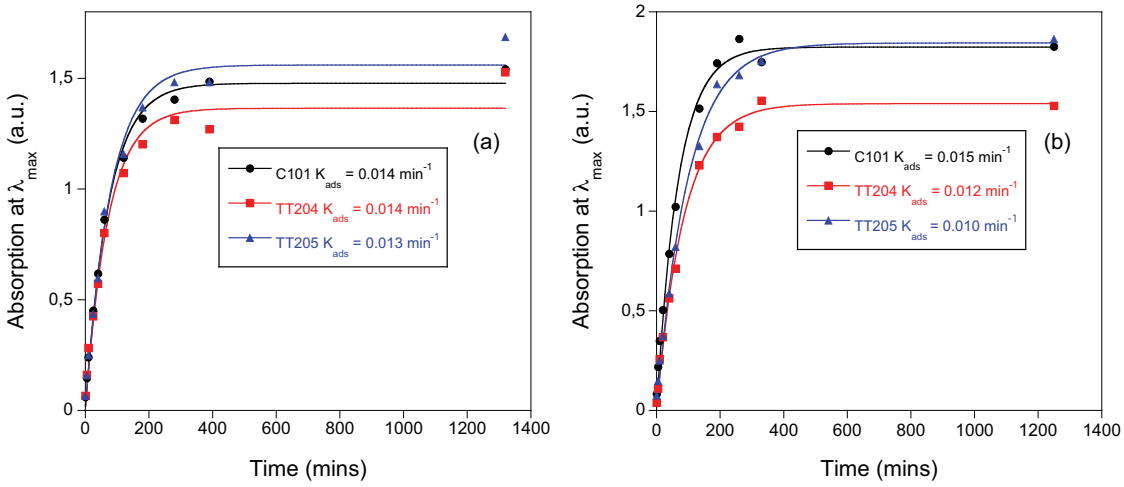

Figure 6.4. Absorption measured for 7 μm TiO_2 films sensitized at R.T. in 300 μM solutions of **C101**, **TT204** and **TT205** in (a) the presence and (b) absence of 1 mM chenodeoxycholic acid. Absoption was measured at 528, 523 and 528 nm for **C101**, **TT204** and **TT205** films respectively. The line corresponds to the fitting of the data to the Lagargren Equation.

Laser transient absorption spectroscopy (L-TAS) was used to measure

the photo-induced electron transfer processes occurring at the dye sensitized TiO_2 electrode in the presence and absence of redox electrolyte. As can be seen in Figure 6.5 the transient decays in the absence of electrolyte show multi-exponential behaviour for all samples as has been observed previously for studies involving similar Ru(II) polypyridine complexes.[14,19] Moreover, the presence of the bulky groups in the structures of **TT204** and **TT205** does not appear to have any significant influence over recombination kinetics if we compare the $t_{50\%}$ values (~3.3 and 2.0 ms for **TT204** and **TT205** respectively) to that of **C101** (~2.4 ms). In the presence of electrolyte the loss of the cation signal due to regeneration of the dye cations by iodide/tri-iodide redox couple appears to be very similar for all samples, indicating that the regeneration efficiency is similar in all cases. This is explained by the HOMO energies (Table 6.1) obtained for these complexes indicating similar driving force energy for the regeneration reaction in all cases.

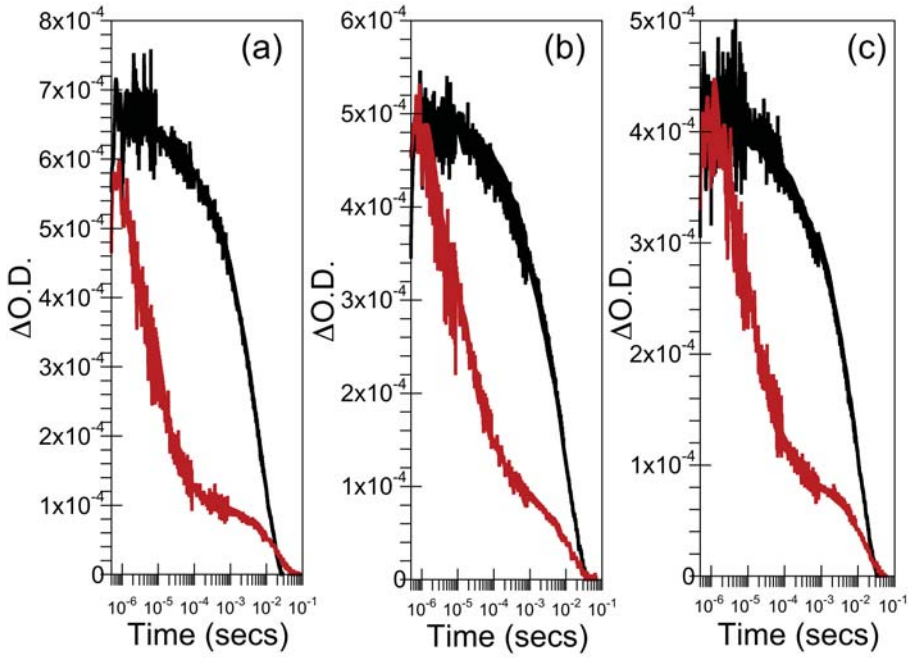

Figure 6.5. Transient absorption kinetics of 4 µm TiO_2 films sensitized with (a) **C101**, (b) **TT204** and (c) **TT205** measured in the presence (red) and absence (black) of electrolyte. Kinetics were recorded at 780 nm following excitation at 580 nm.

TT204 and **TT205** devices show excellent photocurrents even without the use of co-adsorbents. Table 6.2 lists the most important parameters for all devices measured in this work. For the 6 + 5 µm devices, only a negligible increase in photocurrent is observed when chenodeoxycholic acid is used indicating that the bulky groups on **TT204** and **TT205** function just as well as the co-adsorbent in their role of achieving high photocurrents. Both dyes on thicker 12 + 5 µm films sensitized in the presence of chenodeoxycholic acid generated high J_{sc} of 18.2 mA cm^{-2} (**TT204**) and 18.7 mA cm^{-2} (**TT205**) as

shown in Figure 6.6, which is higher than the published value of 17.9 mA cm^{-2} for the **C101** dye.[5]

Table 6.2. Detailed photovoltaic parameters of **C101**, **TT204** and **TT205** DSCs devices. The TiO_2 films were immersed in a 0.3 mM dye ethanol solution containing 1 mM chenodeoxycholic acid (where indicated) overnight at R.T.

Dye	J_{sc}/mA cm^{-2}	V_{oc}/V	FF (%)	$\eta^{a\ (\%)}$
C101[b]	17.94	0.778	78.5	11.0
TT204[c]	18.22	0.682	72.2	8.97
TT204[d]	14.93	0.664	70.9	7.03
TT204[e]	15.05	0.678	71.3	7.32
TT205[c]	18.69	0.715	73.4	9.81
TT205[d]	15.74	0.684	70.8	7.62
TT205[e]	15.85	0.698	70.8	7.84

[a] The efficiencies were measured at 1 sun 1.5 AM G with mask (area = 0.16 cm^2). [b] Data from Gao *et al.*[5] [c] With 1 mM chenodeoxycholic acid in dye solution and 12 + 5 µm thick TiO_2 films. [d] Without chenodeoxycholic acid in dye solution and 6 + 5 µm thick TiO_2 films. [e] With 1 mM chenodeoxycholic acid in dye solution and 6 + 5 µm thick TiO_2 films.

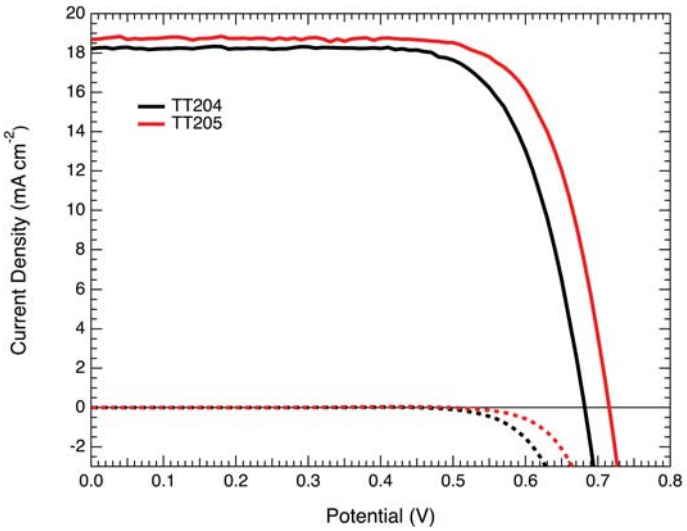

Figure 6.6. IV curves of **TT204** (black) and **TT205** (red) cells made using ethanol sensitization solvent under 1 sun AM 1.5 illumination (solid line) and in the dark (dashed line). The cells were measured with mask (area = 0.16 cm^2). The 12 + 5 µm thick TiO_2 films were immersed in a 0.3 mM dye ethanol solution containing 1 mM chenodeoxycholic acid overnight at R.T.

The IPCE recorded for **TT204** and **TT205** devices (see Figure 6.7) concur with the photocurrents listed in Table 6.2. For the thicker film cells made using chenodeoxycholic acid, J_{sc} varies negligibly, however, V_{oc} varies to a much greater extent (0.78 V, 0.68 V and 0.72 V for **C101**, **TT204** and **TT205** respectively). Particularly striking is the observation of the almost 100 mV difference between **C101** and **TT204** devices. Previous studies by Durrant and co-workers[10,20] investigating the effect of alkyl chain length in ruthenium

complexes on cell performance in both liquid and solid-state DSCs showed increasing V_{oc} and efficiency as chain length became longer. This is due to more effective blocking of recombination between the photo-injected electrons in the titanium and the oxidized electrolyte. However, the introduction of increasingly bulky groups into dye structure in this study clearly does not result in the same outcome.

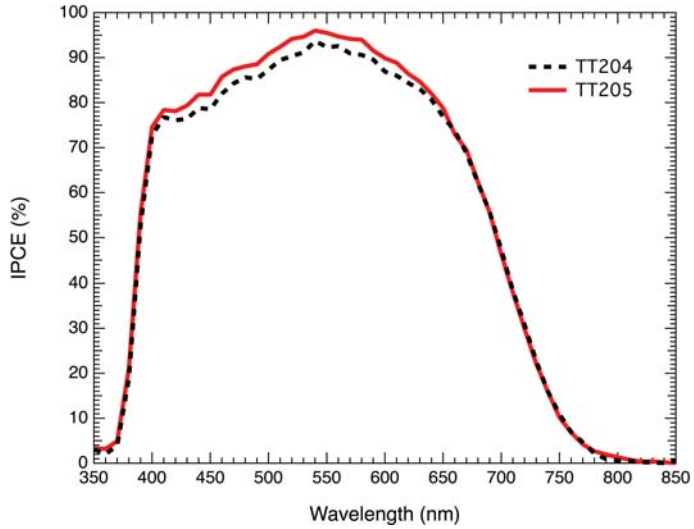

Figure 6.7. Incident photon to current (IPCE) action spectrum for **TT204** (black dashed line) and **TT205** (red solid line) DSCs devices recorded under 1 sun AM 1.5G illumination. The 12 + 5 µm thick TiO_2 films were immersed in a 0.3 mM dye ethanol solution containing 1 mM chenodeoxycholic acid overnight at R.T.

Charge extraction and transient photovoltage studies were carried out in order to investigate electron densities and electron lifetimes in optimized devices composed of 12 + 5 µm thick TiO_2 films under operating conditions. Figure 6.8(a) illustrates charge density as a function of voltage for the different devices. It is clear that there is very little difference in electron densities between the films indicating that the position of the conduction band edge is similar in all devices. Therefore shifts in the Fermi level cannot explain the differences in voltage observed in these devices. However, electron lifetimes measured at identical electron densities using transient photovoltage measurements (Figure 6.8(b)) show a general trend that correlates rather well with the V_{oc} values obtained for these devices, *i.e.* as electron lifetime gets shorter, V_{oc} decreases.

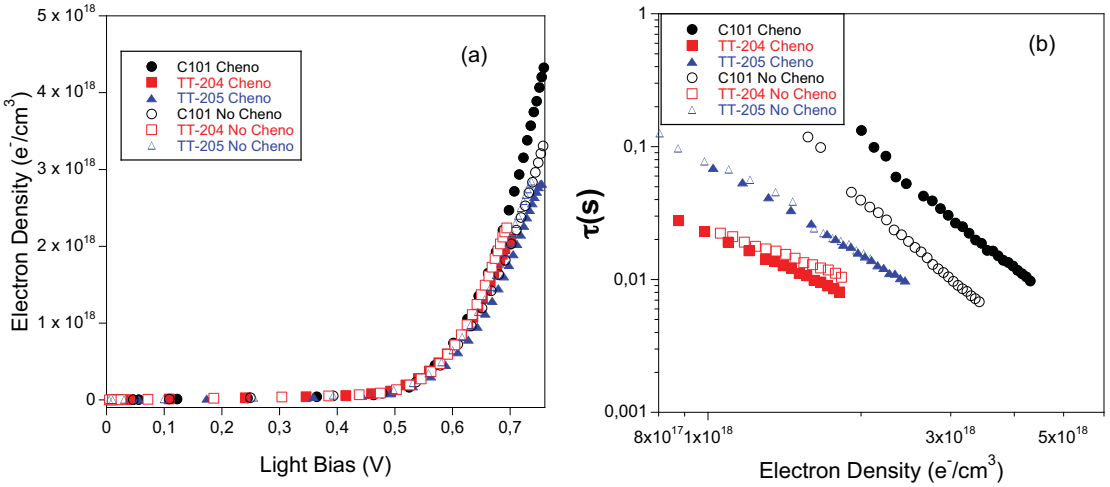

Figure 6.8. (a) TiO_2 electron density *versus* light bias deduced from charge extraction studies and (b) electron lifetime (τ) *versus* electron density deduced from transient photovoltage studies for **C101**, **TT204** and **TT205** devices made with chenodeoxycholic acid.

Though cell voltages (V_{oc}) and electron lifetimes (τ) correlate well for the data presented, it is rather surprising that the bulkier the groups on the sensitizer, the lower the V_{oc} and the shorter τ. Indeed, this is perhaps the opposite of what one might intuitively expect. This observation is particularly pronounced for the 12 + 5 μm cells where the V_{oc} of the **TT204** device is nearly 100 mV smaller than that of the **C101** device. We attribute this to disordered dye packing on the TiO_2 surface when the bulky groups become too big. Moreover, for the thinner 6 + 5 μm cells, devices prepared in the absence of chenodeoxycholic acid show poorer V_{oc} in comparison to devices prepared in the presence of this co-adsorbent. This suggests that dye packing on the TiO_2 is particularly inefficient in the absence of chenodeoxycholic acid and is somewhat confirmed in Figure 6.4(b) where the **TT204** film shows much lower optical density than either **C101** or **TT205**. This may result in bare areas of TiO_2 being exposed to the electrolyte, increasing recombination and lowering cell voltage. This indicates that in addition to its function in DSCs of avoiding aggregation and optimizing photocurrent, chenodeoxycholic acid fulfils a secondary function of facilitating ordered dye packing and optimizing cell voltage.

1.4. Conclusion

Two novel ruthenium complexes, **TT204** and **TT205**, were synthesized and their properties in solution and in DSCs devices investigated and compared against those of **C101**. These dyes showed outstanding photo-currents even in the absence of chenodeoxycholic acid, indicating that the bulky groups can be used as a substitute for co-adsorbents to stop

aggregation and achieve high photocurrents. Despite this, **C101** devices show higher efficiencies, larger cell voltages and longer electron lifetimes under operating conditions. It is postulated that this is because of inefficient dye packing of **TT204** and **TT205** on the TiO_2 surface caused by the bulky groups present on the ancillary ligands of these dyes. Moreover, devices prepared from films sensitized in the presence of chenodeoxycholic acid display both higher efficiencies and cell voltages when compared to devices prepared without this co-adsorbent. This indicates that chenodeoxycholic acid helps form more ordered dye packing on the TiO_2 film. Therefore, though bulky groups may be used as an effective strategy to prevent aggregation and improve photocurrent, avoiding the need for the use of co-adsorbants such as chenodeoxycholic acid, such bulky groups may not be conducive to achieving effective dye packing and higher voltages.

Acknowledgements

Financial support by the MICINN, Spain (CTQ2008-00418/BQU, CTQ2010-18859, CONSOLIDER-INGENIO 2010 CDS 2007-00010 and CONSOLIDER INGENIO CDS-0007 HOPE-2007, PLE2009-0070), and CAM (MADRISOLAR-2, S2009/PPQ/1533), is gratefully acknowledged. EP also thanks the European Research Council for the fellowship PolyDot as well as the Catalan government for the 2009 SGR 207. ICIQ and ICREA financial support is also acknowledged. JNC thanks the MICINN for the Juan de la Cierva Fellowship. MKN thanks the GRL, and World Class University programs (Photovoltaic Materials, Department of Material Chemistry, Korea University) funded by the Ministry of Education, Science and Technology through the National Research Foundation of Korea (No. R31-2008-000-10035-0). MG acknowledge the European Community's Seventh Framework Programme (FP7/2007–2013) under grant agreement nº 246124 of the SANS project.

References

1. O'Regan, B.; Grätzel, M., A low-cost, high-efficiency solar cell based on dye-sensitized colloidal TiO2 films. *Nature* **1991,** *353*, 737-740.
2. (a) Robertson, N., Optimizing dyes for dye-sensitized solar cells. *Angew. Chem., Int. Ed.* **2006,** *45*, 2338-2345; (b) Ardo, S.; Meyer, G. J., Photodriven heterogeneous charge transfer with transition-metal compounds anchored to TiO2 semiconductor surfaces *Chem. Soc. Rev.* **2009,** *38*, 115-164; (c) Hagfeldt, A.; Boschloo, G.; Sun, L.; Kloo, L.; Pettersson, H., Dye-Sensitized Solar Cells. *Chem. Rev.* **2010,** *110*, 6595-6663; (d) Clifford, J. N.; Martínez-Ferrero, E.; Viterisi, A.; Palomares, E., Sensitizer molecular structure-device efficiency relationship in dye sensitized solar cells. *Chem. Soc. Rev.* **2011,** *40*, 1635-1646; (e) Ning, Z.; Fu, Y.; Tian, H., Improvement of dye-sensitized solar cells: what we know and what we need to know. *Energy Environ. Sci.* **2010,** *3*, 1170-1181.
3. Reynal, A.; Palomares, E., Ruthenium Polypyridyl Sensitisers in Dye Solar Cells Based on Mesoporous TiO2. *J. Inorg. Chem.* **2011,** *2011*, 4509-4526.
4. Nazeeruddin, M. K.; Zakeeruddin, S. M.; Humphry-Baker, R.; Jirousek, M.; Liska, P.; Vlachopoulos, N.; Shklover, V.; Fischer, C. H.; Grätzel, M., Acid–Base Equilibria of (2,2‘-Bipyridyl-4,4‘-dicarboxylic acid)ruthenium(II) Complexes and the Effect of Protonation on Charge-Transfer Sensitization of Nanocrystalline Titania. *Inorg. Chem.* **1999,** *38*, 6298-6305.
5. Gao, F.; Wang, Y.; Shi, D.; Zhang, J.; Wang, M.; Jing, X.; Humphry-Baker, R.; Wang, P.; Zakeeruddin, S. M.; Grätzel, M., Enhance the Optical Absorptivity of Nanocrystalline TiO2 Film with High Molar Extinction Coefficient Ruthenium Sensitizers for High Performance Dye-Sensitized Solar Cells. *J. Am. Chem. Soc.* **2008,** *130*, 10720-10728.
6. Chen, C. Y.; Wang, M.; Li, J. Y.; Pootrakulchote, N.; Alibabaei, L.; Ngoc-le, C.-h.; Decoppet, J.-D.; Tsai, J.-H.; Gratzel, C.; Wu, C.-G.; Zakeeruddin, S. M.; Grätzel, M., Highly Efficient Light-Harvesting Ruthenium Sensitizer for Thin-Film Dye-Sensitized Solar Cells. *ACS Nano* **2009,** *3*, 3103-3109.
7. Tatay, S.; Haque, S. A.; O'Reagan, B.; Durrant, J. R.; Verhees, W. J. H.; Kroon, J. M.; Vidal-Ferran, A.; Gavina, P.; Palomares, E., Kinetic competition in liquid electrolyte and solid-state cyanine dye sensitized solar cells. *J. Mater. Chem.* **2007,** *17*, 3037-3044.
8. He, J.; Benko, G.; Korodi, F.; Polivka, T.; Lomoth, R.; Akermark, B.; Sun, L.; Hagfeldt, A.; Sundstrum, V., Modified Phthalocyanines for Efficient Near-IR Sensitization of Nanostructured TiO2 Electrode. *J. Am. Chem. Soc.* **2002,** *124*, 4922-4932.

9. (a) Wang, P.; Zakeeruddin, S. M.; Moser, J. E.; Nazeeruddin, M. K.; Sekiguchi, T.; Grätzel, M., A stable quasi-solid-state dye-sensitized solar cell with an amphiphilic ruthenium sensitizer and polymer gel electrolyte. *Nat. Mater.* **2003,** *2*, 402-407; (b) Wang, P.; Zakeeruddin, S. M.; Comte, P.; Charvet, R.; Humphry-Baker, R.; Grätzel, M., Enhance the Performance of Dye-Sensitized Solar Cells by Co-grafting Amphiphilic Sensitizer and Hexadecylmalonic Acid on TiO2 Nanocrystals. *J. Phys. Chem. B* **2003,** *107*, 14336-14341.

10. Kroeza, J. E.; Hirata, N.; Koops, S.; Nazeeruddin, M. K.; Schmidt-Mende, L.; Grätzel, M.; Durrant, J. R., Alkyl chain barriers for kinetic optimization in dye-sensitized solar cells. *J. Am. Chem. Soc.* **2006,** *128*, 16376-16383.

11. (a) Liu, Y.; Xiang, N.; Feng, X.; Shen, P.; Zhou, W.; Weng, C.; Zhao, B.; Tan, S., Thiophene-linked porphyrin derivatives for dye-sensitized solar cells. *Chem. Commun.* **2009**, 2499-2501; (b) Planells, M.; Forneli, A.; Martínez-Ferrero, E.; Sanchez-Diaz, A.; Sarmentero, M. A.; Ballester, P.; Palomares, E.; O'Reagan, B., The effect of molecular aggregates over the interfacial charge transfer processes on dye sensitized solar cells. *Appl. Phys. Lett.* **2008,** *92*, 153506-153506-3; (c) Koumura, N.; Wang, Z.-S.; Mori, S.; Miyashita, M.; Suzuki, E.; Hara, K., Alkyl-Functionalized Organic Dyes for Efficient Molecular Photovoltaics. *J. Am. Chem. Soc.* **2006,** *128*, 14256-14257; (d) Choi, H.; Baik, C.; Kang, S. O.; Ko, J.; Kang, M.-S.; Nazeeruddin, M. K.; Grätzel, M., Highly Efficient and Thermally Stable Organic Sensitizers for Solvent-Free Dye-Sensitized Solar Cells. *Angew. Chem., Int. Ed.* **2008,** *47*, 327-330.

12. Mori, S.; Nagata, M.; Nakahata, Y.; Yasuta, K.; Goto, R.; Kimura, M.; Taya, M., Enhancement of Incident Photon-to-Current Conversion Efficiency for Phthalocyanine-Sensitized Solar Cells by 3D Molecular Structuralization. *J. Am. Chem. Soc.* **2010,** *132*, 4054-4055.

13. Bessho, T.; Zakeeruddin, S. M.; Yeh, C.-Y.; -G., D. E. W.; Grätzel, M., Highly Efficient Mesoscopic Dye-Sensitized Solar Cells Based on Donor–Acceptor-Substituted Porphyrins. *Angew. Chem., Int. Ed.* **2010,** *49*, 6646-6649.

14. Clifford, J. N.; Palomares, E.; Nazeeruddin, M. K.; Grätzel, M.; Nelson, J.; Li, X.; Long, N. J.; Durrant, J. R., Molecular control of recombination dynamics in dye-sensitized nanocrystalline TiO2 films: free energy vs distance dependence. *J. Am. Chem. Soc.* **2004** *126*, 5225-5233.

15. O'Reagan, B.; Scully, S.; Mayer, A. C.; Palomares, E.; Durrant, J. R., The Effect of Al2O3 Barrier Layers in TiO2/Dye/CuSCN Photovoltaic Cells Explored by Recombination and DOS Characterization Using Transient Photovoltage Measurements. *J. Phys. Chem. B* **2005,** *109*, 4616-4623.

16. Klein, C.; Nazeeruddin, M. K.; Liska, P.; Di Censo, D.; Hirata, N.; Palomares, E.; Durrant, J. R.; Grätzel, M., Engineering of a Novel Ruthenium Sensitizer and Its Application in Dye-Sensitized Solar Cells for Conversion of Sunlight into Electricity. *Inorg. Chem.* **2004,** *44*, 178-180.
17. Nazeeruddin, M. K.; Humphry-Baker, R.; Liska, P.; Grätzel, M., Investigation of Sensitizer Adsorption and the Influence of Protons on Current and Voltage of a Dye-Sensitized Nanocrystalline TiO2 Solar Cell. *J. Phys. Chem. B* **2003,** *107*, 8981-8987.
18. Planells, M.; Pellejà, L.; Ballester, P.; Palomares, E., Utilization of a heterosupramolecular self-assembled trisporphyrin complex in dye-sensitised solar cells. *Energy Environ. Sci.* **2011,** *4*, 528-534.
19. (a) Tachibana, Y.; Haque, S. A.; Mercer, I. P.; Durrant, J. R.; Klug, D. R., Electron Injection and Recombination in Dye Sensitized Nanocrystalline Titanium Dioxide Films: A Comparison of Ruthenium Bipyridyl and Porphyrin Sensitizer Dyes. *J. Phys. Chem. B* **2000,** *104*, 1198-1205; (b) Reynal, A.; Forneli, A.; Palomares, E., Dye structure–charge transfer process relationship in efficient ruthenium-dye based dye sensitized solar cells. *Energy Environ. Sci.* **2010,** *3*, 805-812.
20. Schmidt-Mende, L.; Kroeze, J. E.; Durrant, J. R.; Nazeeruddin, M. K.; Grätzel, M., Effect of hydrocarbon chain length of amphiphilic ruthenium dyes on solid-state dye-sensitized photovoltaics. *Nano Lett.* **2005,** *5*, 1315-1320.

Chapter 7. Conclusions

In this work, the application of different dyes in DSCs is discussed. The device efficiency is simplified in terms of interfacial charge transfer kinetics, which in turn is correlated with the molecular structure. The understanding of these relationships will provide a better and more rational design of new dyes for DSCs.

The main results can be summarized as follows:

- DSCs were performed with two zinc-porphyrins sensitizers employing I^-/I_3^- and $Co(II)(phen)_3$/ $Co(III)(phen)_3$ as red/ox electrolytes in *Paper 1*. In this study it was observed that the optimized sensitization time depends on the electrolyte used. Working with I^-/I_3^-, shorter sensitization times and lower dye loading perform the best results. The use of $Co(II)(phen)_3/Co(III)(phen)_3$ leads to the opposite conditions, longer sensitization times and higher dye loadings.

- The light soaking effect of a D-π-A porphyrin sensitizer with an indoline unit as the donor group was investigated in *Paper 2*. The efficiency of this porphyrin based devices was found to depend upon exposure to illumination with maximum efficiencies observed after 90 minutes with increases in both V_{oc} and J_{sc} observed. Charge extraction and transient photovoltage data indicate that the increase in J_{sc} is due to a downward shift of the TiO_2 conduction band while the increase in V_{oc} is due to an increase in device electron lifetime. The co-sensitization of this porphyrin with another dye with complementary absorbance results in a better efficiency.

- The effect of none, one or two sulfonate anchoring groups in three Ti(IV) phthalocyanines axially coordinated to 2,3- and 1,8-naphthalenediols on DSCs efficiency was examined in *Paper 3*. No differences between them were observed because a ligand exchange with the TiO_2 takes place, giving rise to the same species adsorbed on the inorganic semiconductor.

- One of the highest efficiencies ever recorded for a DSCs device employing a fully organic dye and iodine/iodide electrolytes was

obtained in *Paper 4*. A solvent-free ionic liquid electrolyte was also used and stability studies indicates no degradation of the complete device after 2200 hours at 65ºC.

- A series of organic dyes with alkene and alkyne bridges were tested for DSCs in *Paper 5*. It was resolved that the presence of a alkyne bridge does not consistently leads to faster recombination dynamics between the photo-injected electrons at the TiO_2 and the oxidized electrolyte.

- Finally, in *Paper 6*, two novel ruthenium complexes were compared versus **C101**. In this study was resolved that the bulky groups can be used as a substitute for co-adsorbents to stop aggregation and achieve high photocurrents. The finally dye packing on the TiO_2 surface caused by the bulky groups present on the ancillary ligands must be taken into account.

Annex.

Contributions to the Scientific Community

Utilization of a heterosupramolecular self-assembled trisporphyrin complex in dye-sensitized solar cells. Planells, Miquel; Pellejà, Laia; Ballester, Pablo; Palomares, Emilio.

Energy & Environmental Science, **2011**, 4(2), 528-534.

Energy levels, charge injection, charge recombination and dye regeneration dynamics for donor-acceptor π-conjugated organic dyes in mesoscopic TiO_2 sensitized solar cells. Planells, Miquel; Pellejà, Laia; Clifford, John N.; Pastore, Mariachiara; De Angelis, Filippo; Lopez, Nuria; Marder, Seth R.; Palomares, Emilio.

Energy & Environmental Science, **2011**, 4(5), 1820-1829.

A continuity equation for the simulation of the current-voltage curve and the time-dependent properties of dye-sensitized solar cells. Anta, Juan A.; Idigoras, Jesus; Guillen, Elena; Villanueva-Cab, Julio; Mandujano-Ramirez, Humberto; Oskam, Gerko; Pellejà, Laia; Palomares, Emilio.

Physical Chemistry Chemical Physics, **2012**, 14(29), 10285-10299.

Efficient transparent thin dye solar cells based on highly porous 1D photonic crystals. Colodrero, Silvia; Forneli, Amparo; Lopez-Lopez, Carmen; Pellejà, Laia; Miguez, Hernan; Palomares, Emilio.

Advanced Functional Materials, **2012**, 22(6), 1303-1310.

Effect of bulky groups in ruthenium heteroleptic sensitizers on dye sensitized solar cell performance. Garcia-Iglesias, Miguel; Pellejà, Laia; Yum, Jun-Ho; Gonzalez-Rodriguez, David; Nazeeruddin, Mohammad K.; Grätzel, Michael; Clifford, John N.; Palomares, Emilio; Vazquez, Purificacion; Torres, Tomas.

Chemical Science, **2012**, 3(4), 1177-1184.

Light soaking effects on charge recombination and device performance in dye sensitized solar cells based on indoline-cyclopentadithiophene chromophores. Cabau, Lidia; Pellejà, Laia; Clifford, John N.; Challuri, Vijay; Palomares, Emilio.

Journal of Materials Chemistry A, **2013**, 1(31), 8994-9000.

Ti(IV) phtalocyanines for dye sensitized solar cells. Rodriguez-Morgade, M. Salome; Pellejà, Laia; Torres, Tomas; Palomares, Emilio.

Journal of Porphyrins and Phtalocyanines, **2013**, 17(8-9), 814-820.

Effect of porphyrin loading on performance of dye sensitized solar cells based on iodide/tri-iodide and cobalt electrolytes. Aljarilla, Ana; Clifford, John N.; Pellejà, Laia; Moncho, Antonio; Arrechea, Susana; de la Cruz, Pilar; Langa, Fernando; Palomares, Emilio.

Journal of Materials Chemistry A, **2013**, 1(43), 13640-13647.

The redox pair chemical environment influence on the recombination loss in dye-sensitized solar cells. Idigoras, Jesus; Pellejà, Laia; Palomares, Emilio; Anta, Juan A.

Journal of Physical Chemistry C, **2014**, 118(8), 3878-3889.

A robust organic dye for dye sensitized solar cells based on iodine/iodide electrolytes combining high efficiency and outstanding stability. Joly, Damien; Pellejà, Laia; Narbey, Stephanie; Oswald, Frederic; Chiron, Julien; Clifford, John N.; Palomares, Emilio; Demadrille, Renaud.

Scientific Reports, **2014**, 4, 4033.

D-π-A porphyrin employing an indoline donor group for high efficiency dye-sensitized solar cells. Pellejà, Laia; Challuri, Vijay; Clifford, John N.; Palomares, Emilio.

Journal of Physical Chemistry C, **2014**, article ASAP.

Use of vinyl and ethynyl molecular bridges in organic dyes for dye sensitized solar cells: implications in device performance. Pellejà, Laia; Dominguez, Rocio; Aljarilla, Ana; Clifford, John N.; de la Cruz, Pilar; Langa, Fernando; Palomares, Emilio.

Submitted to ChemElectroChem.